

Sheffield Hallam University

Conformational changes and the self-assembly of alpha-synuclein

MASON, Rebecca

Available from the Sheffield Hallam University Research Archive (SHURA) at:

<http://shura.shu.ac.uk/24181/>

A Sheffield Hallam University thesis

This thesis is protected by copyright which belongs to the author.

The content must not be changed in any way or sold commercially in any format or medium without the formal permission of the author.

When referring to this work, full bibliographic details including the author, title, awarding institution and date of the thesis must be given.

Please visit <http://shura.shu.ac.uk/24181/> and <http://shura.shu.ac.uk/information.html> for further details about copyright and re-use permissions.

Conformational Changes and the Self-assembly of Alpha-synuclein

Rebecca Jane Mason

A thesis submitted in partial fulfilment of the requirements of
Sheffield Hallam University
for the degree of Doctor of Philosophy

October 2018

i. Abstract

Parkinson's disease is the second most common neurodegenerative disease, affecting 0.1 - 0.2% of the population. Incidence of this debilitating disorder rises to 1% of the population over the age of 65, posing a substantial socioeconomic burden on the UK's aging population. There are currently no disease altering treatments for PD, in part due to the incomplete knowledge of the disease mechanism.

The misfolding and aggregation of the protein alpha-synuclein is associated with a range of neurological disorders, including Parkinson's disease. Alpha-synuclein has been irrefutably linked to Parkinson's disease through both genetic and pathological data, with increasing evidence suggesting prefibrillar oligomeric forms of the protein are the toxic species. However, the precise molecular mechanisms through which this protein is linked to the disease are currently unknown. Consequently, increasing knowledge of alpha-synuclein is of great importance, as new discoveries will potentially further the development of new therapeutics for the disease.

In this thesis the primary aim was to conduct investigations into the structural and functional aspects of N-terminally acetylated alpha-synuclein and its oligomers through a combination of Electrospray Ionisation – Ion Mobility Spectrometry – Mass Spectrometry, biochemical and cell culture assays. Alpha-synuclein is a known metal binding protein and the copper binding and subsequent conformational changes and aggregation of modified and mutated forms of the protein were investigated. A novel loss of metal binding function was found for the N-terminally acetylated H50Q form of the protein. The conformational effects of N-terminal acetylation on the oligomeric forms of the protein were also investigated. It was demonstrated that this co-translational modification of alpha-synuclein did not affect oligomer formation or function. Low order oligomers were found to be dynamic during the course of aggregation, by the use of isotopically labelled forms of the protein. Lastly the response of SH-SY5Y cells treated with alpha-synuclein oligomers with the ability to seed intracellular aggregation was investigated, demonstrating that this procedure evokes a stress response in these cells, highlighting a potential mode of action.

Together, investigations presented in this thesis have demonstrated the role of a constitutive co-translational modification in ligand binding and oligomer assembly. Furthermore, the cellular stress response to treatment with these oligomers was also determined giving insights into disease progression. Results have highlighted the importance of using the biologically relevant form of a protein when performing *in vitro* experiments, validated the cellular effects of previously characterised alpha-synuclein oligomers when produced from N-terminally acetylated protein, and extended knowledge of the cellular response of the SH-SY5Y cell line to treatment with a specific class of oligomers.

ii. Candidates statement

I declare that no part of this thesis has been submitted in support of any other degree or qualification at this university or any other institute of learning. All the work presented in this thesis was undertaken by myself.

iii. Dissemination: Scientific Publications

Mason R., Paskins A., Dalton C., Smith D., Copper Binding and Subsequent Aggregation of α -Synuclein Are Modulated by N-Terminal Acetylation and Ablated by the H50Q Missense Mutation. (2016), *Biochemistry*, 55 (34) 4737-474

iv. Dissemination: Conference Presentations

65th ASMS Conference on Mass Spectrometry and Allied Topics 2017 (Indianapolis, USA), **Mason, R.** Dalton, C. Smith, D. *Investigating the dynamics and assembly of alpha-synuclein amyloid oligomers by ESI-IMS-MS* - Poster presentation.

BMSS Annual Meeting 2016 (Eastbourne, UK)/Parkinson's UK Research Conference 2016 (Leeds, UK), **Mason, R.** Dalton, C. Smith, D. *Copper binding and subsequent aggregation of alpha-synuclein is modulated by N-terminal acetylation and ablated by the H50Q mutation* - Poster presentation.

63rd ASMS Conference on Mass Spectrometry and Allied Topics 2015 (St Louis, USA), **Mason, R.** Dalton, C. Smith, D. *Effect of post-translational modifications on the metal binding and conformation of alpha-synuclein* - Poster presentation.

Table of Contents

<i>i. Abstract</i>	2
<i>ii. Candidates statement</i>	3
<i>iii. Dissemination: Scientific Publications</i>	4
<i>iv. Dissemination: Conference Presentations</i>	5
<i>vi. List of Tables</i>	12
<i>vii. List of Figures</i>	13
<i>viii. Abbreviations</i>	16
Chapter 1: General Introduction	18
1.1 Parkinson’s disease	19
1.1.1 Genetics of Parkinson’s disease.....	20
1.1.1.1 SNCA.....	22
1.1.1.2 LRRK2	23
1.1.1.3 DJ-1.....	24
1.1.1.4 PINK1/PRKN	24
1.1.2 Pathophysiology of Parkinson’s disease	25
1.2 Proteins	27
1.2.1 Intrinsically disordered proteins.....	30
1.2.2 Protein aggregation	30
1.3 Alpha-synuclein	32
1.3.1 Physiological role of alpha-synuclein.....	32
1.3.2 Alpha-synuclein structure.....	32
1.3.3 Alpha-synuclein aggregation	34
1.4 Mass spectrometry	35

1.4.1 Electrospray Ionisation	36
1.4.2 Overview of the Synapt G2 HDMS.....	43
1.4.3 Ion mobility spectrometry	46
1.4.3.1 Drift time ion mobility	47
1.4.3.2 Travelling wave ion mobility	49
1.4.4 ESI-IMS-MS of biological systems	53
1.4.4.1 ESI-IMS-MS of alpha-synuclein.....	55
1.4.4.1.1 Alpha-synuclein structure as determined by MS.....	56
1.4.4.1.2 Solution conditions	59
1.4.4.1.3 Ligand binding.....	60
1.4.4.1.4 Aggregation.....	61
1.5 Thesis overview	62
<i>Chapter 2: The effect of N-terminal acetylation and H50Q mutation on copper binding of alpha-synuclein</i>	<i>63</i>
2.1 Introduction	64
2.1.1 Environmental factors and PD.....	64
2.1.2 Metals in PD.....	64
2.1.3 The association between alpha-synuclein and metals	65
2.1.3.1 Alpha-synuclein mutations and metals.....	68
2.1.3.2 Alpha-synuclein modifications and metals	69
2.2 Aims and Objectives	71
2.3 Materials and Methods.....	73
2.3.1 Molecular biology of pET23a-ASYN expression plasmid	73
2.3.2 pACYCduet-naa20-naa25 plasmid purification.....	73
2.3.3 Site directed mutagenesis of pET23a-ASYN	74
2.3.4 Production of chemically competent cells	74
2.3.5 Transformation of competent cells	75

2.3.6 Agarose gel electrophoresis	76
2.3.7 Expression of recombinant proteins	77
2.3.8 Protein purification.....	77
2.3.9 SDS-PAGE.....	78
2.3.10 Sample preparation for mass spectrometry analysis	79
2.3.11 ESI-IMS-MS analysis.....	79
2.3.12 Thioflavin T (ThT) fluorescence	80
2.4 Results and discussion	82
2.4.1 Site directed mutagenesis of pET23a-ASYN	82
2.4.2 Co-transformation of BL21 (DE3) cells	83
2.4.3 Expression and purification of alpha-synuclein recombinant proteins	85
2.4.4 Mass spectrometry confirmation of successful protein production	85
2.4.5 ESI-IMS-MS analysis of recombinant alpha-synuclein reveals a disordered protein with two distinct populations.....	88
2.4.6 Ion mobility analysis of recombinant alpha-synuclein reveals multiple conformations present at each charge state	90
2.4.7 Investigating the effect of N-terminal acetylation and H50Q mutation on alpha-synuclein conformation by ESI-IMS-MS	93
2.4.8 Copper binding to alpha-synuclein is observed by ESI-MS.....	97
2.4.9 Copper binding to alpha-synuclein results in altered populations of conformations detectable by ESI-IMS-MS	100
2.4.10 Copper binding to alpha-synuclein increases the rate of protein aggregation	104
2.4.11 Copper binding to alpha-synuclein is altered by N-terminal acetylation and H50Q mutation	106
2.4.12 Addressing the effect of N-terminal acetylation and H50Q mutation on copper induced conformational change to alpha-synuclein	109
2.4.13 Addressing the effect of N-terminal acetylation and H50Q mutation on copper induced aggregation of alpha-synuclein by Thioflavin T fluorescence.....	112
2.5 Conclusions and future work.....	114

Chapter 3 – Investigating alpha-synuclein aggregation using ESI-MS and ESI-IMS-MS

..... **118**

3.1 Introduction 119

3.2 Aims and Objectives 122

3.3 Materials and Methods..... 124

3.3.1 Production of recombinant alpha-synuclein 124

3.3.2 Production of ¹⁵N labelled recombinant alpha-synuclein 124

3.3.3 Production of MS compatible Type C alpha-synuclein oligomers 124

3.3.4 Aggregation of alpha-synuclein 124

3.3.5 Mass spectrometry 125

3.3.6 Western blot..... 125

3.3.7 Dot blot procedure 125

3.3.8 Thioflavin T (ThT) fluorescence 126

3.4 Results and discussion 127

3.4.1 Low order oligomeric species of alpha-synuclein are detected in both the unmodified and acetylated protein immediately following reconstitution..... 127

3.4.2 Low order oligomeric species of alpha-synuclein are dynamic 130

3.4.3 Structurally comparable species of Type C alpha-synuclein oligomers are present in solutions prepared from both unmodified and acetylated protein..... 133

3.4.4 ESI-MS analysis of alpha-synuclein aggregation 136

3.4.5 Aggregates of alpha-synuclein are formed over the time course utilised for ESI-MS experiments..... 141

3.5 Conclusions and Future Work 144

Chapter 4 - Validation and further characterisation of the effect of alpha-synuclein

oligomers on SH-SY5Y cells..... 147

4.1 Introduction 148

4.1.1 Oligomeric species of alpha-synuclein have been proposed as the toxic form of the protein	148
4.1.1.1 Alpha-synuclein membrane disruption	149
4.1.1.2 Alpha-synuclein propagation	150
4.1.2 Oxidative stress is associated with PD	153
4.1.3 Cell culture models of PD	155
4.2 Aims and Objectives	157
4.3 Methods	158
4.3.1 Production of alpha-synuclein oligomers	158
4.3.2 Maintenance and cryopreservation of SH-SY5Y neuroblastoma cell line	158
4.3.3 CellTox™ Green Cytotoxicity Assay	159
4.3.4 Resazurin reduction assay	159
4.3.5 Immunocytochemistry	160
4.3.6 Preparation of conditioned media	161
4.3.7 Dot blotting	161
4.3.8 GSH/GSSG-Glo™ Assay	162
4.3.9 CellROX™ Green assay	163
4.3.10 Polysome profiling	163
4.3.10.1 Extract preparation	163
4.3.10.2 Preparation of sucrose density gradients	164
4.3.10.3 Sedimentation of extracts on polysome gradients	164
4.3.11 Statistical Analysis	165
4.4 Results and discussion	166
4.4.1 Type A oligomers produced from both unmodified and N-terminally acetylated alpha-synuclein reduce the viability of SH-SY5Y cells	166
4.4.2 Type C oligomers produced from both unmodified and N-terminally acetylated alpha-synuclein cause an increase in cytosolic alpha-synuclein aggregate formation in SH-SY5Y cells	168
4.4.3 Extracellular alpha-synuclein staining is observed in SH-SY5Y cells treated with Type C oligomers and can be detected in conditioned cell media	171

4.4.4 Type C oligomers evoke a stress response in SH-SY5Y cells	176
4.4.4.1 Treatment of SH-SY5Y cells with Type C oligomers results in an increase in ROS	177
4.4.4.2 Treatment of SH-SY5Y cells with Type C oligomers results in an altered GSH/GSSG ratio	179
4.4.4.3 Treatment of SH-SY5Y cells with Type C oligomers results in an altered monosome/polysome ratio	180
4.5 Conclusions and future work.....	183
<i>Chapter 5 - General discussion</i>	<i>189</i>
5.1 H50Q mutation of N-terminally acetylated alpha-synuclein results in a loss of the proteins ability to bind to copper.	191
5.2 N-terminal acetylation of alpha-synuclein was found to not alter the formation of oligomeric species or their function.....	192
5.3 Treatment of SH-SY5Y cells with Type C alpha-synuclein oligomers inducing a stress response.	193
5.4 Concluding remarks	194
<i>Appendix.....</i>	<i>196</i>
<i>Bibliography.....</i>	<i>215</i>

vi. List of Tables

<i>Table 1.1: Summary of monogenic alterations causative of familial PD</i>	21
<i>Table 1.2: Summary of key ESI-MS studies of alpha-synuclein</i>	56
<i>Table 2.1: Plasmids required to produce the various forms of recombinant alpha-synuclein.</i>	75
<i>Table 2.2: Composition of 12% SDS-PAGE gel.</i>	78
<i>Table 2.3: Theoretical vs experimental m/z at the +10 charge state ion of recombinant alpha-synuclein proteins.</i>	85
<i>Table 2.4: Lettering system of alpha-synuclein conformational families.</i>	91
<i>Table 2.5: The percentage population of protein at the +15 CSI in each conformational family, calculated from the area under the fitted curves shown in Appendix Figure 2.</i>	94
<i>Table 3.1: the ratio of monomer to dimer derived from the sum of the intensities of all monomer CSIs and all odd dimer CSIs following an aggregation time course</i>	137

vii. List of Figures

Figure 1.1: Example images of typical PD pathology.	26
Figure 1.2: Diagram of an amino acid.	27
Figure 1.3: Illustration of the various levels of protein structure.	28
Figure 1.4: Illustration of the possible species adopted by proteins during the aggregation process.	31
Figure 1.5: The structure of alpha-synuclein.	34
Figure 1.6: Schematic of electrospray ionisation.	40
Figure 1.7: Summary of electrospray ionization mechanisms.	41
Figure 1.8: Schematic of the Waters Synapt TM G2 HDMS instrument.	45
Figure 1.9: Schematic of ion mobility separation via a stacked-ring ion guide.	50
Figure 1.10: Example calibration curve of denatured standards of known Ω .	53
Figure 2.1: Illustration of proposed localisation of alpha-synuclein metal binding sites.	66
Figure 2.2: Illustration of IRP regulation of translation and stability of IRE-containing mRNAs.	67
Figure 2.3: Schematic of N-terminal acetylation.	70
Figure 2.4: Illustration of lag time calculation from ThT data.	81
Figure 2.5: Sequencing results of the mutated pET23a-ASYN plasmid.	82
Figure 2.6: 1% Agarose gel electrophoresis of plasmid DNA purified from transformed <i>E. coli</i> cells.	84
Figure 2.7: ESI-MS spectra of recombinant alpha-synuclein proteins.	87
Figure 2.8: Drift scope plot and corresponding ESI-MS spectra of unmodified, WT alpha-synuclein.	89
Figure 2.9: ATDs for each CSI of unmodified WT alpha-synuclein	92
Figure 2.10: Driftscope plot and overlaid mass spectrum of each of the four proteins.	95
Figure 2.11: Bar chart showing the percentage conformation of protein in each conformational family at each CSI.	96
Figure 2.12: Spectra of the +10 CSI of unmodified, WT alpha-synuclein alone and in the presence of equimolar Cu ²⁺ .	98
Figure 2.13: CSD of unmodified recombinant alpha-synuclein alone (bottom) and in the presence of equimolar Cu ²⁺ (top).	99
Figure 2.14: ATDs for each charge state ion of unmodified WT alpha-synuclein in the absence and presence of equimolar copper.	102

Figure 2.15: Bar chart showing the percentage conformation of apo (c) and copper bound (1 & 2) unmodified, WT alpha-synuclein in each conformational family at each CSI. _____	103
Figure 2.16: Copper induced aggregation of alpha-synuclein as monitored by Thioflavin T fluorescence. _____	105
Figure 2.17: Alpha-synuclein spectra in the absence and presence of equimolar Cu ²⁺ _____	108
Figure 2.18: Bar chart showing the percentage conformation of apo (c) and copper bound (1 & 2) unmodified and acetylated WT and H50Q alpha-synuclein in each conformational family at each CSI. _____	111
Figure 2.19: Copper induced aggregation of modified and mutated alpha-synuclein as monitored by Thioflavin T. _____	113
Figure 3.1: ESI-IMS-MS analysis of unmodified and acetylated alpha-synuclein. _____	129
Figure 3.2: ESI-MS analysis of unlabelled and nitrogen labelled alpha-synuclein. _____	132
Figure 3.3: ESI-IMS-MS analysis of unmodified and N-terminally acetylated alpha-synuclein Type C oligomers. _____	135
Figure 3.4: ESI-MS analysis of alpha-synuclein aggregation time course. _____	138
Figure 3.5: Western blot, dot blot and ThT evidence that alpha-synuclein is forming aggregates in the duration of time course experiments. _____	143
Figure 4.1: Braak staging of PD brain pathology. _____	152
Figure 4.2: Schematic of polysome profiling traces. _____	165
Figure 4.3: Cell viability assays of SH-SY5Y cells following 16 hour treatment with 10% (v/v) of various forms of unmodified and N-terminally acetylated alpha-synuclein. _____	167
Figure 4.4: Immunocytochemistry of SH-SY5Y cells treated for 16 hours with 10% (v/v) unmodified or N-terminally acetylated Type C oligomers. _____	170
Figure 4.5: ICC and cell viability of SH-SY5Y cells treated with 10% (v/v) Type C oligomers for 1, 16 and 30 hours. _____	173
Figure 4.6: Dot blot of conditioned media from SH-SY5Y cells treated for 16 hours with 10% (v/v) vehicle control, monomeric or Type C oligomeric alpha-synuclein. _____	175
Figure 4.7: CellROX Green oxidative stress assay of SH-SY5Y cells treated for 2 hours with 10% (v/v) vehicle control, positive control (Menadione), monomer or Type C oligomer. _____	178
Figure 4.8: Glutathione assay of SH-SY5Y cells treated for 2 hours with 10% (v/v) vehicle control, positive control (menadione) or Type C oligomers. _____	180

Figure 4.9: Polysome profiling of SH-SY5Y cells treated for 2 hours with 10% (v/v) vehicle control, positive control (menadione) or Type C oligomers. _____ 182

viii. Abbreviations

AA	Ammonium acetate
ATD	Arrival time distributions
AFM	Atomic force microscopy
AD	Autosomal dominant
AR	Autosomal recessive
CSF	Cerebral spinal fluid
CEM	Chain ejection model
CRM	Charged residue model
CSD	Charge state distribution
CSI	Charge state ion
Ω	Collisional cross sectional area
DTIMS	Drift time ion mobility spectrometry
Parkin	E3 ubiquitin-protein ligase parkin
ESI	Electrospray ionisation
EGCG	Epigallocatechin gallate
GWAS	Genome wide association studies
GSH	Glutathione (reduced)
GSSG	Glutathione (oxidised)
IDP	Intrinsically Disordered Protein
IEM	Ion evaporation model
IMS	Ion mobility spectrometry
IRE	Iron response element
IRP	Iron response protein
LRRK2	Leucine rich repeat kinase 2
LB	Lewy-body

MS	Mass spectrometry
<i>m/z</i>	Mass to charge ratio
MAO	Monoamine oxidase
NAT	N-acetyltransferase
NAC	Non-amyloid-beta component
NMR	Nuclear magnetic resonance
OS	Oxidative stress
PD	Parkinson's disease
PMSF	Phenylmethane sulfonyl fluoride
DJ-1	Protein/nucleic acid deglycase DJ-1
Pink1	Phosphate and tensin homolog-induced putative kinase 1
PBS	Phosphate buffered saline
RF	Radio frequency
ROS	Reactive oxygen species
SDS	Sodium dodecyl sulfate
SRIG	Stacked ring ion guides
SNPpc	Substantia nigra pars compacta
ThT	Thioflavin T
3D	Three dimensional
TOF	Time of flight
TWIMS	Travelling wave ion mobility spectrometry
TIC	Total Ion Chromatogram
TH	Tyrosine Hydroxylase
WT	Wild type

Chapter 1: General Introduction

1.1 Parkinson's disease

Parkinson's disease (PD) is a progressive, neurological condition estimated to affect between 1 and 2 of the population per 1000 in industrialised countries (von Campenhausen *et al.*, 2005), meaning there are approximately 65000 - 130000 individuals in the UK with the condition. The three main symptoms of PD are tremor, slowness of movement (bradykinesia) and rigidity. A wide range of other physical and psychological symptoms are often experienced, including depression, anxiety, balance problems, loss of sense of smell, insomnia, problems with urination and constipation, erectile and sexual dysfunction, swallowing difficulties and memory problems (Schapira, Chaudhuri and Jenner, 2017).

The classical motor symptoms of PD are caused by a loss of dopaminergic neurons in the brain, leading to a reduction in dopamine levels. Motor difficulties arise as dopamine plays a vital role in regulating movement through acting as a neurotransmitter. As PD progresses the severity of symptoms escalate, leading it to be increasingly difficult for sufferers to live independently. The primary risk factor of PD is age, with incidence rising to 1% for the over 60's (de Lau and Breteler, 2006) and 2.6% for those between 85 and 89 (de Rijk *et al.*, 2000). Consequently, PD will pose an increased social and economic burden on society in the UK, as the population ages.

Current treatments for PD aim to ease symptoms, maintaining quality of life for as long as possible. However, no new classes of drugs have been introduced within the last 30 years, and symptomatic treatment does not affect the progression of the disease. Medication is used to improve the main movement symptoms of PD by increasing levels of dopamine in the brain (reviewed by Connolly and Lang, 2014). The three main

types of medication commonly used are levodopa, dopamine agonists and monoamine oxidase-B inhibitors. Levodopa is absorbed by neurons, where it is converted into dopamine. Initially levodopa can have a significant positive effect on motor symptoms; however, its effects are gradually reduced as more neurons are lost to the disease, leaving fewer to absorb the levodopa. Dopamine agonists act as substitutes for dopamine in the brain and have a similar, but milder, effect compared to levodopa. Dopamine agonists can have a variety of undesirable side effects, such as hallucinations, confusion and the development of compulsive behaviours. Monoamine oxidase-B inhibitors increase dopamine by blocking the effect of monoamine oxidase-B, an enzyme which breaks down dopamine. This improves symptoms of PD, but to a lesser degree than levodopa. While these treatments can provide relief from some PD symptoms, they lose their effectiveness as the disease progresses, leaving sufferers further debilitated as neurodegeneration continues. Despite decades of research, the cause of the loss of the dopamine producing neurons is still unknown. Therefore, we currently have no treatments to alter the progression of the disease. As such, further research to increase understanding of the cellular and molecular aspects of the aetiology of PD are required in order to develop disease altering treatments.

1.1.1 Genetics of Parkinson's disease

While the aetiology of PD is currently unclear, the majority of cases are sporadic, occurring in people with no clear family history of the disease. These cases are thought to most likely be the result of a complex interplay of environmental and genetic factors (Wirdefeldt *et al.*, 2011). However, a small proportion of sufferers present with a family history of the disease, with familial instances accounting for approximately 5-10% of total cases (Lesage and Brice, 2009). Genetic alterations found in these families

have given insights into the proteins and cellular pathways which may underlie the disease.

Familial PD can be caused by alterations in several genes, with the most significant monogenic causes being highly penetrant mutations in *SNCA*, *LRRK2*, *DJ-1*, *PINK1* and *PRKN*, as summarised in Table 1.1. An overarching theme of the function of these genes is that they are linked to either the protein degradation system, which when disrupted leads to an accumulation of potentially toxic proteins, or to mitochondrial quality and function, impairment of which leads to an accumulation of free radicals and oxidative stress (OS).

Gene	Locus	Protein	Inheritance	Reference
SNCA	4q21-23	Alpha-synuclein	AD	(Polymeropoulos <i>et al.</i> , 1996)
LRRK2	12q12	Leucine rich repeat kinase 2	AD	(Paisán-Ruíz <i>et al.</i> , 2004)
DJ-1	1p36	Protein/nucleic acid deglycase DJ-1	AR	(Bonifati <i>et al.</i> , 2003)
PINK1	1p35-36	Phosphate and tensin homolog-induced putative kinase 1	AR	(Valente <i>et al.</i> , 2004)
PRKN	6q25.2-27	E3 ubiquitin-protein ligase parkin	AR	(Kitada <i>et al.</i> , 1998)

Table 1.1: Summary of monogenic alterations causative of familial PD

The inheritance pattern of PD is dependent on the affected gene, with *SNCA* and *LRRK2* alterations being inherited in an autosomal dominant (AD) fashion and *DJ-1*, *PINK1* and *PRKN* having autosomal recessive (AR) inheritance. A summary of these genes and their association with PD is provided below.

1.1.1.1 *SNCA*

The first genetic link to PD occurred in 1996, when Polymeropoulos *et al.* discovered a locus at 4q21-q23 which was associated with AD PD in a large Italian family (Polymeropoulos *et al.*, 1996). Shortly after, the *SNCA* gene, encoding the protein alpha-synuclein, was mapped to this locus. Upon sequencing of the *SNCA* gene a mutation causing the substitution of an alanine at amino acid 53 with a threonine (A53T) was identified in this Italian family, in addition to three unrelated Greek families with high incidence of PD (Polymeropoulos *et al.*, 1997). Subsequently the A53T mutation, along with five other point mutations (A30P, E46K, H50Q, G51D, and A53E), has been identified in many families of varied origin from around the world (Krüger *et al.*, 1998; Zarranz *et al.*, 2004; Lesage *et al.*, 2013; Proukakis *et al.*, 2013; Pasanen *et al.*, 2014). Copy number variation of *SNCA* have also been found to be associated with PD (La Cognata *et al.*, 2017) displaying a dose-related phenotype, with severity of clinical presentation and disease progression correlating to *SNCA* dosage (Ross *et al.*, 2008).

In addition to the known, disease causing variants of alpha-synuclein, single nucleotide polymorphisms in the *SNCA* gene have consistently been found to be one of the main risk factors for sporadic PD by genome wide association studies (GWAS), with variants throughout the 5' region, 3' region and introns having a statistically significant effect on PD susceptibility (Loureiro, Campêlo and Silva, 2017). While the function of alpha-synuclein is not well characterised, studies have shown a role for the protein in the

regulation of neurotransmitter release through mediation of vesicular trafficking (Vargas *et al.*, 2014) and the maintenance of synaptic function and plasticity of dopaminergic neurons (Burré, 2015). Alpha-synuclein is the major constituent of Lewy-bodies (LBs), amyloid containing structures which are found in surviving cells in PD patients on post mortem (Spillantini *et al.*, 1997).

1.1.1.2 LRRK2

The first evidence that the *LRRK2* gene was associated with PD came in 2002, when a locus at 12p11.2-q13.1 was linked to autosomal dominant Parkinsonism in a Japanese family (Funayama *et al.*, 2002). In 2004 the *LRRK2* gene was mapped to this locus (Paisán-Ruíz *et al.*, 2004). *LRRK2* mutations are the most common known contributor to PD, estimated to account for between 1-5% of sporadic cases and 5-20% of familial cases worldwide (Correia Guedes *et al.*, 2010). Mutations in this gene display variable penetrance, depending largely on ethnicity (Ross *et al.*, 2010), and usually present as mid-to-late onset with slow disease progression. Single nucleotide polymorphisms in the *LRRK2* gene have also been consistently found as one of the main risk factors for sporadic PD by GWAS (Nalls *et al.*, 2014).

LRRK2 encodes for the highly conserved, multi-domain protein leucine rich repeat kinase 2 (LRRK2). Evidence suggests that LRRK2 plays an important role in the regulation of autophagy, vesicular trafficking and lysosome function (Roosen and Cookson, 2016). Many PD associated *LRRK2* mutations affect the protein's enzymatic core (Rudenko and Cookson, 2014), with pathogenic mutations leading to altered kinase activity (Liao *et al.*, 2014; Cookson, 2015). Mutations in *LRRK2* have also been linked to mitochondrial impairment, resulting in a loss of mitochondrial function in neuronal cells and an increase in OS (Sanders *et al.*, 2014).

1.1.1.3 DJ-1

In 2003 it was discovered that mutations in *DJ-1*, encoding protein/nucleic acid deglycase DJ-1 (DJ-1), were associated with early onset, AR PD (Bonifati *et al.*, 2003). DJ-1 has been associated with a number of cellular processes and is most widely accepted as having a role in the protection of neuronal cells from OS (Cookson, 2012). Mutations in the DJ-1 protein cause a loss of its protective properties against OS and DJ-1 knockout increases the vulnerability of cells to oxidative insult (Goldberg *et al.*, 2005).

1.1.1.4 PINK1/PRKN

In 1998 mutations in the *PRKN* gene were identified in a Japanese family with AR juvenile Parkinsonism (Kitada *et al.*, 1998). Mutations in *PRKN* have since been identified in patients of many ethnicities, and are the most common cause of familial, early onset PD (Schulte and Gasser, 2011). *PRKN* encodes the E3 ubiquitin-protein ligase parkin (parkin) which plays a role in the proteasome degradation system through the ubiquitination of proteins, targeting them for degradation. PD associated parkin mutations result in a loss of E3 ligase function and subsequent toxic accumulation of proteins which cannot be degraded by the parkin dependent ubiquitin/proteasome pathway (Shimura *et al.*, 2000).

In 2004 mutations in the *PINK1* gene were identified in an Italian family with AR, early onset PD (Valente *et al.*, 2004). *PINK1* encodes the phosphate and tensin homolog-induced putative kinase 1 (PINK1), which is believed to work together in a common pathway with parkin to regulate mitochondrial quality control. PINK1 accumulates on the outer membrane of damaged mitochondria, recruiting and activating parkin, which

ubiquitinates proteins on the outer membrane of the mitochondria, triggering autophagy (Pickrell and Youle, 2015).

In addition to the five well characterised PD causative genes described here, polymorphic variants in many additional genes have been linked to PD susceptibility, with GWAS highlighting new associations as more studies are carried out. A recent meta-analysis of GWAS identified 41 risk loci for PD, many of which encoded genes involved in lysosomal biology, mitochondrial biology and autophagy (Chang *et al.*, 2017). Overall, mutations associated with PD mainly appear to disrupt the protein degradation system or affect mitochondrial quality and function. The genetics of PD is complex but has contributed to understanding of the pathogenesis of the disease, which may by extension ultimately be leveraged for therapeutic benefit.

1.1.2 Pathophysiology of Parkinson's disease

While external examination of the PD brain is typically unremarkable, two major neuropathological findings are most commonly found (Mackenzie, 2001). The first is a loss of pigmented dopaminergic neurons in the substantia nigra pars compacta (SNpc), found upon examination of brain sections, an example of which is shown in Figure 1.1 (a). It is thought that around 50% of nigral neurons are lost before the motor symptoms of PD begin to appear, and on autopsy a loss of over 80% is typically seen (Hartmann, 2004). The significant loss of neuromelanin-pigmented neurons in the SNpc, and subsequent dopamine deficit in the nigrostriatal system, represent the most important hallmark of PD, leading to the major motor symptoms observed in patients.

The second major neuropathological finding in PD is the presence of LBs, metal rich proteinaceous inclusions found in surviving neurons which are comprised mainly of

alpha-synuclein in the form of amyloid fibrils (Spillantini *et al.*, 1997). A variety of other proteins are detectable in LBs, most notably ubiquitin, neurofilament protein, heat shock proteins and tau (Goedert *et al.*, 2012). The presence of ubiquitin is indicative of LBs representing a structural manifestation of a protective cellular response. Classical LBs are spherical, intracytoplasmic neuronal inclusions with a typical diameter between 8 μm and 30 μm . Upon H&E staining they have an eosinophilic hyaline core and a pale peripheral halo, as shown in Figure 1.1 (b).

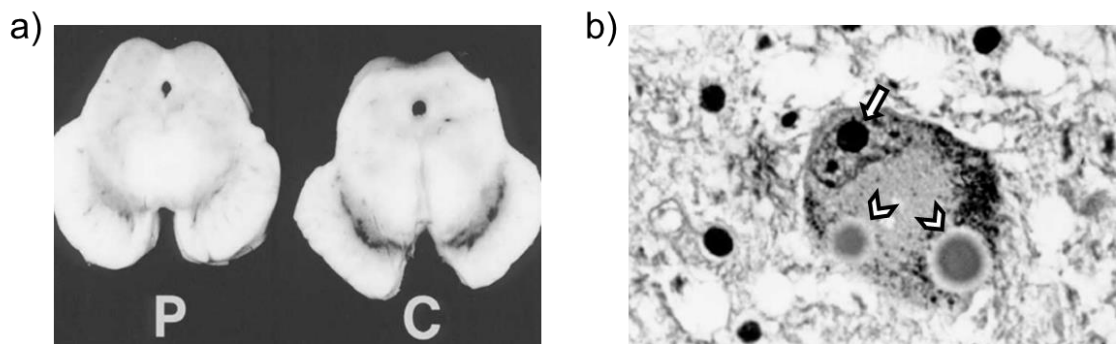


Figure 1.1: Example images of typical PD pathology. Shown in (a) is horizontal sections of midbrain from a patient with PD (P) and a normal control (C), where a loss of pigmentation in the SN in PD can be seen. Shown in (b) is H&E staining of a pigmented neuron from a PD patient (nucleus highlighted with an arrow), containing two Lewy bodies, highlighted with arrowheads. Image adapted from Mackenzie (2001).

The presence of alpha-synuclein in LBs has warranted significant attention, particularly as the protein is strongly linked to PD through genetic evidence, as described in Section 1.1.1.1. Therefore, both genetic and pathological evidence point towards alpha-synuclein playing a key role in the pathogenesis of PD. Research into alpha-synuclein has been an extremely active field over the past 20 years and investigations of this protein are the focus of this thesis.

1.2 Proteins

Proteins constitute the major building blocks of the cell, being fundamental components of almost every function involved in life. Proteins are biological polymers of amino acids linked by an amide bond. Amino acids are small, organic molecules consisting of an amino group (-NH₂), a carboxyl group (-COOH), a hydrogen atom and a variable R group, as shown in Figure 1.2. It is this variable R group which defines the properties of an amino acid. Proteins have innumerable cellular functions, and typically adopt a unique structure which determines this function. There are four levels of protein structure, as shown in Figure 1.3.

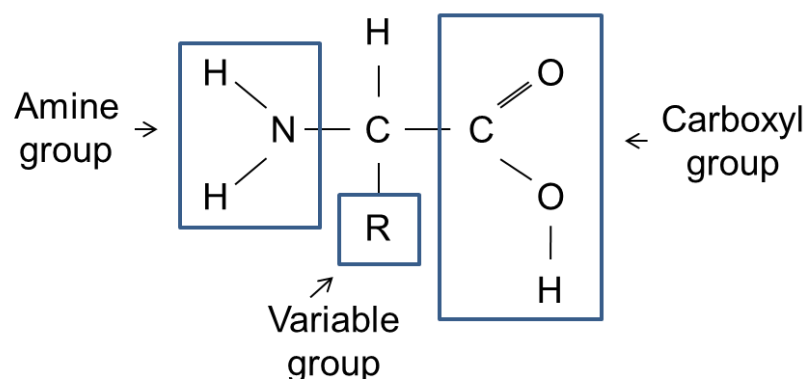


Figure 1.2: Diagram of an amino acid. The common structure of amino acids, consisting of an amino group, a carboxyl group, a hydrogen atom and a variable R group.

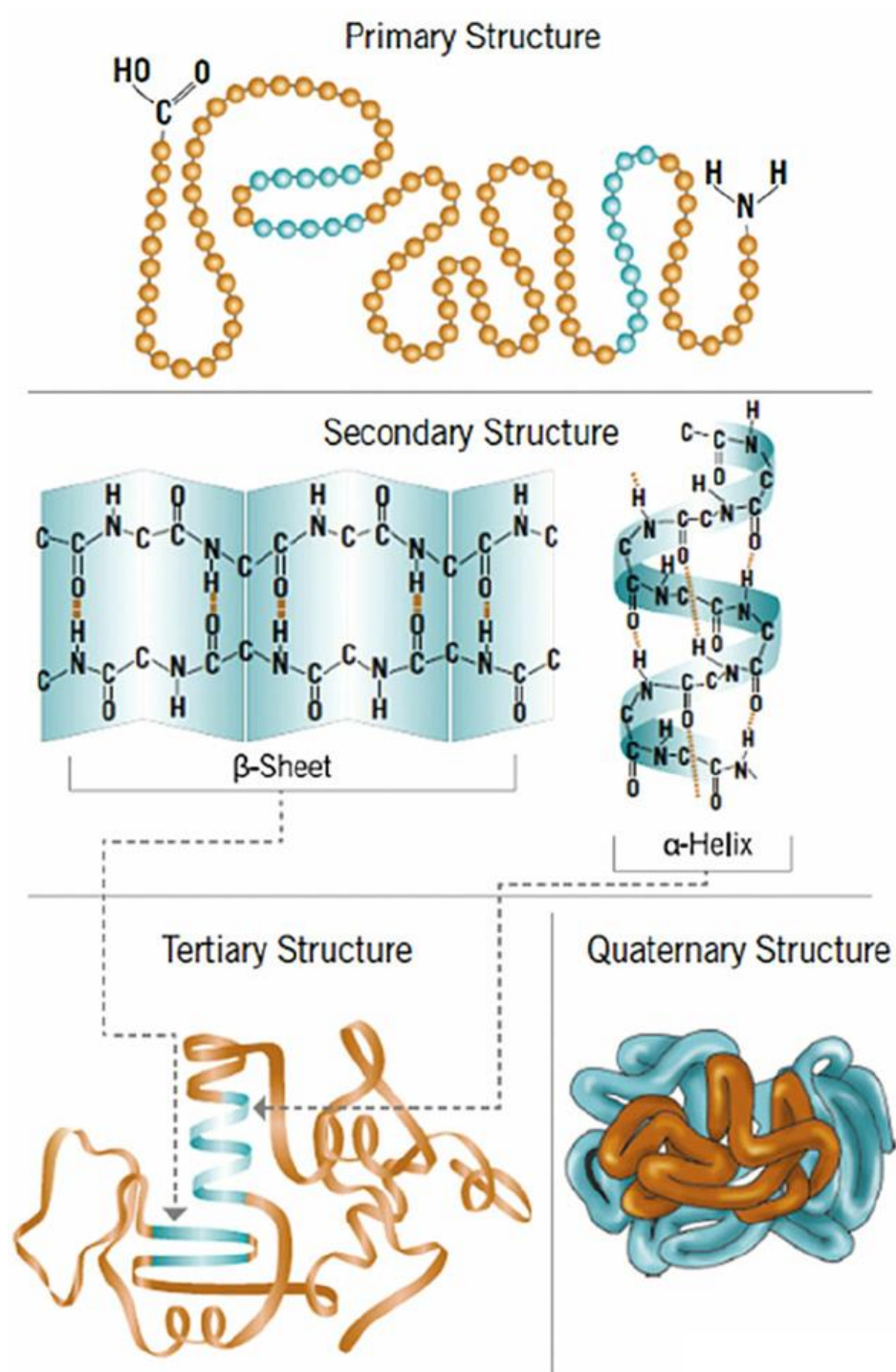


Figure 1.3. Illustration of the various levels of protein structure. Adapted from (Wijaya, Wijaya and Mehta, 2015).

Primary structure refers to the order of amino acids which make up the polypeptide chain of a protein. It is this sequence of amino acids which determines a protein's ultimate structure, with the variable R groups of the amino acids interacting and forming non-covalent bonds. Secondary structure refers to stretches of proteins adopting distinct, characteristic local conformations dependent on hydrogen bonding, with the two main types being α -helices and β -sheets. Tertiary structure refers to the three dimensional (3D) arrangement of these local structural conformations, with the protein adopting a conformation to achieve maximum stability or lowest energy state. In a protein made up of multiple polypeptide chains, quaternary structure is the 3D arrangement of these protein subunits. Most proteins require a complex folding process after they are synthesised to be able to acquire their correct tertiary or quaternary structure. Proteostasis, the management of this folding procedure, comprises a quality control network of hundreds of proteins (Hartl, Bracher and Hayer-Hartl, 2011). If this process becomes impaired, protein folding is compromised, which can lead to abnormal aggregation or mislocalisation of proteins (Schneider and Bertolotti, 2015).

1.2.1 Intrinsically disordered proteins

Challenging the traditional model that protein structure governs its function, many biologically active proteins possess substantial regions lacking a stable secondary structure, which are termed Intrinsically Disordered Proteins (IDPs). Alpha-synuclein is an example of such a protein. Despite lacking significant secondary structure, IDPs have been shown to be involved in many biological functions (Uversky, 2011) such as cell signalling (Iakoucheva *et al.*, 2002) and transcription (Minezaki *et al.*, 2006), often gaining structure on the binding of ligands. IDPs typically contain a low proportion of hydrophobic and order promoting amino acids, and a high proportion of charged and disorder promoting amino acids (Dyson, 2016; Uversky, 2016), leading to flexible and highly heterogenic conformations. Numerous IDPs have been implicated in disease, such as p53 in cancer, amyloid beta in Alzheimer's disease and alpha-synuclein in Parkinson's disease (reviewed by Babu, 2016).

1.2.2 Protein aggregation

Protein aggregation is a common feature in nature, with functional amyloids playing important roles in processes such as structure and protection, cell-cell recognition and epigenetic inheritance (Pham, Kwan and Sunde, 2014). However, the misfolding and subsequent aggregation of proteins is known to be implicated in the pathogenesis of many disease states, termed protein misfolding diseases.

A common feature of protein misfolding diseases is the presence of amyloid fibrils found deposited in various organs and tissues. Amyloid fibrils are protein aggregates, formed from normally soluble proteins which assemble to form insoluble fibers which are resistant to degradation. Despite being made from various different proteins,

amyloid fibrils share many characteristics, including a common structure, a typical X-ray diffraction pattern and common histological characteristics. The common structure of amyloid fibrils consists of a regular cross beta structure, with beta sheets stacked parallel to the fibril axis. The fibrils are unbranching assemblies, many μm in length and typically 5 - 15 nm wide under electron microscopy (Toyama and Weissman, 2011). A variety of possible protein species can be populated during the aggregation pathway, as described in Figure 1.4.

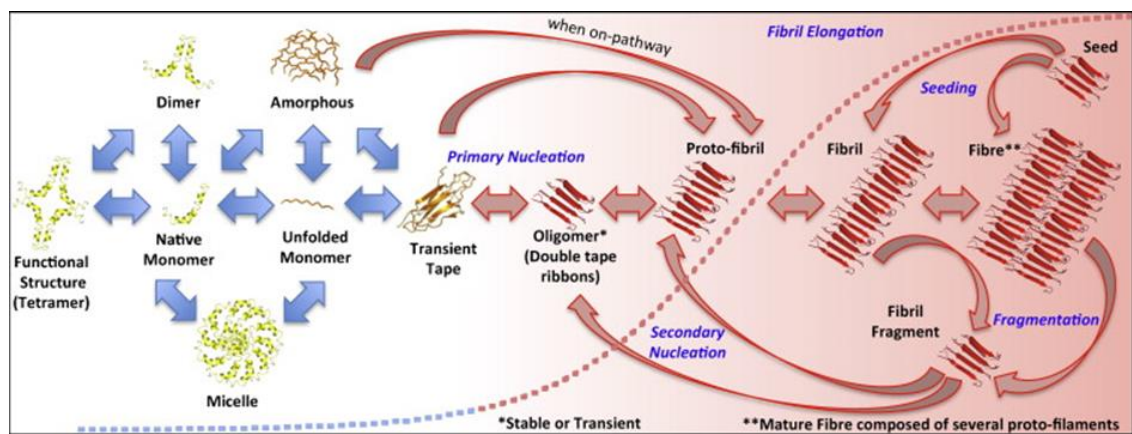


Figure 1.4: Illustration of the possible species adopted by proteins during the aggregation process. Image taken from (Invernizzi *et al.*, 2012).

Many neurodegenerative diseases are associated with abnormal protein aggregation and the proteins implicated in such disease states are frequently IDPs. Understanding the aggregation process of proteins implicated in these diseases is an important area of research, in order to facilitate the design of therapeutics capable of disrupting the aggregation process. However, the precise mechanisms by which aggregation occurs and triggers disease remain largely unknown (Eisele *et al.*, 2015).

1.3 Alpha-synuclein

1.3.1 Physiological role of alpha-synuclein

Alpha-synuclein is a highly abundant protein in the brain. Accounting for approximately 1% of total protein in neuronal cells (Mizuno *et al.*, 2012), alpha-synuclein is mainly localised to the presynaptic terminals of neurons (Iwai *et al.*, 1995). While the precise physiological function of alpha-synuclein is largely unknown, it is believed to contribute to activity at the synapse (reviewed by Burré, 2015). Specifically, it is thought to be involved in the regulation of neurotransmission through participation in vesicular trafficking and neurotransmitter release (Clayton and George, 1998), and has been demonstrated to interact with various components of the SNARE complex (Burré *et al.*, 2010). In addition to being abundant in the brain, alpha-synuclein is found in many other tissues, including the skin (Rodríguez-Leyva *et al.*, 2014), heart (Iwanaga *et al.*, 1999) and gastrointestinal tract (Shannon *et al.*, 2012), suggesting its function may be more varied than purely the regulation of neurotransmission. Animal and cellular models have implicated a possible involvement of alpha-synuclein in many biological functions, including dopamine biosynthesis (Perez *et al.*, 2002), metal binding (Tavassoly *et al.*, 2014), mitochondrial function (Pozo Devoto and Falzone, 2017) and microtubule organisation (Cartelli *et al.*, 2016).

1.3.2 Alpha-synuclein structure

Structurally, alpha-synuclein is generally agreed to be an intrinsically disordered, negatively charged protein comprised of 140 amino acids. However, in recent years alpha-helical tetrameric forms of the protein have been reported (Bartels, Choi and Selkoe, 2011; Wang *et al.*, 2011). However this theory remains to be confirmed, as

other groups report an intrinsically disordered structure when the protein is purified under similar conditions (Fauvet *et al.*, 2012). In addition, in-cell nuclear magnetic resonance spectroscopy (NMR) has shown the protein remains in an intrinsically disordered state when introduced to the cell by electroporation (Theillet *et al.*, 2016).

Alpha-synuclein can be split into three main regions as shown in Figure 1.5; the N-terminal region (amino acids 1-65), the central region (amino acids 66-95) and the C-terminal region (amino-acids 96-140). The N-terminal region contains seven series of 11 amino acid imperfect repeats, with a conserved KTKEGV hexameric motif, which is similar to repeats found in the alpha-helical domain of apolipoproteins (George *et al.*, 1995). This region of alpha-synuclein is known to be able to bind to lipids, forming amphipathic alpha-helices (Bussell and Eliezer, 2003). The alpha-helical form of alpha-synuclein has been found to have a reduced tendency to aggregate *in vitro* (Zhu and Fink, 2003) and these repeats have been linked to inhibition of this protein adopting a beta-sheet structure (Kessler, Rochet and Lansbury, 2003). Interestingly, all six of the familial alpha-synuclein mutations (A30P, E46K, H50Q, G51D, A53T and A53E) reside within this N-terminal region, and it has been suggested that the KTKEGV motif plays an important role in maintaining the intrinsically disordered structure of the protein (Sode *et al.*, 2007). The central region of alpha-synuclein contains the non-amyloid- β component (NAC) sequence between residues 71 and 82, which has been shown to be essential to the protein's aggregation (Giasson *et al.*, 2001). The C-terminal region is largely unfolded and rich in acidic residues, giving the protein its overall negative charge. This region of the protein is known to be important in the inhibition of alpha-synuclein assembly through interfering with molecular interactions of the NAC region (Murray *et al.*, 2003). The C terminus of the protein contains the most common post-

translational modification site of the protein; the phosphorylation of the serine residue at position 129. This modification is highly associated with PD, with approximately 90% of the alpha-synuclein found in LBs being phosphorylated at this site compared to approximately 4% which is found to be phosphorylated within the cytosol (Walker *et al.*, 2013).

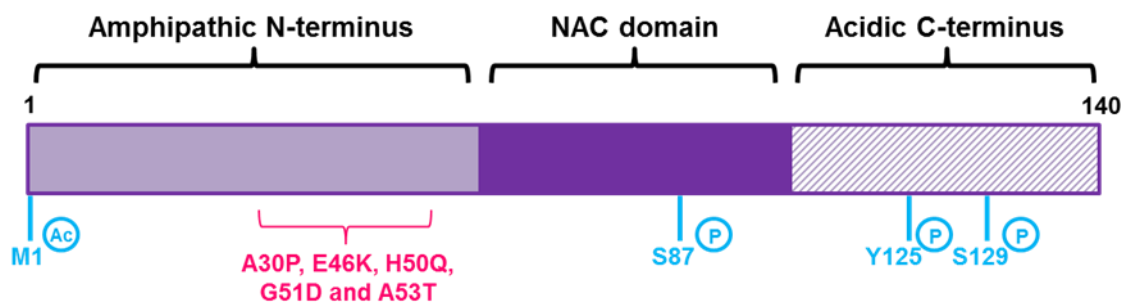


Figure 1.5: The structure of alpha-synuclein. Alpha-synuclein is a 140-residue protein comprised of three distinct regions; the highly conserved N-terminus, containing a series of imperfect KTKEGV repeats involved in lipid binding, the central non amyloid- β component (NAC) which is essential for the protein's aggregation, and the largely unfolded, negatively charged C-terminus. Known familial mutations are shown in pink and acetylation/phosphorylation sites are shown in blue.

1.3.3 Alpha-synuclein aggregation

Alpha-synuclein is thought to be natively unfolded at neutral pH due to its low intrinsic hydrophobicity and high net negative charge, evidence for which has been provided by a number of techniques including far-UV circular dichroism and NMR (Eliezer *et al.*, 2001). However, there has been debate regarding its *in vivo* conformational state as described above, with some believing the physiological form of the protein to be the tetramer. What is clear is that the highly ordered fibrillar form of alpha-synuclein

found in LBs is not the normal state of the protein in healthy individuals. However, the exact mechanism of alpha-synuclein aggregation is still uncertain, and currently it is not known whether the aggregation of the protein is a cause or a consequence of PD.

It is thought that alpha-synuclein is involved in PD through misfolding of the usually disordered monomer into highly structured, beta-sheet rich amyloid fibrils via a population of potentially transient toxic soluble oligomers and protofibrils (discussed in detail in Section 4.1.1). The formation of these oligomers is preceded by the collapse of extended forms of the protein into a partially folded intermediate (Uversky, Li and Fink, 2001a). Further fibrillation of alpha-synuclein is a nucleation dependent process (Conway, Harper and Lansbury, 2000), where the disordered monomer first assembles into soluble oligomers during an initial lag phase until a nucleus is formed. Aggregates then form rapidly around this nucleus during an elongation phase, until a thermodynamic equilibrium between fibrillar aggregates and monomer is established. The familial PD mutations have been shown to alter alpha-synuclein oligomerisation and subsequent aggregation (Winner *et al.*, 2011), demonstrating a probable role for alpha-synuclein misfolding and aggregation in PD. Ligand binding has also been demonstrated to effect alpha-synuclein aggregation, with binding of some compounds such as divalent metal cations (Han, Choi and Kim, 2018) and biological polyamines (Krasnoslobodtsev *et al.*, 2012) increasing aggregation, and others such as squalamine (Perni *et al.*, 2017) and curcumin (Herva *et al.*, 2014) decreasing aggregation.

1.4 Mass spectrometry

Mass spectrometry (MS) is a powerful analytical technique used to identify the molecular mass and relative abundance of ions within a sample and is particularly

suites to the study of diverse and transient non-covalent complexes such as amyloid oligomers. Mass spectrometers consist of three fundamental components; an ionisation source, analyser and detector. Samples are introduced into the mass spectrometer via an ionisation source, which generates gas phase ions from the analyte. Ions are then separated by one or more mass analysers, based on their mass (m) to charge (z) ratios (m/z). The separated ions then reach a detector which measures the relative abundance of each ion of a particular m/z , converting it to an electrical signal and presenting this information in the form of a mass spectrum.

Many different configurations of mass spectrometers are commercially available, with diverse combinations of ionisation source, mass analysers and detectors. MS data presented in this thesis were predominantly obtained on a Waters SynaptTM G2 HDMS instrument (Waters Corporation, Wilmslow, Manchester, UK), using a TriVersa NanoMate electrospray ionisation (ESI) source (Advion, Ithaca, USA). The ESI process is described in detail below.

1.4.1 Electrospray Ionisation

ESI is an atmospheric pressure ionisation technique, well suited to the analysis of polar molecules of a wide range of molecular mass. It is a soft ionisation technique, meaning a sample is ionised by the addition or removal of a proton with little extra energy remaining. This allows the sample to be analysed with little or no fragmentation and, depending on the conditions used, can preserve sample conformation and non-covalent interactions (Gaskell, 2009). As such, ESI is one of the main ionisation methods used in the analysis of biomolecules. ESI commonly uses samples dissolved in a polar, volatile solvent such as ammonium acetate (AA). The sample passes through a fine needle to which a high voltage is applied. In positive ion mode (which is frequently

used for protein analysis, and used exclusively in this thesis) a positive voltage is applied to the needle and a negative voltage applied to the counter-electrode in the instrument. This leads to a build-up of protons at the tip of the needle. As a consequence of this strong electric field the sample emerging from the tip is dispersed into an aerosol of highly charged droplets, aided by introducing nitrogen as a nebulising gas flowing around the outside of the capillary. This flow of gas directs the Taylor cone towards the mass spectrometer. As the charged droplet travels towards the sample cone, evaporation of the solvent occurs. This results in a reduction of droplet size, which becomes unstable as it reaches its Raleigh limit, where the surface tension is balanced by Coulombic repulsion. At this stage the droplet undergoes Coulombic explosion, resulting in many smaller, more stable droplets which in turn undergo desolvation and consequently more Coulombic explosion events.

NanoElectroSpray Ionisation (nESI) is a variant of conventional ESI developed by Wilm and Mann (Wilm and Mann, 1994) where needle tip openings of only a few μm are used rather than the $\sim 100 \mu\text{m}$ openings seen in conventional ESI. In nESI a reduced flow rate is used ($< 10 \text{ nL}$ per minute versus $\sim 1\text{-}10 \mu\text{L}$ per minute typically utilised in conventional ESI), resulting in lower sample consumption. nESI is a softer ionisation mechanism than conventional ESI, requiring lower capillary voltages and gas flows. The initial nESI droplet size is smaller than ESI and therefore droplets undergo fewer solvent evaporation and Coulombic explosion cycles prior to ion production. This soft ionisation mechanism makes nESI ideal for acquiring mass spectra of intact, noncovalent complexes. nESI also allows improvements in sensitivity and ionisation efficiency (Karas, Bahr and Dülcks, 2000; Konermann *et al.*, 2013).

Gas phase ions are formed when the ion is released from the droplet and the charge is transferred onto the analyte (Figure 1.6). It is believed that the exact mechanism through which an analyte is released from the droplet is dependent on the properties of the analyte. Three main models by which ions may be released from the charged droplet have been proposed; the ion evaporation model (IEM), the charged residue model (CRM) and the chain ejection model (CEM). In the IEM, low molecular weight charged species are emitted from nanometer-sized droplets, which have shrunk by evaporation until the field strength at the surface of the droplet is large enough for ions to be expelled (Nguyen and Fenn, 2007). In the CRM a solvent droplet containing a single analyte fully evaporates, with the residual charge being transferred to the analyte inside (Fernandez de la Mora, 2000). The most recently proposed model is the CEM, in which a disordered polymer is partially ejected from the droplet after migrating to the surface of the droplet due to the exposure of hydrophobic residues. This leads to protons attaching to the exposed portion of the ion, followed by further extrusion and ultimate ejection of the extended chain (Konermann *et al.*, 2013). Much of the current evidence suggests that folded proteins formed by ESI from buffered aqueous solution ionize by the CRM, small ions by the IEM, and unfolded, disordered proteins by the CEM (Donor *et al.*, 2017). A schematic illustrating these three models of ion formation by ESI is shown in Figure 1.7.

The ESI process gives rise to multiply charged protein ions, with the number of charges transferred onto an analyte being dependent on its accessible surface area and presence of ionisable functional groups. During acquisition a range of different charge states of the same protein may be observed, referred to as the proteins charge state distribution (CSD). The CSD is largely influenced by the folded state of the solution

phase protein. Folded proteins are known to display a narrow CSD with lower average charge, due to a limited number of charged residues on their surface. An unfolded protein will display a wide CSD with higher average charge, due to a higher number of charged ionisation sites being accessible (Vahidi, Stocks and Konermann, 2013).

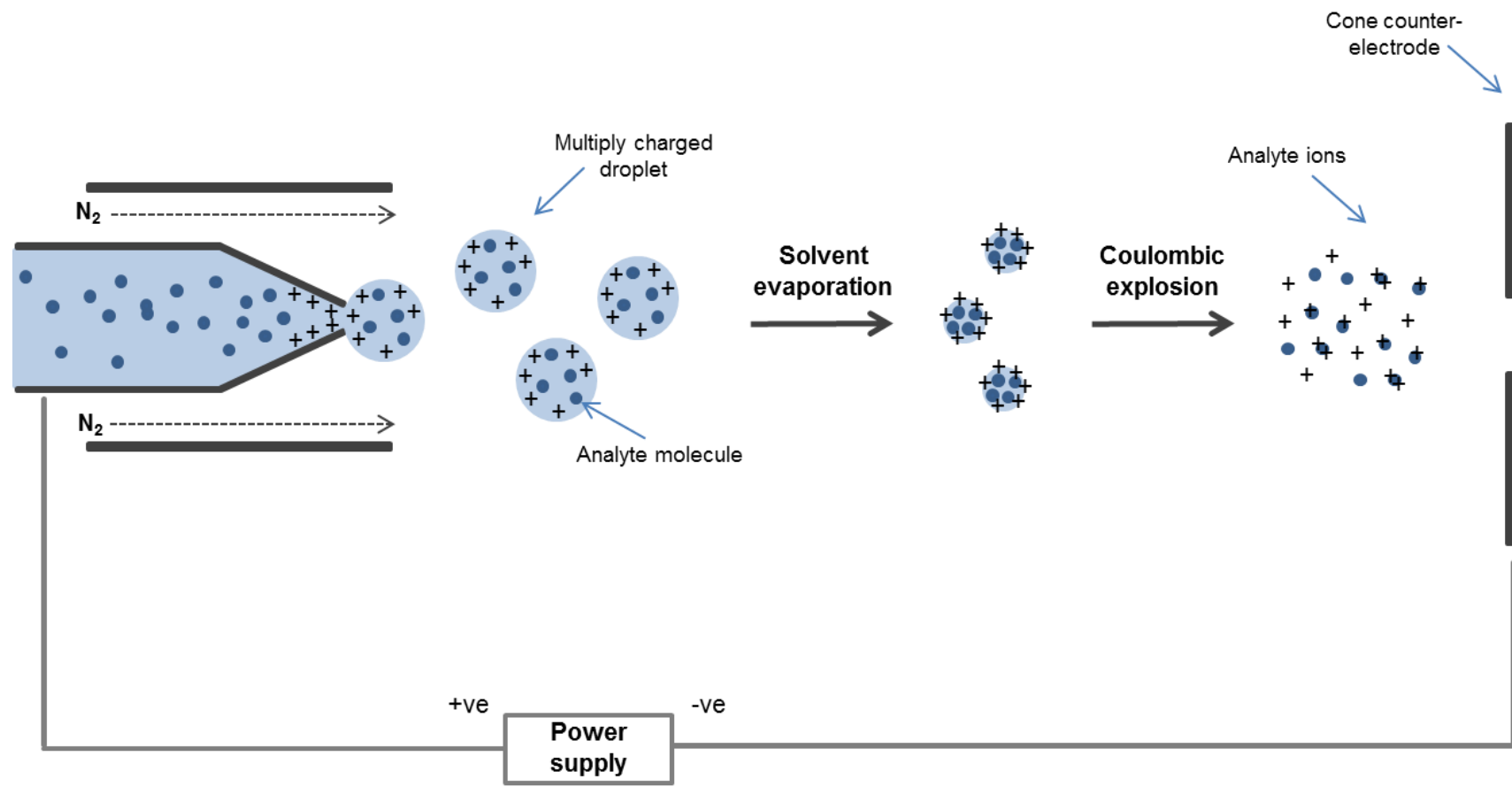


Figure 1.6: Schematic of electrospray ionisation. Multiply charged droplets are expelled from the needle. Solvent evaporation occurs followed by coulombic explosion, resulting in protonated analyte ions which enter the mass spectrometer in the gas phase.

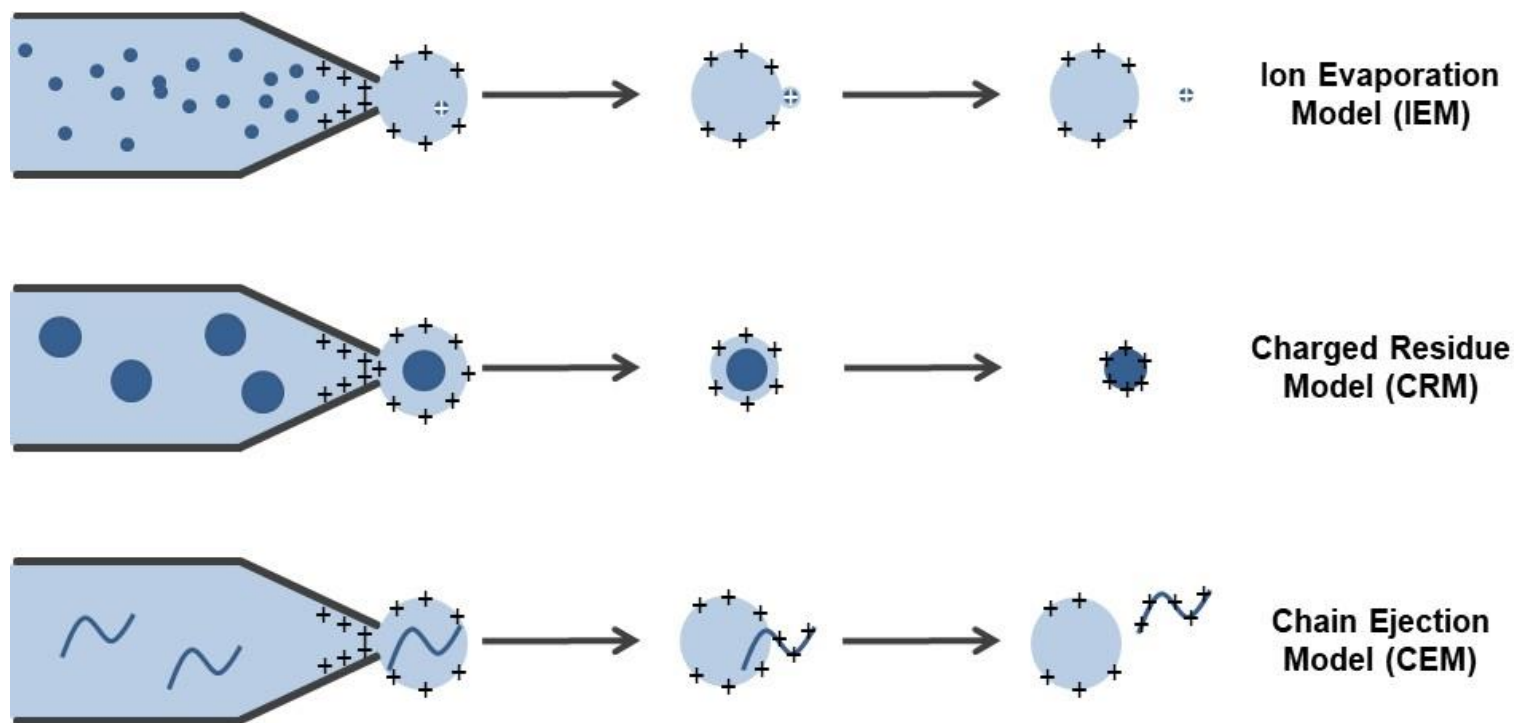


Figure 1.7: Summary of electro spray ionization mechanisms. Schematic of the three main proposed mechanisms of ESI. In the IEM small ions are emitted from droplets which have shrunk until the field strength at the surface is large enough for ions to be expelled. In the CRM a droplet containing a single analyte evaporates with the residual charge being transferred to the analyte. In the CEM a disordered polymer is partially ejected from the droplet where protons attach to the exposed portion, followed by further extrusion and ultimate ejection of the extended chain.

Based on the CRM, the number of charges that a protein will obtain can be estimated based on the mass of the protein when acquired from aqueous ammonium acetate at neutral pH (Peschke, Blades and Kebarle, 2002). The calculated charge can be estimated by the Rayleigh limit, with the size equivalent to the protein in question as follows.

$$z^R = 8\pi/e(\gamma\epsilon_0R^3)^{\frac{1}{2}}$$

Equation 1: Predicted charge calculation, where γ is the surface tension of the aqueous solution droplet, ϵ_0 is the empirical permittivity of the vacuum, e is the elementary charge and R is the radius of the droplet.

Making the assumption that the radius of the protein correlates to its mass, and its density is similar to water, a simplified equation can be created as shown below:

$$z^R = 0.078 M^{\frac{1}{2}}$$

Equation 2: Calculated charge of a protein (z^R), in which M is the Mass in Da.

Therefore an 18.4 kDa folded globular protein for example would be expected to have 11 charges and a 36.9 kDa globular dimer would accommodate 15 charges and a 72.7 kDa heptamer would possess 21 charges (Heck and Van Den Heuvel, 2004). If the 14 kDa alpha-synuclein monomer had a folded, globular conformation it would be expected to acquire 9 charges if ionised by the CEM.

1.4.2 Overview of the Synapt G2 HDMS

Following ionisation of the sample, resulting ions were analysed using a Synapt™ G2 HDMS on the basis of both their m/z values and their arrival time through a drift tube, from which collisional cross sectional area (Ω) was calculated. Figure 1.8 shows an overview of the transit of the ions through the Synapt™ G2 HDMS used within this thesis. Analyte ions in the gas phase first pass through the sample cone where they enter an intermediate vacuum region, and from here pass into the mass spectrometer, which is held under high vacuum to prevent ions being hindered by air molecules on their journey through the instrument. Ions travel through a stacked ring ion guide towards the quadrupole mass analyser, where ions of a certain m/z can be selected if required for tandem MS analysis. Ions subsequently enter the tri-wave region of the instrument, where ion mobility spectrometry (IMS) is carried out, allowing the detection of an ions arrival time, and subsequent calculation of Ω . The tri-wave region consists of three cells; the trap cell, IMS cell and transfer cell. Ions enter the trap cell, which is pressurised by argon, where pockets of ions are collected before entering the IMS cell. The IMS cell consists of a helium pressurised gate region where ions are pulsed into the nitrogen pressurised section of the IMS cell, where ion mobility separation occurs. The process of IMS is described in detail in Section 1.4.3. Ions then enter the argon pressurised transfer cell, where ions are collected before being pushed as packets of ions into the time-of-flight (TOF) mass analyser. TOF analysers are based on the principle that the time taken for an ion to travel a known distance under high vacuum is directly related to its m/z ratio. A reflectron at the end of the flight tube aids in the correction of the difference in kinetic energy distributions of ions of the same

m/z , reducing peak broadening and therefore increasing resolution (Wollnik and Przewloka, 1990).

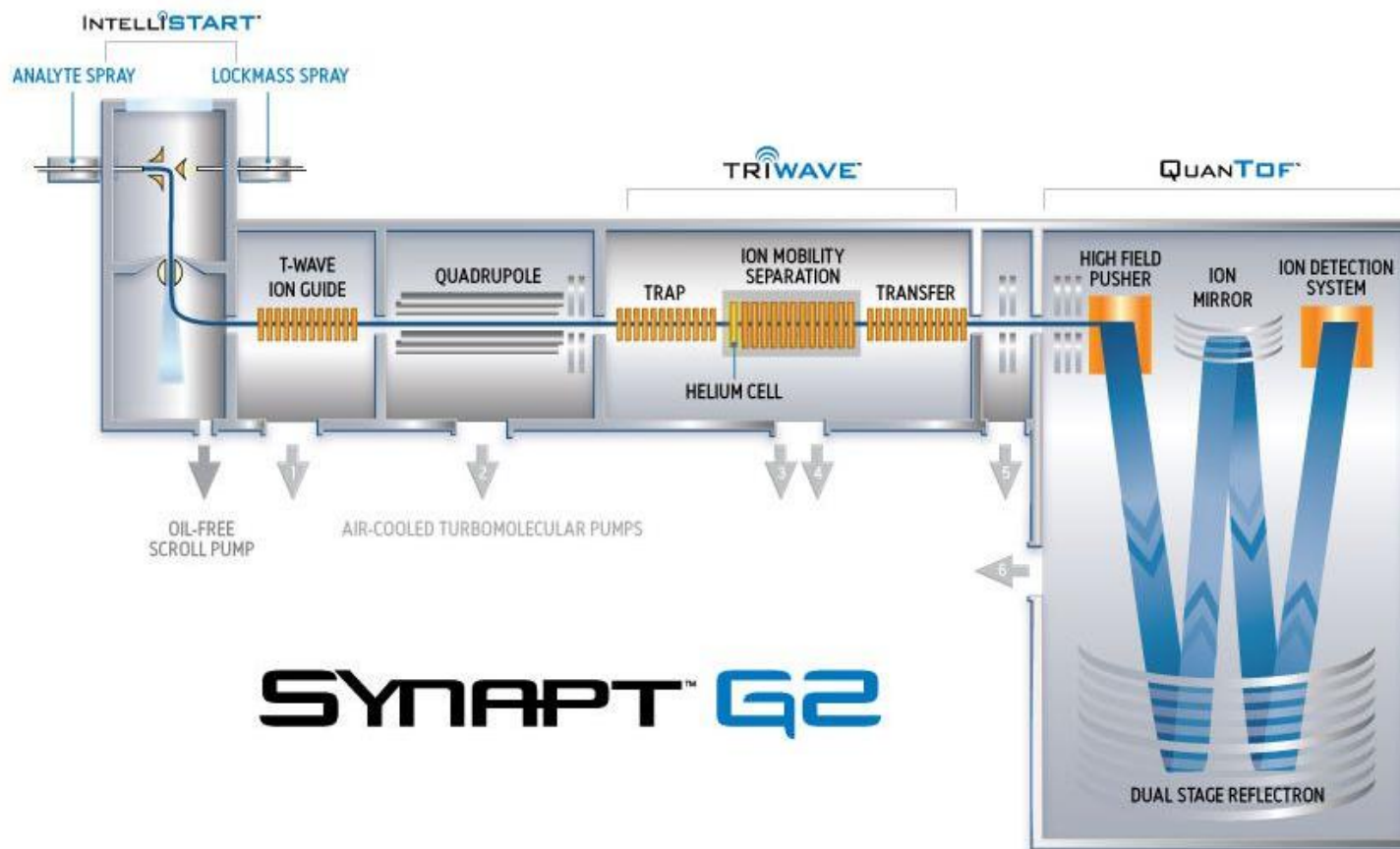


Figure 1.8: Schematic of the Waters Synapt™ G2 HDMS instrument. Image reproduced from The University of Warwick showing the main components of the Synapt G2 HDMS; the ionisation source, the quadrupole mass analyser, the triwave ion mobility separation region and the QuantTOF mass analyser.

1.4.3 Ion mobility spectrometry

IMS is a widely used technique which separates gas phase ions based on differences in their mobility through a buffer gas under a weak electric field. Mobility is quantified as the time taken for an ion to traverse through a drift tube of a given length. The time an ion will take is dependent on its charge, mass and conformation. IMS provides structural information in the form of calculated rotationally averaged Ω , providing a valuable structural biology tool for characterising co-populated protein conformations under varying conditions. The Ω of an ion is a calculation of the momentum transfer of its average area as it tumbles through a gas, and is typically measured in Angstroms squared (\AA^2). Ω is related to the chemical structure (mass and size) and three-dimensional conformation (or shape) of an ion. Ω is not an intrinsic property of an analyte, as measured Ω is additionally dependent on the identity of drift gas used, experimental temperature and the electric field used during the measurements (May, Morris and McLean, 2017).

Coupled to MS, IMS is capable of separating isobaric species in complex samples, enabling structural information about a given ion to be gained often in comparison to model structures whose Ω has been determined *in silico*. IMS is able to distinguish isobaric species as the mobility of an ion is dependent on its conformation (in addition to its m and z). If two given ions have identical m and z , but different conformations, the ion with the smaller Ω will traverse the length of a drift tube more rapidly than the ion with larger Ω . This occurs as the larger ion is slowed due to increased collisions with the buffer gas (Cumeras *et al.*, 2015).

1.4.3.1 Drift time ion mobility

There are two main types of drift tubes commonly used for IMS of proteins, traditional drift time ion mobility (DTIMS) and travelling wave ion mobility (TWIMS). DTIMS measures the time taken for an ion to traverse through a drift tube filled with a buffer gas (typically nitrogen or helium), in the presence of a uniform electric field. Ω can be directly measured from DTIMS using the Mason-Schamp equation (Mason and Schamp, 1958), described below.

$$K = \frac{v_D}{E}$$

Equation 3

The mobility of a gas phase ion (K) is defined by its drift velocity (v_D) divided by the electric field (E). As the drift velocity (v_D) is related to the drift time (t_D) taken to traverse the length (L) of the drift tube, the mobility of an ion can be experimentally determined from its observed drift time as shown in Equation 4:

$$K = \frac{v_D}{E} = \frac{L}{t_D E}$$

Equation 4

As the density of the buffer gas influences the mobility of an ion, reduced mobility (K_0) is generally used, where P is the pressure of the buffer gas and T is the temperature of the buffer gas, which are normalised to a standard buffer gas pressure of 760 torr and temperature of 273.2K to provide a basis for comparison of results:

$$K_0 = K \times \frac{273.2}{T} \times \frac{P}{760}$$

$$= \frac{L}{t_D E} \times \frac{273.2}{T} \times \frac{P}{760}$$

Equation 5

Once the mobility of an ion (K) has been established, Ω can then be calculated using the following equation, where z is the number of charges on the analyte ion, e is the charge on an electron (1.6022×10^{-19} C), k_b is the Boltzmann constant, T is the temperature and N is the number density of the buffer gas and $\left[\frac{1}{m_I} + \frac{1}{m_N}\right]$ is the reciprocal of the reduced mass between the analyte ion (m_I) and the buffer gas (m_N):

$$K = \frac{(18\pi)^{\frac{1}{2}}}{16} \frac{ze}{(k_b T)^{\frac{1}{2}}} \left[\frac{1}{m_I} + \frac{1}{m_N}\right]^{\frac{1}{2}} \frac{1}{N} \frac{1}{\Omega}$$

Equation 6

Substituting the definition for K in terms of K_0 and rearranging the equation to make Ω the subject describes the proportionality between Ω and average drift time (t_D):

$$\Omega = \frac{(18\pi)^{\frac{1}{2}}}{16} \frac{ze}{(k_b T)^{\frac{1}{2}}} \left[\frac{1}{m_I} + \frac{1}{m_N}\right]^{\frac{1}{2}} \frac{760}{P} \frac{T}{273.2} \frac{1}{N} \frac{t_D E}{L}$$

Equation 7

From this equation the Ω of an ion can be determined by recording its drift time through a buffer gas filled conventional ion mobility cell at a range of electric fields.

1.4.3.2 Travelling wave ion mobility

Ion mobility data presented in this thesis was acquired by TWIMS. This technique is similar to DTIMS, but rather than the ions being under the influence of a constant, uniform electric field they are subject to a voltage pulse, creating a travelling wave of electric potential that varies with both time and the length of the mobility device. The drift tube of the TWIMS cell in the SynaptTM G2 HDMS is composed of a series of stacked ring ion guides (SRIG) which carry opposite radio frequency (RF) voltages on adjacent rings, providing a radially confining potential barrier for the ions. Ion mobility separation occurs due to the combination of a SRIG with a travelling voltage wave superimposed on the confining RF voltage, causing ions to roll over the top of the travelling waves as they traverse the cell, with lower mobility ions rolling over more times than the higher mobility ions, giving a longer drift time, as illustrated in Figure 1.9 (Giles *et al.*, 2004). Unlike DTIMS, it is not possible to directly measure Ω from TWIMS as the traveling-wave transport of ions is not well characterised. Although the arrival time obtained from a TWIMS device cannot be used to directly derive Ω , it can be accurately estimated through calibration of the T wave against standards of known Ω , protocols for which have been described in detail by a number of groups (Ruotolo *et al.*, 2008; Smith *et al.*, 2009; Thalassinos *et al.*, 2009; Bush *et al.*, 2010).

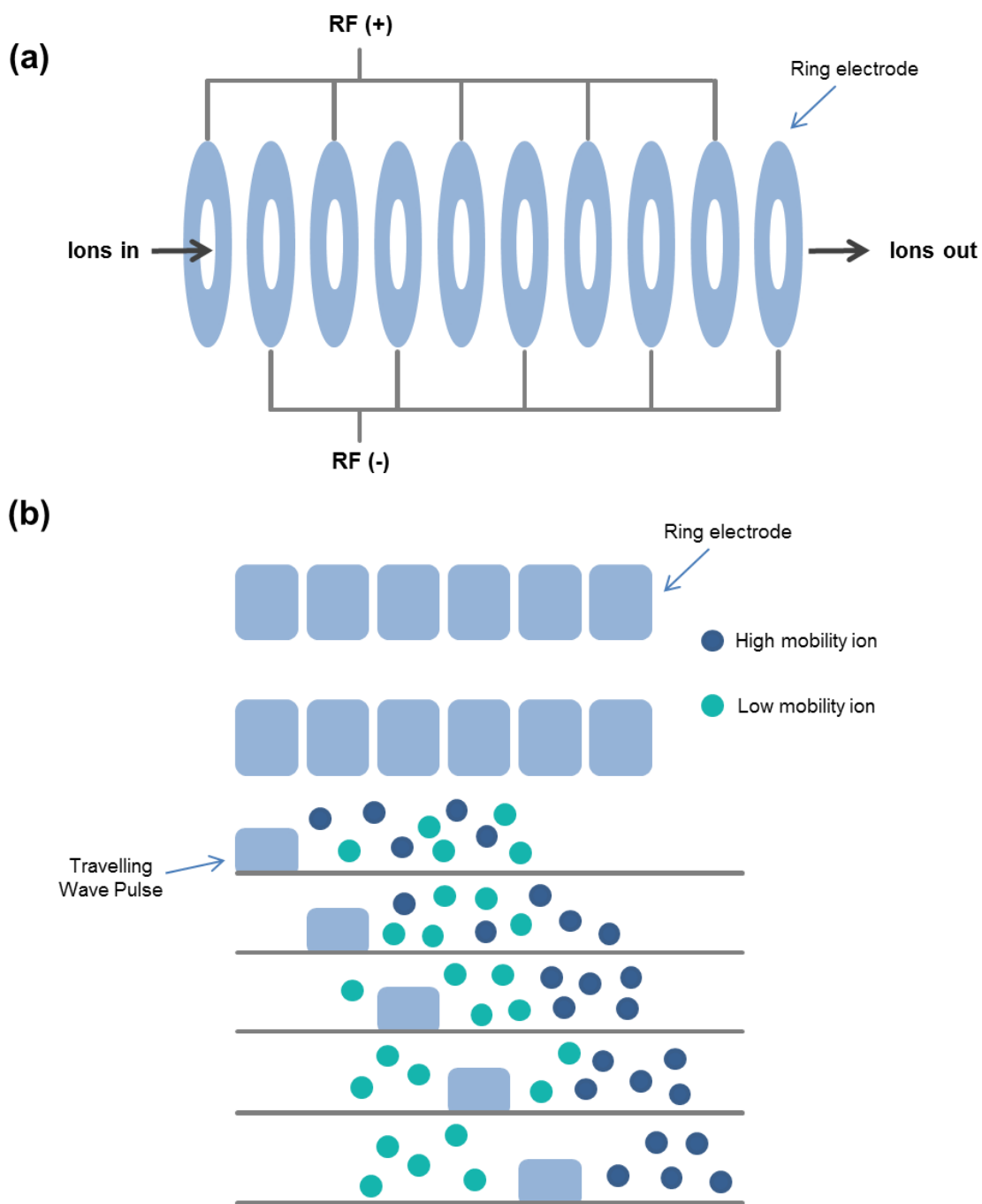


Figure 1.9: Schematic of ion mobility separation via a stacked-ring ion guide. Schematic of the SRIG carrying opposite RF voltages on adjacent rings found in the TWIMS cell of the Synapt G2 HDMS shown in (a). An illustration of the motion of the travelling wave superimposed on the confining RF voltage, causing ions of lower mobility to roll over the top of the travelling waves as they traverse the cell, allowing separation on the basis of mobility shown in (b).

In order to calculate Ω from TWIMS, correction factors must be incorporated into the conventional ion mobility equations developed for linear drift tubes to take into account the non-linear effects of the TWIMS instruments. These correction factors can be determined empirically through experimental calibration once acquisition parameters have been optimised. In the following equation, A is the correction factor for the electric field parameters (E and L in conventional ion mobility equations) and B is a compensatory factor for the non-linear effect of the TWIM instrumentation:

$$\Omega = \frac{(18\pi)^{\frac{1}{2}}}{16} \frac{ze}{(k_b T)^{\frac{1}{2}}} \left[\frac{1}{m_I} + \frac{1}{m_N} \right]^{\frac{1}{2}} \frac{760}{P} \frac{T}{273.2 N} \frac{1}{A} t_D^B$$

Equation 8

Ω can be defined as a charge and mass independent measure, reduced Ω (Ω'), by dividing the above equation by the absolute charge (ze) and reduced mass as shown in equation 9:

$$\Omega' = \frac{(18\pi)^{\frac{1}{2}}}{16} \frac{1}{(k_b T)^{\frac{1}{2}}} \frac{760}{P} \frac{T}{273.2 N} \frac{1}{A} t_D^B$$

Equation 9

These parameters can then be incorporated into one constant, A' as shown in equation 8. A' is a correction factor for the temperature, pressure and electric field and B is a correction factor for the non-linear effects of the TWIMS device:

$$\Omega' = A' t_D^B$$

Equation 10

Ω can therefore be expressed as equation 11:

$$\begin{aligned}\Omega &= ze \left[\frac{1}{m_I} + \frac{1}{m_N} \right]^{\frac{1}{2}} A' t_D^B \\ &= ze \left[\frac{1}{m_I} + \frac{1}{m_N} \right]^{\frac{1}{2}} \Omega'\end{aligned}$$

Equation 11

It is also necessary to compensate for the mass dependent transit time of an ion outside of the mobility region of the instrument, which is achieved by use of equation 12:

$$t'_D = t_D - (C\sqrt{m/z} / 1000)$$

Equation 12

Where t'_D is the corrected drift time (msec), t_D is the measured drift time (msec) and C is a constant, found in the control software as the enhanced duty cycle delay coefficient.

Given a known charge, mass and Ω , the Ω' of an ion can be determined empirically. A' and B can be determined experimentally from drift times (t_D) obtained from a range of multiply charged ions of known protein standards with known Ω . Ω can then be plotted against t_D , an example of which is shown in Figure 1.10. A calibration curve can then be obtained from fitting these data to the equation $y = A'x^B$, giving empirically determined values for A' and B. From this calibration curve the calculation of Ω of an analyte of interest can be determined from its drift time (Smith *et al.*, 2009).

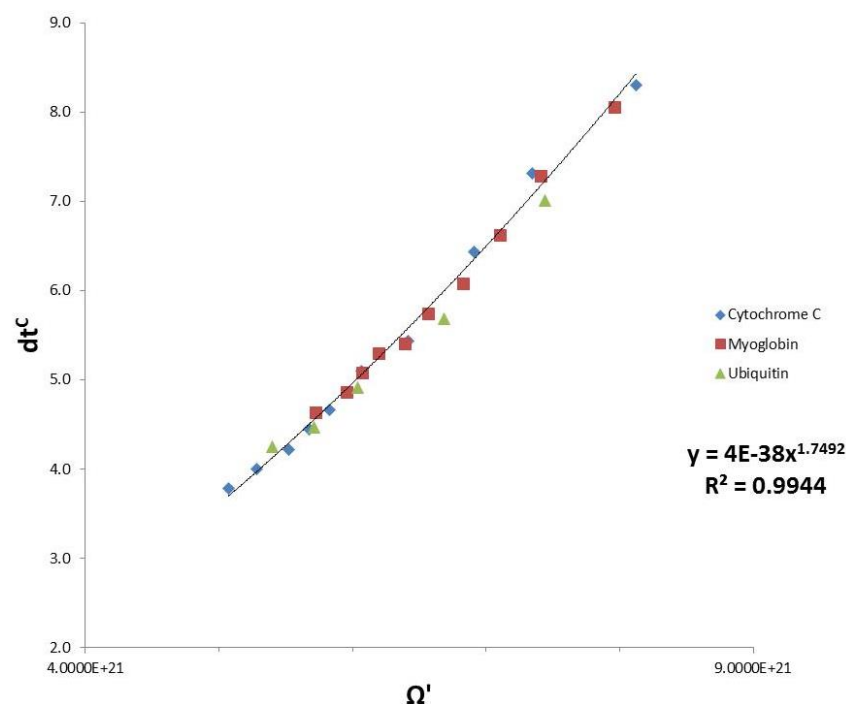


Figure 1.10: Example calibration curve of denatured standards of known Ω' versus drift time (msec) for multiply charged ions of cytochrome c, myoglobin and ubiquitin under denaturing solution conditions.

1.4.4 ESI-IMS-MS of biological systems

The study of proteins by IMS-MS was enabled through the development of ESI, allowing intact proteins and protein complexes to be transferred into the gas phase. ESI-MS and ESI-IMS-MS have emerged as useful tools for the study of many biological systems, with applications in many areas, such as the study of protein subunit stoichiometry, protein modifications and ligand binding and protein-metal interactions (reviewed by Sharon and Robinson, 2007).

ESI-MS and ESI-IMS-MS have also proved to be key techniques in the study of protein structure. In order to apply MS based techniques to the study of protein structure, successful retention of structure must be maintained on transition from solution phase to the gas phase. Early papers within the field reported that experimentally observed

Ω s were in good agreement with measurements obtained from more traditional analysis techniques such as X-ray crystallography and NMR, or from theoretical values (Scarff *et al.*, 2008; Smith *et al.*, 2009; Leney *et al.*, 2014). Growing evidence supports the retention of solution structures in the gas phase (Ruotolo *et al.*, 2002; Ouyang *et al.*, 2003; Florance *et al.*, 2011), providing experimental design and instrumental conditions have been carefully considered (Breuker and McLafferty, 2008; Chen and Russell, 2015).

Gross structural information of a protein can be inferred from MS alone through assessment of its CSD. Typically, compact proteins will present with few charge states due to limited ionisable sites being present on their surface, while more disordered or unfolded proteins have more exposed ionisable sites, and therefore a wider CSD (Testa *et al.*, 2013). Gaussian fitting of a protein's CSD can aid in the investigation of different conformers present in the sample, and in this way the effect of variables such as solution conditions or ligand binding on gross conformation can be analysed. However, such analysis is complicated by multiple species presenting at the same m/z , either through overlapping conformational families or the presence of oligomeric species. The presence of such species can be resolved through the addition of IMS, which enables their separation and interrogation, providing another dimension to conformational analysis. Pivotal examples where IMS and MS have been utilised in the study of protein structure include studies from the Robinson group into the self-assembly of insulin aggregates, demonstrating that MS can identify the solution states of oligomeric proteins (Nettleton *et al.*, 2000), studies from the Bowers group investigating the conformation of biological molecules such as Bradykinin (Wyttenbach, von Helden and Bowers, 1996) and trinucleotides (Gidden and Bowers,

2003), studies from the Jarrold group investigating the conformations of bovine pancreatic trypsin inhibitor and cytochrome C (Shelimov *et al.*, 1997), and studies from the Clemmer group investigating the effect of experimental conditions on ubiquitin conformers (Li *et al.*, 1999).

The study of amyloid formation is one biological system which has benefited greatly from the advances in ESI-IMS-MS, as understanding the morphological transitions which occur at early stages of protein aggregation is of critical importance for developing diagnostic and therapeutic strategies for amyloid diseases. This technique has been used extensively in the study of early stages of aggregation of proteins implicated in protein misfolding diseases, providing valuable information on the co-existing, transient conformations which often exist during this process. Key examples include investigations into the Alzheimer's disease associated amyloid- β (Bernstein *et al.*, 2009; Gessel *et al.*, 2012) and tau (Larini *et al.*, 2013), dialysis-related amyloidosis associated β -2-microglobulin (Smith *et al.*, 2011; Woods *et al.*, 2011; Leney *et al.*, 2014) and type 2 diabetes mellitus associated amylin (Bernstein *et al.*, 2009; Young *et al.*, 2014). This body of work has increased knowledge of the process of protein aggregation through structural characterization of intermediate, oligomeric species of aggregate formation, differentiation of isobaric peaks in the mass spectrum and investigation of the binding mode and subsequent conformational changes of enhancers and inhibitors of aggregation.

1.4.4.1 ESI-IMS-MS of alpha-synuclein

The focus of this thesis is the investigation of the structural changes and aggregation of alpha-synuclein, with one of the main techniques utilised being ESI-IMS-MS. Due to alpha-synuclein's lack of well-defined secondary structure and structural heterogeneity

it has proved challenging to investigate the conformation of this protein using conventional structural biology tools such as X-ray crystallography or NMR. In an attempt to overcome these challenges, alpha-synuclein has been studied using MS methods by a number of groups. Areas of interest included attempts to characterise the structure of alpha-synuclein, investigations into the effect of solution conditions and ligand binding on alpha-synuclein conformation, and studies of oligomeric species of the protein and its aggregation. Summaries of findings from key studies in these areas are provided below.

1.4.4.1.1 Alpha-synuclein structure as determined by MS

The intrinsic structure of alpha-synuclein has been investigated using MS methods, with varying results. Alpha-synuclein has been extensively analysed in both positive and negative ionisation mode by several groups. Table 1.2 summarises findings from key studies into the structure of alpha-synuclein under native conditions using ESI-MS.

Ionisation mode	Protein conc.	Buffer	CSD (mon)	CSD (dimer)	Reference
Negative	50 μ M	5 mm AA pH 7	$6 \leq z \leq 16$	$17 \leq z \leq 21$	(Bernstein <i>et al.</i> , 2004)
Negative	12 μ M	10 mm AA pH 7.4	$6 \leq z \leq 18$	-	(Natalello <i>et al.</i> , 2011a)
Positive	10 μ M	10 mm AA	$6 \leq z \leq 22$	$13 \leq z \leq 26$	(Frimpong <i>et al.</i> , 2010)
Positive	40 μ M	50 mm AA pH 6.8	$6 \leq z \leq 18$	$13 \leq z \leq 21$	(Illes-Toth <i>et al.</i> , 2013)
Positive	70 μ M	50 mm AA pH 6.8	$5 \leq z \leq 20$	-	(Beveridge <i>et al.</i> , 2015)
Positive	70 μ M	50 mm AA pH 7	$5 \leq z \leq 21$	$10 \leq z \leq 23$	(Phillips <i>et al.</i> , 2015)

Table 1.2: Summary of key ESI-MS studies of alpha-synuclein

For studies in positive ion mode, Frimpong *et al.* (2010), Illes-Toth *et al.* (2013), Beveridge *et al.* (2015) and Phillips *et al.* (2015) all found a wide CSD of the protein, with +5 being the lowest CSI detected and +22 being the highest, providing supporting evidence to alpha-synuclein being a disordered protein. A wide CSD of dimers was also noted in several of the studies, ranging from the +10 to the +26 ion, while a range of dimers, trimers and tetramers was detected by Phillips *et al.* (2015). The presence of dimeric species in the spectra demonstrates that alpha-synuclein is capable of self-association under native conditions. Another common finding of these investigations is indications of the presence of multiple conformational families of alpha-synuclein, within its wide CSD. A characteristic, multimodal distribution of monomeric ions is a common feature across all studies, with Frimpong *et al.* (2010) detecting maxima at the +19, +14 and +8 CSIs and Illes-Toth *et al.* (2013) detecting maxima at the +13 and +7 CSIs. Meanwhile, Beveridge *et al.* (2015) noted significant variation in the CSD in terms of peak intensities, highlighting the variability and plasticity of this protein. Deconvolution of the CSD by Frimpong *et al.* (2010) identified four conformational envelopes within the $+6 \leq z \leq +22$ CSD, with a degree of overlap. IMS data also supports the notion of multiple conformational families of alpha-synuclein, with Illes-Toth *et al.* (2013) detecting two distinguishable conformations at the +6, +11, +12 and +13 CSIs, three distinguishable conformations at the +7 CSI and four distinguishable conformations at the +8 CSI. Upon converting the IMS data to Ω , the most compact conformations were found to correspond to expected values for a globular protein of alpha-synuclein's mass, while the conformations with largest Ω corresponded to values expected from an expanded/alpha-helical conformation. Multiple conformational families were also detected using IMS by Beveridge *et al.* (2015), who found two distinguishable conformations between +8 and +16 CSIs, and one conformation at CSIs

above and below this range. A minimum Ω of 1043 Å² and a maximum Ω of 2742 Å² was observed, comparable to those observed by Illes Toth *et al.* (2013). A high level of variance in measured Ω was noted, indicating conformational inconsistency, which they theorised could be due to either unresolved species or interconversion of species within the timescale of the experiment. Phillips *et al.* (2015) utilised IMS to investigate conformations of alpha-synuclein present following chemical crosslinking, which identified three distinct conformational families, compact (~1200 Å²), extended (~1500 Å²) and unfolded (~2350 Å²). These measurements correlated to those observed in solution and correspond well to IMS findings for the non-crosslinked protein.

Due to alpha-synuclein being a negatively charged protein under physiological conditions, several investigations into this protein have been conducted using negative mode ESI, with results mirroring those seen in positive ionisation mode. An early study by Bernstein *et al.* (2004) found the alpha-synuclein monomer to have a CSD of $-6 \leq z \leq -16$, with a CSD of dimers from $-17 \leq z \leq -21$, and a study by Natello *et al.* (2011) bimodal CSD centered at the -14/-15 and -7/-8 CSIs. Consistent with positive mode studies, these reports indicate the protein is intrinsically disordered.

Although a certain degree of inconsistency is found in the various reports of the CSD/conformational families of alpha-synuclein, all investigations have noted the presence of coexisting conformational families with both compact and more extended species present. The discrepancies seen are likely due to a combination of differences in instrumentation, sample acquisition, buffer composition and starting material, as well as a result of the natural fluctuation of the protein. Indeed, the conformational heterogeneity of alpha-synuclein when studied by ESI-IMS-MS has been highlighted in

reports by Phillips *et al.* (2015) and Beveridge *et al.* (2015), where spectra obtained from identically prepared alpha-synuclein samples taken under highly similar source conditions displayed significant differences in the relative population of different charge states, as well as differences in the distribution between monomeric and oligomeric CSIs.

1.4.4.1.2 Solution conditions

In addition to looking at the native structure of alpha-synuclein, investigations into the effect of solution conditions on structure have been an active area of research, due to the known link between solution condition and alpha-synuclein aggregation.

The effect of altered pH has been investigated in a number of studies. Bernstein *et al.* (2004) found that reducing the pH from neutral to 2.5 resulted in a significant narrowing of CSD, from $-6 \leq z \leq -16$ to $-6 \leq z \leq -11$, suggesting the presence of predominantly compact conformations in acidic conditions. Using IMS the average Ω across all CSIs was calculated to be 2530 \AA^2 at pH 7, which reduced to 1690 \AA^2 at pH 2.5, corresponding to a more globular, compact structure. It was also found that the acidic conditions employed altered dimer formation, as the CSD of dimers from $-17 \leq z \leq -21$ found when ionised from a pH 7 solution was not detected in the pH 2.5 solution. Studies by Frimpong *et al.* (2010) and Beveridge *et al.* (2015) produced similar results, with an increase in low CSIs found with decreasing pH. Frimpong *et al.* (2010) also looked at the effect on dimers, which were found clustered around the +11 CSI at pH 2.5, broadening at pH greater than 4 to $+13 \leq z \leq +26$. These results demonstrate the enrichment of particular conformations in response to solution pH.

The effect of various alcohols has also been investigated, which has further demonstrated the enrichment of particular conformations in response to solution conditions. Frimpong *et al.* (2010) found an abundance of compact forms upon addition of 10% - 60% alcohol while Natello *et al.* (2011) found methanol stabilised compact forms and hexafluoro-2-propanol and tetrafluoroethylene promoted partially folded, intermediate forms.

1.4.4.1.3 Ligand binding

Another key area of interest has been research into the effect of various ligands on alpha-synuclein. As with altered solution conditions, it is known that binding of certain ligands can enhance or inhibit alpha-synuclein aggregation, and as such investigations into early conformational changes which occur upon binding to these ligands is of great interest due to the insights it could potentially give into alpha-synuclein pathology.

The effect of metal ion binding on alpha-synuclein conformation has been the subject of much research, with a particular emphasis on copper binding, due to its known ability to promote oligomerisation and aggregation of alpha-synuclein (discussed in detail in Section 2.1.3). A study employing negative mode QTOF-MS to investigate conformational transitions following copper binding found a decrease of the disordered conformer and a shift towards the compact conformer. A substantial shift was seen, with the dominant CSI changing from -15 to -8 (Natalello *et al.*, 2011b). The role of copper in its ability to induce aggregation and alter the conformation of alpha-synuclein will form the central focus of Chapter 2.

The binding of many other small molecules has been investigated using IMS-MS, including investigations into spermine (Grabenauer *et al.*, 2008), calcium (Han, Choi and Kim, 2018), dopamine (Illes-Toth, Dalton and Smith, 2013), epigallocatechin gallate (EGCG) (Konijnenberg *et al.*, 2016) and gallic acid (Liu *et al.*, 2014). A common finding of these studies was an increase in compact conformations upon binding of compounds known to increase alpha-synuclein aggregation, such as spermine (Grabenauer *et al.*, 2008), and prevention of the formation of compact conformations by compounds which inhibit aggregation, such as gallic acid (Liu *et al.*, 2014).

1.4.4.1.4 Aggregation

Various studies have utilised ESI-IMS-MS in an attempt to further understanding of the early stages of alpha-synuclein aggregation. Vlad *et al.*, (2011) reported specific autoproteolytic truncation and degradation products of alpha-synuclein which arose during aggregation. A fragment with high aggregation tendency was identified and aggregation studies of the carboxy-terminal fragment (72-140) showed increased fibrillisation compared to the intact protein. Philips *et al.* (2015) saw an increase in dimer to monomer ratio following aggregation, but no gross conformational change, while Illes-Toth *et al.*, (2015) characterised a specific population of oligomers, from dimers through to hexamers, which were able to induce intracellular alpha-synuclein aggregation. While some progress has been made in this area, characterising the early stages of alpha-synuclein using this technique has lagged behind progress made for other amyloidogenic proteins (discussed in Section 1.4.4), and such knowledge is vital to develop potential PD treatments to directly target the aggregation process. An investigation of the structure and dynamics of these oligomeric species will be the central focus to Chapter 3.

1.5 Thesis overview

The overall aim of this thesis was to investigate the structural and functional aspects of alpha-synuclein and its oligomers. In Chapter 2 investigations into the copper binding and subsequent alterations to conformation and aggregation propensity of alpha-synuclein were performed. Specifically, the effects of a familial PD mutation and a co-translational modification on these factors were characterised. In Chapter 3 investigations into the aggregation of alpha-synuclein, both into specific oligomers of known function and into amyloid fibrils were conducted. Chapter 4 set out to further characterise the effect of alpha-synuclein oligomers with the ability to seed intracellular aggregation on an SH-SY5Y cell culture model.

Chapter 2: The effect of N-terminal acetylation and H50Q mutation on copper binding of alpha-synuclein

2.1 Introduction

Various metal ions are known to bind to alpha-synuclein and are found in LBs along with aggregated forms of the protein. Characterising the metal binding ability and subsequent conformational changes of alpha-synuclein can give important insights into the association between metal binding and protein aggregation. In this chapter, the effect of the H50Q familial mutation and N-terminal acetylation on the copper binding of alpha-synuclein was investigated.

2.1.1 Environmental factors and PD

Epidemiological studies have linked various environmental factors to increased incidence of PD. Well established factors include exposure to pesticides and herbicides (Elbaz *et al.*, 2009; Tanner *et al.*, 2011), metals (Gorell *et al.*, 1999; Willis *et al.*, 2010), solvents (Goldman *et al.*, 2012) and Polychlorinated Biphenyls (Caudle *et al.*, 2012).

2.1.2 Metals in PD

High metal exposure is known to be a potential risk factor in certain non-familial forms of PD (Gorell *et al.*, 2004), and alterations in metal homeostasis have been associated with many neurodegenerative diseases (Chen, Miah and Aschner, 2016). The maintenance of metal homeostasis is vital for biological function, as metals play essential roles as co-factors in many biological processes (Tapiero, Townsend and Tew, 2003). One example relevant to PD is that in dopaminergic neurons the enzyme tyrosine hydroxylase (TH), responsible for catalysing the first step in the conversion of tyrosine to dopamine, requires ferrous iron as a cofactor (Fitzpatrick, 1989). Accumulation and abnormal distributions of various metals (including iron, copper and

zinc) in the SNpc and striatum of PD patients has been widely reported (Kozlowski *et al.*, 2012; Dusek *et al.*, 2015; Gardner *et al.*, 2017). However, it remains to be established whether these alterations in metal homeostasis are a cause or consequence of PD (for a review see Rasheed *et al.*, 2017).

2.1.3 The association between alpha-synuclein and metals

Due to the established link between alpha-synuclein and PD, the interaction of this protein with various metals has been investigated (reviewed by Carboni and Lingor, 2015). As discussed in Section 1.3.2, alpha-synuclein is known to exhibit significant conformational heterogeneity, undergoing considerable conformational transitions depending on environmental conditions. Collapsed conformers of alpha-synuclein have been linked to its aggregation (Uversky, Li and Fink, 2001b). Certain environmental conditions have been demonstrated to be capable of inducing such collapsed conformational states, including the presence of various divalent metal ions (Santner and Uversky, 2010). While most interactions between alpha-synuclein and metals occur at the C-terminus of the protein and appear to be low-specificity (Binolfi *et al.*, 2006), high affinity binding sites for Cu^{2+} have been reported (Han, Choi and Kim, 2018). Evidence suggests alpha-synuclein is capable of binding Cu^{2+} at three specific sites, shown in Figure 2.1; a high-affinity N-terminal site where copper is anchored by the freely available amino-terminal nitrogen, a site anchored by the imidazole ring of the histidine at residue 50, and a low-affinity site at the C-terminus of the protein (Binolfi *et al.*, 2012). Mapping studies employing circular dichroism, calorimetric titrations, NMR and electron paramagnetic resonance spectroscopy have all demonstrated the population of a collapsed species of alpha-synuclein in the presence of this metal (Drew *et al.*, 2008; Binolfi *et al.*, 2010; Natalello *et al.*, 2011b).

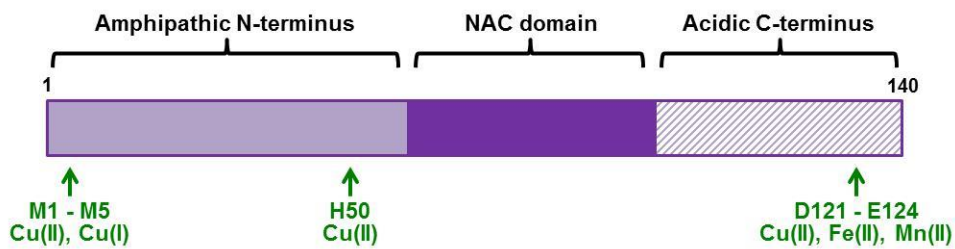


Figure 2.1: Illustration of proposed localisation of alpha-synuclein metal binding sites. Alpha-synuclein has a high affinity for copper, with two main binding sites at the N-terminus. A third, lower affinity copper binding site exists at the C-terminus, which can bind other divalent metals, including Fe(II) Cu(II) and Mn(II). Figure adapted from Carboni and Lingor (2015).

In addition to being a known metal binding protein, recent reports have also linked alpha-synuclein to the maintenance of cellular iron homeostasis; a carefully regulated process crucial for correct biological functioning. An important component of iron homeostasis is achieved by iron regulatory proteins (IRPs); cytosolic proteins which post-transcriptionally regulate the expression of iron metabolism genes in response to cytosolic iron levels (Wang and Pantopoulos, 2011). As illustrated in Figure 2.2, through binding to iron response elements (IREs), motifs of around 30 nucleotides found within mRNA, which form hairpin-loop structures, IRPs can enhance or inhibit translation of a gene, depending on the location of the IRE. In conditions of low iron, IRPs bind to IREs. If the IRE is located in the 5'-UTR the IRPs prevent translation of that gene by blocking the mRNA from binding to the ribosome. If the IRE is located in the 3'-UTR, binding of IRPs protect these genes from endonuclease cleavage, making them more stable and promoting translation. In conditions of high iron, IRPs do not bind to IREs, resulting in translation of mRNAs with IREs in the 5'-UTR, and degradation of mRNAs with IREs in the 3'-UTR. IREs are commonly found in proteins involved in iron

homeostasis, such as transferrin receptor protein 1 and ferritin. A predicted IRE has been identified in the 5'-UTR of SNCA, and it has been demonstrated that alpha-synuclein translation can be regulated by iron (Febbraro *et al.*, 2012).

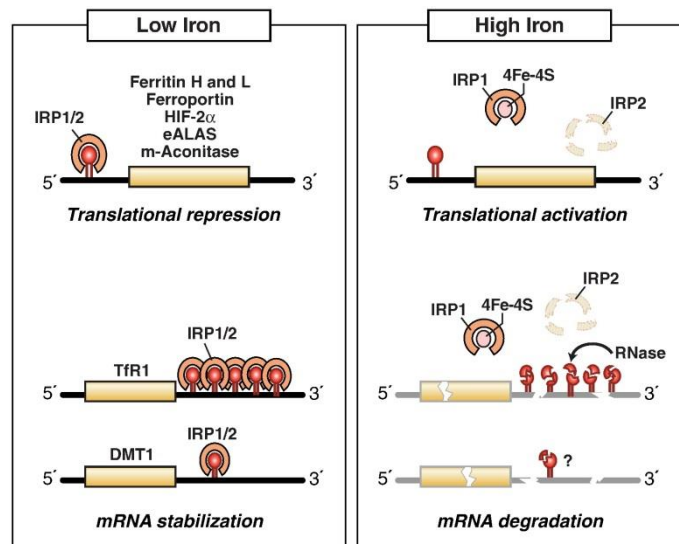


Figure 2.2: Illustration of IRP regulation of translation and stability of IRE-containing mRNAs. IRPs bind to IREs located in either the 5' or 3' untranslated regions of specific mRNAs. When iron is limited, IRPs bind with high affinity to 5' IRE mRNAs and repress translation, and to 3' IRE mRNAs, stabilize these mRNAs. When iron is abundant, IRPs do not bind IREs, resulting in the translation of 5' IRE-containing mRNAs and degradation of 3' IRE-containing mRNAs. Figure taken from Anderson *et al.* (2012).

A further link between alpha-synuclein and iron homeostasis comes from data showing the protein is able to act as a ferrireductase. Enzymes with ferrireductase activity reduce iron from its ferric form to its ferrous form, a vital function to ensure sufficient availability of Fe²⁺ for a range of cellular processes. It has been demonstrated that both recombinant alpha-synuclein and the lysate of cells overexpressing alpha-synuclein are capable of reducing Fe³⁺ to Fe²⁺, requiring NADH as an electron donor and copper bound to the protein to cycle between its oxidized and reduced forms (Davies, Moualla

and Brown, 2011). Further research has implied that the major catalytically active form of alpha-synuclein is a membrane-associated tetramer (McDowall, Ntai, Hake, *et al.*, 2017a) and the associated ferrireductase activity is also detectable *in vivo* (McDowall, Ntai, Honeychurch, *et al.*, 2017b). These studies provide substantial evidence for alpha-synuclein being involved in iron homeostasis, and points to a physiological function for alpha-synuclein as a metalloprotein. Therefore a paradoxical situation exists between the ability of alpha-synuclein to undergo metal induced aggregation *in vitro* and its potential role as a metal binding protein *in vivo*.

2.1.3.1 Alpha-synuclein mutations and metals

As discussed in Section 1.1.1.1, several point mutations in SNCA which cause AD forms of PD have been identified. The recently identified H50Q missense mutation in SNCA exon 4 was reported by two research groups in 2013 (Appel-Cresswell *et al.*, 2013; Proukakis *et al.*, 2013). This mutation has been shown to accelerate fibril formation of the protein (Ghosh *et al.*, 2013), reduce its solubility (Porcari *et al.*, 2015) and increase its secretion and toxicity in cell culture (Khalaf *et al.*, 2014). This mutant is of particular interest in relation to copper binding, as the loss of the histidine imidazole ring would presumably affect alpha-synuclein's copper binding ability. However, studies investigating copper binding of alpha-synuclein *in vitro* where the H50 residue was mutated to an alanine found negligible effects on copper binding; contrary to what would be predicted upon the removal of a copper anchoring site (Davies *et al.*, 2011). The effect of the H50Q familial mutation on copper binding was investigated by Proukakis *et al.* (2013) who found the mutant was able to bind to copper, but in a different manner to the WT protein, with binding mainly involving the N-terminus site.

2.1.3.2 Alpha-synuclein modifications and metals

The diversity of the human proteome is much greater than would be predicted by the genome. A large part of this diversity is due to protein modifications; alterations to proteins which occur co- or post-translationally, allowing a protein to act in multiple ways. *In vitro* studies of alpha-synuclein have historically used recombinant protein obtained from bacterial overexpression. Such expression produces unmodified alpha-synuclein. However, *in vivo* alpha-synuclein has been shown to be constitutively acetylated at its N-terminus (Anderson *et al.*, 2006), a common co-translational modification of nascent polypeptides, particularly those which retain their initiating methionine residue such as alpha-synuclein (Bradshaw, 1989).

Acetylation is one of the most common modifications in eukaryotes, in which the acetyl group from acetyl coenzyme A is transferred onto a protein's N-terminus (Fig. 2.3). In mammalian cells, N-terminal acetylation is carried out by the N-acetyltransferase (NAT) group of enzymes which catalyse the transfer of an N-acetyl group from acetyl-coA to the alpha-amino group of a protein's N-terminus (Varland, Osberg and Arnesen, 2015). This process neutralizes the positive charge of the free alpha-amino group, blocking it from further modifications. The NatB complex is responsible for N-terminal acetylation of alpha-synuclein as it has substrate specificity for proteins with starting N-termini Met-Glu-, Met-Asn- and, as is the case with alpha-synuclein, Met-Asp- (Van Damme *et al.*, 2012). A method of producing acetylated recombinant proteins was established in 2010 (Johnson *et al.*, 2010). This technique utilised co-expression of the protein of interest with its corresponding NAT enzyme, which has allowed *in vitro* studies of acetylated, recombinant alpha-synuclein to be performed.

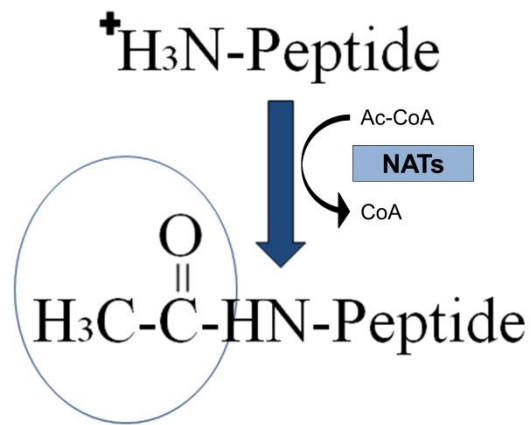


Figure 2.3: Schematic of N-terminal acetylation. N-acetyltransferase enzymes catalyse the transfer of an N-acetyl group from acetyl-coA to the alpha-amino group of a protein's N-terminus.

Alpha-synuclein was first identified as being acetylated when purified from Lewy bodies using LC-MS/MS (Anderson *et al.*, 2006), which has since been confirmed in alpha-synuclein isolated from brain tissue homogenate (Ohrfelt *et al.*, 2011) and erythrocytes (Fauvet *et al.*, 2012). In recent years a number of *in vitro* studies have aimed to elucidate the effect of acetylation on alpha-synuclein structure and function. Such studies have shown that acetylation results in an increase in lipid binding affinity (Dikiy and Eliezer, 2014), altered transient secondary structure (Kang *et al.*, 2013) and decreased aggregation rates (Kang *et al.*, 2012). N-terminal acetylation is also an important modification in relation to its Cu^{2+} binding as the transfer of an acetyl group to the copper anchoring amino-terminal nitrogen has the potential to alter the protein's Cu^{2+} binding ability. Indeed, it has been demonstrated that N-terminally acetylated alpha-synuclein lacks this high affinity N-terminal Cu^{2+} binding site and undergoes altered fibril formation in the presence of this metal (Moriarty *et al.*, 2014).

2.2 Aims and Objectives

Prior studies investigating wild type N-terminally acetylated alpha-synuclein have successfully used ensemble based spectroscopy techniques to probe structural changes brought about by metal binding (Moriarty *et al.*, 2014). However, changes to individual conformational states of alpha-synuclein have not been investigated. To date, the effect of the familial H50Q mutation on Cu²⁺ binding of biologically relevant N-terminally acetylated alpha-synuclein has not been investigated. In this chapter, ESI-IMS-MS has been employed to observe the copper binding and subsequent conformational transitions of individual conformational states of unmodified and N-terminally acetylated forms of wild type (WT) and H50Q alpha-synuclein, using conditions suitable to maintain protein-metal complexes in the gas-phase. ESI-IMS-MS has been utilized due to its ability to interrogate dynamic ensembles of the same mass by separating extended and collapsed conformations (Jenner *et al.*, 2011), with changes in solution conformation detected in the gas phase as changes in Ω . This method also allows the binding of ligands to specific conformational states to be determined (Hopper and Oldham, 2009).

The specific aims of this chapter were:

1. To produce N-terminally acetylated and H50Q mutated recombinant forms of alpha-synuclein.
2. To establish whether N-terminal acetylation or H50Q mutation alter the conformational state of alpha-synuclein.

3. To establish whether N-terminal acetylation or H50Q mutation alter the aggregation propensity of alpha-synuclein.
4. To establish the effect of N-terminal acetylation in the context of the H50Q mutation on the copper binding affinity, conformation states and aggregation propensity of alpha-synuclein.

2.3 Materials and Methods

2.3.1 Molecular biology of pET23a-ASYN expression plasmid

A modified pET23a expression plasmid containing the nucleotide sequence for the expression of alpha-synuclein was provided by Dr David Smith (Sheffield Hallam University, UK). Throughout this thesis this plasmid will be referred to as pET23a-ASYN.

2.3.2 pACYCduet-naa20-naa25 plasmid purification

In order to produce acetylated alpha-synuclein the pNatB (pACYCduet-naa20-naa25) plasmid, allowing expression of the fission yeast NatB complex, was obtained from Addgene in the form of an agar stab. *E.coli* from the stab was streaked onto an agar plate containing 25 mg/mL chloramphenicol and incubated overnight at 37 °C/5% CO₂. A 500 mL starter culture was grown from a single colony from the agar plate, and plasmid DNA purified using an OriGene PowerPrep HP® Plasmid Maxiprep kit, following manufacturer guidelines. Briefly, the starter culture was pelleted and resuspended in Cell Suspension Buffer. Cells were lysed through addition of Cell Lysis Solution before addition of Neutralisation Buffer. The lysate was centrifuged at 15000 xg for 10 minutes at room temperature, and the supernatant added to a pre-equilibrated column provided with the kit. The column was washed with Wash Buffer and bound DNA eluted with Elution Buffer. Eluted DNA was subjected to isopropanol precipitation and the DNA pellet resuspended in TE Buffer. Glycerol stocks from excess overnight culture were produced by the addition of an equal volume of 50% glycerol to the culture, and storage at -80 °C.

2.3.3 Site directed mutagenesis of pET23a-ASYN

H50Q mutant alpha-synuclein was created by modification of the pET23a-ASYN plasmid via site directed mutagenesis, using a QuikChange® II XL Site-Directed Mutagenesis Kit by Stratagene following manufacturer's instructions.

Briefly, two complimentary oligonucleotides containing the desired mutation, flanked by unmodified nucleotide sequence were designed in house and synthesized by Sigma Aldrich LTD. Primers used were:

Forward: 5' GCGTTGTCCAAGGGGTTGCG 3'

Reverse: 5' CGCAACCCCTTGGACAACGC 3'

Oligonucleotide primers, each complementary to opposite strands of the vector, were extended during temperature cycling by PfuUltra HF DNA polymerase without primer displacement. Extension of the oligonucleotide primers generated a mutated plasmid containing staggered nicks. Following temperature cycling, the product was treated with Dpn I endonuclease to digest the parental DNA template and to select for mutation containing synthesized DNA. The nicked vector DNA incorporating the desired mutations was then transformed into XL10-Gold ultracompetent cells. Mutated plasmids were then isolated using a QIAprep Spin Miniprep Kit, following manufacturer's instructions. Throughout this thesis this mutated plasmid will be referred to as pET23aH50Q-ASYN.

2.3.4 Production of chemically competent cells

Stocks of chemically competent BL21 (DE3) *E.coli* cells were prepared for use in transformations and subsequent overexpression of proteins. *E.coli* were streaked from

glycerol stocks onto an agar plate containing 100 mg/mL ampicillin and incubated overnight at 37 °C/5% CO₂. A single colony was used to inoculate a 5 mL starter culture of LB (containing 10 g/mL Tryptone, 10 g/mL NaCl, 5 g/mL yeast extract and 100 mg/mL ampicillin). 500 µL of starter culture was transferred to 50 mL pre warmed LB and cultured at 37 °C until the OD₆₀₀ reached between 0.5 and 0.7. The culture was then aliquoted into chilled 50 mL falcon tubes and centrifuged at 4000 rpm for 5 minutes at 4 °C. The supernatant was discarded, the pellet resuspended in 30 mL TBF1 (30 mM KOAc, 100 mM RbCl, 50 mM MnCl, 10 mM CaCl₂, pH 5.8) and incubated on ice for one hour. They were then centrifuged again at 4000 rpm for 5 minutes at 4 °C and the pellet resuspended in 4 mL TBFII (10 mM MOPS, 10 mM RbCl, 75mM CaCl₂, 15% Glycerol, pH 7.0). 200 µL aliquots of chemically competent cells were flash frozen in liquid nitrogen and stored at -80 °C.

2.3.5 Transformation of competent cells

100 µL of BL21 (DE3) chemically competent cells were transformed with 1 µL of the appropriate plasmids required to express each protein, as shown in Table 2.1, with the addition of β-mercaptoethanol to a final concentration of 24 mM.

	pET23a-ASYN	pET23aH50Q-ASYN	pNatB
Unmodified, WT	✓	✗	✗
Acetylated WT	✓	✗	✓
Unmodified H50Q	✗	✓	✗
Acetylated H50Q	✗	✓	✓

Table 2.1: Plasmids required to produce the various forms of recombinant alpha-synuclein.

Reaction mixtures were incubated for 30 minutes on ice. The mixture was then exposed to 45 second heat shock in a 42 °C water bath and returned to ice for 2 minutes. 900 µL of preheated, sterile SOC medium (2% tryptone, 0.5% yeast extract, 10 mM NaCl, 2.5 mM KCl, 10 mM MgCl₂, 10 mM MgSO₄, and 20 mM glucose) was added and the reactions incubated at 37 °C with aggitation at 200 rpm for one hour to allow the bacteria to express antibiotic resistance. 100 µL of the reaction was spread onto agar plates containing 100 mg/mL ampicillin (for those transformed with the pET23a plasmids only) or 100 mg/mL ampicillin and 25 mg/mL chloramphenicol (for those transformed with both pET23a and pNatB plasmids) to select for bacteria which had been successfully transformed. Agar plates were incubated at 37 °C/5% CO₂ overnight.

2.3.6 Agarose gel electrophoresis

Plasmid DNA was separated on a 1% agarose gel to check quality and purity. A 1% agarose gel was prepared by dissolving 400 mg of agarose in 40 mL of TAE buffer (89 mM Tris-HCL pH 7.8, 89 mM borate, 2 mM EDTA), followed by heating in a microwave until agarose was dissolved. The solution was then allowed to cool before the addition of 0.5 µg/mL ethidium bromide and the gel poured into a Bio-Rad gel tray sealed with a Bio-Rad gel caster. An 8 well comb was inserted into the agarose solution and the gel allowed to set at room temperature. Agarose gels were then placed in a Bio-Rad horizontal electrophoresis tank and submerged in TAE buffer. DNA samples were mixed with loading dye and loaded into the wells. exACTGene Mid Range DNA Ladder; 300 to 5000bp (Fisher BioReagents), was added into a separate well to aid DNA size estimation. The electrophoresis tank was connected to an electrical power pack and 100 volts applied to the gel for 40 minutes. Gels were imaged on a UVP epi dark room trans-illuminator under ultra violet light.

2.3.7 Expression of recombinant proteins

Single colonies from agar plates were incubated in 100 mL LB media (containing 100 mg/mL ampicillin or 100 mg/mL ampicillin and 25 mg/mL chloramphenicol as appropriate) overnight at 37 °C with agitation at 200 rpm. Expression was induced by inoculating 15 mL of this overnight culture into 1 L of auto induction media (Formedium, UK) containing 100 mg/mL ampicillin or 100 mg/mL ampicillin and 25 mg/mL chloramphenicol. This was incubated for 18 hours at 28 °C with agitation at 180 rpm. Cells were then harvested by centrifugation at 8,000 rpm, 4 °C for 20 minutes.

2.3.8 Protein purification

The cell pellets were resuspended in a lysis buffer containing 10 mM Tris-HCl, pH 8.0, 100 µg/mL lysozyme, 20 µg/mL DNase, 20 µg/mL RNase, one bacterial protease inhibitor cocktail tablet (Sigma Aldrich) and 2 mM phenylmethylsulfonyl fluoride (PMSF). The lysate was incubated on ice for 30 minutes before the addition of 1 mM ethylenediaminetetraacetic acid (EDTA) and then further lysed by sonication. The lysate was centrifuged at 10000 xg, 4 °C for 40 minutes to remove debris and the supernatant acidified to pH 4.5, centrifuged again at 10000 xg, 4 °C for 30 minutes to remove precipitated proteins and the lysate neutralised to pH 8.0. This crude lysate was passed through a 0.2 µm filter and loaded on to a 50 mL Q-Sepharose column (GE Healthcare) for anion exchange at 4 °C. Prior to this the column was equilibrated with two column volumes of buffer A (25 mM Tris-HCl, 10 mM NaCl pH 8.0) and the protein eluted with a 0-100% linear gradient of buffer B (25 mM Tris-HCl, 1M NaCl pH 8.0). SDS-PAGE analysis of Q-Sepharose fractions was performed and the fractions enriched with alpha-synuclein were pooled, dialysed at 4 °C against ultrapure water and

lyophilised. Lyophilised protein was dissolved in buffer A and injected onto a HiLoad® 26/600 Superdex™ 200 Prep Grade size exclusion column (Amersham Biosciences) using 25 mM Tris-HCl, 10 mM NaCl pH 8.0 as running buffer. SDS-PAGE analysis of size exclusion fractions was performed and purified fractions containing only alpha-synuclein were pooled, dialysed at 4 °C against ultrapure water, re-lyophilised and stored at -20 °C for further experiments. Protein concentration was measured by absorbance at 280 nm using an extinction coefficient of 5960 M⁻¹cm⁻¹ on a nanodrop spectrophotometer.

2.3.9 SDS-PAGE

Separating and stacking gels were prepared as shown in Table 2.2. Glass plates were assembled according to manufacturer's instructions. The separating gel was cast and allowed to polymerise, followed by casting of the stacking gel and insertion of a comb to form sample wells.

	Separating gel (mL)	Stacking gel (mL)
ddH₂O	3.4	2.9
40% acrylamide	2.4	0.75
1.5 M Tris-HCL pH 8.8	2	-
0.5 M Tris-HCL pH 6.8	-	1.25
10% SDS	0.08	0.05
10% APS	0.08	0.05
TEMED	0.008	0.005

Table 2.2: Composition of 12% SDS-PAGE gel.

10x running buffer of 250 mM Tris-HCl, 1920 mM glycine and 1% w/v SDS, pH 8.3 was diluted to 1x before use. Samples were diluted with 4x Laemmli protein sample buffer

(Bio-rad) and electrophoresed in 1x running buffer at 100 V. To aid molecular weight determination 5 μ L protein marker (broad range, P7702S, New England Biolabs) was loaded into one well. On completion of electrophoresis, gels were stained with InstantBlue Protein Stain (Expedeon) and visualised using a LI-COR Odyssey and Odyssey Infrared Imaging software (LI-COR, Nebraska, USA).

2.3.10 Sample preparation for mass spectrometry analysis

Protein samples were prepared for MS analysis by dissolving lyophilized protein and CuCl_2 to a final concentration of 20 μ M in 50 mM ammonium acetate pH 7.0. Protein to metal ratios of 1:0 and 1:1 were prepared and mixed immediately prior to analysis.

2.3.11 ESI-IMS-MS analysis

All experimentation was performed on a Synapt G2 HDMS instrument (Waters, Manchester, UK) equipped with a Triversa (Advion Biosciences) automated nano-ESI interface in positive mode. Positive ESI was used with a capillary voltage of 1.7 kV and nitrogen nebulizing gas pressure of 0.7 psi. The following instrument parameters were used unless stated otherwise: cone voltage 45 V, source temperature 60 $^{\circ}$ C, backing pressure 3.0 mbar, trap collision energy 4 V, transfer 20 V, IMS wave velocity 600 m/s, IMS wave height 4 V, IMS gas flow 90 mL/min. Mass calibration was carried out by an infusion of CsI cluster ions. For attaining denatured spectra, calibrants were prepared before injection at 10 μ M dissolved in 50% acetonitrile, 10% formic acid and 40% ultrapure water (v/v/v). A calibration curve for collision cross-sectional areas was obtained based on of multiple charge states of cytochrome C from equine heart, myoglobin from equine heart and ubiquitin from bovine erythrocytes as described in detail in Section 1.4.3.2. Drift times were corrected for both mass-dependent and

independent time of flight (Ruotolo *et al.*, 2008). Arrival time distributions (ATD) were determined using the Mass Lynx v4.1 software (Waters, Manchester, UK). ATD for each charge state at its respective m/z value were extracted from the Driftscope plots available within the MassLynx suite of software. Plots were then fitted with Microsoft Excel using least square regression to a minimum number of Gaussian distributions using multiples of the following equation:

$$y = \frac{A}{w\sqrt{\pi/2}} e^{-\frac{(x-x_0)^2}{2.w^2}}$$

Where A = total area under the curve from the baseline, x_0 = center of the peak, and w = width of the peak at half height. This model describes a normal (Gaussian) probability distribution function.

2.3.12 Thioflavin T (ThT) fluorescence

Lyophilized alpha-synuclein was reconstituted to a final concentration of 70 μ M with 10 μ M ThT, with and without equimolar CuCl_2 . 100 μ l of sample was placed into a black walled 96 well plate with a 4 mm diameter glass bead, which has been shown to increase the reproducibility of ThT assays (Giehm, Lorenzen and Otzen, 2011). The plate was incubated at 37 °C with agitation at 300 rpm using a BMG Labtech CLARIOstar plate reader. ThT fluorescence readings (excitation 440 nm/emission 488 nm) were taken at 60 minute intervals over the course of an aggregation experiment. Lag time was determined from raw data by calculating the intercept between the maximum derivative and the pre-transitional base line as shown in Figure 2.4.

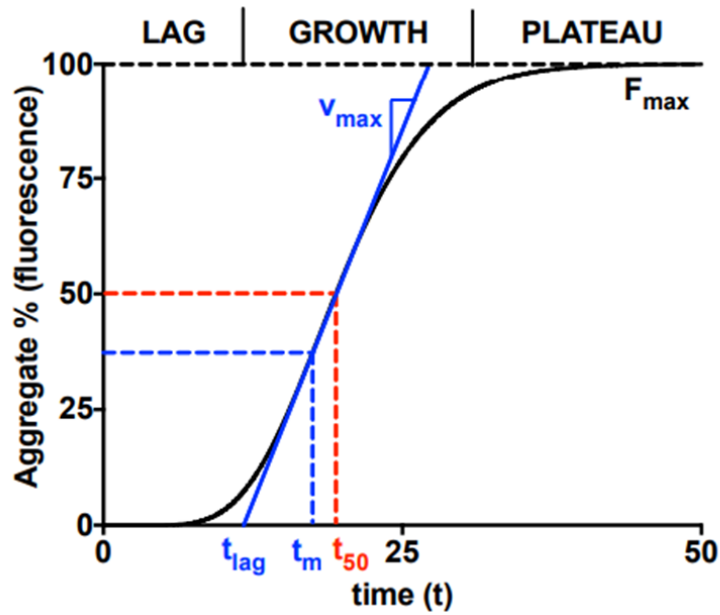


Figure 2.4: Illustration of lag time calculation from ThT data. An increase in aggregates over time results in a characteristic sigmoidal curve for amyloid fibril formation. F_{\max} = fluorescence intensity of final aggregates. t_{50} = the time at which half of the plateau aggregates are formed. t_m = the time at which the growth rate reaches its maximum, v_{\max} . t_{lag} is estimated by extending the tangent at t_m down to the time axis. Figure taken from Shoffner and Schnell, (2016).

2.4 Results and discussion

In order to determine the effect of protein modification and mutation of a key metal binding residue on alpha-synuclein, recombinant protein was produced with and without N-terminal acetylation, with and without the histidine at residue 50 mutated to the PD associated glutamine.

2.4.1 Site directed mutagenesis of pET23a-ASYN

In order to produce mutated alpha-synuclein site directed mutagenesis was performed. The H50Q mutant was successfully produced as confirmed by sequencing, shown in Figure 2.5. Highlighted in red, it can be seen that the usual CAT codon at residue 50 (encoding a histidine) has been successfully replaced by a CAA codon (encoding a glutamine) using the primers described in Section 2.3.3.

a) ATG GAT GTC TTC ATG AAA GGG CTg^{tcG} AAA GCG AAA GAA GGT GTC GTA
GCA GCT GCG GAA AAG ACC AAA CAA GGC GTA GCC GAA GCA GCC GGT
AAA ACG AAG GAA GGT GTG CTG TAT GTC GGC AGC AAG ACC AAA GAA
GGC GTT GTC **CAA** GGG GTT GCG ACT GTT GCG GAG AAA ACG AAA GAG
CAG GTG ACA AAC GTG GGA GGA GCC GTT GTG ACC GGT GTG ACC GCA
GTA GCC CAG AAA ACG GTG GAA GGT GCT GGC TCC ATT GCA GCG GCG
ACT GGC TTT GTG AAG AAA GAC CAG TTA GGG AAA AAC GAG GAA GGT
GCT CCT CAA GAA GGC ATC TTG GAG GAT ATG CCG GTT GAT CCG GAT
AAT GAG GCC TAT GAG ATG CCG AGT GAA GAA GGC TAC CAG GAC TAC
GAA CCA GAA GCG TAA

b) MDVFMKGLSKAKEGVVAAAEKTKQGVAEAAGKTKEGVLYVGSKTKEGVV**Q**GVA
TVAEKTKEQVTNVGGAVVTGVTAVAQKTVEGAGSIAAATGFVKKDQLGKNEEGA
PQEGILEDMPVDPDNEAYEMPSE EGYQDYEP EA

Figure 2.5: Sequencing results of the mutated pET23a-ASYN plasmid. The DNA sequence (a) and amino acid sequence (b) of the alpha-synuclein coding region of the pET23a-ASYN plasmid, mutated via site directed mutagenesis. The mutated amino acid to which primers were designed is highlighted in red.

2.4.2 Co-transformation of BL21 (DE3) cells

To achieve N-terminal acetylation of recombinant alpha-synuclein produced in *E. coli* cells, co-transformation with both the pNatB plasmid (encoding the catalytic subunit (Naa20) and auxiliary subunit (Naa25) of the NatB complex) and the pET23a-ASYN plasmid was performed, as described by Johnson *et al.* (2013). Successful co-transformation was confirmed by agarose gel electrophoresis, shown in Figure 2.6. In lanes 2 and 3, containing the product of plasmid prep from *E.coli* cells transformed with either pET23a-ASYN or pNatB alone, three bands are seen, corresponding to the nicked, linear and supercoiled forms of the individual plasmids. Conversely in lane 4, containing the product of plasmid prep from *E. coli* cells transformed with both the pET23a-ASYN and the pNatB plasmids, six bands are present, corresponding to the nicked, linear and supercoiled forms of both plasmids. This demonstrates that the *E.coli* cells were successfully co-transformed with both plasmids.

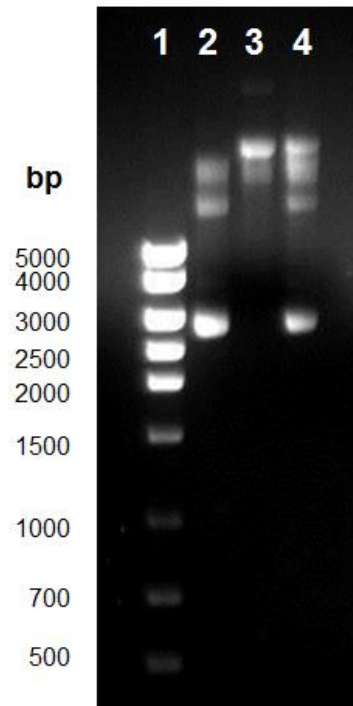


Figure 2.6: 1% Agarose gel electrophoresis of plasmid DNA purified from transformed E. coli cells. Agarose gels containing ethidium bromide for DNA visualisation used to analyse plasmids purified from transformed E. coli cells. Lane 1 contains DNA Ladder to aid DNA size estimation. Lane 2 contains the product of plasmid prep from E. coli cells transformed with pET23a-ASYN, lane 3 the product from E. coli cells transformed with pNatB and lane 4 the product from E. coli cells transformed with both pET23a-ASYN and pNatB.

2.4.3 Expression and purification of alpha-synuclein recombinant proteins

Unmodified and N-terminally acetylated forms of WT and H50Q alpha-synuclein were produced via transformation of *E.coli* with the appropriate plasmids, overexpression of the target protein via auto induction, and purification using column chromatography as described in Section 2.3.8. Typical chromatograms and SDS-PAGE results obtained from this purification process can be found in Appendix Figure 1. Following the purification procedure a single band corresponding to overexpressed alpha-synuclein is seen with no visible contaminants, demonstrating that the protein is suitably pure.

2.4.4 Mass spectrometry confirmation of successful protein production

In order to confirm modified and mutated forms of the alpha-synuclein protein had been produced, protein samples were analysed by ESI-MS to confirm they were of the expected mass. Example spectra of the +10 charge state ions are shown in Figure 2.7, with theoretical and experimental m/z shown in Table 2.3.

	Theoretical m/z	Experimental m/z
WT unmodified	1447.0114	1446.9948
H50Q unmodified	1446.1150	1446.1312
WT acetylated	1451.2197	1451.3160
H50Q acetylated	1450.3187	1450.3348

Table 2.3: Theoretical vs experimental m/z at the +10 charge state ion of recombinant alpha-synuclein proteins.

As shown in Table 2.3, all four proteins were found to be of the expected mass. The H50Q mutation resulted in a decrease in molecular mass of 9 Da (due to the substitution of a glutamine (146 Da) for a histidine (155 Da)) and N-terminal acetylation resulted in an increase in molecular mass of 42 Da (due to the replacement

of one of the hydrogens from the amine group with an acetyl group). Also observable in the spectra of acetylated proteins in Figure 2.7 is a peak of lower intensity corresponding to the non-acetylated protein, demonstrating that the acetylation process in our experimental set up was not 100% efficient. This is thought to be due to the pET23a-ASYN and pNatB plasmids making use of the same induction system, meaning they will both start being expressed at a similar time. Due to N-terminal acetylation being a co-translational modification this means that for the alpha-synuclein protein expressed early following induction may not have the NatB complex present to carry out the modification. An improved system utilising a sequential induction system with improved acetylation efficiency has recently been described (Eastwood *et al.*, 2017). Despite the acetylation procedure not being 100% efficient, the majority of the protein did undergo this modification. Therefore, MS results confirm that all four versions of the protein had been successfully produced.

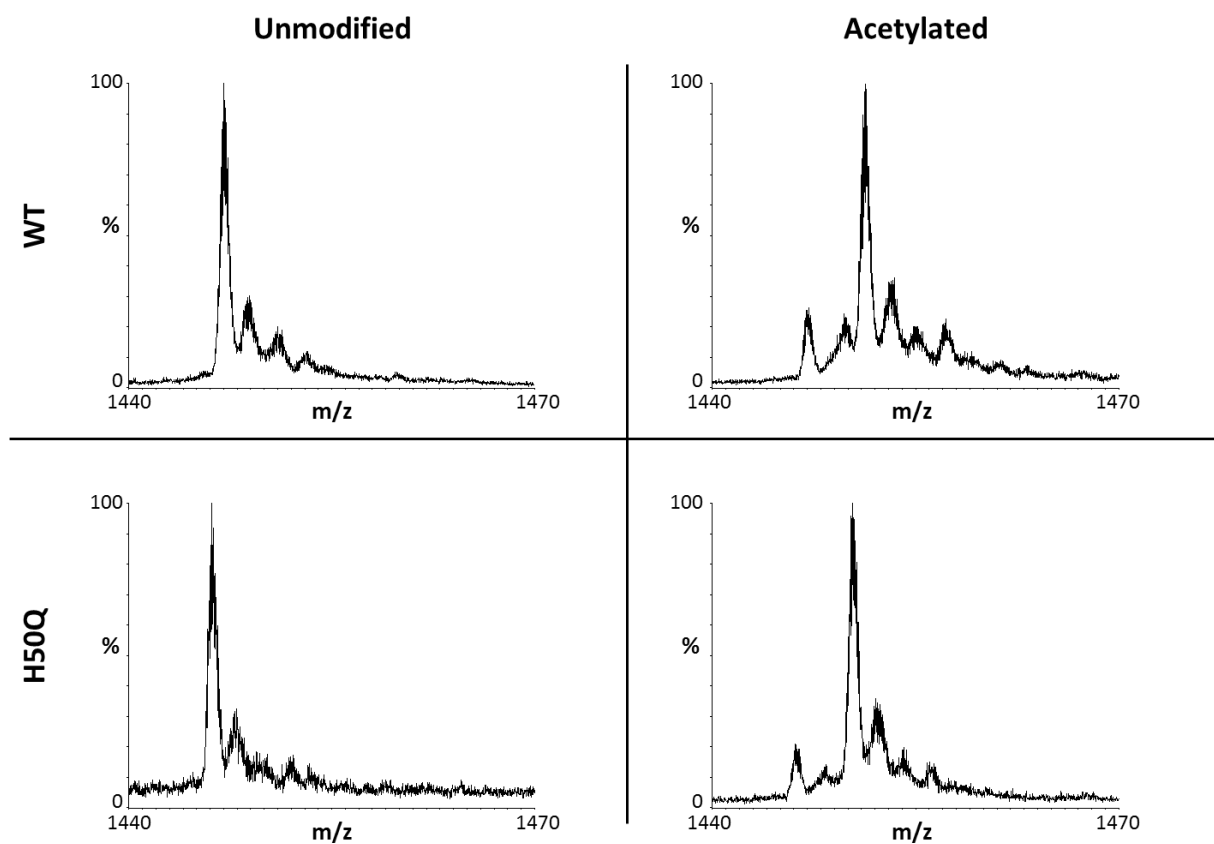


Figure 2.7: ESI-MS spectra of recombinant alpha-synuclein proteins. Representative spectra of the +10 charge state of unmodified and N-terminally acetylated WT and H50Q mutant alpha-synuclein, acquired in 50 mM ammonium acetate (pH 7) in positive ion mode, with the x-axis representing mass to charge ratio and the y-axis representing normalised relative intensity.

2.4.5 ESI-IMS-MS analysis of recombinant alpha-synuclein reveals a disordered protein with two distinct populations

Although alpha-synuclein is predominantly described as a natively unstructured protein, it is known to co-populate a range of conformational families under equilibrium, which have been investigated using ESI-IMS-MS by various groups (Bernstein *et al.*, 2004; Frimpong *et al.*, 2010; Natalello *et al.*, 2011b; Phillips *et al.*, 2015). Positive mode ESI-MS of the recombinant alpha-synuclein used in this thesis is indicative of an intrinsically disordered protein. As shown in Figure 2.8, the spectrum displays a wide CSD of monomeric alpha-synuclein of $+5 \leq z \leq +15$. As discussed in Section 1.4.1, a protein with a defined tertiary structure will typically display a narrow CSD, while a wider distribution of charge states, as seen here, is characteristic of a disordered protein. Also notable in the spectra is the presence of at least two major distinct populations of alpha-synuclein, with some degree of overlap. This bi-modal distribution consists of an extended conformational state (with corresponding high charge states) centred on the +11 ion and a compact conformational state (with corresponding lower charge states) centred on the +7 ion, shifted in favour of the extended conformational state. The presence of these two major conformational families is equivalent to those previously reported by our group (Illes-Toth *et al.*, 2013) and others (discussed in Section 1.4.4.1). Ion mobility analysis further supports the presence of two major distinct populations, shown in the drift scope plot in Figure 2.8. Here, two distinct populations can be distinguished; a primarily extended conformation between the +15 and +8 CSIs with longer drift times, and a more compact conformation between the +8 and +5 ions, with comparatively shorter drift times.

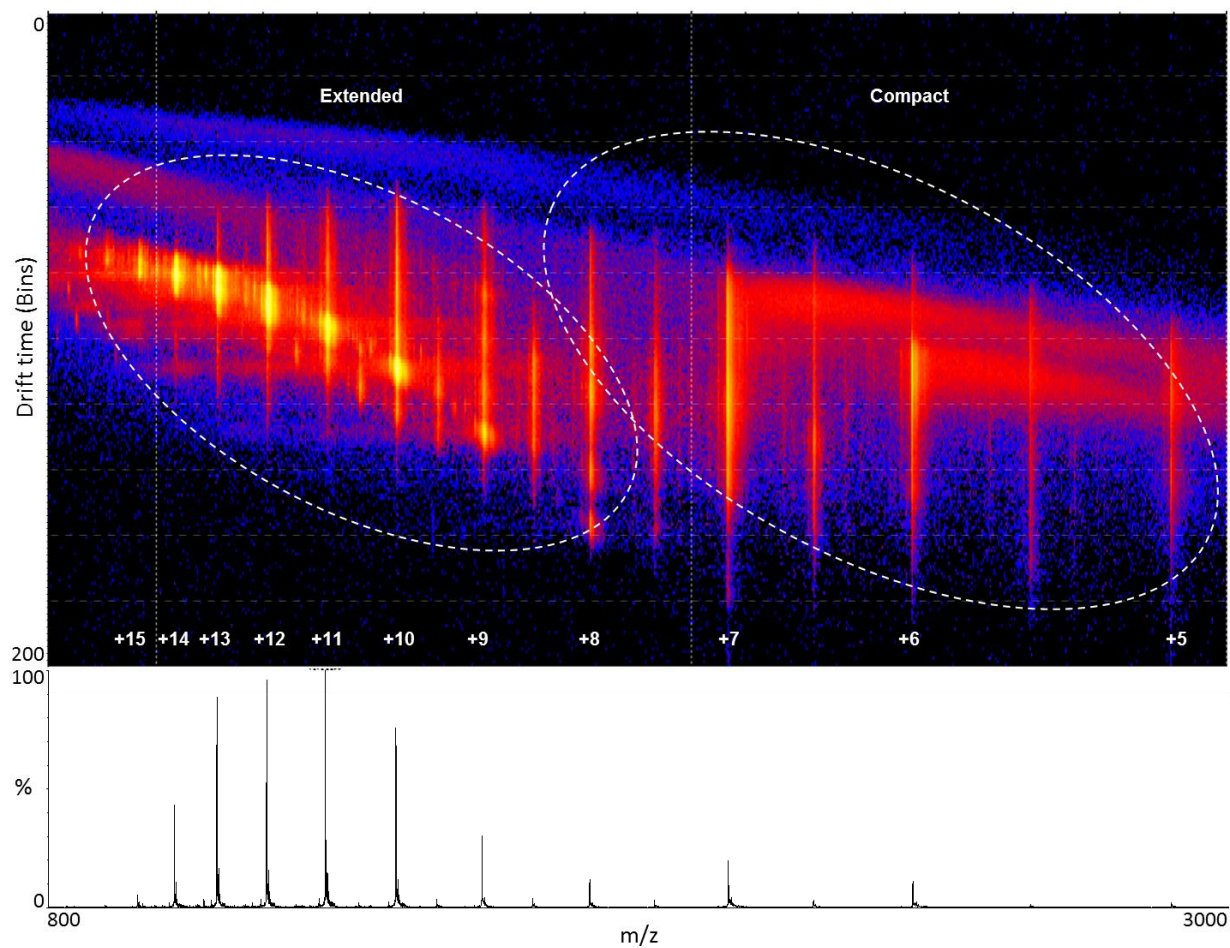


Figure 2.8: Drift scope plot and corresponding ESI-MS spectra of unmodified, WT alpha-synuclein. Representative drift scope plot and mass spectra of unmodified, WT alpha-synuclein, acquired in 50 mM ammonium acetate (pH 7) in positive ion mode.

2.4.6 Ion mobility analysis of recombinant alpha-synuclein reveals multiple conformations present at each charge state

In addition to the two major populations distinguishable in Figure 2.8, numerous conformational families, with multiple populations of both extended and compact conformations, can be observed on deeper analysis of the individual ATD of each CSI. Figure 2.9 (a) shows the ATDs extracted from each CSI and fitted to the minimum number of Gaussian distributions required to resolve the multiple conformations present. Drift time has been converted to Ω through calibration with standards of known Ω following the method described in Section 1.4.3.2. The calibration curve used for the conversion of drift time to Ω is shown in Figure 1.10, with the celebrants' used chosen to bracket the arrival times of all alpha-synuclein species identified under the experimental conditions used in this thesis. Figure 2.9 (b) shows the Ω value from the peak top of each resolvable conformational family, plotted against its respective z . In addition, theoretical values of alpha-synuclein modelled to a globular or all helical conformation (Bernstein *et al.*, 2004) have been superimposed onto the experimental data to aid in visualisation of the differing conformations.

A total of eight resolvable conformational families spanning a wide range of Ω were detected, which have been assigned a letter from A to H as outlined in Table 2.4, with A representing the most compact of the states and H the most extended. In the majority of cases each conformational family is seen across multiple CSIs, with a slight increase in Ω within the same conformational family observed as charge state increases, presumably as a result of Coulombic repulsion. A primarily extended population (F - H) is seen between the +8 and +15 charge state ions and a subpopulation of more compact conformations (A - E) seen predominantly between

the +5 and +9 charge state ions, with multiple overlapping features in both series. Ω ranged from the most compact value of 1339 Å² at the +5 CSI to the most extended of 3221 Å² at the +15 CSI. The most compact conformation corresponded to a predicted globular conformation and the most extended corresponded to the predicted random coil conformation. It can be seen that the various conformational families occupy Ω values throughout the full range between these theoretical values, demonstrating again the conformational heterogeneity of this protein.

	Conformational family	Chromatogram colour	CSI range	Average Ω
Compact  Extended	A	Yellow	+5	1339
	B	Green	+5 to +9	1681 ± 142
	C	Purple	+6 to +9	1930 ± 115
	D	Black	+7 to +12	2269 ± 118
	E	Red	+8 to +12	2511 ± 104
	F	Blue	+8 to +15	2749 ± 178
	G	Lilac	+11 to +15	2916 ± 167
	H	Orange	+13 to +15	3121 ± 91

Table 2.4: Lettering system of alpha-synuclein conformational families. Conformational families determined through Gaussian fitting of ATDs of each CSI from ESI-IMS-MS spectrum of 10 µM unmodified WT alpha-synuclein (50 mM ammonium acetate)

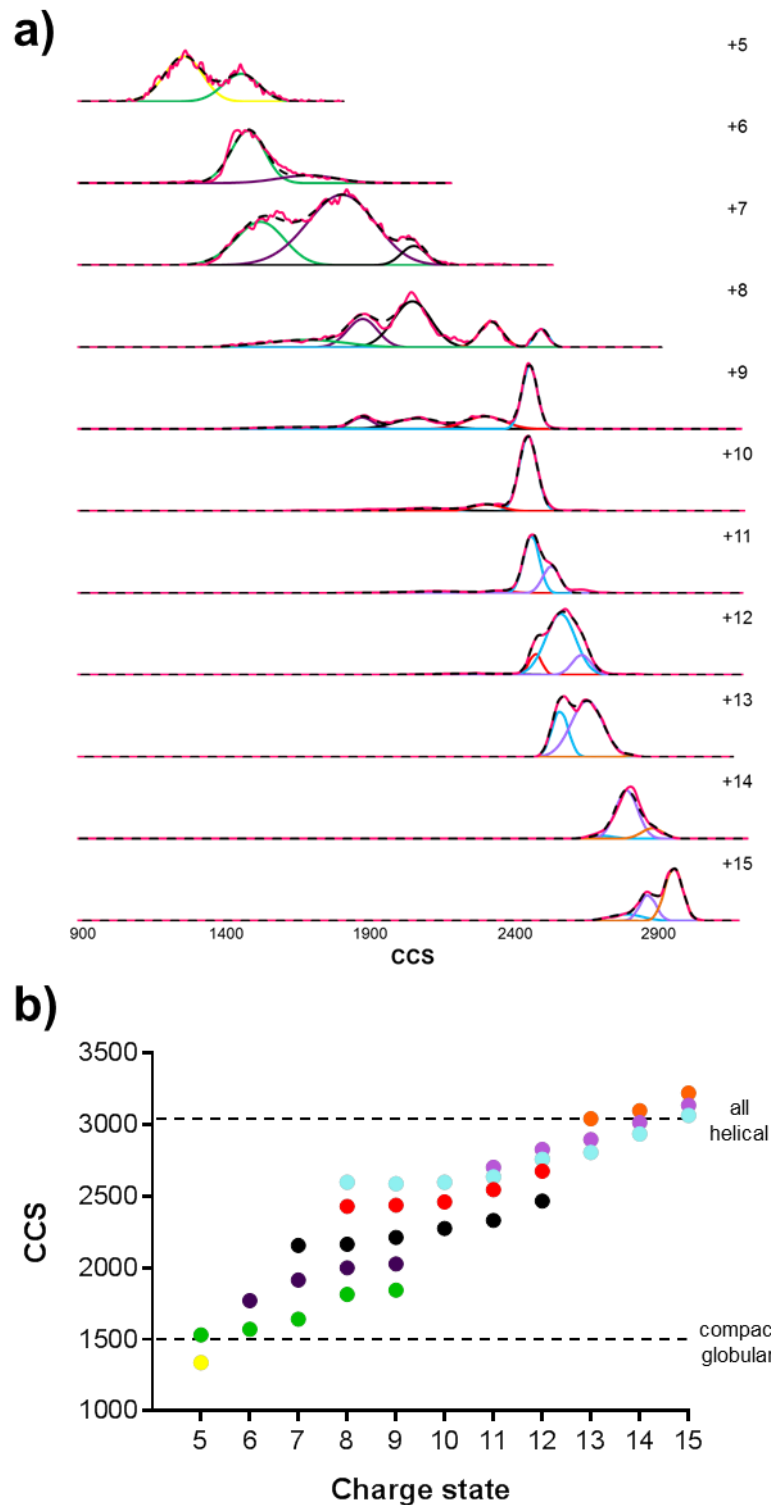


Figure 2.9: ATDs for each CSI of unmodified WT alpha-synuclein. (a) The peak area of each alternate population of differing Ω was calculated from Gaussian distributions. The raw ATD is displayed in pink and the sum of the fitted Gaussians is shown as a black broken line. (b) The peak top of resolvable conformational families as presented in (a) plotted against charge state, with dotted lines representing theoretical Ω calculated for structures having an all helical or compact globular structure, as reported by Bernstein *et al.* (2004).

2.4.7 Investigating the effect of N-terminal acetylation and H50Q mutation on alpha-synuclein conformation by ESI-IMS-MS

In order to address the effect of N-terminal acetylation and the H50Q mutation on alpha-synuclein conformation, these modified proteins were also analysed by ESI-IMS-MS, enabling comparison to the unmodified, WT protein. The driftscope plot and corresponding mass spectrum of each of the four proteins are shown in Figure 2.10. The spectra of all four versions of the protein are similar, with a CSD of $+5 \leq z \leq +15$, a bi-modal distribution centered on the +7 and +11/+12 CSI's, and a similar pattern of relative peak intensities. The driftscope plots are also similar, with two distinct populations being observed for each of the proteins.

When looking in detail at the eight conformational families described in Section 2.4.6, some slight differences are apparent. These differences are presented in Figure 2.11, a bar chart plotting the percentage population of protein attributed to each conformational family (A to H) at each CSI. The percentage population in differing conformational families at each CSI was obtained through Gaussian fitting of the ATD and calculation of the area under the curve for each resolvable conformation. The extracted driftscope plots and Gaussian fitting for each individual protein can be seen in Appendix Figure 2. While a degree of variability is to be expected, there are some notable differences between the WT and H50Q proteins in the percentage of protein populating each family at the +15 CSI. This CSI contains three resolvable conformations, F, G and H. The proportion of protein in the most extended state (H) is lower in the H50Q mutants than the WT proteins. Conversely the percentage of protein in the less extended states (F and G) is higher in the H50Q mutants than the WT proteins. These differences are summarised in Table 2.5.

	WT		H50Q	
	Unmodified	Acetylated	Unmodified	Acetylated
F	14%	13%	25%	19%
G	26%	34%	59%	79%
H	60%	53%	16%	2%

Table 2.5: The percentage population of protein at the +15 CSI in each conformational family, calculated from the area under the fitted curves shown in Appendix Figure 2.

These results suggest that, compared to unmodified WT alpha-synuclein, neither N-terminal acetylation nor the H50Q mutation result in significant changes in CSD, conformational families, Ω s or abundance of each CSI. This demonstrates that the unbound metal free conformational states of these proteins are largely comparable, and therefore the introduction of the point mutation and modification has not altered the gross gas phase conformation of this protein. However, some slight differences were observed in the proportion of protein in each conformational family at specific CSIs.

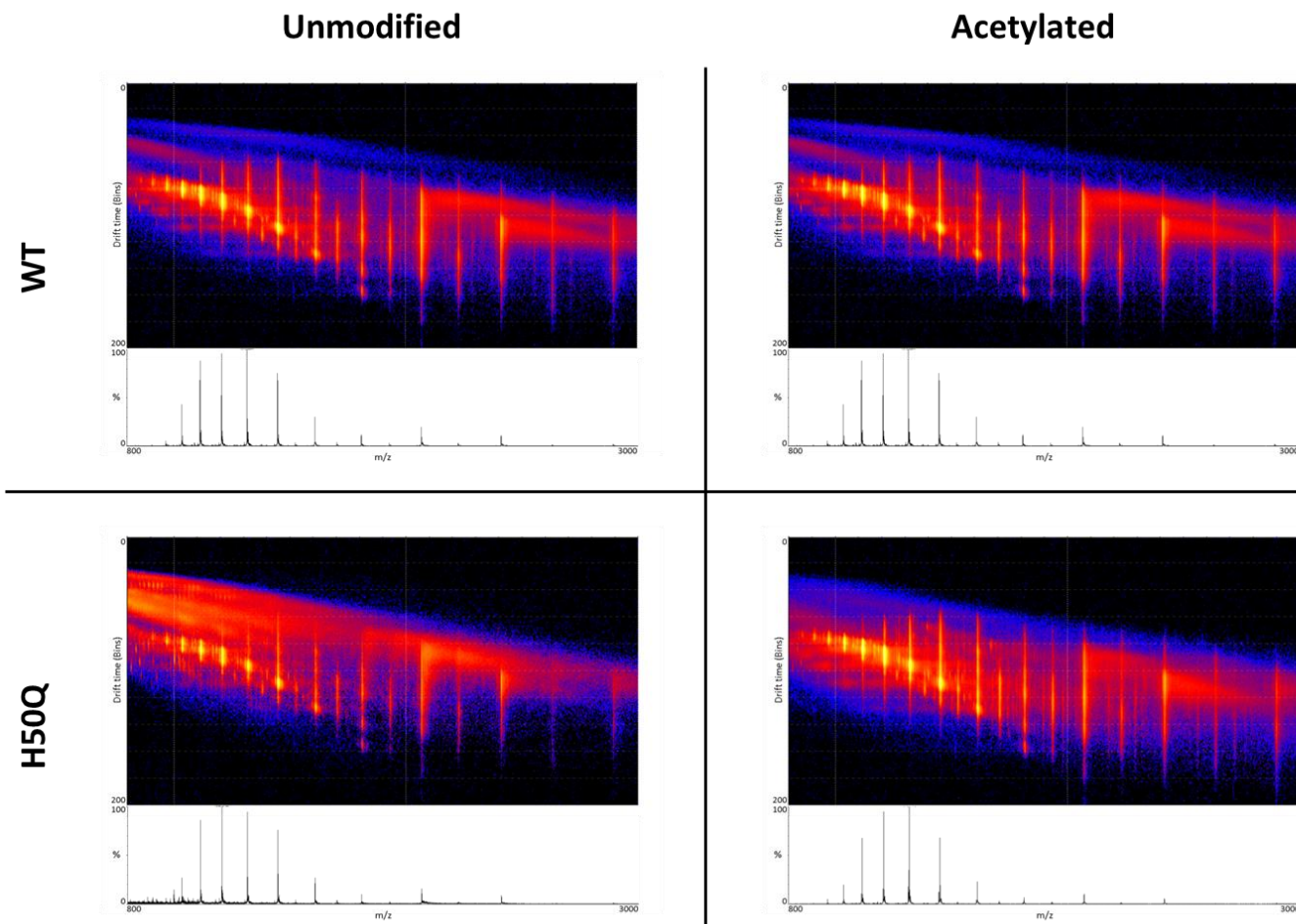


Figure 2.10: Driftscope plot and overlaid mass spectrum of each of the four proteins. Driftscope plot/spectra obtained from 50 mM ammonium acetate (pH 7) solution of 10 μ M unmodified, acetylated, H50Q and acetylated H50Q alpha-synuclein in positive ion mode.

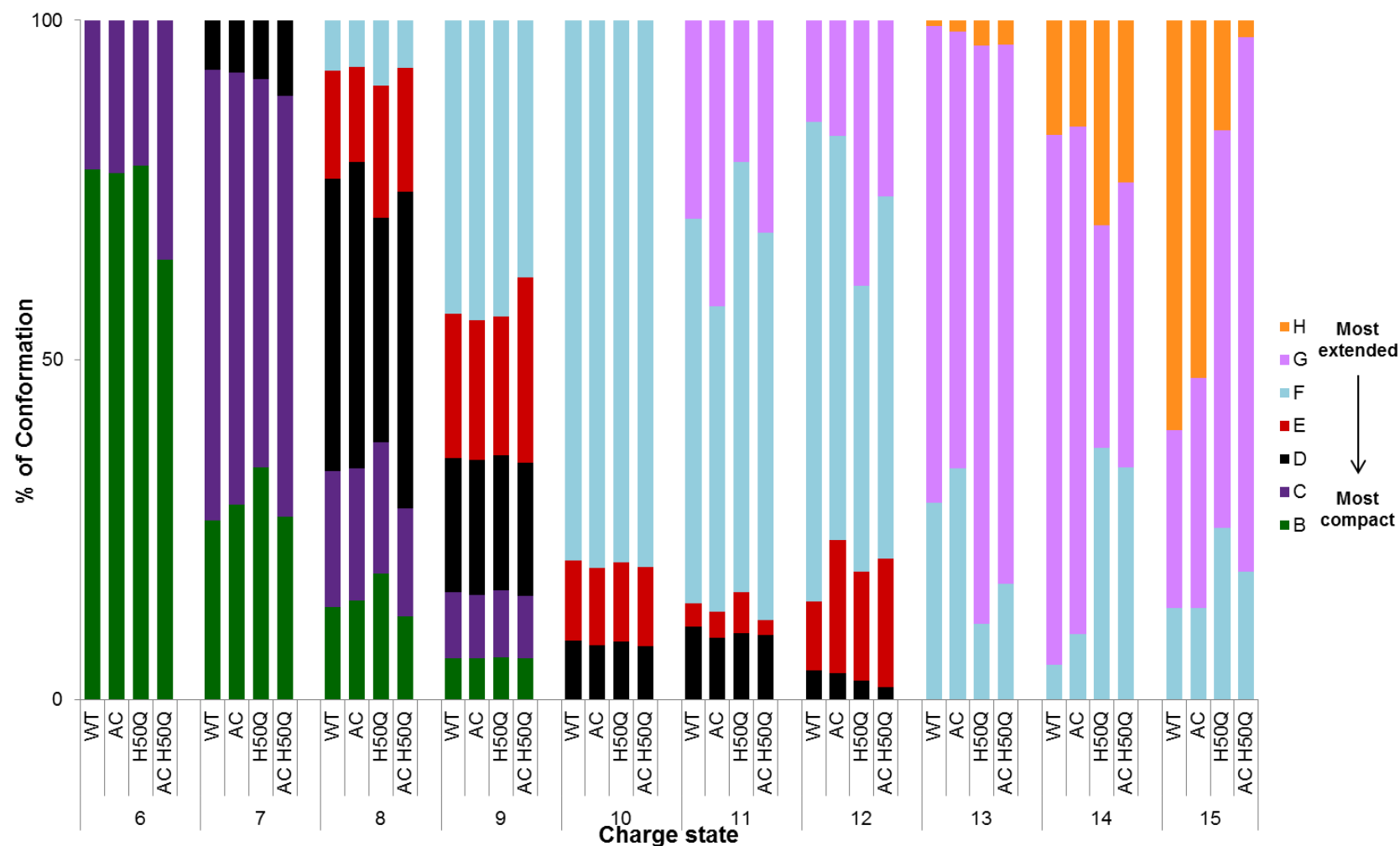


Figure 2.11: Bar chart showing the percentage conformation of protein in each conformational family at each CSI. Percentage in each conformation calculated through fitting the ATD of 10 μ M unmodified and acetylated WT and H50Q alpha-synuclein (50 mM ammonium acetate (pH 7)) of each CSI to the minimum number of Gaussians and calculating the area under the curve.

2.4.8 Copper binding to alpha-synuclein is observed by ESI-MS

As discussed in Section 2.1.3.1, alpha-synuclein is known to be a copper binding protein (Binolfi *et al.*, 2010; De Ricco *et al.*, 2015). However, while techniques such as NMR and electron paramagnetic resonance allow the detection of copper binding, they do not allow the detection of conformational change to specific protein species in the detail achieved by ESI-IMS-MS. To determine the degree of Cu²⁺ binding to alpha-synuclein, mass spectra were acquired at a 1:1 protein to metal ratio, immediately upon the addition of CuCl₂.

Figure 2.12 shows the ESI spectra of the +10 CSI of alpha-synuclein, alone and in the presence of equimolar CuCl₂. It is clear that alpha-synuclein is binding to copper, with an increase in mass equivalent to the addition of one or two copper ions (an increase of the overall mass of 61.5 Da per copper bound, given that each ion repels two protons from the protein to conserve charge) being detected. Virtually the entire population of monomeric alpha-synuclein can be seen to bind to copper, with the majority of the protein found bound to one ion and a smaller proportion bound to two. This pattern of binding is seen across all charge state of the protein, demonstrating that all CSIs, and hence conformational states, of monomeric alpha-synuclein are able to bind to copper (shown in Figure 2.17).

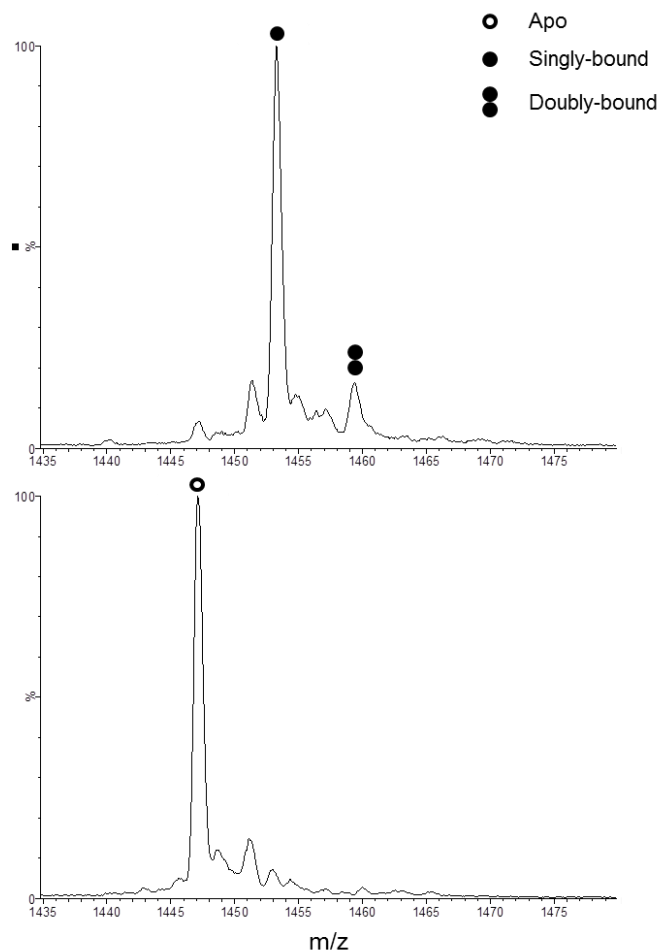


Figure 2.12: Spectra of the +10 CSI of unmodified, WT alpha-synuclein alone and in the presence of equimolar Cu²⁺. Spectra acquired at a protein concentration of 10 μ M with a CuCl₂ ratios of 1:0 and 1:1. The x axis represents m/z and the y axis represents relative abundance.

The CSD of alpha-synuclein alone or in the presence of equimolar copper is shown in Figure 2.13. Here, a change in CSD can be seen, with a broadening from the $+5 \leq z \leq +15$ seen in the absence of copper to $+5 \leq z \leq +17$ in the presence of copper. The most abundant ion also differs, from the +11 CSI in the absence of copper to the +13 CSI in the presence of copper. This would indicate an alteration in the conformation distribution on metal binding, with higher CSIs, and therefore more extended forms of the protein, being observed in the presence of copper.

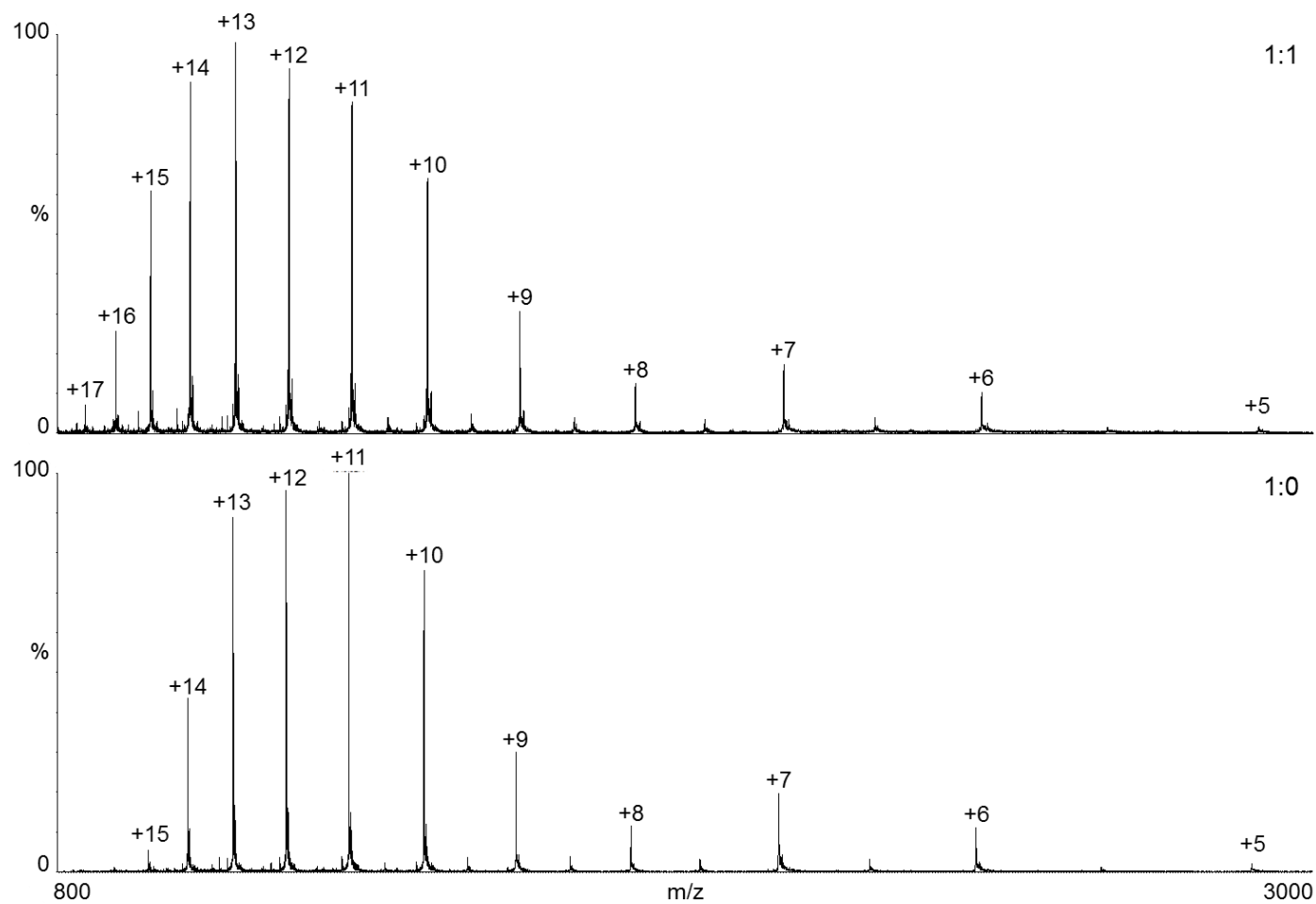


Figure 2.13: CSD of unmodified recombinant α -synuclein alone (bottom) and in the presence of equimolar Cu^{2+} (top). Spectra acquired at a protein concentration of $10 \mu\text{M}$ with a CuCl_2 ratios of 1:0 and 1:1. The x axis represents m/z and the y axis represents relative abundance.

2.4.9 Copper binding to alpha-synuclein results in altered populations of conformations detectable by ESI-IMS-MS

Compact conformations of alpha-synuclein are known to be aggregation prone, and the equilibrium of conformations can be shifted towards compact states under certain conditions. Polyvalent metal ions have the propensity to shift the conformational equilibrium and trigger structural rearrangements (Santner and Uversky, 2010). Ion-mobility spectra were acquired in order to investigate changes in alpha-synuclein conformations that occur upon Cu^{2+} binding.

Figure 2.14 shows the ATD of each CSI of alpha-synuclein alone (a) or bound to one copper ion (b). It can be seen that the same conformational families (A-H) are present in both the apo- and holo- conditions, demonstrating that binding of a copper ion does not result in monomeric alpha-synuclein adopting any new conformations detectable by this method. However, what can be noted is the proportion of protein populating these conformations being altered upon copper binding. A shift to the more compact conformations of the protein can be seen at the majority of CSIs, most notably at +7, +8, +9, +14 and +15. Figure 2.15 summarises these data, showing the percentage population of protein in each conformational family at all CSIs, for alpha-synuclein alone or bound to 1 or 2 copper ions. A clear pattern of an increase in the more compact conformations at each charge state can be seen. The data also demonstrates that alpha-synuclein bound to two copper ions undergoes a greater conformational shift than the protein bound to one copper ion or the apo protein. As an example, the +10 CSI contains 3 conformations: D, E and F, which occupy 9%, 12% and 79% of the protein at the CSI respectively. Upon binding to copper the proportion of protein in the most compact of these three conformations, D, increases to 24% when one copper ion

is bound and further to 30% when two copper ions are bound. On the contrary, the proportion of protein in the most extended conformation at this CSI, F, decreases to 58% when one copper ion is bound and further to 47% when two copper ions are bound. This demonstrates that, compared to the unbound protein, a greater proportion of the protein is in a compact conformation at these CSIs when copper is bound.

Also of note are the CSIs detectable in the presence (but not the absence) of copper at +16 and +17 (shown in Figure 2.14). The conformations detected at these CSIs do not represent new conformations of the protein, but rather a continuation of the most extended conformational families present in the unbound spectra, F, G and H.

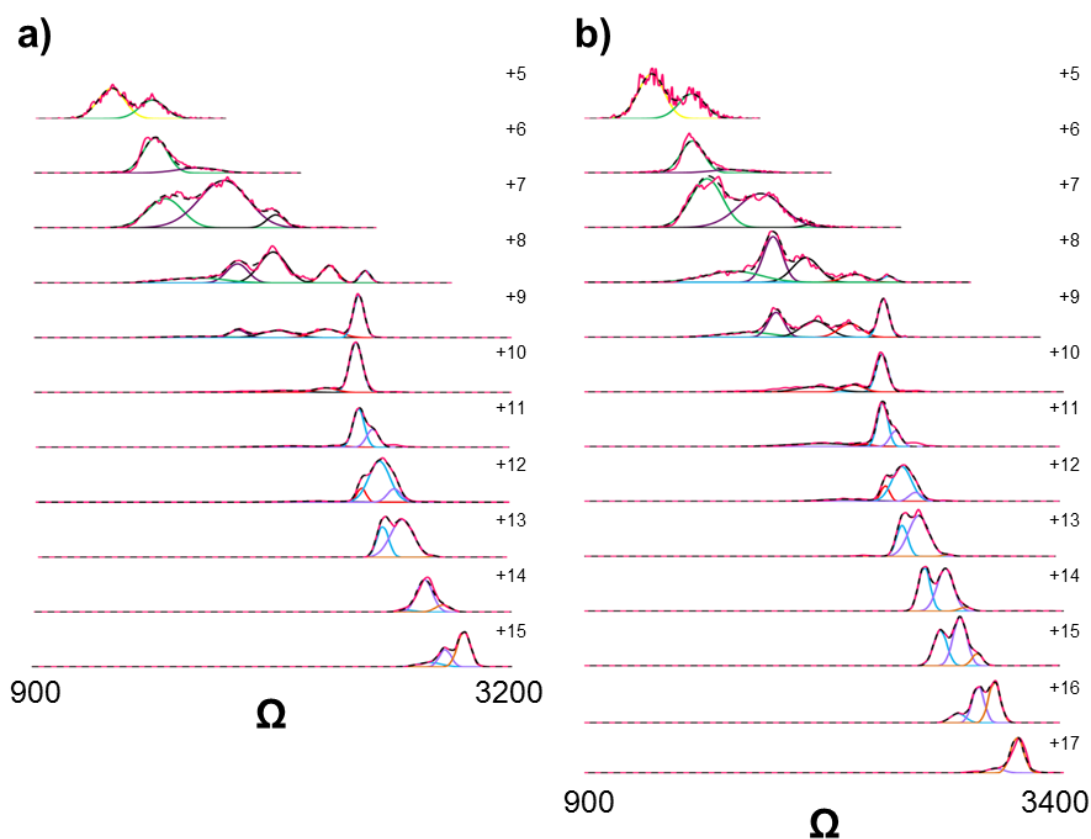


Figure 2.14: ATDs for each charge state ion of unmodified WT alpha-synuclein in the absence and presence of equimolar copper. The peak area of each alternate population of differing Ω was calculated from Gaussian distributions using a least square fitting method. Spectra were acquired at protein to CuCl_2 ratios of 1:0 (a) and 1:1 (b) in 50 mM ammonium acetate. The x axis represents Ω values and the y axis represents relative abundance at each charge state.

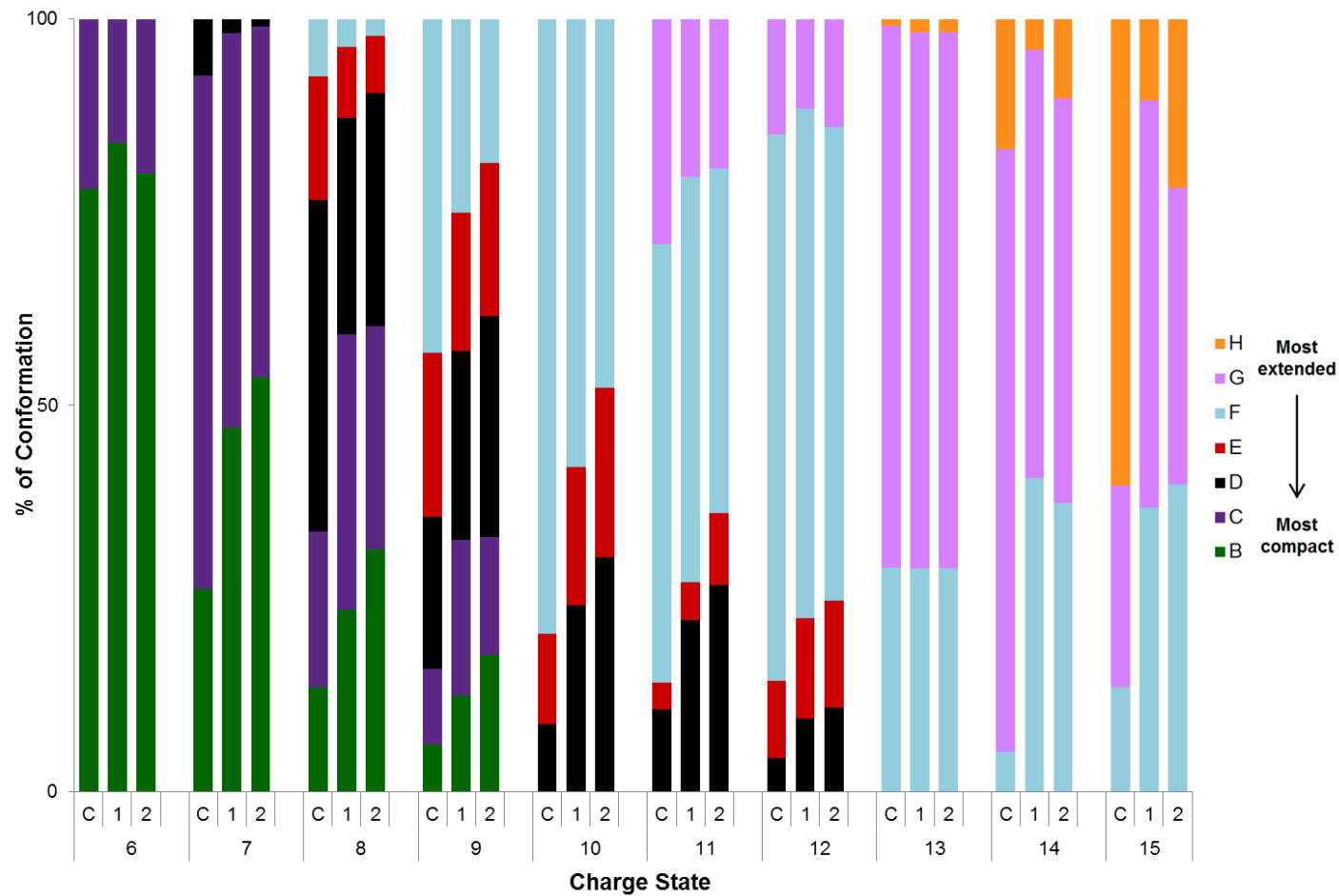


Figure 2.15: Bar chart showing the percentage conformation of apo (c) and copper bound (1 & 2) unmodified, WT alpha-synuclein in each conformational family at each CSI. Percentage in each conformation calculated through fitting the ATD of 10 μ M unmodified WT alpha-synuclein (with and without equimolar copper) of each CSI to the minimum number of Gaussians and calculating the area under the curve.

2.4.10 Copper binding to alpha-synuclein increases the rate of protein aggregation

As discussed in Section 1.3.3, alpha-synuclein is a protein which can aggregate into amyloid fibrils, and certain environmental conditions, including the presence of various metals, are known to alter the rate of aggregation. It is thought that one or more species of alpha-synuclein that arises during the aggregation pathway may be the toxic form of the protein, and conditions which increase aggregation rate are known to be associated with incidence of PD (Manning-Bog *et al.*, 2002; Munishkina, Fink and Uversky, 2009). The aggregation propensity of alpha-synuclein in the presence and absence of Cu^{2+} was investigated using ThT fluorescence, a conventional method used to probe the emergence of beta-sheet rich protein structures on the amyloid fibril forming pathway (LeVine, 1999). ThT is used to monitor *in vitro* amyloid fibril formation as upon binding to amyloid fibrils it emits a strong fluorescence signal at approximately 482 nm when excited at 450 nm (Naiki *et al.*, 1989).

Results are displayed in Figure 2.16, with individual traces of five replicate aggregation experiments shown in (a) and the median and standard deviation aggregation lag time of the repeats shown in (b). Lag time was determined by calculating the intercept between the maximum derivative and the pre-transitional base line as described in Figure 2.4. When alpha-synuclein was incubated in the presence of copper, the lag time was significantly decreased from a lag time of 677 minutes for alpha-synuclein incubated alone to a lag time of 323 minutes in the presence of copper, indicating that material rich in beta-sheet material was being formed at an earlier time point. These results demonstrate that Cu^{2+} increases the rate at which unmodified, WT alpha-synuclein forms amyloid fibrils.

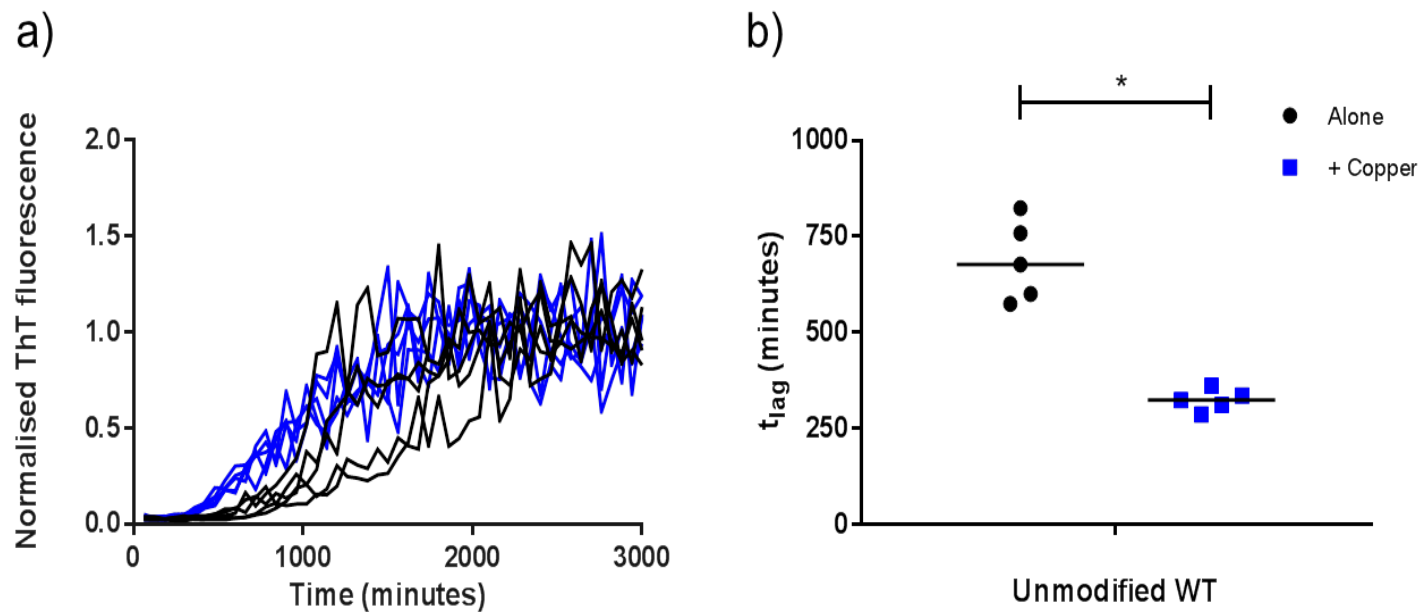


Figure 2.16: Copper induced aggregation of alpha-synuclein as monitored by Thioflavin T fluorescence. Alpha-synuclein was incubated at 70 μ M alone (black) or in the presence of equimolar CuCl₂ (blue) and aggregation monitored by ThT fluorescence assay. Shown in (a) are the individual traces of 5 replicates experiments for each condition. Shown in (b) is the calculated median of these replicates. Statistical significance determined by the Kruskal–Wallis with Conover–Inman post hoc analysis test ($P < 0.05$).

2.4.11 Copper binding to alpha-synuclein is altered by N-terminal acetylation and H50Q mutation

Once the pattern of copper binding to unmodified, WT alpha-synuclein and subsequent conformational change and aggregation propensity had been established, the effect of N-terminal acetylation and H50Q mutation on these factors was investigated. To determine the degree of Cu^{2+} binding to the modified and mutated proteins, ESI-MS mass spectra were again acquired at a 1:1 protein to metal ratio immediately upon the addition of CuCl_2 . Figure 2.17 shows resulting spectra for the +6 to the +14 charge state ions of all 4 proteins in the absence and presence of equimolar CuCl_2 .

As shown in the spectra in Figure 2.17, in contrast to the unmodified protein, in the presence of equimolar Cu^{2+} the majority of N-terminally acetylated alpha-synuclein remained in its apo form with this being the base peak in the spectra of each CSI. The N-terminally acetylated protein does bind to copper, with peaks of lower intensity being present corresponding to the protein being bound to either one or two copper ions. These results in agreement with previous studies (Moriarty *et al.*, 2014) indicate that acetylation reduces the ability of alpha-synuclein to bind Cu^{2+} , likely as a result of the high-affinity N-terminal copper binding site becoming inaccessible upon acetylation.

In agreement with previous studies (Davies *et al.*, 2011), it was found that the unmodified H50Q mutant protein (i.e. the non-acetylated version of H50Q alpha-synuclein) displayed no alterations in binding of Cu^{2+} by ESI-MS. As with the unmodified WT protein, the base peak at every CSI of the protein corresponded to the

binding of one copper ion and the entire population of monomeric H50Q alpha-synuclein was found bound to either one or two copper ions. The lack of alterations seen with this protein implies that the H50Q mutation does not hinder copper binding, indicating that the H50 residue does not play a prominent role in copper binding to the unmodified protein under the conditions investigated here.

In contrast, the previously unstudied N-terminally acetylated H50Q mutant showed greatly impaired copper binding, with only a negligible proportion of protein binding to one Cu^{2+} ion, and the vast majority remaining in its unbound form. This can clearly be seen at every CSI shown in Figure 2.17. This indicates that, although the histidine at residue 50 does not appear to play a prominent role in copper binding to the unmodified protein, it does play a major role in copper binding to the acetylated H50Q mutant. This novel finding is of great interest, as in PD families with the H50Q mutation the N-terminally acetylated H50Q mutant would be the form found *in vivo*. Therefore the data presented here implies that the form of alpha-synuclein found in these PD patients would have greatly impaired ability to bind to copper.

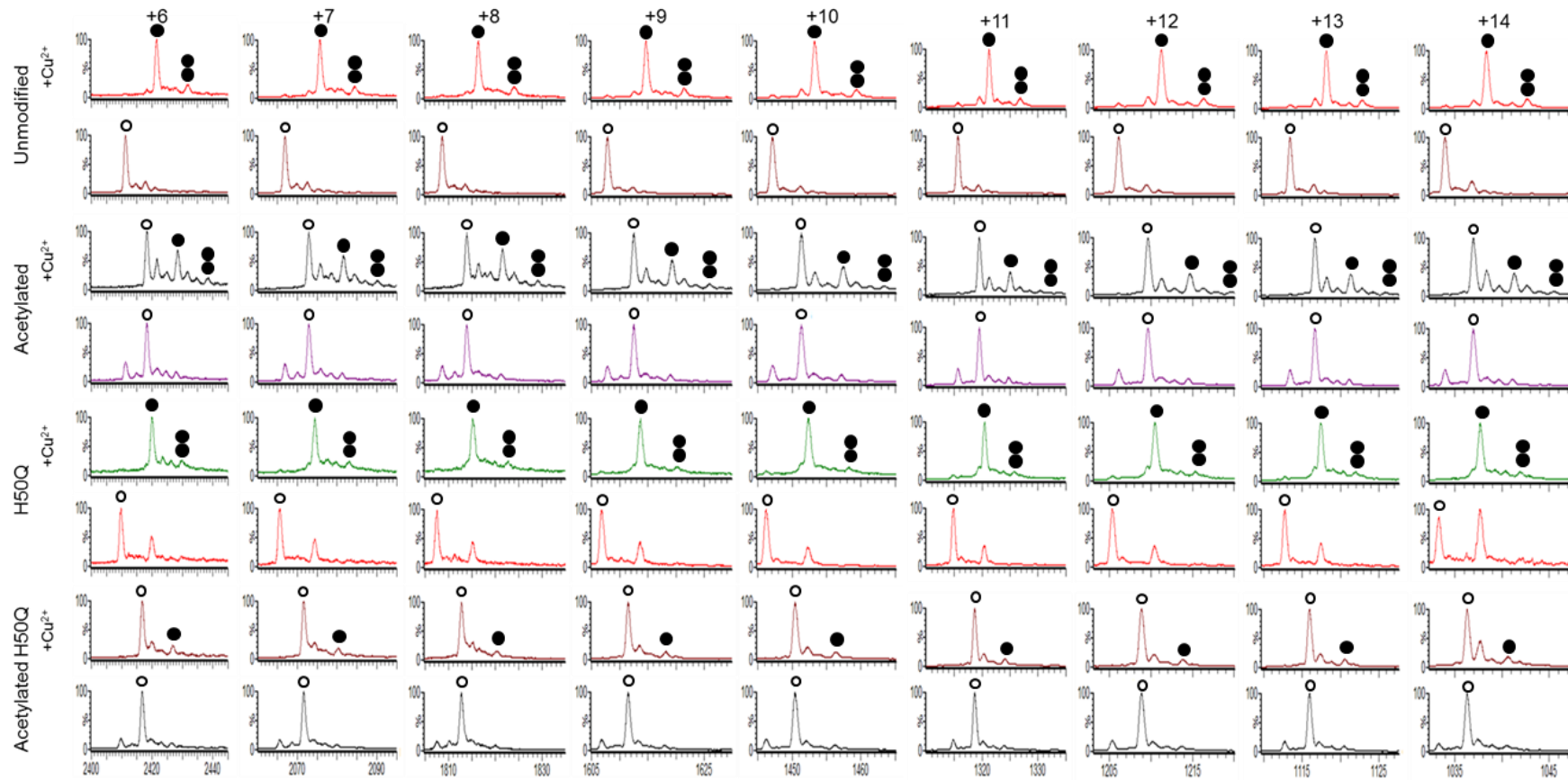


Figure 2.17: Alpha-synuclein spectra in the absence and presence of equimolar Cu^{2+} . Binding of Cu^{2+} to unmodified and acetylated WT and H50Q alpha-synuclein at the +6 to +14 CSIs. Spectra were acquired at protein to CuCl_2 ratios of 1:0 and 1:1 in 50 mM ammonium acetate (pH 7). The x axis represents m/z values and the y axis represents relative abundance.

2.4.12 Addressing the effect of N-terminal acetylation and H50Q

mutation on copper induced conformational change to alpha-synuclein

In order to investigate the effect of N-terminal acetylation and H50Q mutation on the conformational changes which occur following copper binding, IMS experiments were performed. ATDs were extracted for each CSI of unmodified and N-terminally acetylated WT and H50Q alpha-synuclein, in the presence and absence of equimolar Cu^{2+} . The data were converted to Ω and fitted to the minimum number of Gaussian distributions. The area under each curve was then used to gain estimates of the population of each conformational state. Results are presented in summarised form in Figure 2.18, a bar chart plotting the percentage population of protein attributed to each conformational family (A to H) at each CSI. The Gaussian fitting of the extracted ATDs used for the production of Figure 2.18 can be seen in Appendix Figure 2.

The copper induced conformational change to the unmodified WT protein is as shown previously in Figure 2.15, with an overall shift to the more compact conformational families seen across the majority of CSIs. In the case of the N-terminally acetylated WT alpha-synuclein, it can be seen that the unbound form of the protein (in the presence of copper) does not undergo any notable conformational changes compared to the protein in the absence of copper, indicating that the majority of the acetylated protein is indeed unable to interact with the copper. The N-terminally acetylated WT protein which is bound to copper undergoes similar conformational change to the unmodified protein, with an increase in protein occupying the more compact conformations seen at the majority of CSIs. However at some of the higher CSIs the opposite affect is seen, with an increase in the more extended conformational families being observed which is particularly evident at the +13 and +14 CSIs in Figure 2.18. This demonstrates that

acetylation is not only altering alpha-synuclein's affinity for copper, but also altering the conformational changes which occur when copper is bound.

The unmodified H50Q mutant form of the protein displays a pattern of conformational change similar to that of the unmodified WT protein. This would indicate in the absence of acetylation H50 is not required for binding and the conformational changes which occur as a result of this. A significant proportion of acetylated H50Q alpha-synuclein was unable to bind to copper and hence no conformational changes occurred with this protein when copper is present in solution.

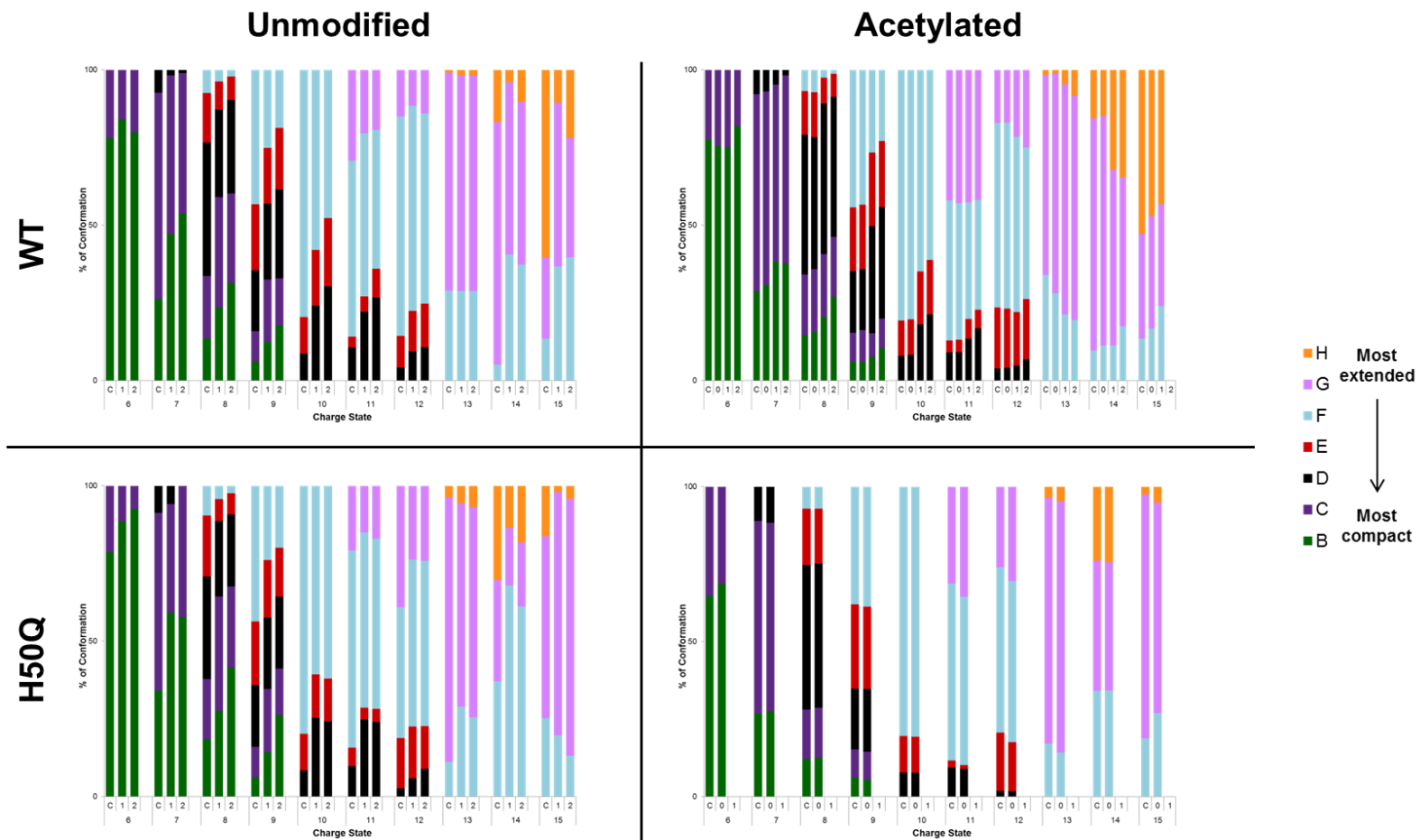


Figure 2.18: Bar chart showing the percentage conformation of apo (c) and copper bound (1 & 2) unmodified and acetylated WT and H50Q alpha-synuclein in each conformational family at each CSI. Percentage in each conformation calculated through fitting the ATD of 10 μ M unmodified WT alpha-synuclein (with and without equimolar copper) of each CSI to the minimum number of Gaussians and calculating the area under the curve.

2.4.13 Addressing the effect of N-terminal acetylation and H50Q mutation on copper induced aggregation of alpha-synuclein by Thioflavin T fluorescence

The effect of acetylation and the H50Q mutation on alpha-synuclein aggregation propensity, in the presence and absence of Cu^{2+} , was investigated using Thioflavin-T fluorescence as shown in Figure 2.19.

In agreement with previous reports (Kang *et al.*, 2012) it was found that the N-terminally acetylated WT alpha-synuclein had an increased average lag time ($t_{\text{lag}} = 886$ minutes) compared to that of the unmodified WT protein ($t_{\text{lag}} = 677$ minutes). Therefore acetylation of the protein reduces its tendency to aggregate. The H50Q mutant displayed a higher aggregation propensity than the WT protein, with a reduced average lag time of 228 minutes, which again has been reported in the literature (Khalaf *et al.*, 2014). This lag time was further reduced with the addition of Cu^{2+} ($t_{\text{lag}} = 159$ minutes). The previously unstudied N-terminally acetylated H50Q mutant displayed the same increased aggregation propensity as the unmodified H50Q mutant ($t_{\text{lag}} = 181$ minutes), but in this case no further decrease in lag time was observed upon the addition of Cu^{2+} ($t_{\text{lag}} = 186$ minutes). This is consistent with the impaired Cu^{2+} binding and lack of conformational change seen with this protein by ESI-IMS-MS.

Hence, N-terminal acetylation decreases and the H50Q mutation increases the intrinsic rate of aggregation of alpha-synuclein. This aggregation rate is increased by the presence of copper, with the exception of the acetylated H50Q mutant, where copper binding is ablated and therefore no further increase in aggregation is observed.

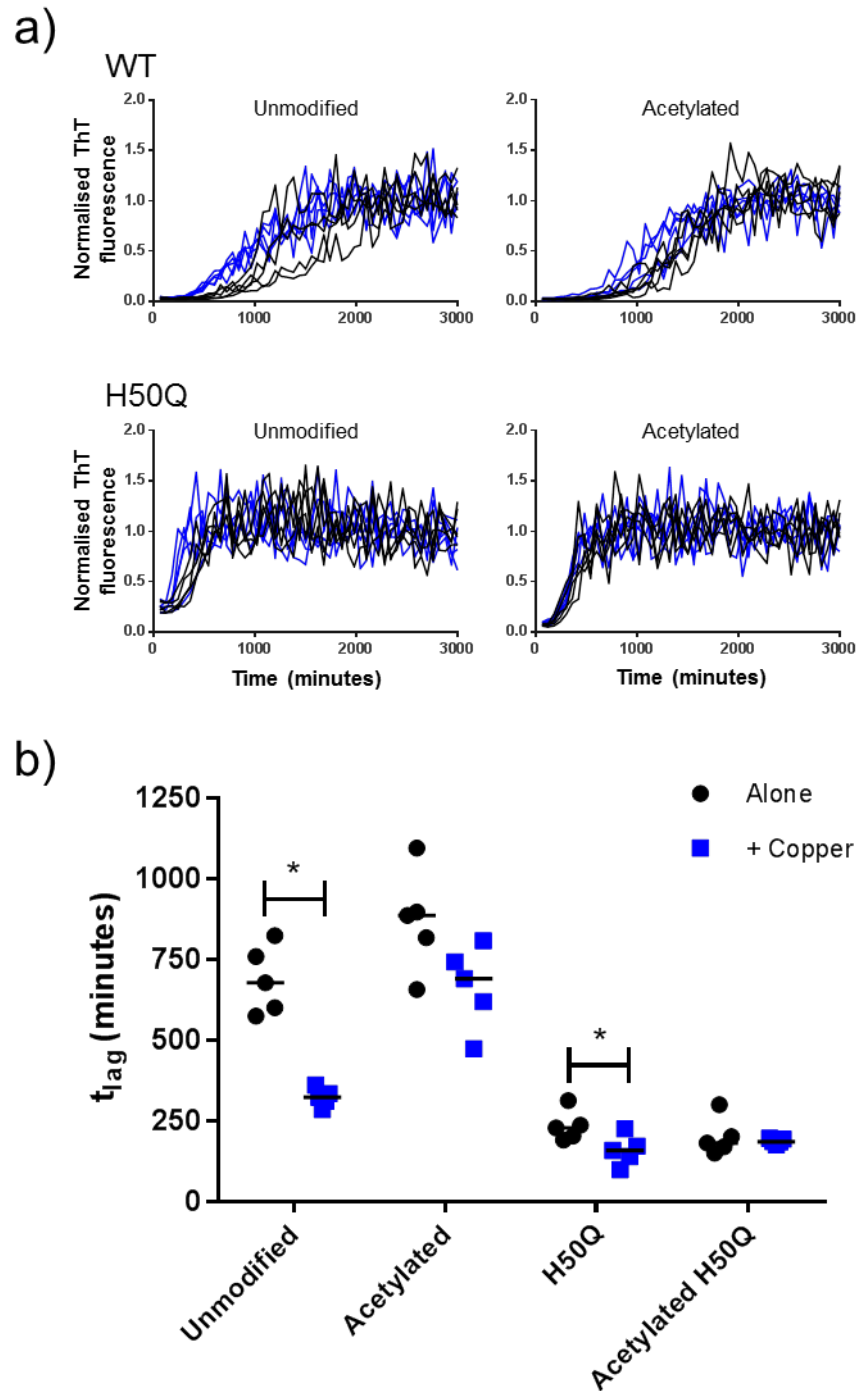


Figure 2.19: Copper induced aggregation of modified and mutated alpha-synuclein as monitored by Thioflavin T. Alpha-synuclein was incubated at 70 μ M alone (black) or in the presence of equimolar CuCl_2 (blue). Statistical significance determined by the Kruskal–Wallis with Conover–Inman post hoc analysis test ($P \leq 0.05$).

2.5 Conclusions and future work

The aim of this chapter was to ascertain whether N-terminal acetylation or H50Q mutation of alpha-synuclein resulted in alterations to, firstly, the conformation of the protein, and secondly, the copper binding and subsequent changes in conformation and aggregation propensity. To facilitate these investigations, N-terminal acetylation of recombinant alpha-synuclein was achieved through co-transformation and H50Q mutation was achieved through site directed mutagenesis. Resulting proteins were then investigated via ESI-MS, IMS and ThT fluorescence.

Results presented in this chapter demonstrate that the alpha-synuclein monomer presents as a heterogeneous, dynamic protein; existing simultaneously in a number of conformational states. This is evidenced in both its wide, bi-modal CSD and the multiple conformational families co-populating each CSI. These findings are in keeping with previous investigations utilising ESI-IMS-MS in the study of alpha-synuclein, as discussed in detail in Section 1.4.4.1.

In comparison to the unmodified, WT protein, neither N-terminal acetylation nor H50Q mutation appeared to significantly alter the overall conformation of alpha-synuclein. However some slight differences were observed in the percentage of protein populating the most extended conformational family, H. The H50Q mutants (both unmodified and N-terminally acetylated) displayed a reduced proportion of protein in this most extended conformation at the +15 CSI compared to their WT counterparts. It would be of interest to investigate other familial PD mutants known to alter alpha-synuclein aggregation, to see if a common pattern emerges.

The copper binding characteristics of unmodified, WT alpha-synuclein under our experimental set up was first established to allow comparison of the modified proteins. It was seen that at a 1:1 ratio of protein to Cu^{2+} , the entire population of alpha-synuclein monomer bound to either 1 or 2 copper ions, demonstrating a high affinity for this metal. Binding was seen across all CSIs, in agreement with alpha-synuclein peptide binding studies (Brown, 2009). These results indicate that initial Cu^{2+} binding is determined at the primary structural level, as the extended, disordered state was capable of binding Cu^{2+} ions without a pronounced conformational change.

ESI-IMS-MS data presented here provides evidence for two concurrent events occurring when alpha-synuclein binds to copper. The first is a shift to more compact forms of the protein, which is evident when looking at the ATDs of individual CSIs. This result is in agreement with previous reports of the protein shifting to a partially folded conformation in the presence of this metal, which is thought to be associated with an increased tendency to aggregate (Natalello *et al.*, 2011b). The second observation is the somewhat contradictory finding of an increased CSD in the presence of copper, with an increase in the higher CSIs in particular. This suggests an increase in extended forms of alpha-synuclein upon copper binding, which has recently been reported in the literature by Ranjan *et al.* (2017), who found a resultant destabilisation of long-range tertiary interactions of alpha-synuclein, exposing the highly amyloidogenic NAC region, with a resultant increase in the rate of fibril formation.

N-terminal acetylation of alpha-synuclein reduced copper binding ability, with the majority of the protein remaining in an unbound state. This is in agreement with previous studies (Moriarty *et al.*, 2014), and is not surprising when taking into account that the initiating methionine residue which is altered upon N-terminal acetylation is a

key anchor of alpha-synuclein highest affinity copper binding site. The H50Q mutant was found to have the same copper binding affinity as the WT protein, with the entire monomeric population binding to either 1 or 2 copper ions. This is in contrast to what would be anticipated from the loss of the histidine residue, which is involved in the second highest affinity main copper binding site, but is in agreement with previous studies on the topic (Davies *et al.*, 2011). Lastly, the previously unstudied N-terminally acetylated H50Q mutant was investigated. Here it was found that copper binding was drastically impaired, with virtually all of the protein remaining unbound in the presence of copper. This result suggests that in the unmodified H50Q mutant the N-terminus site is largely responsible for the copper binding seen here by ESI-MS.

In vivo the N-terminus of alpha-synuclein is known to be acetylated; this implies that the familial H50Q mutation would result in impaired copper binding. This finding is of great importance if the ability of alpha-synuclein to bind copper is important for its (as yet uncertain) physiological role. As discussed in Section 2.1.3, one proposed function of alpha-synuclein is the protein having ferrireductase activity, requiring copper bound to carry out this function. Results presented here would imply that the H50Q mutation would leave alpha-synuclein impaired in its ability to act as a ferrireductase, as the acetylated form of this protein (the form that would be found *in vivo*) is not able to bind to copper. Copper is required for many reactions in cellular metabolism, which is particularly true in the brain due to this organ having a high respiratory rate and being prone to OS. Copper is involved in many vital functions in the brain, including the control of reactive oxygen species (ROS), neurotransmitter synthesis and metabolism and extracellular matrix formation (reviewed by Tapiero, Townsend and Tew, 2003). In addition to being vital for many cellular processes, copper can also participate in the

cascade of free radical generation as a catalyst in Fenton chemistry. The Fenton reaction, $\text{Cu(I)} + \text{H}_2\text{O}_2 \leftrightarrow \text{Cu(II)} + \text{OH}^- + \text{OH}^\cdot$ converts relatively stable hydrogen peroxide into the highly reactive hydroxyl radical. This is important in brain areas metabolising biological amines (such as dopamine), as hydrogen peroxide is a by-product of monoamine oxidase (MAO) metabolism. Damaging aspects of copper are present when this metal exists as a free ion, and therefore alterations to a protein's copper binding ability has the potential to alter the equilibrium of free copper ions, resulting in a possible increase in ROS. Therefore it would be pertinent to assess the ability of N-terminally acetylated H50Q alpha-synuclein to act as a ferrireductase *in vivo*, and if alterations are found to assess cellular metal homeostasis and ROS balance.

Through all experiments presented in this chapter the H50A mutant was also investigated in parallel to the H50Q mutant, with identical results seen (data not shown). This demonstrates that it is the loss of the histidine residue, rather than the presence of the glutamine residue, which is responsible for the loss of copper binding seen in the acetylated H50Q mutant.

Results presented in this chapter are the first to describe the effect of a familial mutation on the copper binding ability of the biologically relevant, N-terminally acetylated alpha-synuclein protein. Data presented in this chapter highlight the need to take into account N-terminal acetylation when conducting *in vitro* investigations of alpha-synuclein.

Chapter 3 – Investigating alpha-synuclein aggregation using ESI-MS and ESI-IMS-MS

3.1 Introduction

Protein misfolding diseases arise from a protein's inability to retain its native conformation. Many neurodegenerative diseases such as Alzheimer's, Huntington's and PD share the common feature of a usually soluble protein aggregating and forming amyloid deposits in the brain. The proteins implicated in these three diseases (amyloid beta in Alzheimer's disease, huntingtin in Huntington's disease and alpha-synuclein in PS) are IDPs, with reported levels of disorder of > 80%, > 81% and > 75% respectively (Raychaudhuri *et al.*, 2009). Understanding the aggregation process involved in protein misfolding diseases is critical to be able to develop therapeutics designed to inhibit aggregation as a whole or to inhibit the formation of or dissociate toxic species which arise during the aggregation process.

The aggregation of alpha-synuclein into amyloid fibrils is thought to be associated with PD pathogenesis, with evidence pointing towards one or more of the oligomeric species which arises during the aggregation process being the pathogenic form. The protein's ability to self-assemble has been investigated by numerous techniques, including ThT assay (Buell *et al.*, 2014), dynamic light scattering (Dusa *et al.*, 2006), small-angle X-ray scattering (Rekas *et al.*, 2010), transmission electron microscopy (Anderson and Webb, 2011) and atomic force microscopy (AFM) (Fink, 2006). Disadvantages of such techniques include low sensitivity, low throughput nature and, in some cases, their inherent biased nature (Giehm, Lorenzen and Otzen, 2011). However, these investigations have identified multiple intermediate oligomeric species, including spherical and ring-shaped structures populated during assembly (Conway *et al.*, 2000; Lashuel *et al.*, 2013). Consequently, it has been theorised that the transition from the native, soluble form of alpha-synuclein into amyloid fibrils is

not a single step process, or even one single pathway, making it of great importance to characterise the individual species populated during the aggregation process.

ESI-MS is able to provide a high throughput, high sensitivity, unbiased technique which is capable of characterising oligomeric species present in the early stages of protein aggregation. ESI-IMS-MS emerged in the 1990's as an alternative to more traditional techniques such as X-ray crystallography and NMR for the investigation of protein structure (Shelimov *et al.*, 1997). While ESI-IMS-MS is not able to provide the atomistic resolution of these techniques it offers the valuable advantage of the ability to study both the conformational dynamics of a protein and the interrogation of multiple overlapping conformers and oligomeric species. This makes ESI-IMS-MS an invaluable tool for the study of aggregating proteins, allowing the frequently diverse array of species which arise during early aggregation to be investigated. A further benefit of ESI-IMS-MS is the lower sample concentrations required compared to techniques such as NMR and X-ray crystallography. This is an important advantage for proteins such as alpha-synuclein, where concentration is known to affect aggregation (Uversky *et al.*, 2001). Consequently, ESI-MS and ESI-IMS-MS have been used to investigate a range of aggregating proteins and peptides. However, investigations into the aggregation of alpha-synuclein using these techniques have been lacking, particularly when compared to the progress which has been made for other amyloidogenic proteins, most notably β_2 -microglobulin (Lim and Vachet, 2004; Smith *et al.*, 2006; Mendoza *et al.*, 2010, 2011; Smith *et al.*, 2011; Woods *et al.*, 2011; Dong *et al.*, 2014; Leney *et al.*, 2014; Hall, Schmidt and Politis, 2016) and amyloid- β (Bernstein *et al.*, 2005, 2009; Murray *et al.*, 2009; Gessel *et al.*, 2012; de Almeida *et al.*, 2017; Jin Lee *et al.*, 2018). Although ligand binding studies have been performed with alpha-synuclein little has been published on

the oligomeric conformations by mass spectrometry. Several modes of action have been proposed as to how alpha-synuclein oligomers can elicit cytotoxicity, with protocols established to enable the formation of oligomers with known cellular effects. Exogenous application of Type C alpha-synuclein oligomers characterised by Danzer *et al.* (2007) are known to increase cytosolic alpha-synuclein aggregation, as described in detail in Section 4.1.1.2. The production of these oligomers has been adapted for MS analysis by Illes-Toth *et al.* (2015). ESI-IMS-MS revealed that in preparations of Type C oligomers the unmodified protein is capable of forming species from dimers to hexamers that are accessible by this technique. These oligomers, through comparison with model structures, were shown to be consistent with ring-like assemblies. In parallel, MS compatible Type C oligomers were demonstrated to be able to induce intracellular aggregation in neuronal cell lines via a prion-like mechanism (Illes-Toth *et al.*, 2015). However, the assembly and dynamics of alpha-synuclein oligomers has not yet been investigated. It is also unknown if N-terminally acetylated versions of the protein are able to form these oligomeric species in the same manner as the unmodified protein.

3.2 Aims and Objectives

ESI-MS and ESI-IMS-MS have proved to be valuable tools for the investigation of protein aggregation. The aim of this chapter was to apply MS methods to investigate the species present of alpha-synuclein during the early stages of aggregation. The presence of low order oligomers, most commonly dimers, of alpha-synuclein in non-aggregated samples has been a common finding in studies utilising MS, as discussed in Section 1.4.4.1. Here, the low order oligomeric species present in samples of the unmodified and N-terminally acetylated protein were investigated to determine their oligomeric state and the dynamics of these low order oligomers in MS experiments was investigated using isotope labelling. ^{14}N and ^{15}N versions of the protein were created and through mixing at various time points used to determine the extent of inter conversion between the oligomers. Such approaches have been previously for other amyloidogenic proteins, showing alterations in oligomer dynamics over time (Smith *et al.*, 2011).

The specific aims of this chapter were:

1. To characterise the species and dynamics of low order oligomers of unmodified and N-terminally acetylated alpha-synuclein present in samples prior to aggregation.
2. To determine if Type C oligomers of alpha-synuclein assembled from both unmodified and N-terminally acetylated recombinant protein share a common structure.

3. To monitor the aggregation of alpha-synuclein under MS compatible conditions, looking at the oligomeric species present and their dynamics over the aggregation time course.

3.3 Materials and Methods

3.3.1 Production of recombinant alpha-synuclein

Unmodified and N-terminally acetylated alpha-synuclein were produced as described in Section 2.3.7/2.3.8.

3.3.2 Production of ¹⁵N labelled recombinant alpha-synuclein

¹⁵N labelled alpha-synuclein was produced in the manner described in Section 2.3.1, with the alteration of culturing transformed *E. coli* in ¹⁵N Overnight Express™ Autoinduction NMR Medium (Novagen), following manufacturer guidelines, rather than the autoinduction media used for unlabelled protein production.

3.3.3 Production of MS compatible Type C alpha-synuclein oligomers

In order to produce MS-compatible Type C oligomers protocols described by Illes-Toth *et al.* (2015) were followed. Alpha-synuclein was reconstituted to a final concentration of 7 µM in 50 mM AA (pH 7.0) containing 20% ethanol, followed by overnight incubation at 21 °C with continuous shaking. The following day solutions were concentrated 1:14 using ultracentrifugation (VivaSpin 500 columns, MWCO 30 kDa, GE Healthcare) allowing the separation of oligomeric species from monomeric protein. Type C oligomeric species were then analysed immediately following production.

3.3.4 Aggregation of alpha-synuclein

Lyophilised alpha-synuclein was reconstituted in 50 mM AA (pH 7) to a final concentration of 70 µM and incubated at 37 °C in a 96 well plate, with agitation at 300 rpm. A 4 mm diameter glass bead was added to each well. Samples were taken at 0,

3.5, 19.5, 46.5 and 71.5 hour time points and an aliquot used immediately for MS analysis and the remainder snap frozen and stored at -80 °C for western blot, dot blot and ThT analysis. All samples endured the same number of freeze-thaw cycles.

3.3.5 Mass spectrometry

Mass spectrometry was performed as described in Section 2.3.11 with the following alterations; cone voltage 70 V, backing pressure 6.45 mbar.

3.3.6 Western blot

For western blot analysis 5 µL of sample from each time point of the aggregation experiment were subjected to SDS-PAGE using a homemade 12% SDS gel and transferred to a polyvinylidene fluoride membrane for 90 minutes at 75 V. The membrane was then blocked in TBS-T containing 5% (w/v) non-fat milk (NFM) for 1 hour at room temperature, followed by overnight incubation with mouse monoclonal anti-alpha-synuclein antibody [syn211] (1:5000, abcam, ab80627) in TBS-T with 1% (w/v) NFM at 4 °C under gentle shaking. Following primary antibody incubation, membranes were washed 3 times for 10 minutes with TBS-T before incubation with IRDye® 680LT Goat anti-Mouse IgG antibody (H + L) (1:15,000, Licor, 925-68070) in 1% (w/v) NFM for 1 hour at room temperature. Visualisation was performed using the LI-COR Odyssey and Odyssey Infrared Imaging software (LI-COR, Nebraska, USA).

3.3.7 Dot blot procedure

Nitrocellulose membranes (0.45 µM, GE Healthcare, Sweden) were spotted with 1 µL of sample from each aggregation time point, allowed to air dry and blocked for 1 hour in 5 % (w/v) NFM TBS-T. Primary antibody (Anti-Amyloid Fibrils LOC Antibody (1:2000,

Merk, AB2287)) was diluted in 1% (w/v) NFM TBS-T and incubated with the membrane overnight under continuous gentle shaking at 4 °C. Three wash steps were performed with TBS-T before incubation with secondary antibody (IRDye® 800CW Goat anti-Rabbit IgG (H + L) (1:15,000 dilution, LI-COR)) diluted in 1 % (w/v) NFM TBS-T for one hour under continuous gentle shaking at room temperature. Visualisation was performed using the LI-COR Odyssey and Odyssey Infrared Imaging software (LI-COR, Nebraska, USA).

3.3.8 Thioflavin T (ThT) fluorescence

For ThT analysis 20 µL of sample from each time point of the aggregation process were mixed with 100 µL of 100 µM ThT and fluorescence intensity between 474 and 594 was measured using a CLARIOstar plate reader (BMG LABTECH, Buckinghamshire, UK).

3.4 Results and discussion

3.4.1 Low order oligomeric species of alpha-synuclein are detected in both the unmodified and acetylated protein immediately following reconstitution

Chapter 2 details how alpha-synuclein is a highly dynamic protein which exists in multiple conformations including a dynamic equilibrium between the monomeric form of the protein and low order oligomers. In this chapter low order oligomers of unmodified and N-terminally acetylated alpha-synuclein were investigated using ESI-IMS-MS to ascertain whether any differences were observable between the oligomeric forms of the protein.

Figure 3.1 (a) shows the mass spectra of freshly reconstituted, unmodified and N-terminally acetylated alpha-synuclein (70 μ M, 50 mM AA, pH 7.0) prior to incubation. In both the unmodified and N-terminally acetylated preparations, low abundance dimers, trimers and tetramers can be observed in addition to the more abundant monomer CSIs. The alpha-synuclein dimer peaks display a wide range of CSIs from $10 \leq z \leq 23$, suggesting that the dimer, like the monomer, is dynamic and flexible and that N-terminal acetylation has had no effect on this structure. The observed CSD for the trimeric forms of the protein was $15 \leq z \leq 29$ and $20 \leq z \leq 31$ for the tetramers. This decrease in the width of the CSD would suggest that the oligomers of both forms of the protein become more compact on assembly. Figure 3.1 (b) shows mass spectra in the 1400 - 3000 m/z range where the majority of low order oligomer CSIs reside. The inset in (b) shows an expanded view of the 1840 - 2035 m/z region, where the +15 dimer, +22 and +23 trimer and +29 and +31 tetramer peaks can be seen for both

proteins. Driftcope plots of these species are shown in Figure 3.2 (c) where again dimers, trimers and tetramers are detectable in both preparations, as highlighted on the figure, with the intensity of species decreasing as mass increases.

Comparison of spectra acquired for unmodified and N-terminally acetylated alpha-synuclein indicates that acetylation does not affect the formation of low order oligomers, as both versions of the protein produced very similar spectra. These results are in keeping with a previous investigation of N-terminally acetylated alpha-synuclein by ESI-IMS-MS by Kang *et al.* (2012), where no differences from the unmodified protein were found. However, in this previous study the largest species found for both forms of the protein was the dimer, whereas here the trimer and tetramer were additionally observed. Slight variations in the low order oligomer species present in different alpha-synuclein solutions were however commonly found in ESI-MS experiments conducted throughout this thesis, with the monomer dimer and trimer being found in all protein solutions and the tetramer frequently being detectable, but occasionally being absent. This is in keeping with the known variability found when analysing this protein using MS methods (Phillips *et al.*, 2015).

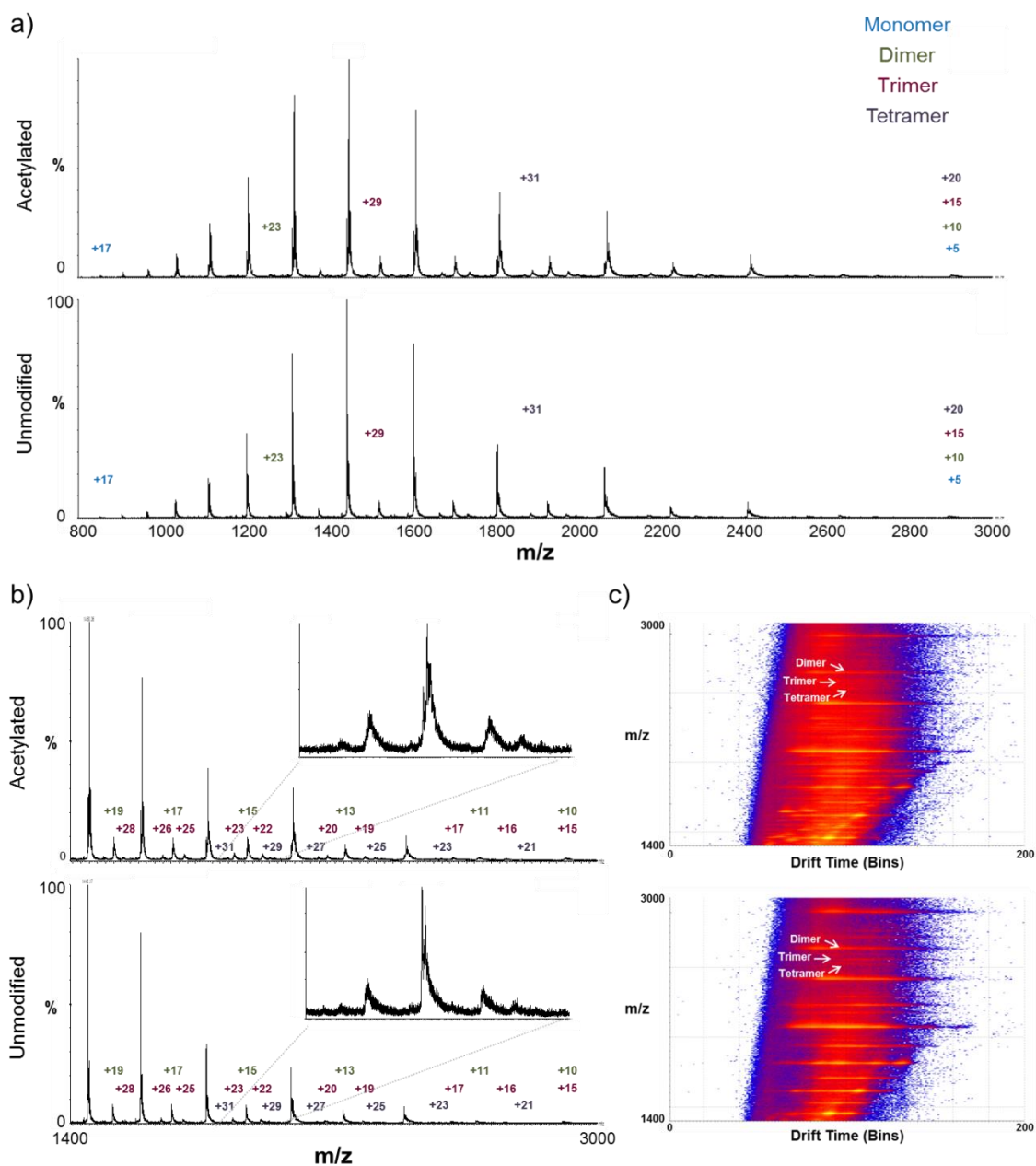


Figure 3.1: ESI-IMS-MS analysis of unmodified and acetylated α -synuclein. Mass spectra in the 800 - 3000 range of recombinant proteins (70 μ M, 50 mM AA pH 7) shown in (a), with the extremes of the CSD of monomeric, dimeric, trimeric and tetrameric species labelled. Mass spectra in the 1400 - 3000 range containing low order oligomers shown in (b), with CSIs of dimers highlighted in green, trimers in purple and tetramers in blue. Inset shows the expanded region of 1840 - 2035 m/z . Driftscope plots of both proteins in the 1400 - 3000 range is shown in (c), with one example of a dimer, trimer and tetramer CSI highlighted on each.

3.4.2 Low order oligomeric species of alpha-synuclein are dynamic

In order to gain insight into the stability of the low order oligomers of alpha-synuclein described above, isotopic labelling of proteins was utilised. ^{15}N alpha-synuclein was produced using ^{15}N as the sole source of nitrogen for the *E.coli* cells during the recombinant protein expression process, resulting in a form of the protein with a mass shift sufficient to detect by MS. Through incubating equal concentrations of ^{14}N and ^{15}N labelled alpha-synuclein separately and then mixing samples immediately prior to ESI-MS analysis, the rate of subunit exchange of oligomeric species can be determined. If the subunits are in rapid exchange the oligomers detected will be formed indiscriminately from the protein pool. For a dimer CSI this would result in three peaks in a 1:2:1 ratio, corresponding to dimers comprised of two ^{14}N subunits, one ^{14}N and one ^{15}N subunit, or two ^{15}N subunits respectively. However, if the dimer did not interconvert, a ratio of 1:1 between the ^{14}N and ^{15}N peaks would be seen.

Figure 3.2 shows spectra from ^{14}N and ^{15}N alpha-synuclein reconstituted to equal concentrations and either analysed alone or mixed immediately prior to acquisition. Full spectra are shown in (a), where two peaks can be seen for each monomeric CSI in the mixed sample. Spectra of the +11 monomer CSI is shown in (b), where in the mixed sample only peaks attributable to the ^{14}N or ^{15}N are seen. Spectra of the +13 dimer CSI is shown in (c), where in the mixed sample a new, most abundant peak is present, attributable to this dimer comprising one ^{14}N subunit and one ^{15}N subunit. This indicates that this dimer CSI is dynamic in nature, as the monomeric subunits are in exchange. The 2150 - 3000 m/z range is shown in (d), where a variety of low order oligomers can be seen. Full subunit exchange was detected for all distinguishable low order oligomers in the spectrum, demonstrating that following reconstitution of

lyophilised recombinant alpha-synuclein, the low order oligomers detectable by ESI-MS are dynamic in nature and fully exchange during the time course of the experiment. Both the trimer and tetramer higher order oligomers appear to be fully exchanged during the time course of the experiment, with broad peaks being observed in the mixed ^{14}N and ^{15}N sample.

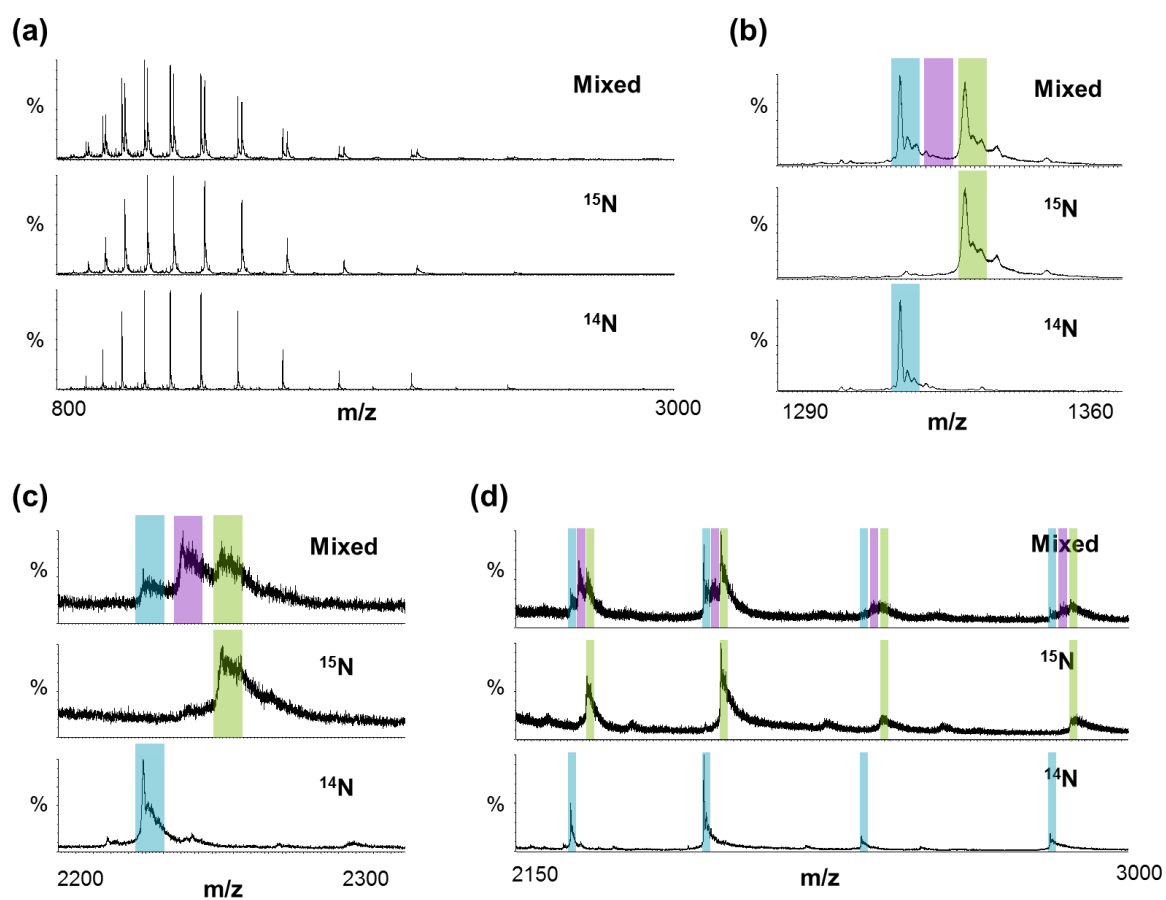


Figure 3.2: ESI-MS analysis of unlabelled and nitrogen labelled alpha-synuclein. Mass spectra in the 800 - 3000 range of ^{14}N , ^{15}N and combined proteins (70 μM , 50 mM AA pH 7.0) shown in (a). Spectra of the +11 monomer CSI is shown in (b) and the +13 dimer CSI is shown in (c). Spectra of the +11 and +13 dimer CSIs and +5/+10 and +6/+12 monomer/dimer CSIs are shown in (d), with peaks attributable to the ^{14}N protein highlighted in blue, ^{15}N protein highlighted in green and mixed ^{14}N and ^{15}N highlighted in purple.

3.4.3 Structurally comparable species of Type C alpha-synuclein

oligomers are present in solutions prepared from both unmodified and acetylated protein

As will be discussed in detail in Section 4.1.1 increasing evidence suggests that it is the oligomeric species of alpha-synuclein which may be the toxic form of protein, rather than mature aggregates. Type C oligomers adapted to be compatible with MS analysis, while retaining their cellular effects, have previously been characterised by ESI-IMS-MS (Illes-Toth *et al.*, 2015).

Figure 3.3 shows the drift scope plot (i) and spectra (ii) of Type C alpha-synuclein oligomers, adapted for MS analysis, assembled from unmodified (a) and N-terminally acetylated (b) protein. Here both low order (dimers, trimers and tetramers) and higher order (pentamers and hexamers) oligomeric species can be observed, interspersed with peaks that could not be assigned, consistent with the previous report of Illes-Toth *et al.*, (2015). In addition to the oligomeric species, a CSD of monomeric CSIs is present, despite the use of a 30000 Da MWCO spin concentrator in the Type C preparation protocol. This may be a result of the dynamic nature of the oligomers and the re-establishment of an equilibrium state. Also notable in the spectra is a greater proportion of monomeric protein coming from the more compact CSIs (centred on the +7 ion) when compared to the spectra of freshly reconstituted alpha-synuclein shown in Figure 3.1 and Figure 3.2. Previous work has provided evidence for an increase in the compact state of alpha-synuclein, centred on the +7 CSI under conditions which are known to increase aggregation of the protein, such as the presence of high concentrations of alcohols (Natalello *et al.*, 2011). As accumulation of this compact state correlates with increased aggregation, it is plausible that this partially folded

form of alpha-synuclein seen here represents an intermediate in conformational transitions to oligomeric species of the protein. This shift in CSI intensity was not seen in control experiments of the Type C oligomer sample prior to incubation, demonstrating that the increase in the more compact CSIs seen following incubation is not an artefact of the 10% ethanol used in the oligomerisation protocol. No notable differences were observed in the driftscope plot or spectra of Type C oligomers prepared from unmodified or N-terminally acetylated alpha-synuclein. This indicates that N-terminal acetylation does not affect the assembly of alpha-synuclein into Type C oligomers. These results support data shown in Figure 4.4, where N-terminal acetylation was found to not alter the ability of Type C oligomers to induce intracellular aggregation of alpha-synuclein.

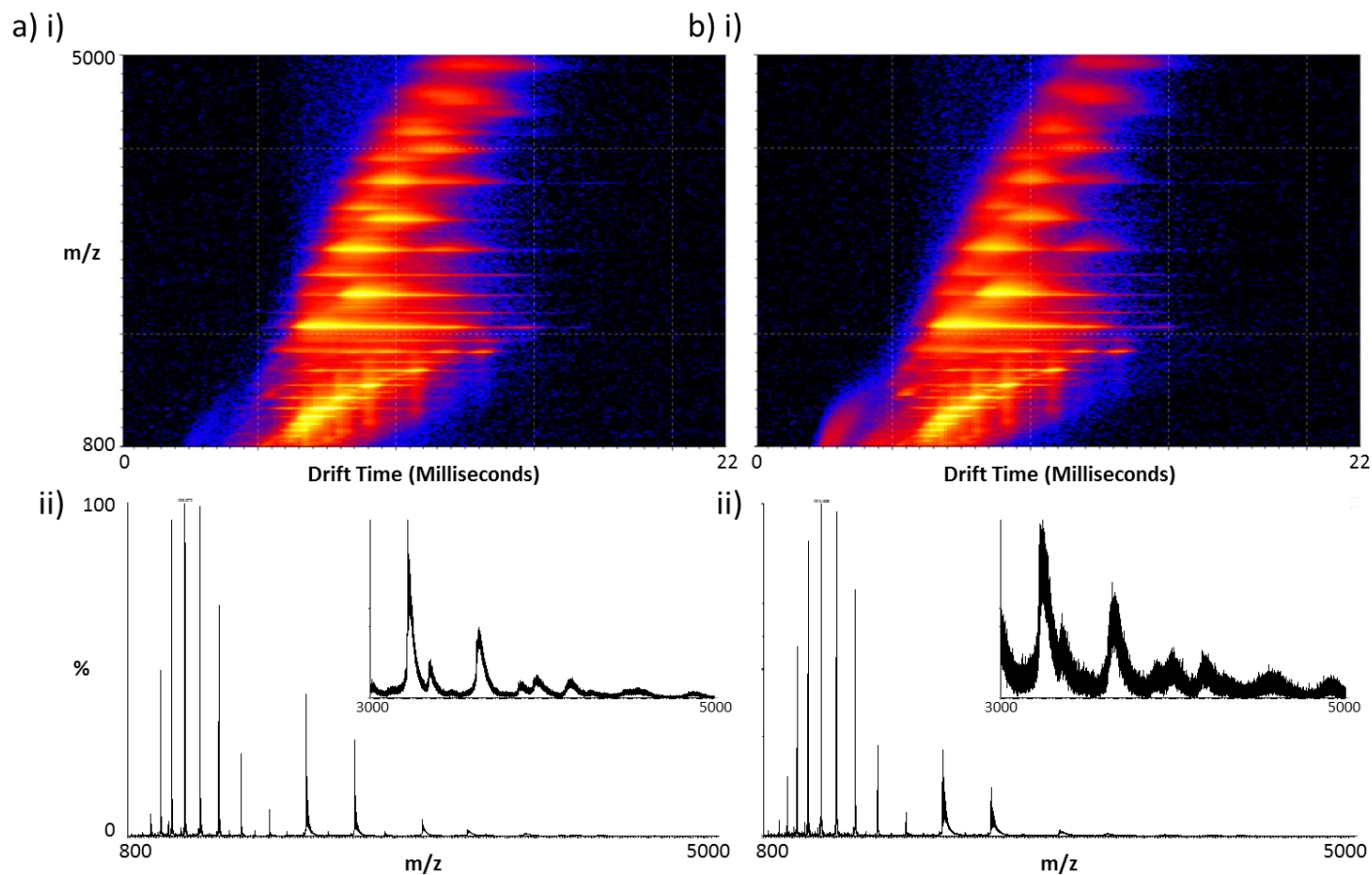


Figure 3.3: ESI-IMS-MS analysis of unmodified and N-terminally acetylated alpha-synuclein Type C oligomers. Driftscope plots of unmodified (a) and N-terminally acetylated (b) Type C oligomers in the 800 - 5000 m/z range is shown in (i) and corresponding spectra shown in (ii) (inset shows the expanded region of 3000 - 5000 m/z).

3.4.4 ESI-MS analysis of alpha-synuclein aggregation

In order to investigate the assembly mechanism of alpha-synuclein into amyloid material ESI-MS was used to characterise the transitional species present during the early stages of alpha-synuclein aggregation. Incubation of 70 μ M alpha-synuclein under agitation is known to produce amyloid material that is ThT positive (Figure 2.16). Investigations were carried out over a three day time course, as this length of time was shown to be adequate for alpha-synuclein to form aggregates in earlier experiments using ThT fluorescence, as shown in Figure 2.19.

Figure 3.4 (a) shows spectra of 0, 3.5, 19.5, 46.5 and 71.5 hour time points of an *in vitro* alpha-synuclein aggregation time course. The 0 hour spectrum displays the same characteristics as described in Figure 3.1 of wide CSDs and low order oligomeric species present in addition to the monomer. The monomer CSD spans $5 \leq z \leq 17$ and features a predominantly mono-modal distribution centred on the +12 CSI at 0 hour incubation. From the 3.5 hour time point the CSDs of the monomeric and oligomeric species begin to narrow, with the CSD of the various species at each time point summarised in Figure 3.4 (b). The dimer CSD reduced from $10 \leq z \leq 23$ at 0 h to $11 \leq z \leq 15$ at 71.5 h, indicative of a collapse in the conformation of the dimer with time. In addition to the alterations in CSD, the Total Ion Chromatogram (TIC) was found to decrease at each time point (as highlighted on the spectra of Figure 3.4 (a) in purple), as it became increasingly difficult to achieve a stable nESI spray. This would indicate that as the time course progresses alpha-synuclein monomers and low order oligomers are depleted from the solution, possibly as a result of these species aggregating to higher order oligomers beyond the mass range able to be detected in this experiment.

Alpha-synuclein aggregation is a nucleation dependent process, and it has been suggested that the dimer acts as the nucleus for aggregation (Roostae *et al.*, 2013). A previous study by Phillips *et al.*, (2015) monitoring the aggregation of alpha-synuclein using MS methods found, in contrast to data presented here, that the CSD of the dimeric species remained consistent throughout the aggregation experiment (despite a reduction in TIC as found here) and a shift in the ratio of dimer to monomer CSIs over time. In contrast, the ratio of monomer to dimer was found here to increase over time, suggesting a preferential depletion of the dimeric species. This is shown in Table 3.1, where the ratio of monomer to dimer, calculated by summing the absolute intensities of all monomeric CSIs and all odd dimeric CSIs at each time point, is displayed. This is in keeping with the suggestion of the dimer as a nucleus for aggregation, as it is possible the dimer CSIs would be depleting at a greater rate than the monomer CSIs if they were nucleating the formation of higher order oligomers or fibrils.

	Incubation time (hours)				
	0	3.5	19.5	46.5	71.5
Monomer : Dimer	27.4	31.4	59.2	76.1	132.6

Table 3.1: the ratio of monomer to dimer derived from the sum of the intensities of all monomer CSIs and all odd dimer CSIs following an aggregation time course.

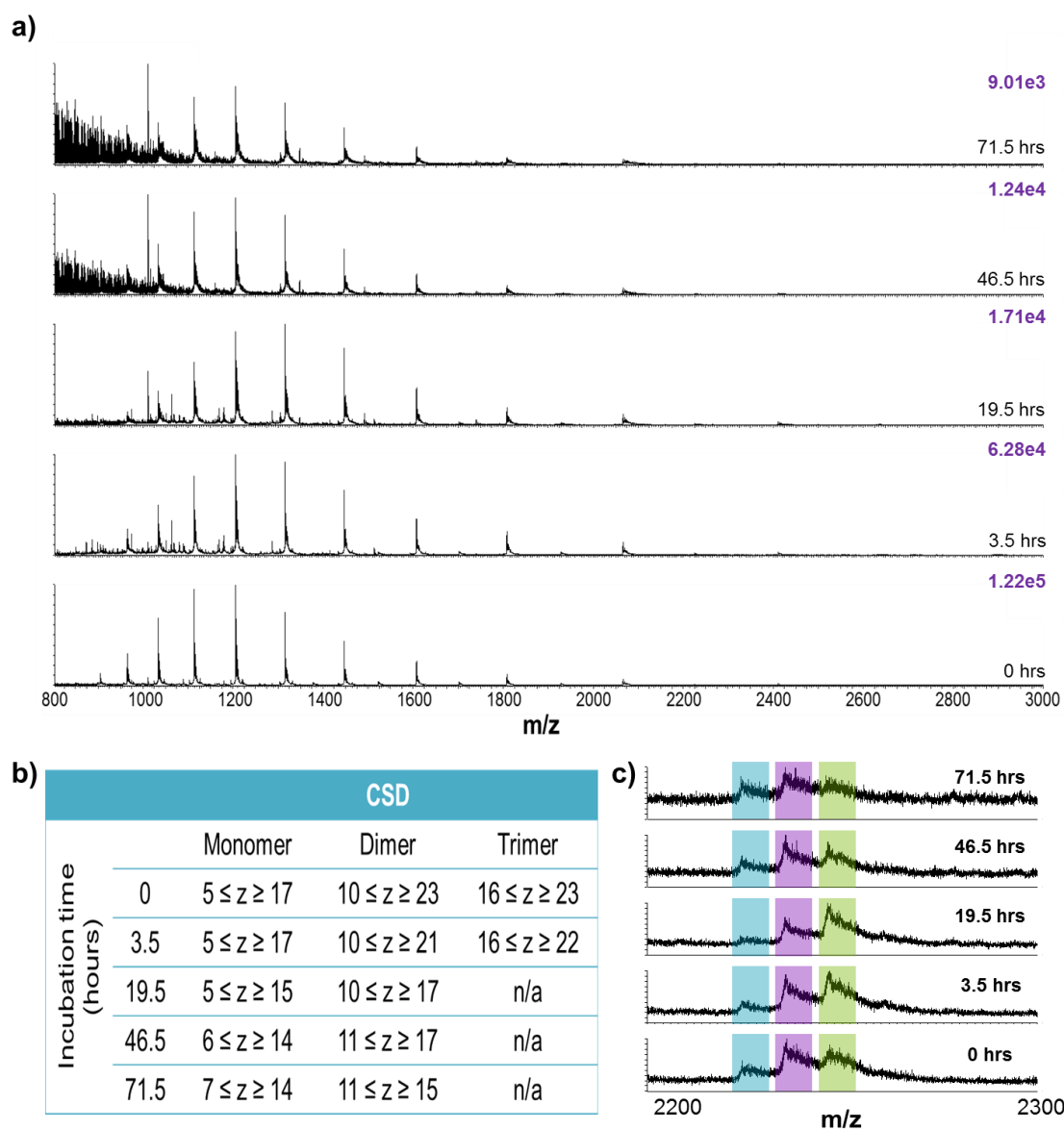


Figure 3.4: ESI-MS analysis of alpha-synuclein aggregation time course. Spectra acquired following 0, 3.5, 19.5, 46.5 and 71.5 hour incubations are shown in (a), with the total ion count over 20 scans shown in purple. Table showing the CSD of monomeric, dimeric and trimeric species present at corresponding time points shown in (b). Spectra of the +13 dimer CSI of ^{14}N and ^{15}N incubated separately and combined immediately before acquisition is shown in (c), with peaks attributable to the ^{14}N protein highlighted in blue, ^{15}N protein highlighted in green and mixed ^{14}N and ^{15}N highlighted in purple.

The data presented in this chapter appear to present a paradox in results with monomer to hexamers being observed in the Type C oligomer specific protocol yet larger species absent during fibril formation. Larger oligomeric species would be expected, and results presented in Figure 3.3 demonstrate that species up to at least the hexamer are able to be detected under our experimental conditions. The lack of higher order oligomers during fibril formation conditions could potentially be due to aggregating species of alpha-synuclein quickly reaching a size making them undetectable by our MS method due to the increased concentration of the total protein 70 μM compared to the 7 μM used in the oligomer protocol. A plausible explanation is that the time points selected missed the presence of aggregating species or that the absence of either ethanol or a pre-concentration step prevented their formation. This could indicate that the low order oligomeric species present throughout the aggregation time course experiment may easily form and dissociate, but are not part of the fibril formation pathway. It has been demonstrated in the case of other proteins that reconstitution of lyophilised protein can result in the formation of low order oligomers on short time frames (Smith, Radford and Ashcroft, 2010) and the storage conditions of alpha-synuclein can affect the oligomeric state of the protein (Stephens *et al.*, 2018).

Alternatively the low order oligomers which persist at later time points could potentially be an artefact of the electrospray process, however higher order pentamers and hexamers were shown to require incubation before being observed. The lack of the higher order oligomeric species similar to the Type C preparation found during the aggregation time course suggests that these oligomers are either transient in nature, only being detectable for a defined period of time before aggregating

further and becoming undetectable, or that they are off pathway oligomers not related to the eventual formation of amyloid fibrils.

To address the dynamic nature of the oligomers populated during the early stages of aggregation isotopic labelling of proteins was utilised in the manner described in Section 3.3.2. This allowed the investigation of the dynamics of alpha-synuclein oligomer subunit exchange over the course of the aggregation experiment. Equal concentrations of ^{14}N and ^{15}N labelled alpha-synuclein were incubated under aggregation conditions separately and mixed immediately prior to ESI-MS analysis at discrete time points. Figure 3.4 (c) shows the spectra of the +13 dimer CSI of ^{14}N and ^{15}N incubated separately and combined immediately before acquisition, with peaks attributable to the ^{14}N protein highlighted in blue, ^{15}N protein highlighted in green and mixed ^{14}N and ^{15}N highlighted in purple. The presence of a peak attributable to both ^{14}N and ^{15}N was detected at every time point, demonstrating that this dimer is remaining dynamic throughout the aggregation experiment. This pattern was seen across all detectable oligomeric species in the spectra, which were found to undergo subunit exchange at each time point tested. The finding of all low order oligomers remaining dynamic at the end of the aggregation experiment is in contrast to previous studies using a similar technique to analyse the aggregation of β_2 microglobulin, where alterations in dynamics were found for both particular oligomeric CSIs and over the time course of an aggregation experiment (Smith *et al.*, 2010, Smith *et al.*, 2011). This provides support to the possibilities mentioned above, that low order alpha-synuclein oligomers detectable by ESI-MS either easily form and dissociate, but are not a part of the aggregation pathway, or are an artefact of the electrospray process. What can be determined from ESI-MS is that soluble protein is consumed during the aggregation

process and that the oligomeric species become compacted upon incubation. The absence of high order oligomers akin to those observed with the oligomer specific protocol raises the possibility that the Type C oligomers form on an amyloid independent pathway.

3.4.5 Aggregates of alpha-synuclein are formed over the time course utilised for ESI-MS experiments

Due to the absence of any oligomeric species larger than those present prior to sample aggregation, alternate techniques were employed on samples taken at corresponding time points to confirm that protein aggregation had occurred on the timescale investigated.

Figure 3.5 (a) shows the result of western blot analysis of the samples using an antibody to detect alpha-synuclein. A band corresponding to the monomeric form of the protein can be seen at all time points, which correlates to the presence of a monomeric CSD at each time point seen with MS analysis. Also detectable is the presence of a high molecular weight species of alpha-synuclein at the 19.5 hour, 46.5 hour and 71.5 hour time points. These aggregates reside at the very top of the sample well of the SDS-PAGE gel used to separate out the samples before western blot transfer, demonstrating that these aggregates are too large to enter the gel and be analysed by SDS-PAGE analysis. Figure 3.5 (b) shows the result of dot blot analysis of the samples using the LOC antibody which recognise generic epitopes common to amyloid fibrils and fibrillar oligomers. It can be seen that the intensity of fluorescence from this antibody increases at each time point, with the most intense fluorescence, and therefore the most fibrillar material in the sample, being at the 71.5 hour time

point. No signal is detected at the 0 hour time point, demonstrating that the starting material is not recognised by this antibody. Figure 3.5 (c) shows the result of ThT analysis of the 5 samples. No notable fluorescence above the vehicle control is detected in the 0 hour and 3.5 hour samples, indicating that no significant β -sheet structure is present in these samples, correlating to both the lack of signal from the LOC antibody by dot blot analysis and lack of large aggregates seen through western blot analysis. At the later time points (19.5 hour, 46.5 hour and 71.5 hour) an increase in ThT fluorescence is seen, indicating that the protein in the sample has assembled into a form containing significant β -sheet structure.

The data presented here confirms that amyloid material has been formed under MS compatible conditions during the time course aggregation experiment used for MS analysis, despite the lack of larger species seen in the ESI-MS spectra, validating the time points chosen for MS experiments.

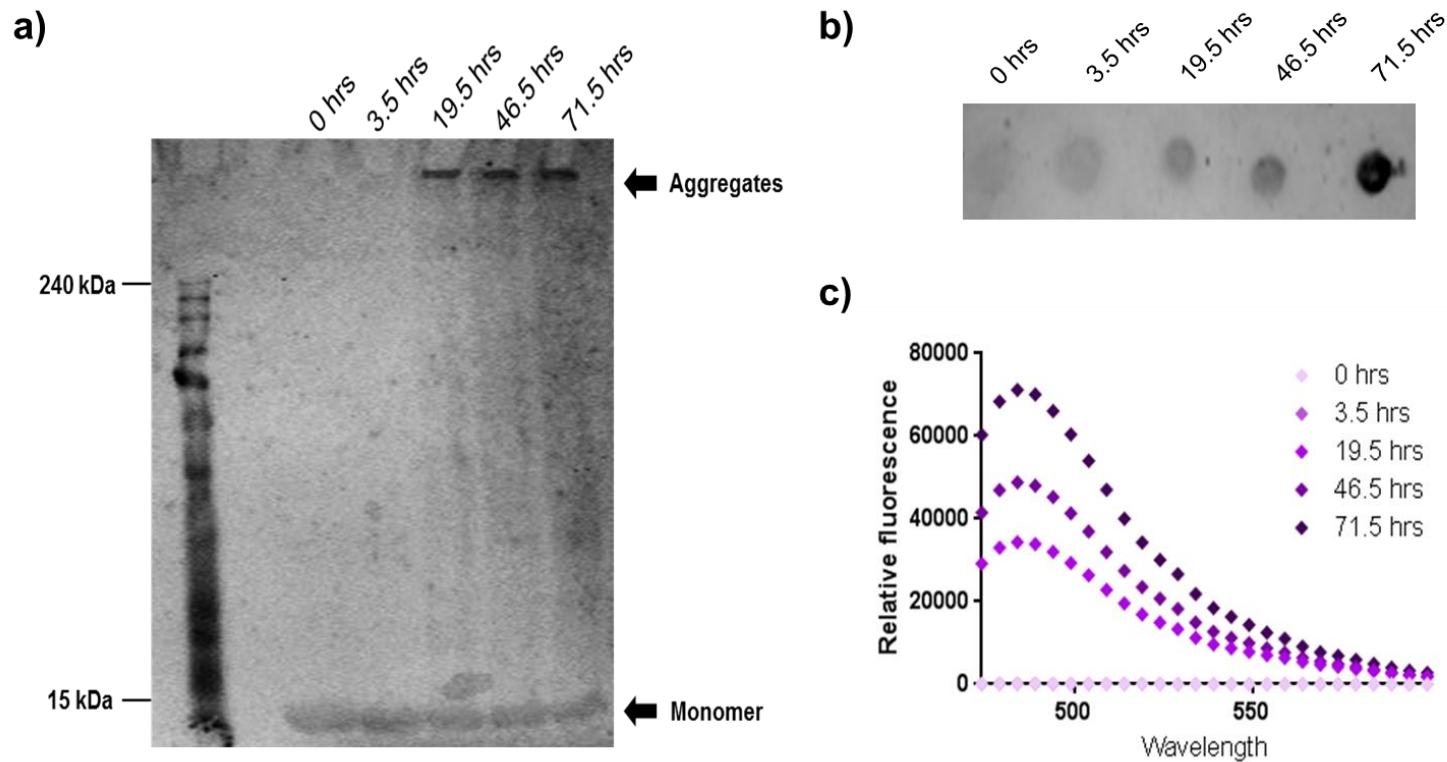


Figure 3.5: Western blot, dot blot and ThT evidence that alpha-synuclein is forming aggregates in the duration of time course experiments. Western blot using an antibody to detect alpha-synuclein of samples taken following 0, 3.5, 19.5, 46.5 and 71.5 hour incubations is shown in (a). The same samples were subject to dot blot analysis using an antibody to recognise generic epitopes common to amyloid fibrils and fibrillar oligomers shown in (b) and ThT assay, shown in (c).

3.5 Conclusions and Future Work

Characterizing prefibrillar oligomers is key to understanding the aberrant aggregation of misfolding proteins and provides vital insights which can aid in the design of potential therapeutics for protein misfolding diseases. The aim of this chapter was to apply MS methods to investigate the species of alpha-synuclein which arise during the early stages of its aggregation.

Data presented in this chapter has characterised the species of low order oligomers which are present in non-aggregated samples of both unmodified and N-terminally acetylated alpha-synuclein. The same species were present for both forms of the protein, indicating that acetylation does not alter the formation of low order alpha-synuclein oligomers. To investigate the dynamic nature of low order oligomers, the rate of subunit exchange was monitored using $^{14}\text{N}/^{15}\text{N}$ labelling. The data revealed that all oligomer ions present in the non-aggregated samples underwent rapid exchange, demonstrating that they are dynamic entities.

Experiments presented here also confirmed that the species of Type C alpha-synuclein oligomers, characterised using MS by Illes-Toth *et al.*, (2015) were also present when these oligomers were assembled from the acetylated protein. The dynamics of the higher order oligomeric species present in Type C oligomer samples were not able to be analysed during the course of this PhD, due to a combination of difficulty in obtaining two independent preparations displaying these species at similar intensities on the same time scale, and due to broad peaks masking exchange.

Lastly, the characteristics of ESI-MS spectra acquired over the course of an aggregation experiment was assessed. As fibrillar forms of the protein were formed (as confirmed

by various biochemical assays) evidence was seen in the spectra for depletion of solution phase constituents. It was also notable that the low order oligomers present throughout the aggregation time course remained dynamic, continuing to undergo subunit exchange. This suggests that these oligomeric species may not be on pathway oligomers or that the early stages of aggregation are highly dynamic. What was observed was a decrease in the CSD with time, indicative of more compact conformation being populated during the aggregation process. An alternative explanation is that these oligomers could be an artefact of the electrospray process, and not representative of the protein in solution, however further experiments would be required to determine this. There are various lines of evidence supporting the idea of low order oligomeric forms of the protein (particularly tetramers) *in vivo*. It may be the case that the monomeric protein pool present at the end of the aggregation experiment is in equilibrium with large aggregates, and that the low order oligomers seen are able to form whenever there is monomer present.

It is important to note that some variations were found between results presented here and previously published work, with one example being the opposite trend in monomer to dimer ratio found here compared to that shown in a similar experiment by Phillips *et al.*, (2015). One possible explanation for the contrasting results lays in the instrumental settings used in each study. While sample preparation conditions were virtually identical in both studies, different cone voltages were applied, with 70 V being used for spectra presented in this chapter and 165 V being used in the study of Phillips *et al.*. This higher cone voltage could potentially be resulting in the dissociation of higher aggregates of alpha-synuclein, resulting in alterations to the spectra seen compared to where dissociation was not occurring. Alpha-synuclein is a notoriously

conformational plastic protein, and significant day to day variability in MS spectra under near identical conditions has been reported. Also apparent on review of the literature is a significant degree of variability in the findings of different research groups. For example, when using MS to investigate conformational shifts in response to altered pH studies by Bernstein *et al.*, (2004) and Frimpong *et al.*, (2010) found a shift to more compact conformations at low pH while Natalello *et al.*, (2011) found a shift to the more extended conformations. The known variability of alpha-synuclein may also account for the differences in results presented here and previous reports.

The failure in identifying higher order oligomers than those present at the 0 hour time point, or alterations in the dynamics of low order oligomers during the aggregation process perhaps goes some way to explain the lack of progress made in characterising alpha-synuclein aggregation species by ESI-MS. Much progress has been made in the characterisation of other amyloidogenic proteins by the methods employed here, but no one has yet successfully applied these techniques to the analysis of alpha-synuclein aggregation. It may be the case that alpha-synuclein is not a protein suitable for analysis by these methods, or these oligomers are never populated, and consequently different approaches may need to be developed to progress the field.

Chapter 4 - Validation and further characterisation of the effect of alpha-synuclein oligomers on SH-SY5Y cells

4.1 Introduction

4.1.1 Oligomeric species of alpha-synuclein have been proposed as the toxic form of the protein

Much research has implicated alpha-synuclein aggregation and, more specifically, the generation of prefibrillar oligomeric species, as the toxic form of the protein which contributes to the neurodegeneration seen in PD. Key evidence supporting the hypothesis of oligomers, rather than the fibrillar aggregates, being the toxic species comes from the observation of LBs being present in approximately 10% of neurologically normal individuals over the age of 60 (Frigerio *et al.*, 2011), LB load correlating poorly to PD symptoms and certain familial forms of the disease presenting with neuronal degeneration with the absence of LBs (Cookson, Hardy and Lewis, 2008). Further evidence includes increased levels of alpha-synuclein oligomers in brains with LB pathology (Paleologou *et al.*, 2009) and in the cerebrospinal fluid (CSF) of PD patients (Parnetti *et al.*, 2014). Animal models have provided supporting evidence, with 3 month old female Fisher F344 rats (Harlan Laboratories) expressing artificial E57K and E53K alpha-synuclein variants, designed to promote 'off-pathway' oligomer formation, displaying a more severe loss of dopaminergic neurons compared to these rats expressing artificial WT alpha-synuclein. Conversely, a peptide encompassing amino acid 30 – 110 of alpha-synuclein, designed to have increased aggregation propensity, did not induce toxicity in this rat model (Winner *et al.*, 2011). Additionally, injection of pre-formed oligomeric species into the SNpc Sprague Dawley rats (300–350 gram) has been shown to induce nigral degeneration (Dimant *et al.*, 2013). *In vitro*, cell culture studies have demonstrated that exogenously applied pre-formed oligomers are capable of inducing cellular pathology in both the SH-SY5Y cell line and neuron-

enriched cerebral cortical cells prepared from embryonic mice brains (Danzer *et al.*, 2007), and that inducing intracellular alpha-synuclein oligomerisation in human H4 neuroglioma cells, Human Embryonic Kidney cells and Chinese Hamster Ovary cells results in increased toxicity (Outeiro *et al.*, 2008).

Despite strong evidence that alpha-synuclein oligomers can be toxic, identifying the mechanism of oligomer induced toxicity is hindered by the heterogeneity of its aggregation products and the complex interactions which occur between oligomers and various cellular pathways implicated in PD. Mechanisms of oligomer induced toxicity which have been implicated to date include mitochondrial defects (Parihar *et al.*, 2009, Di Maio *et al.*, 2016), endoplasmic reticulum stress (Colla *et al.*, 2012a, Colla *et al.*, 2012b), inflammatory response (Zhang *et al.*, 2005, Wilms *et al.*, 2009), synaptic dysfunction (Diogenes *et al.*, 2012, Choi *et al.*, 2013, Kaufmann *et al.*, 2016), autophagic and lysosomal dysfunction (Klucken *et al.*, 2012, Bliederhaeuser *et al.*, 2016), membrane disruption (Volles and Lansbury, 2002, Danzer *et al.* 2007) and cell to cell propagation (Kordower *et al.*, 2008, Li *et al.*, 2008, Mendez *et al.*, 2008, Danzer *et al.*, 2009, Lee *et al.*, 2010, Danzer *et al.*, 2012). Alpha-synuclein oligomer membrane disruption and cell to cell propagation have been investigated in this chapter, and will be described in more detail below.

4.1.1.1 Alpha-synuclein membrane disruption

One well studied mechanism of alpha-synuclein toxicity is through its interactions with cellular membranes. As described in Section 1.3.2 monomeric alpha-synuclein is known to be capable of binding to membranes, and it is thought this ability may be important for its physiological function, supported by the observation that the six known PD causing variants in alpha-synuclein occur within the membrane binding

region of the protein. Aside from the physiological membrane binding of alpha-synuclein, it has been shown that certain oligomeric species of the protein can form pores in biological membranes, leading to calcium influx and subsequent cell death (Danzer *et al.*, 2007; Feng *et al.*, 2010; E Illes-Toth *et al.*, 2015; Pacheco *et al.*, 2015). It has also been demonstrated that alpha-synuclein is able to bind to mitochondrial membranes, resulting in the production of ROS and subsequent cellular damage (Parihar *et al.*, 2008, 2009; Paillusson *et al.*, 2017; Ludtmann *et al.*, 2018) and that targeting the interaction of oligomers and membranes can reduce alpha-synuclein toxicity through displacement of the protein from the membrane, interfering with membrane-induced self-assembly and vesicle disruption (Wrasidlo *et al.*, 2016).

4.1.1.2 Alpha-synuclein propagation

A second potential mechanism of alpha-synuclein oligomer induced toxicity which has received much attention in recent years is the possibility of the protein spreading pathology in a prion-like manner. This theory originated from the observation that upon neuropathological examination, LB pathology tended to follow a stereotypical pattern *in vivo*, undergoing an ascending distribution from the lower brainstem and olfactory bulb to the limbic system and, finally, the neocortex (Braak *et al.*, 2003). This typical propagation of alpha-synuclein pathology between anatomically interconnected brain areas correlates with the characteristic progression of PD symptoms observed clinically, as detailed in Figure 4.1, with the Braak model of PD proposing that LB pathology spreads over time between axonally connected structures (Braak *et al.*, 2006). Moreover it has been proposed that this process is initiated by a 'causative agent' affecting the olfactory bulb and autonomic nerves before spreading pathology through the interconnected neuronal pathways (Hawkes, Del Tredici and

Braak, 2007). This hypothesis was supported in 2008 by ground breaking findings of LB pathology in foetal dopaminergic neuron grafts which had been transplanted into PD subjects 11 – 16 years prior to their death (Kordower *et al.*, 2008; Li *et al.*, 2008); a phenomenon which has been successfully replicated in animal models (Angot *et al.*, 2012). The discovery of LB pathology in these relatively young neurons was strongly suggestive of alpha-synuclein pathology spreading from diseased to healthy cells in a prion-like manner, a hypothesis with important implications for our understanding of PD and the development of potential therapeutics. Consequently, much research has been undertaken to attempt to elucidate the mechanism of prion-like alpha-synuclein spread. It has been shown that Lewy body extracts derived from PD brains were able to trigger alpha-synuclein pathology and neurodegeneration in animal models (Recasens and Dehay, 2014), providing further evidence that alpha-synuclein is capable of spreading from diseased to healthy cells. Data from *in vitro* and *in vivo* models suggests that certain oligomeric forms of alpha-synuclein are able to promote cell-to-cell propagation, aiding in the spread of pathology (for a review see Longhena *et al.*, 2017). The species of alpha-synuclein oligomer appears to be crucial to its seeding capability, as *in vitro* and *in vivo* studies have demonstrated that both fully formed fibrils (Luk *et al.*, 2012) and certain oligomeric populations (Danzer *et al.*, 2007; Fagerqvist *et al.*, 2013) do not have seeding capabilities.

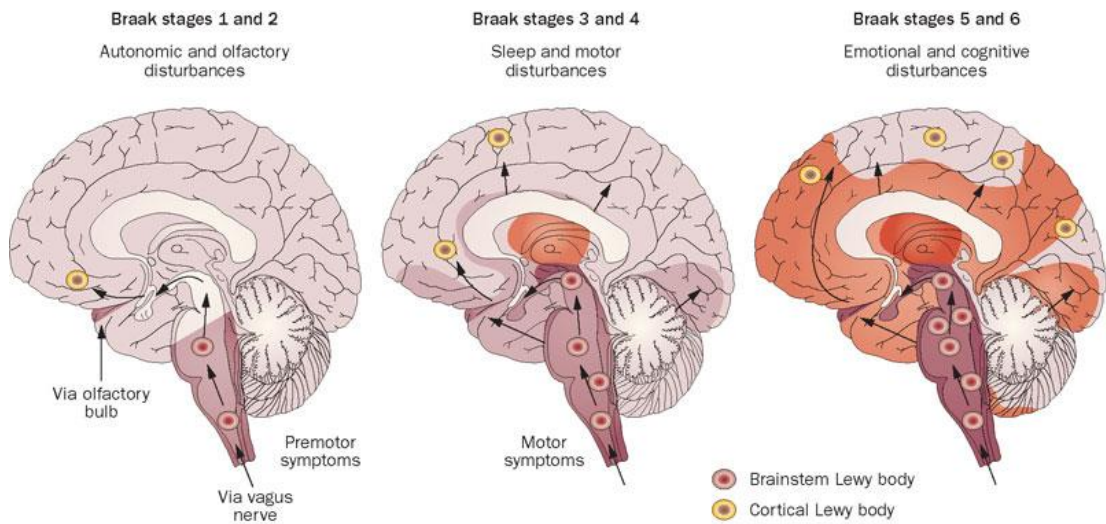


Figure 4.1: Braak staging of PD brain pathology. Proposed mechanism of the progression of PD brain pathology, showing the initiation sites in the olfactory bulb and the medulla oblongata, through to the later infiltration of Lewy pathology into cortical regions. Image taken from Doty (2012).

The molecular events at each step of alpha-synuclein propagation (the seeding of aggregates, release of aggregates from diseased cells and entry of aggregates into healthy cells) have been the subject of intense investigation (reviewed by Brundin and Melki, 2017). In order for alpha-synuclein to be capable of seeding aggregates it must have the ability to induce conformational change and aggregation in another molecule. This property is well established for alpha-synuclein both *in vitro* (Luk *et al.*, 2009) and *in vivo* (Masuda-Suzukake *et al.*, 2013). One mechanism through which alpha-synuclein is thought to be released from cells is via misfolding-associated protein release, which occurs under conditions of proteasomal dysfunction and has been repeatedly linked to PD (Lee *et al.*, 2016). Other proposed mechanisms of alpha-synuclein release include exocytosis (Lee, 2005; Jang *et al.*, 2010) and secretion in exosomes (Danzer *et al.*, 2012; Fussi *et al.*, 2018). Released alpha-synuclein is thought to be able to enter donor cells through several possible mechanisms, such as through endocytosis (Desplats *et*

al., 2009), direct penetration (Jiang *et al.*, 2017), tunnelling nanotubules (Abounit *et al.*, 2016) and membrane receptor mediated access (Lee *et al.*, 2008; Mao *et al.*, 2016).

4.1.2 Oxidative stress is associated with PD

Strong evidence suggests that OS may play a key role in the cascade of events leading to the loss of dopaminergic neurons seen in PD (Gaki and Papavassiliou, 2014). OS is the result of an imbalance between ROS and the ability of an organism to counteract their action by antioxidative protection systems. At normal physiological levels ROS act as signalling molecules which are involved in the regulation of cell proliferation, apoptosis and gene expression (Poljsak, Šuput and Milisav, 2013). However ROS which are not counteracted by antioxidants can cause damage to many components of the cell, including DNA, lipids and proteins. Up until a threshold level the cell is able to counteract the OS and promote survival. However, if the balance of ROS to antioxidants becomes too dysregulated, cellular damage caused by ROS will eventually lead to cell death, which is believed to be one mechanism involved in the development of PD (Dias, Junn and Mouradian, 2013). ROS have various intra and extracellular origins. The largest source of intracellular oxidants is the mitochondria and its respiratory chain. Free radicals of oxygen are generated as a normal result of oxygen metabolism as during aerobic respiration mitochondria reduce O₂ to H₂O and through this process produce the superoxide anion radical (O₂⁻), hydrogen peroxide (H₂O₂) and the hydroxyl radical (OH[•]). Other sources of ROS production include microbial infections involving phagocyte activation, interactions between redox-active metals and oxygen species, the degeneration of fatty acids by peroxisomes and the oxidative metabolism of ingested toxins. The human body is equipped with a variety of

antioxidants which counteract ROS, including superoxide dismutase, glutathione (GSH) and catalase (for a review see Rahal *et al.*, 2014).

There are several pathways specific to nigrostriatal dopaminergic neurons which leave them particularly vulnerable to OS. Firstly, the process of dopamine metabolism is a source of ROS. Certain enzymes involved in dopamine metabolism, such as MAO, TH and L-amino acid oxidase, produce H_2O_2 as a by-product of their activity (Segura-Aguilar *et al.*, 2014). MAO is known to catabolize excess cytosolic dopamine, producing ROS (Segura-Aguilar *et al.*, 2014). Excess cytosolic dopamine can occur as a result of neuron damage or levodopa treatment (Blesa, Lanciego and Obeso, 2015). Mitochondrial impairment is a second mechanism which seems to affect nigrostriatal dopaminergic neurons in particular. Impairment or inhibition of mitochondrial complex I are known to lead to an increase in ROS production and subsequent apoptosis (Franco-Iborra, Vila and Perier, 2015). Studies have shown that mitochondrial complex I inhibitors such as 1-methyl-4-phenyl-1,2,3,6-tetrahydropyridine (MPTP) (Langston *et al.*, 1983) and rotenone (Betarbet *et al.*, 2000) result in the highly specific degeneration of nigrostriatal dopaminergic neurons, resulting in a Parkinsonian phenotype. Mutations in many PD associated genes are known to affect the mitochondria, and these changes are associated with an increase in OS in dopaminergic SNpc neurons (Blesa, Lanciego and Obeso, 2015). A third source of ROS specific to these cells is iron, stored in neuromelanin. Neuromelanin has high affinity for transition metals, with both high and low affinity binding sites for iron. At physiological iron levels the majority of iron is found bound to the high affinity sites, where it is stored in an inactive form. At increased concentrations of iron, neuromelanin's high affinity sites are saturated and more iron will bind to the low

affinity sites, where it can accumulate in an inactive form and catalyse the Fenton reaction (Zucca *et al.*, 2017). Additionally, neuromelanin saturated with iron has been shown to oxidise dopamine, exacerbating OS (Zecca *et al.*, 2008).

Considerable evidence from both PD patients and experimental models supports that increased OS is seen in both sporadic and familial cases of PD. Evidence of OS has been provided through detection of oxidised DNA, lipids and proteins in the brains of PD patients (Bosco *et al.*, 2011). A meta-analysis of studies designed to identify oxidative stress markers in PD demonstrated that patients have increased levels of the OS damage markers 8-OHdG and malondialdehyde and the reactive nitrogen species nitrite in peripheral blood. Conversely, decreased levels of the antioxidants catalase, uric acid and glutathione were found (Wei *et al.*, 2018).

4.1.3 Cell culture models of PD

Despite advances in PD research, the mechanisms underlying neuronal degeneration remain unclear. *In vitro* cellular models are a useful tool to investigate molecular pathologies underlying PD and provide an opportunity to develop therapeutic strategies to alter these pathologies. A major challenge of conducting research into age-related neurodegenerative disorders is that there are no cellular or animal models capable of recapitulating all features of the disease. When attempting to investigate the molecular mechanisms underlying complex disorders such as PD it can be useful to break down and investigate each pathological disease process individually, which is particularly important when there is limited understanding of the pathogenic mechanisms underlying the disease. The use of *in vitro* cellular models can be a helpful tool to increase understanding in this area. A range of cell culture models are commonly used in PD research, most frequently immortalized human and animal cell

lines, primary cells and stem cells. In PD multiple types of neuronal cells are known to degenerate. However, due to the importance of motor symptoms in PD there has been a focus on the use of dopaminergic cell models to try to recapitulate the mechanisms underlying the degeneration of dopaminergic neurons in the SNpc, which gives rise to these motor symptoms. SH-SY5Y cells are a popular choice in PD research, and the cell model used in this thesis (for a review of the use of SH-SY5Y cells in PD research see Xicoy, Wieringa and Martens (2017)). SH-SY5Y cells are a subline of the SK-N-SH line, established in 1970 from a bone marrow biopsy of a metastatic neuroblastoma of a 4 year old female. The SH-SY5Y line undergoes 3 rounds of clonal selection, from SK-N-SH to SH-SY to SH-SY5 to SH-SY5Y. These cells have many advantages. They are inexpensive to obtain and culture and they amplify rapidly, allowing experiments requiring large numbers of cells to be performed. These cells are of human origin, and so express human specific proteins. SH-SY5Y cells express dopamine receptors and transporters, and are vulnerable to oxidative stress. It is important to note that while there are genetic alterations in these cells, being from a neuroblastoma, PD related pathways which they are commonly used to study (such as the UPS, ROS metabolism and DA metabolism) remain unaffected (Krishna *et al.*, 2014). However, SH-SY5Y cells are difficult to differentiate into a post-mitotic mature dopaminergic state (Constantinescu *et al.*, 2007) and, at present, there is no consensus on many fundamental aspects of their use such as culture media composition and differentiation protocols (Xicoy, Wieringa and Martens, 2017).

4.2 Aims and Objectives

The purpose of this chapter was to further investigate the calcium influx inducing Type A and intracellular aggregation seeding Type C oligomers first characterised by Danzer *et al.* (2007). Previous investigations into these oligomeric species have been conducted using oligomers produced from unmodified recombinant alpha-synuclein. As discussed in detail in Section 2.1.3.2, alpha-synuclein is known to be constitutively acetylated *in vivo*. In this chapter the SH-SY5Y cell line was used as a model to investigate the effect of N-terminal acetylation on the cellular effects of these two oligomeric populations. Furthermore, the response of these cells following treatment with Type C oligomers was further investigated, with an emphasis on OS.

The specific aims of this chapter were:

1. To establish whether N-terminal acetylation affected the cytotoxicity of Type A and C oligomers.
2. To establish whether N-terminal acetylation affected the ability of Type C oligomers to induce intracellular aggregation.
3. To further investigate the effect of Type C oligomers inducing intracellular alpha-synuclein aggregation in SH-SY5Y cells.
4. To establish whether Type C oligomers are able to induce a stress response in SH-SY5Y cells.

4.3 Methods

4.3.1 Production of alpha-synuclein oligomers

Unmodified and N-terminally acetylated alpha-synuclein was produced as described in Section 2.3.7/2.3.8. 'Type A' and 'Type C' oligomeric species were prepared as described by Danzer *et al.* (2007), unless otherwise stated. In brief, Type A oligomers were prepared by reconstituting lyophilised alpha-synuclein in 50 mM sodium phosphate buffer (SPB) (pH 7.0) containing 20% ethanol to a final concentration of 7 μ M. Following a four hour incubation at 21 °C with continuous shaking, solutions were lyophilised and resuspended in one half the starting volume in 50 mM SPB (pH 7.0) containing 10% ethanol. These solutions were shaken at 21 °C for 24 hours with open lids to evaporate residual ethanol, followed by 6 days of shaking at 21 °C with closed lids. Type C oligomers were prepared by reconstituting lyophilised protein in 50 mM SPB (pH 7) containing 20% ethanol to a final concentration of 7 μ M and incubating at 21 °C overnight with continuous shaking, followed by concentration 1:14 using ultracentrifugation (VivaSpin 500 columns, MWCO 30 kDa, GE Healthcare) allowing the separation of oligomeric species from monomeric protein. Type A and Type C oligomeric species were used for experiments immediately after production.

4.3.2 Maintenance and cryopreservation of SH-SY5Y neuroblastoma cell line

All cell culture methods were carried out under sterile conditions in a class II laminar flow cabinet. SH-SY5Y human neuroblastoma cells were purchased from the European Collection of Authenticated Cell Cultures (Cat. No. 94030304, Public Health England, Salisbury, UK). Cell cultures were maintained in high glucose Dulbecco's modified

Eagle's GLUTAMAX™ medium (DMEM) (Gibco) supplemented with 10% (v/v) foetal bovine serum (FBS) and 1% (v/v) penicillin-streptomycin (Invitrogen) at 37 °C in a humidified atmosphere containing 5% CO₂. Cells were purchased at passage 16 and used up to a maximum of passage 25. Stocks of 1x10⁶ cells per cryovial were preserved in liquid nitrogen dewars for long-term storage in a solution of 90% FBS/10% dimethyl sulfoxide.

4.3.3 CellTox™ Green Cytotoxicity Assay

Following manufacturer guidelines the Express, No-Step Addition at Dosing method of the CellTox™ Green Cytotoxicity Assay (Promega) was performed on SH-SY5Y cells. Briefly, SH-SY5Y cells were seeded at 1x10⁴ cells per well and cultured for 48 hours in black-walled 96-well plates before treatment with test compounds. 1 µL of CellTox™ Green Dye was added to each 500 µL of test compound diluent and/or vehicle control before adding to the cells and incubating at 37 °C/5% CO₂ for the desired treatment time. Following treatment fluorescence was measured using a CLARIOstar plate reader (BMG LABTECH, Buckinghamshire, UK) with excitation at 485 nm and emission at 520 nm.

4.3.4 Resazurin reduction assay

Resazurin sodium salt (Sigma-Aldrich) was dissolved in PBS to 3 mg/mL, sterilised through a 0.2 µm filter into a light protected container and stored at 4 °C before use. SH-SY5Y cells were seeded at 1x10⁴ cells per well in opaque-walled 96-well plates and cultured for 48 hours before treatment with test compounds. Following treatment with various alpha-synuclein species and appropriate controls, test medium was replaced with growth medium containing 0.03 mg/mL resazurin and the cells

incubated for a further two hours at 37 °C/5% CO₂. Culture media was incubated with resazurin in parallel as a blank control. Fluorescence was then measured using a CLARIOstar plate reader with excitation at 560 nm and emission at 590 nm.

4.3.5 Immunocytochemistry

For immunofluorescence staining SH-SY5Y cells were seeded at 4×10^4 cells per well and cultured and treated with test compounds in 8 well Lab-Tek II chamber slides (Nunc, 154534). Following treatment, culture medium was removed from each well and cells washed with PBS before fixation and permeabilisation in ice-cold methanol for 15 minutes at -20 °C. The cells were then washed in PBS containing 0.1% (v/v) Tween-20 (PBS-T). Non-specific binding sites were blocked using 1% (w/v) BSA in PBS for one hour at room temperature under continuous gentle shaking. After blocking, cells were washed three times in PBS-T before incubation with primary antibody (anti- α -synuclein syn211 monoclonal antibody (1:2000, Fisher, AFMA112874)) in blocking solution for 1 hour at room temperature under continuous gentle shaking. Three more PBS-T wash steps were performed before cells were incubated with secondary antibody (Texas Red[®] goat anti-mouse polyclonal IgG H+L (1:1000, Invitrogen; T6390)) in blocking solution for 1 hour at room temperature under continuous gentle shaking. Cells were washed four times with PBS-T before mounting using ProLong[™] Diamond Antifade Mountant with DAPI (Invitrogen[™], ThermoFisher Scientific, Loughborough, UK). To assess background fluorescence primary antibody was omitted in a designated chamber and all other steps were performed as described above. Slides were left to cure overnight at 4 °C in the dark prior to image capture using an Olympus BX60 bright field/fluorescence microscope. Evaluation of percentage of cells containing alpha-synuclein inclusions was performed by counting the number of cells per field of vision

containing clear alpha-synuclein immunopositive inclusions, expressed as a percentage of total cell count. To quantify total fluorescence per cell, images were analysed using the image analysis software ImageJ 1.50i using the corrected total cell fluorescence (CTCF) calculation shown below, where the background fluorescence of a selected area is subtracted from the fluorescence value of a measured area:

$$CTCF = \frac{\text{Integrated density} - (\text{mean background fluorescence} \times \text{area})}{\text{cell number}}$$

4.3.6 Preparation of conditioned media

To prepare conditioned cell culture media for dot blot analysis, SH-SY5Y cells were cultured and treated with test compounds as described in Section 4.3.5. Following treatment, media containing test compounds was removed; the cells washed once with PBS-T and then incubated with fresh culture media for one hour. This conditioned media was removed from the cells, 2 mM of PMSF added and the media centrifuged at 16000 x g for 15 minutes at 4 °C. The supernatant was aliquoted and stored at -80 °C for future analysis.

4.3.7 Dot blotting

0.05% Triton X-100 was added to samples of conditioned media. Nitrocellulose membranes (0.45 µM, GE Healthcare, Sweden) were spotted with 1 µL of sample or positive/negative control, allowed to dry and blocked for 1 hour in 5% (w/v) non-fat milk (NFM) in TBS-T. Primary antibody (anti-α-synuclein syn211 monoclonal antibody

(1:2000, Fisher, AFMA112874)/anti-alpha-synuclein phospho S129 antibody (1:2000, abcam, ab51253)) was diluted in 1% NFM TBS-T and incubated with the membrane overnight under continuous gentle shaking at 4 °C. Three wash steps were performed with TBS-T before incubation with secondary antibody (goat anti-mouse IRDye® 800 nm CW secondary antibody (1:15,000 dilution, Cat. No. 925-32210, LI-COR)/donkey anti-rabbit IRDye® 680 nm CW secondary antibody (1:15,000 dilution, Cat. No. 925-68073, LI-COR) diluted in 1% (w/v) NFM TBS-T for 1 hour under continuous gentle shaking at room temperature. Visualisation was performed using the LI-COR Odyssey and Odyssey Infrared Imaging software (LI-COR, Nebraska, USA).

4.3.8 GSH/GSSG-Glo™ Assay

Following manufacturer guidelines (Promega) the Assay Procedure for Measuring GSSG and Total Glutathione in Adherent Mammalian Cells was performed. Briefly, SH-SY5Y cells were seeded at 2×10^4 cells per well, cultured and treated in white opaque-walled 96-well plates. Test compounds were 10% (v/v) Type C alpha-synuclein oligomers, 10 µM menadione as a positive control and corresponding vehicle controls. Test compound and/or vehicle control was removed from the cells and replaced with 50 µl per well of Total Glutathione Lysis Reagent or Oxidized Glutathione Lysis Reagent as appropriate. 50 µL of Total Glutathione Lysis Reagent was also added to no-cell controls and wells containing a range of glutathione concentrations to produce a standard curve. The plate was then shaken for 5 minutes at room temperature. 50 µL per well of Luciferin Generation Reagent was added to all wells and incubated at room temperature for 30 minutes. 100 µL per well of Luciferin Detection Reagent was added and incubated at room temperature for 15 minutes. Luminescence was recorded using a CLARIOstar plate reader. The concentration of total and oxidised glutathione in

treated cells was extrapolated from the standard curve and the GSH/GSSG ratio calculated.

4.3.9 CellROX™ Green assay

Following manufacturer guidelines the assay procedure for measuring oxidative stress using CellROX™ Green Reagent was performed on SH-SY5Y cells. Briefly, SH-SY5Y cells were cultured and treated with test compounds on coverslips. The CellROX™ Green Reagent was then added to a final concentration of 5 μ M and the cells incubated for 30 minutes at 37 °C. Medium was then removed and cells washed with PBS. Cells were then fixed with 10% formalin and mounted using ProLong™ Diamond Antifade Mountant with DAPI. Slides were left to cure overnight at 4 °C in the dark prior to image capture using an Olympus BX60 bright field/fluorescence microscope. Corrected total cell fluorescence was calculated as described in Section 4.3.5.

4.3.10 Polysome profiling

4.3.10.1 Extract preparation

SH-SY5Y cells were plated at a density of 4×10^6 cells per T175 flask and cultured for 48 hours before treatment. Following treatment cells were incubated with the translation inhibitor cycloheximide (100 μ g/mL) for five minutes at 37 °C, washed and cells scraped in 5 ml of ice-cold PBS containing 100 μ g/mL cycloheximide. Cells were then pelleted by centrifugation at 500 x g for 5 min at 4 °C and resuspended in 450 μ l of hypotonic buffer (20 mM HEPES KOH (pH 7.4), 2 mM Magnesium Acetate, 0.1 M Potassium Acetate, 100 μ g/mL cycloheximide, 500 μ M DTT, 1x protease inhibitor cocktail and 100 units RNase inhibitor in DEPC treated distilled water). The mixture was vortexed for five seconds, before the addition of 25 μ L of 10% Triton X-100 and 25

μ l of 10% SDS, and vortexed for five more seconds. Lysates were incubated at 4 °C for five minutes before centrifugation at 16000 xg and the supernatant frozen at -80 °C for future analysis.

4.3.10.2 Preparation of sucrose density gradients

Varied concentrations of sucrose ranging from 15-50 % were prepared from a 60 % (w/v) DEPC treated sucrose stock and 10X polysome buffer (100 mM Tris acetate, pH 7.4, 700 mM NH₄OAc, 40 mM MgOAc). To generate a gradient, 2.25 mL of each solution was sequentially dispensed into open-top 12.0 mL polylallomer centrifuge tubes (Seton Scientific), starting with the 50% (w/v) sucrose solution and ending with the 15% (w/v) solution. Each layer was snap-frozen in liquid nitrogen before the next layer was added. Sucrose gradients were stored at -80 °C and thawed overnight at 4 °C prior to use.

4.3.10.3 Sedimentation of extracts on polysome gradients

The concentration of polysome extracts was determined using a NanoDrop 1000 spectrophotometer (ThermoFisher Scientific). 2.5 A₂₆₀ units of extract were layered on top of sucrose gradients. Sucrose gradients were centrifuged using a Th-641 swing-out rotor in a Sorvall WX Ultracentrifuge for 150 minutes at 4 °C. Polysomes were measured by upward displacement using 60% (w/v) sucrose; gradients were displaced using a fractionator that was connected to a UV-vis detector which measured polysomes at 254nm, producing a polysome trace as shown in the diagram in Figure 4.2. Monosomes/polysomes were measured and compared using NIH ImageJ software. 1 mL fractions were collected. 750 μ L of Trizol was added to each fraction before being frozen at -80 °C.

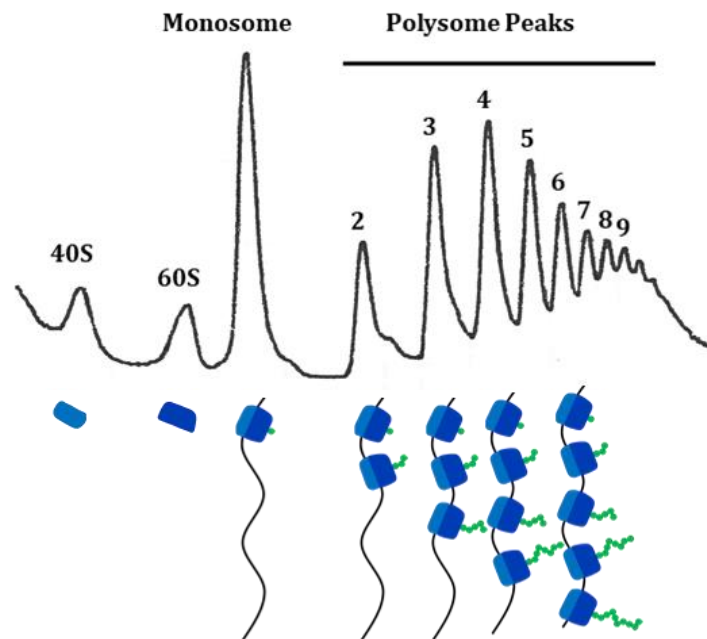


Figure 4.2: Schematic of polysome profiling traces. Following the addition of cycloheximide, ribosomes decoding mRNA become stalled. Cell extracts are then separated on a sucrose gradient before being passed through a UV detector to produce a polysome trace. With the exception of the 40S and 60S peaks, the peaks relate to the number of ribosomes attached to any given mRNA. As efficient translation can be attributed to multiple ribosomes translating along mRNAs, the area underneath the monosome peak can be compared to the polysome peaks to calculate a polysome/monosome ratio which can be compared to evaluate translational control and translation initiation.

4.3.11 Statistical Analysis

Statistical analysis was undertaken using StatsDirect version 3.0.126. Data was determined to be non-parametric following Shapiro-Wilk test of normality therefore a Kruskal-Wallis test was undertaken with post hoc analysis. Dwass-Steel- Critchlow - Flinger post hoc analysis was undertaken for data points > 6 and Conover-Inman post hoc analysis < 6 data points. *P* value < 0.05 is denoted on graphs by *.

4.4 Results and discussion

Several modes of action have been proposed as to how alpha-synuclein oligomers can elicit cytotoxicity and protocols have been established to enable the formation of oligomers with known cellular effects. Exogenous application of Type A and Type C alpha-synuclein oligomers characterised by Danzer *et al.* (2007) are known to reduce cell viability and increase cytosolic alpha-synuclein aggregation respectively. However, oligomers used in these studies were prepared from unmodified, recombinant alpha-synuclein. As discussed in detail in Chapter 2, *in vivo* alpha-synuclein is known to be constitutively acetylated at its N-terminus. The effect of Type A and Type C oligomers prepared from N-terminally acetylated alpha-synuclein on a cell culture model has, to the best of our knowledge, not previously been investigated.

4.4.1 Type A oligomers produced from both unmodified and N-terminally acetylated alpha-synuclein reduce the viability of SH-SY5Y cells

Exogenous application of the Type A pore forming oligomers of alpha-synuclein has been shown to result in an influx of calcium into SH-SY5Y cells, leading to reduced cell viability (Danzer *et al.* 2007). In order to assess the effect of N-terminal acetylation on alpha-synuclein cytotoxicity the viability of SH-SY5Y cells following 16 hour treatment with 10% (v/v) unmodified and N-terminally acetylated forms of monomer, Type A and Type C oligomers was assessed using both a CellTox Green Cytotoxicity Assay and a resazurin reduction assay, with results displayed in Figure 4.3.

The CellTox Green Cytotoxicity Assay allows the assessment of cell viability through detecting changes in membrane integrity which occur upon cell death. This allows the CellTox Green assay dye to enter cells and bind to their DNA, enhancing the dye's

fluorescent properties. Consequently fluorescence is proportional to cytotoxicity, with an increase in fluorescence correlating to a decrease in cell viability. Results following 16 hour incubation with the various treatments are shown in Figure 4.3 (a). Type A oligomers were the only treatment found to have a significant effect on cell viability. Type A oligomers were significantly cytotoxic to cells when made from both unmodified ($p = 0.0157$) and N-terminally acetylated ($p = 0.0035$) alpha-synuclein. Conversely, monomeric and Type C oligomeric forms of the protein were found not to have an effect on cell viability.

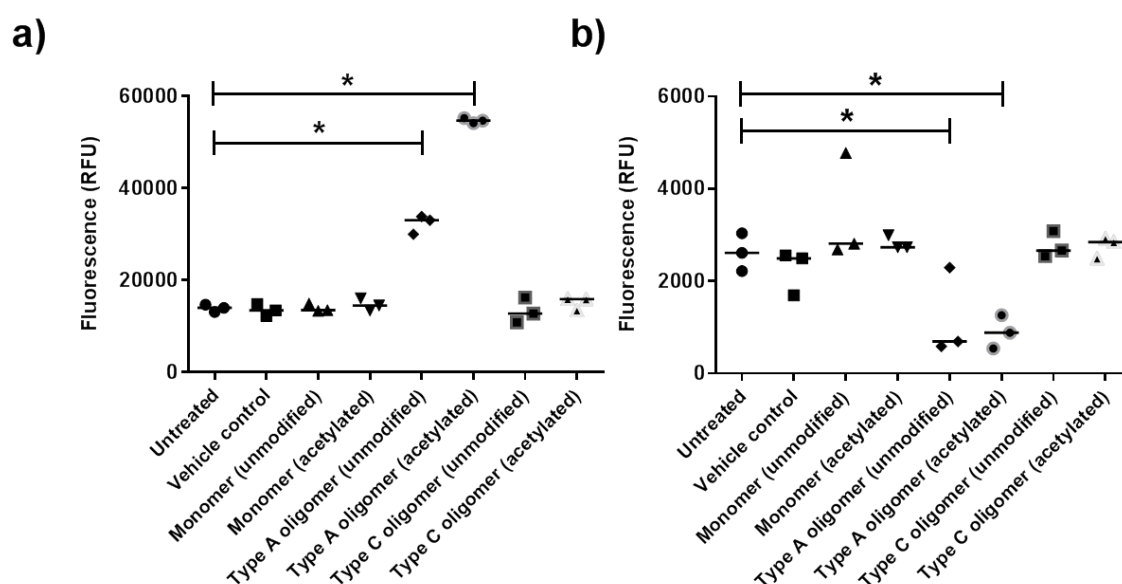


Figure 4.3: Cell viability assays of SH-SY5Y cells following 16 hour treatment with 10% (v/v) of various forms of unmodified and N-terminally acetylated alpha-synuclein. Results of CellTox Green Cytotoxicity Assay shown in a) and results of resazurin reduction assay shown in b). Statistical significance determined by Kruskal-Wallis test * = $P < 0.05$.

An alternate approach to assessing cell viability is through monitoring the metabolic activity of cells. Resazurin is a cell permeable, redox indicator which can be used to assess metabolic activity, and therefore cell viability. Metabolically active cells

maintain a reducing environment within their cytoplasm and mitochondria, which allows reduction of oxidised resazurin to reduced resorufin, which has detectable fluorescence. By monitoring this fluorescence the relative metabolic activity of cells can be determined. Resazurin reduction assay results following 16 hour incubation with the various treatments are shown in Figure 4.3 (b). The results of this assay are, in agreement with the CellTox Green Cytotoxicity Assay. Again, Type A oligomers were found to cause a significant decrease in viability when produced from both unmodified ($p = 0.0256$) and N-terminally acetylated ($p = 0.0152$) alpha-synuclein.

The results of these two viability assays demonstrate, in agreement with previous reports (Danzer *et al.* 2007, Illes-Toth *et al.* 2015), that Type A alpha-synuclein oligomers have a cytotoxic effect on the SH-SY5Y cell line. Monomeric and Type C oligomeric forms of the protein did not display a cytotoxic effect, indicating that this cytotoxic property is dependent on the oligomer species, and not a shared feature of all forms of alpha-synuclein. The previously unstudied N-terminally acetylated Type A oligomers were found to have a comparable effect on cell viability to the unmodified species, demonstrating for the first time that N-terminal acetylation does not alter the cytotoxic properties of these oligomers.

4.4.2 Type C oligomers produced from both unmodified and N-terminally acetylated alpha-synuclein cause an increase in cytosolic alpha-synuclein aggregate formation in SH-SY5Y cells

While the concept of intracellular propagation of alpha-synuclein has been extensively studied over the last decade, the precise mechanisms underlying this process remain uncertain. Exogenous application of Type C oligomers has been shown to cause a

reduction in homogeneous, cytoplasmic alpha-synuclein staining and an increase of punctate, aggregate formation in the cytosol and near the nucleus in neuronal cultures (Danzer *et al.* 2009).

The propensity of Type C oligomers, made from either unmodified or N-terminally acetylated alpha-synuclein, to induce aggregation when added extracellularly to SH-SY5Y cells was investigated here using immunocytochemistry. Representative images of cells treated with Type C oligomers or vehicle control, stained for DAPI (blue) and alpha-synuclein (red) are shown in Figure 4.4 (a). In agreement with previous work (Danzer *et al.*, 2009) an alteration in alpha-synuclein staining is seen in treated cells. The homogeneous, cytoplasmic staining seen in the vehicle control (and in untreated cells; representative image shown in Appendix Figure 3) is altered upon treatment with Type C oligomers, with punctate spots of heightened fluorescence observed, that are indicative of intracellular aggregates of the protein. This alteration was specific to Type C oligomers, as treatment with the equivalent concentration of monomer did not result in significant changes compared to the vehicle control (representative images on monomer treated cells shown in Appendix Figure 3). Figure 4.4 (b) shows analysis of this experiment, with fold change in CTCF normalised to the vehicle control shown in (i) and percentage of cells containing intracellular alpha-synuclein inclusions shown in (ii). It was found that the CTCF was significantly higher following treatment with both unmodified and N-terminally acetylated Type C oligomers, which could feasibly be due to the exogenously added oligomers or due to an increase in endogenous protein of the cells.

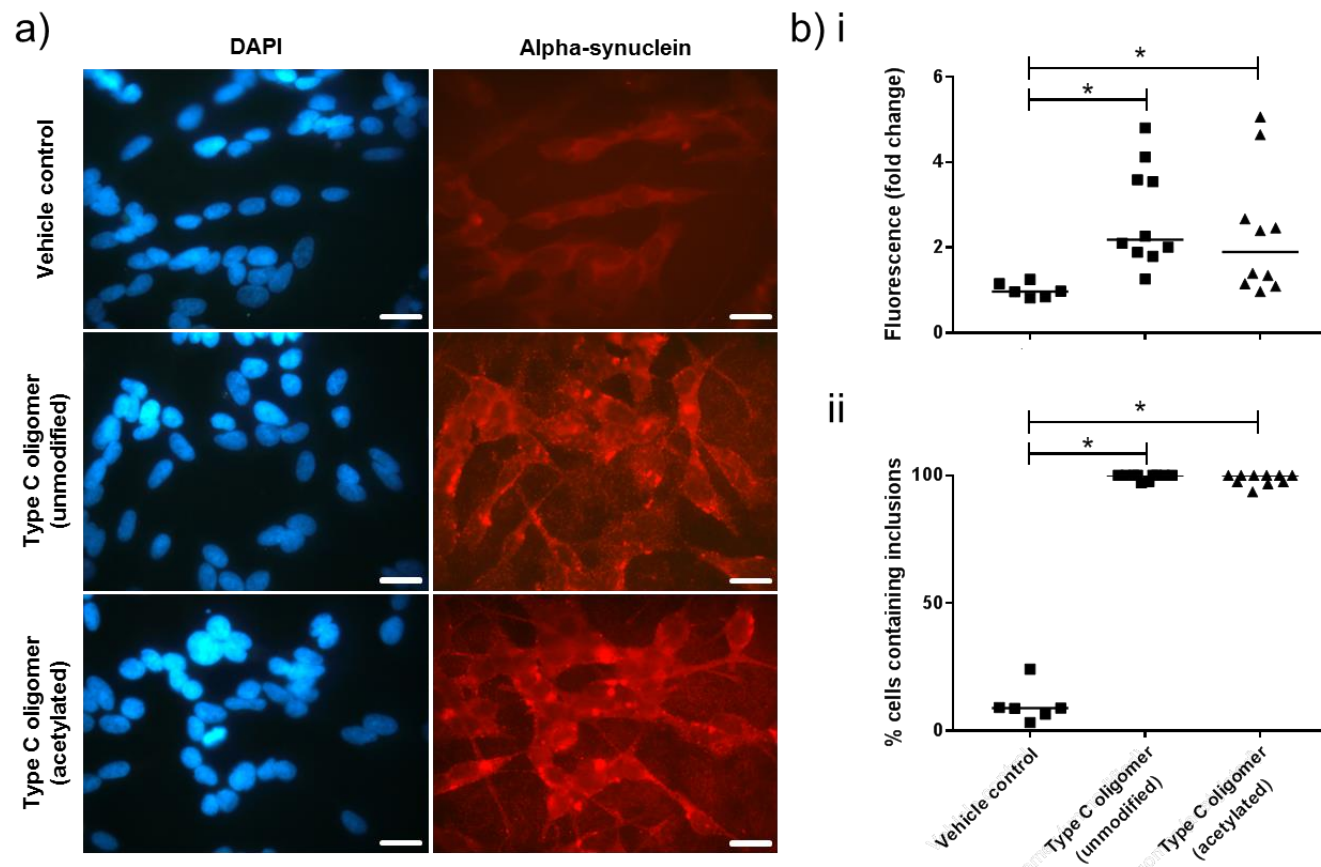


Figure 4.4: Immunocytochemistry of SH-SY5Y cells treated for 16 hours with 10% (v/v) unmodified or N-terminally acetylated Type C oligomers. Representative ICC images at 100x magnification of nuclear staining in blue and alpha-synuclein in red shown in (a) (scale bar = 20 μ m). CTCF of the red channel (alpha-synuclein) shown in (b) i, presented as fold change in fluorescence normalised to vehicle control. Percentage of cells per field of view containing alpha-synuclein inclusions shown in (b) ii. Statistical significance determined by Kruskal-Wallis test * = $P < 0.05$.

While a small proportion of vehicle treated cells were found to contain alpha-synuclein inclusions, in cells treated with Type C oligomers the percentage of cells containing inclusions was significantly increased for both unmodified and N-terminally acetylated oligomers. Representative results presented in Figure 4.4 were consistent upon biological repeats (n>3). This demonstrates, in agreement with previous reports (Danzer *at al.*, 2009), that the localisation of alpha-synuclein is altered in cells following treatment with these Type C oligomers. The presence of this protein in inclusions, rather than the usual homogenous cytoplasmic distribution is important as it provides supportive evidence for certain forms of the protein having the potential to seed fibril formation of endogenous alpha-synuclein, which has important implications as one potential explanation of the propagation of alpha-synuclein pathology observed in PD.

These results demonstrate that Type C oligomers are able to induce the formation of intracellular aggregates containing alpha-synuclein in SH-SY5Y cells. Assembling these oligomers from N-terminally acetylated alpha-synuclein did not alter this function, demonstrating for the first time that acetylation does not affect the capability of these oligomers to induce this cellular response. Throughout the rest of this chapter results presented were obtained following treatment with N-terminally acetylated alpha-synuclein species, as the more physiologically relevant form of the protein.

4.4.3 Extracellular alpha-synuclein staining is observed in SH-SY5Y cells treated with Type C oligomers and can be detected in conditioned cell media

As shown in Figure 4.4, treatment of SH-SY5Y cells with Type C oligomers results in an increase in fluorescence and the presence of punctate alpha-synuclein inclusions in the

cytoplasm. It was noted in the analysis of these images that with this treatment extracellular fluorescence was also repeatedly present, which was not seen in the vehicle control or monomer treated experiments. It was hypothesised that this extracellular staining could potentially result from original treatment protein not being taken up by the cell, debris from dead cells or secreted alpha-synuclein. To investigate this further, SH-SY5Y cells were treated with 10% (v/v) Type C oligomers for varied amounts of time.

Figure 4.5 (a) shows representative images from immunocytochemistry experiments performed following 1, 16 and 30 hour treatments with 10% (v/v) Type C oligomers. Following 1 hour treatment the extracellular region remains relatively clear of fluorescence, comparable with vehicle controls (Appendix Figure 3). In contrast, extracellular fluorescence is clearly present at both the 16 and 30 hour time points, indicating that an alpha-synuclein species is being secreted from the cells. Figure 4.5 (b) shows analysis of extracellular fluorescence in the red channel which has been quantified using ImageJ. It can be seen that there is no significant difference in extracellular fluorescence (compared to the vehicle control) at the 1 hour time point. Conversely, extracellular fluorescence significantly increased at the 16 and 30 hour time points. If extracellular fluorescence was a result of exogenous alpha-synuclein oligomers not being taken up by cells it would be anticipated that any extracellular fluorescence would be detectable immediately following treatment, and stay consistent throughout treatment times. As background fluorescence was low at the one-hour time point then increased over time, these results support the idea that the extracellular fluorescence cannot be singularly attributable to original treatment protein.

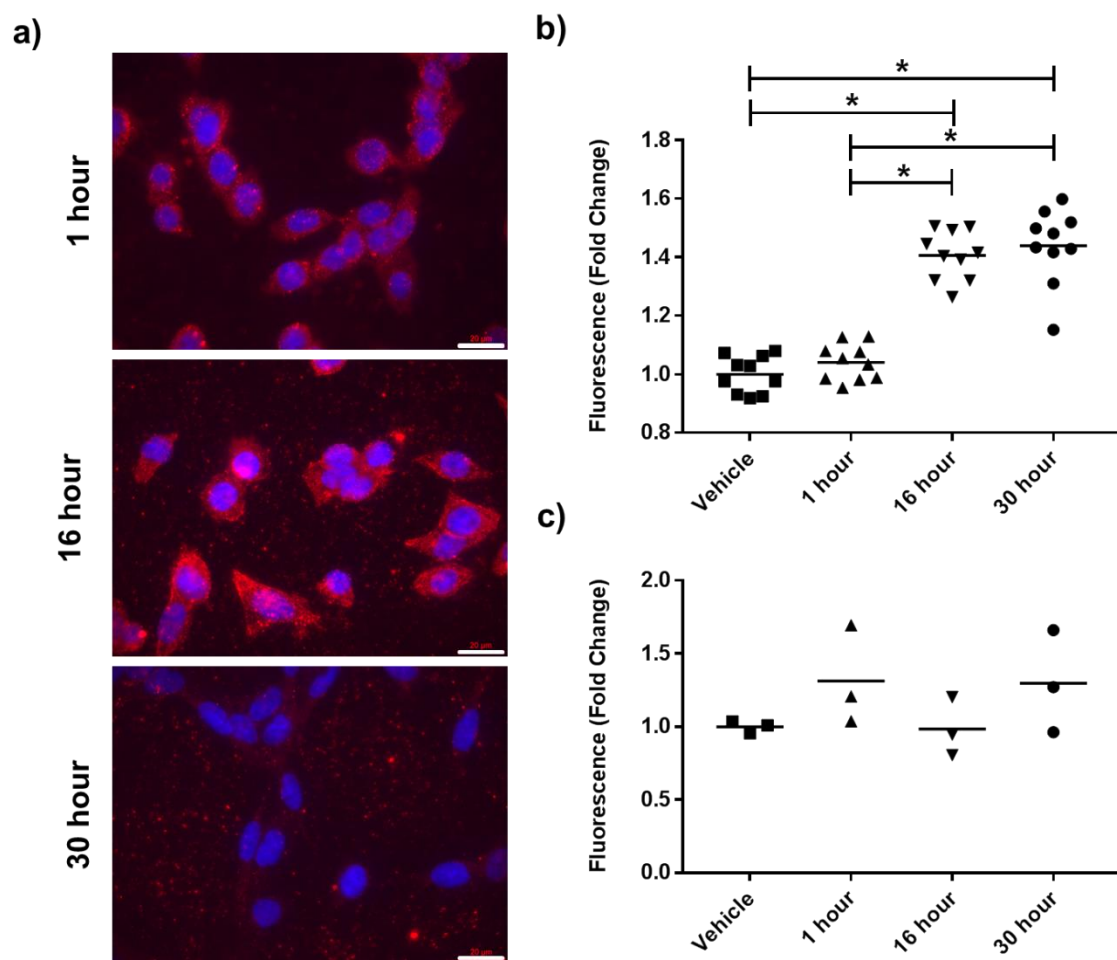


Figure 4.5: ICC and cell viability of SH-SY5Y cells treated with 10% (v/v) Type C oligomers for 1, 16 and 30 hours. Representative ICC images at 100x magnification of nuclear staining in blue and alpha-synuclein in red shown in (a) (scale bar = 20 μ m). Quantification of extracellular fluorescence in the red channel normalised to the vehicle control shown in (b). CellTox Green Cytotoxicity Assay at corresponding time points displayed as fold change, normalised to vehicle control shown in (c). Statistical significance determined by Kruskal-Wallis test * = $P < 0.05$.

In order to investigate cell death as a potential cause of extracellular fluorescence cell viability was assessed in parallel using the CellTox Green Cytotoxicity Assay, with results shown in Figure 4.5 (c). No significant differences in cells treated with Type C oligomers were seen compared to the vehicle control at any of the time points tested. As the vehicle control contains little extracellular fluorescence this provides evidence against the background fluorescence in oligomer treated cells being attributable to debris from cell death, as no significant difference in viability was seen. This leaves the possibility of the extracellular fluorescence being attributable to alpha-synuclein being secreted from the viable, treated cells.

While alpha-synuclein was originally thought of as an exclusively intracellular protein (due to its lack of a signalling sequence), it is now well established that this protein is detectable in extracellular fluids including the plasma (El-Agnaf *et al.*, 2003) and CSF (Borghi *et al.*, 2000) of both PD patients and unaffected individuals. To investigate whether alpha-synuclein was being secreted from SH-SY5Y cells treated with Type C oligomers a dot blot assay was performed on conditioned media using antibodies to detect both alpha-synuclein and alpha-synuclein phosphorylated specifically at serine 129 (ps129). The conditioned media was analysed for the presence of ps129 due to the known association between this post-translational modification and PD, as discussed in Section 1.3.2. Vehicle control, monomeric or Type C oligomeric treatments were applied to SH-SY5Y cells for 16 hours in the same manner as for immunocytochemistry experiments. Following 16 hour treatment media was removed, cells washed and fresh growth media applied. Cells were incubated in this growth media for 1 hour. Conditioned media was then collected and subject to dot blot analysis. As shown in Figure 4.6, negligible signal was detected from either antibody in conditioned media of

cells treated with vehicle control or monomeric alpha-synuclein. This demonstrates that these cells do not release alpha-synuclein to a significant degree able to be detected by this method, which corresponds to the lack of extracellular fluorescence seen in immunocytochemistry images. The lack of signal from the anti-alpha-synuclein antibody in the monomeric treatment demonstrates that the removal of treatment media and wash steps were sufficient to remove any treatment protein which had not been internalised by the cells.

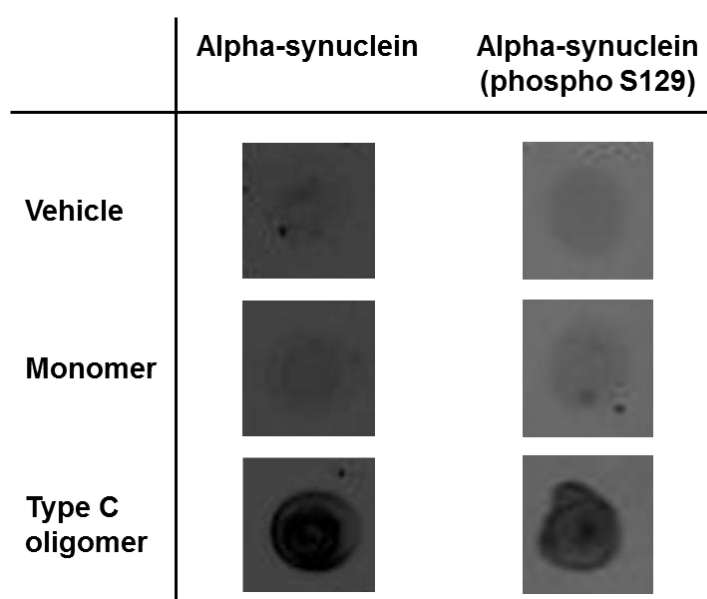


Figure 4.6: Dot blot of conditioned media from SH-SY5Y cells treated for 16 hours with 10% (v/v) vehicle control, monomeric or Type C oligomeric alpha-synuclein.

On the contrary, cells treated with Type C oligomers display a signal clearly detectable from the alpha-synuclein antibody, demonstrating that alpha-synuclein is being released into the media by these treated cells. This provides supporting evidence to the extracellular fluorescence seen in Figure 4.4 and 4.5 being attributable to treated SH-SY5Y cells secreting alpha-synuclein into the culture media. It is plausible that the alpha-synuclein detected could be from either the original treatment oligomers, or

endogenous alpha-synuclein produced by the cells themselves. More notably signal was also detected in the conditioned media of Type C oligomer treated cells from the antibody to ps129. Under physiological conditions approximately 4% of alpha-synuclein is phosphorylated at one or more of its sites (Fujiwara et al, 2002). In contrast, approximately 90% of the alpha-synuclein deposited in LBs is ps129 (Anderson *et al.*, 2006), suggesting phosphorylation at this site may be associated with PD. Several lines of evidence point towards phosphorylation of alpha-synuclein being associated with its secretion from cells. PD patients have been shown to have increased ps129 alpha-synuclein in their blood plasma compared to controls (Foulds *et al.*, 2013). It has been demonstrated that ps129 is important for modulating the clearance of alpha-synuclein inclusions through autophagy (Tenreiro *et al.*, 2014), and moreover it has recently been shown that alpha-synuclein can be secreted in exosomes as a compensatory mechanism of clearance when autophagy is impaired (Fussi *et al.*, 2018). An increase in alpha-synuclein ps129 has also been associated with conditions of cellular stress, with studies demonstrating that conditions which result in oxidative stress correlate to an increase in ps129 (Arawaka *et al.*, 2017).

4.4.4 Type C oligomers evoke a stress response in SH-SY5Y cells

While no significant effect on cell viability was found in SH-SY5Y cells treated with Type C oligomers, due to the finding of ps129 alpha-synuclein in conditioned media of treated cells various cellular stress assays were conducted to investigate the possibility of these oligomers inducing a stress response. Three cellular stress assays were performed; CellROX green assay, glutathione assay and polysome profiling. Menadione, a compound known to generate intracellular ROS (Criddle *et al.*, 2006; Loor *et al.*, 2010) was used as a positive control in each experiment at 10 μ M, a

concentration chosen to induce OS but not significantly reduce cell viability, based on IC50 calculations on SH-SY5Y cells under our laboratory conditions (IC50 curve shown in Appendix Figure 4).

4.4.4.1 Treatment of SH-SY5Y cells with Type C oligomers results in an increase in ROS

CellROX Green Reagent is a cell-permeable fluorogenic probe which exhibits fluorescence upon oxidation by ROS and subsequent binding to DNA. Therefore this assay directly detects changes in ROS levels. Figure 4.7 displays results from a CellROX Green Assay conducted on SH-SY5Y cells treated with 10% (v/v) vehicle control, positive control, alpha-synuclein monomer or Type C oligomers following a 2 hour incubation. Figure 4.7 (a) shows representative images of DAPI and CellROX Green staining under each condition. CTCF was used as a method of analysing experimental images, with results displayed in Figure 4.7 (b). Here it can be seen that treatment with both Menadione and Type C oligomers resulted in an increase in CTCF, and therefore an increase in ROS in these cells, showing that both of these treatments are evoking an oxidative stress response from the cells. No increase in CTCF was found following 2 hour treatment with either vehicle control or alpha-synuclein monomer. This demonstrates that the increase in ROS following treatment with Type C oligomers is not a general response to the alpha-synuclein protein, but is conformation specific.

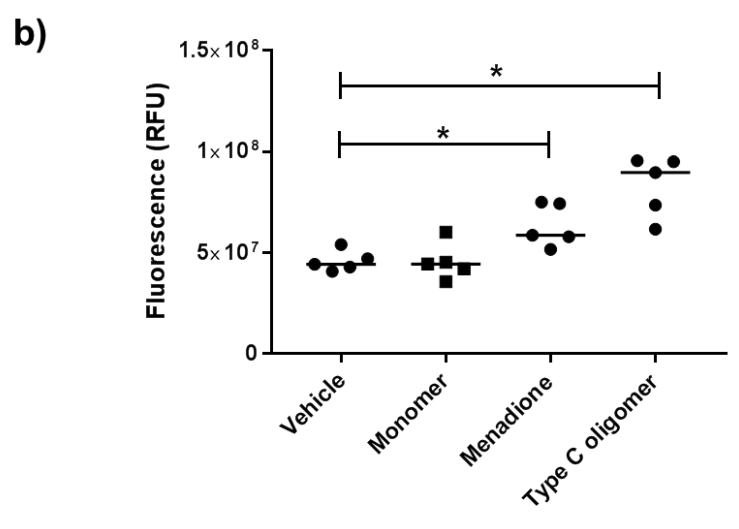
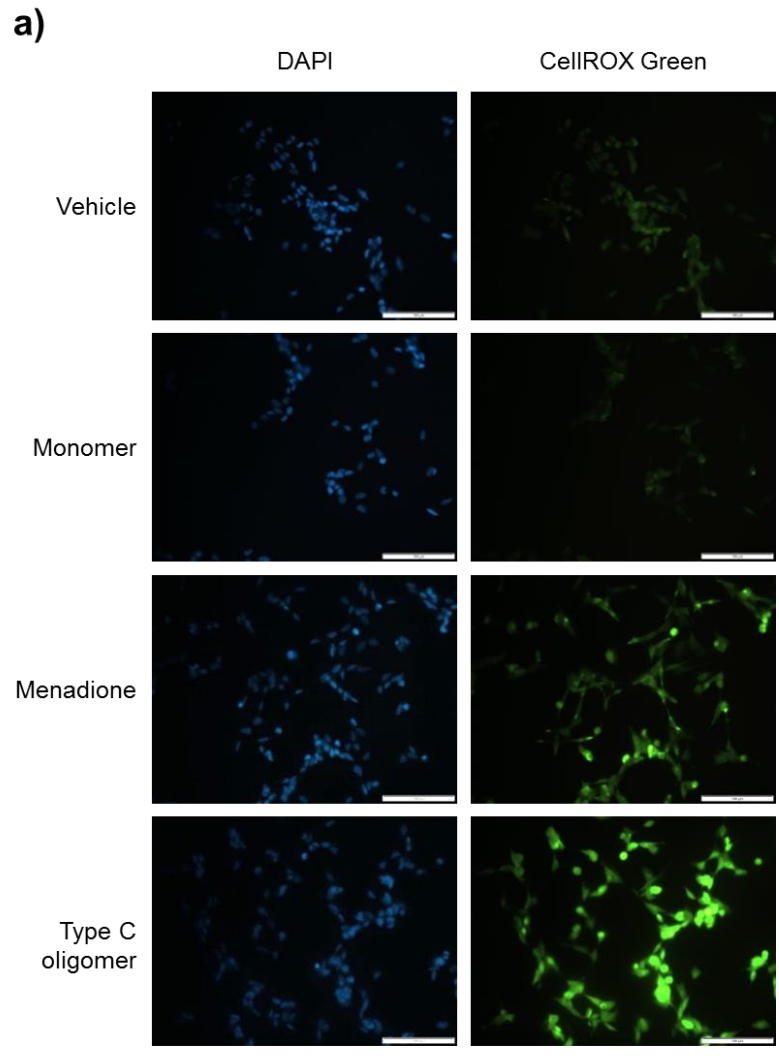


Figure 4.7: CellROX Green oxidative stress assay of SH-SY5Y cells treated for 2 hours with 10% (v/v) vehicle control, positive control (Menadione), monomer or Type C oligomer. Representative images at 40x magnification shown in (a) (scale bar = 100 μ m) and CTCF of the green channel shown in (b). Statistical significance determined by Kruskal-Wallis test * = $P < 0.05$.

4.4.4.2 Treatment of SH-SY5Y cells with Type C oligomers results in an altered

GSH/GSSG ratio

As described in Section 4.1.2, OS can be a result not only of an increase in ROS, but also a disruption in the balance of ROS to antioxidants. One important antioxidant is glutathione, a tripeptide consisting of glutamate, cysteine and glycine, with the reactive thiol group of the cysteine residue acting as an effective antioxidant. Glutathione exists *in vivo* in reduced (GSH) and oxidised (GSSG) forms, with the majority found as GSH under normal physiological conditions. During OS a decrease in GSH and increase in GSSG is seen, and therefore the ratio of GSH/GSSG decreases. Consequently, GSH/GSSG ratio can be used as an indicator of the health of a cell. Figure 4.8 shows the results of a glutathione assay on SH-SY5Y cells treated for 2 hours with vehicle control, positive control or Type C oligomers. Figure 4.8 shows the concentration following treatment of GSH (a) and GSSG (b), the value of which has extrapolated from the calibration curve shown in Appendix Figure 5. Following treatment with both Type C oligomers and Menadione a reduction in GSH and increase in GSSG is seen, indicative of OS. In contrast to the results obtained from the CellROX Green assay, this result was more pronounced with menadione treatment than Type C oligomer treatment. Nevertheless, Type C oligomer treatment did result in a considerable alteration to the concentration of total and reduced glutathione in the cells, which is evidenced in Figure 4.8 (c), where GSH/GSSG ratio (normalised to vehicle control) is shown. Decreases in GSH/GSSG ratio in the SNpc have also been found in the analysis of brain tissue from PD patients compared to controls (Dias, Junn and Mouradian, 2013) and results here suggest that the alteration in GSH/GSSG ratio observed during PD could be partially due to certain species of alpha-synuclein.

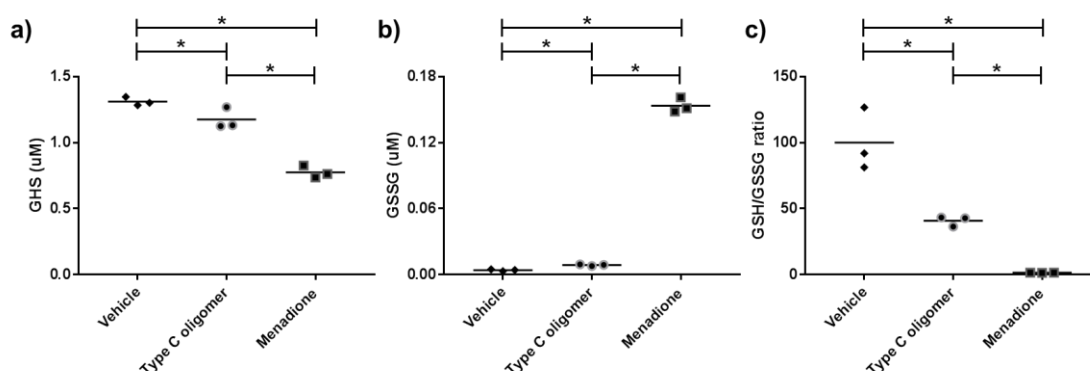


Figure 4.8: Glutathione assay of SH-SY5Y cells treated for 2 hours with 10% (v/v) vehicle control, positive control (menadione) or Type C oligomers. Concentration of GSH shown in (a) and GSSG shown in (b). Ratio of GSH/GSSG (normalised to the vehicle control) shown in (c). Statistical significance determined by Kruskal-Wallis test * = $P < 0.05$.

4.4.4.3 Treatment of SH-SY5Y cells with Type C oligomers results in an altered monosome/polysome ratio

Polysome profiling was used as a third method of investigating cellular stress. Eukaryotic cells are able to adapt to environmental changes by modulating the expression of specific gene products. The expression of protein-coding genes can be regulated by many processes at both the transcriptional and post-transcriptional level. Precise regulation of mRNA translation is fundamental for cellular homeostasis, particularly for cellular processes which require rapid changes in protein expression patterns, such as in response to conditions of physiological and environmental stress. Regulation of mRNA translation can alter cellular phenotype, with a decrease in the rate of translation causing a predominant loss of short lived proteins, which can affect important cellular processes (Johannes *et al.*, 1999). Specific changes in protein expression can also occur as cells are able to alter their pool of efficiently translated

mRNA in response to stress conditions (Rajasekhar *et al.*, 2003; Thomas and Johannes, 2007). mRNA translation is a complex process which can be divided into three major phases: initiation, elongation and termination. While all phases are highly regulated it is the initiation phase which is most controlled, and therefore thought to be the major rate limiting step of protein synthesis (Jackson, Hellen and Pestova, 2010). The analysis of polysomes - mRNA molecules attached to multiple ribosomes - has been used as an approach to analyse the efficiency of translation initiation. Polysome profiling allows the determination of translational efficiency of both the whole transcriptome and individual mRNAs. It provides information on the transcriptional status of mRNA depending on the number of ribosomes that it is associated with. mRNAs associated with no or few ribosomes are thought to be translated poorly while those associated with many are believed to be actively translated. Under conditions of cellular stress, where translation is inhibited, a reduction in polysomes is seen along with an increase of 80S monosomes. Thereby the ratio of polysomes to monosomes from a polysome profiling experiment can be used as a measure of translational activity, as the integrated area under the curve is proportional to the amount of ribosomal RNA, and therefore the number of ribosomes.

SH-SY5Y cells were treated for 2 hours with vehicle control, positive control or Type C oligomers, followed by the addition of cyclohexamide to freeze translating ribosomes to their mRNA, permitting the measurement of polysomes. Cells were then lysed and the RNA separated on a sucrose gradient, allowing the production of a polysome trace for each condition. Figure 4.9 displays the results from these experiments, with representative polysome traces following each treatment shown in (a) and the polysome/monosome ratio shown in (b). It was found that following treatment with

both the positive control and Type C oligomers there was a reduction in polysome to monosome ratio, indicative of translational stress. Therefore Type C oligomer treatment appears to have a major effect on global mRNA translation, providing further evidence that these oligomers are causing a stress response in the cells. Combined results from these three assays provide strong evidence that treatment of SH-SY5Y cells with Type C alpha-synuclein oligomers evokes a stress response from the cells.

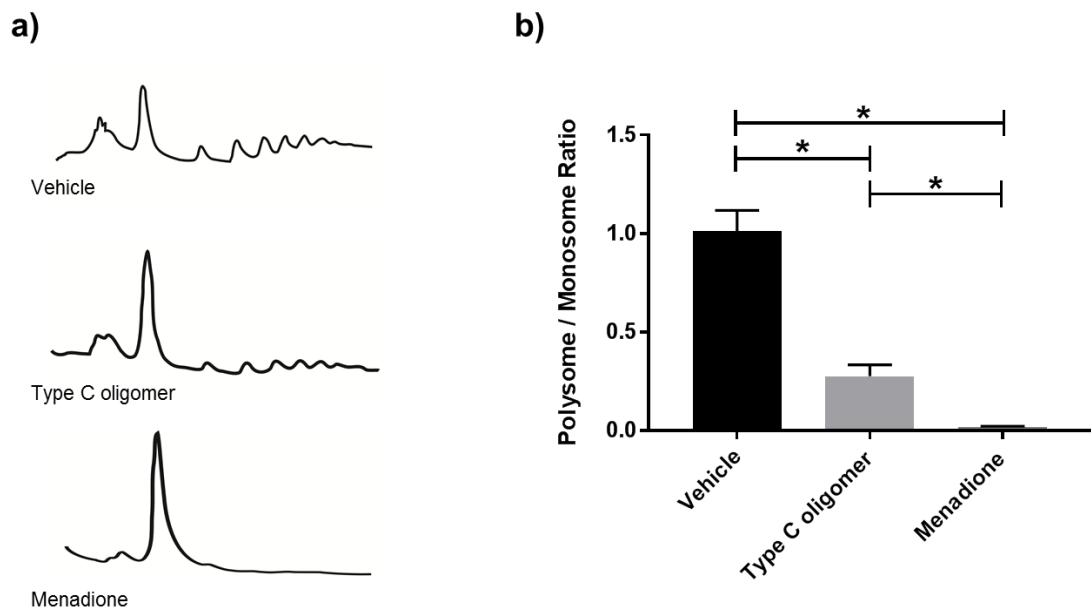


Figure 4.9: Polysome profiling of SH-SY5Y cells treated for 2 hours with 10% (v/v) vehicle control, positive control (menadione) or Type C oligomers. Representative polysome traces for each condition shown in (a) and calculated polysome/monosome ratio shown in (b). Statistical significance determined by Kruskal-Wallis test * = $P < 0.05$.

4.5 Conclusions and future work

Results presented in this chapter demonstrate that N-terminal acetylation of alpha-synuclein does not affect the function of Type A or Type C oligomers, suggesting that either N-terminal acetylation of the protein does not affect its oligomerisation, or that the N-terminal region is not critical in self-assembly. This is in contrast to the recent report of Bu *et al.* (2017) showing a significant decrease in oligomerisation of the N-terminally acetylated protein, thought to result from preventing the formation of intermolecular hydrogen bonds. One possible explanation for this difference could be that the Type A and Type C oligomers investigated in this study may exert their cellular effects on different timescales. The Bu *et al.* (2017) study demonstrated a reduction in the rate of oligomer assembly in the acetylated protein, however in this thesis an overnight incubation was used for the preparation of Type C oligomers which was presumably long enough to allow oligomers formed from both types of the protein to reach their endpoint by the time of analysis. In addition, the technique used to monitor aggregation in the study of Bu *et al.* was limited to the detection of small oligomers of less than 8 nm. An alternate explanation of the conflicting results found in work presented in this chapter is that the biologically active oligomers investigated here are larger than can be detected by the method of Bu *et al.*. Indeed, in the original study by Danzer *et al.* characterising Type A and Type C oligomers, through using AFM Type A oligomer preparations were found to contain structures between 2 and 45 nm in size, while Type C preparations were between 4 and 10 nm.

Results presented here are the first to our knowledge validating the cellular effects of Type A and Type C oligomers characterized by Danzer *et al.* (2007) when produced from N-terminally acetylated alpha-synuclein. Findings that acetylation did not appear

to perturb the function of these oligomers implies that oligomers made from endogenous protein have the potential to induce the same cellular effects as those applied externally. Although N-terminal acetylation was not found to affect the function of the two oligomeric species investigated here, it would be advisable to use the acetylated form of the recombinant protein for future *in vitro* experiments because, as shown by data presented in Chapter 1. In addition, N-terminal acetylation of alpha-synuclein does have the potential to modulate the kinetics if not the final structure of protein assemblies.

The response of SH-SY5Y cells to treatment with Type C oligomers was also further investigated in this chapter, leading to novel results. It has previously been shown that the seeding effect of Type C oligomers occurs in a time dependent manner, and that the aggregates are comprised of both exogenous and endogenous alpha-synuclein (Danzer *et al.*, 2009). SH-SY5Y cells overexpressing alpha-synuclein have also been shown to secrete alpha-synuclein oligomers into the media, both free and in exosomes (Danzer *et al.*, 2012). However, the release of alpha-synuclein from cells treated with Type C oligomers has not previously been reported, nor has the release of ps129 alpha-synuclein from these treated cells which indicates that the released material has been processed by the cell. Due to the addition of Triton to conditioned media before dot blot analysis it is possible that the alpha-synuclein detected in our experiments exists freely in the media or in a membrane bound vesicle such as an exosome. It would be of interest to clarify this point, which could be achieved by using differential ultracentrifugation to separate vesicles from the conditioned media alongside the detection of exosomal markers. This would provide additional information on the mechanisms by which alpha-synuclein is being secreted within this model, and

establish whether unmodified and phosphorylated alpha-synuclein are being secreted via the same mechanisms. It would also be worthwhile to confirm whether the secreted protein is exogenous or endogenous protein, or a mixture of both. This could be achieved for example by using ^{15}N labelled protein when creating the Type C oligomers and then analysing the conditioned media using LC-MS. Using this technique could also be useful to validate the results presented in Figure 4.5 (b) and Figure 4.6 giving a fully quantitative output, as opposed to the more qualitative analysis by ImageJ and dot blot analysis.

Alpha-synuclein is known to aggregate under stress conditions and age is the number one risk factor for PD. In addition to the presumed decades needed for misfolded proteins to reach a critical threshold to induce neuronal damage, age associated impairment of mitochondrial function and subsequent increase in ROS are thought to be key factors in age related neurodegenerative disorders (Schapira, 2008; Greaves *et al.*, 2012). Intracellular generation of free radicals has been shown to induce alpha-synuclein aggregation, as has exposure of cells in culture to H_2O_2 and ferrous iron, MPP^+ , NO and superoxide (Ostrerova-Golts *et al.*, 2000; Kakimura *et al.*, 2001; Paxinou *et al.*, 2001). The overexpression of alpha-synuclein is also known to increase intracellular ROS (Junn and Mouradian, 2002) and cause structural and functional alterations to mitochondria (Ingelsson, 2016). Additionally, it has recently been described that treatment of iPSC-derived neurons with an oligomeric species first described by Hoyer *et al.* (2002) induced OS through interactions with metal ions (Deas *et al.*, 2016). However the oligomers used in this study were assembled through a very different method to the Type C oligomers investigated here and, importantly, are not known to be associated with intracellular seeding of endogenous alpha-synuclein.

Phosphorylation of alpha-synuclein is known to be increased in conditions of stress and ps129 alpha-synuclein was detected here in conditioned media from Type C treated cells. In addition OS was observed by fluorescence and luminescence based assays, and polysome analysis shows a characteristic stress response. Results presented in this chapter therefore provide strong evidence that treatment of SH-SY5Y cells with Type C oligomers leads to an increase in OS.

An interesting extension of work presented here is in relation to the polysome profiling experiment shown in Figure 4.9. As mentioned previously, specific changes in protein expression can occur in response to different conditions as cells are able to alter their pool of efficiently translated mRNA (Rajasekhar *et al.*, 2003; Thomas and Johannes, 2007). Results presented here demonstrate that, following treatment of SH-SY5Y cells with Type C oligomers, a global reduction in mRNA translation occurs. Through analysing the mRNA present in the monosome and polysome peaks, the specific expression of individual proteins in response to treatment could be investigated to determine whether they are up regulated or down regulated under these conditions. RT-PCR or northern blot polysome analysis could be used for the targeted analysis of specific mRNAs. Alternately, global translational changes occurring following treatment with Type C oligomers could be analysed by identifying the translational status of polysomal mRNAs through microarray or deep-sequencing analysis, giving a genome-wide perspective of the mRNA pool being translated following treatment.

This chapter provides further knowledge of the mechanism of action of Type C oligomers, and provides a potential explanation of OS being involved in the ability of these oligomers to induce aggregation. While it has previously been hypothesised that these oligomers cause intracellular alpha-synuclein aggregation through a self-

propagation prion-like mechanism, results presented here raise the possibility of OS as an additional explanation of the increased aggregation of alpha-synuclein following treatment. The concept of alpha-synuclein acting in a prion-like manner is not without controversy. One main point of contention is that not all post-mortem analyses of PD cases display the typical spread of LB pathology described by the Braak staging scheme (Burke, Dauer and Vonsattel, 2008; Brundin and Melki, 2017). Results presented here provide evidence that rather than certain oligomeric species of alpha-synuclein directly self-propagating aggregation of endogenous protein, OS is playing an important role in this process.

While the cells in our experiments do not display reduced viability in response to Type C oligomer treatment, it is important to take into account the treatment time tested and, more importantly, the nature of these cells. PD develops gradually over many decades, with the cells lost to the disease being post-mitotic neurons. While the SH-SY5Y cells used in this chapter seem to be able to cope with the OS induced by Type C oligomers (on the time scale tested here), the experiments in this chapter were conducted on undifferentiated SH-SY5Y cells. These cells are commonly used in PD research however, as with all *in vitro* models, using these cells has disadvantages. One of the main disadvantages is that they are an actively dividing cancer cell line. Many lines of evidence suggest that a build-up of aberrant proteins in neurons contributes to PD, and metabolically active dividing cells are not likely to share this characteristic build up over time. Whether oligomer treatment would prove toxic to post-mitotic neurons which are potentially already vulnerable to stress due to age, the build-up of environmental toxins or genetic alterations which cause vulnerability to PD is open to investigation. This highlights the importance of future work being conducted on more

representative cell culture models. One possibility would be the use of iPSC derived neurons is an exciting, though more technically and financially challenging, alternative. Deriving neurons from the somatic cells of patients would provide an excellent opportunity to investigate the effect of the oligomeric species investigated here in one of the most relevant cell culture models currently available. The use of iPSC models also importantly allows the investigation of disease progression, from early progenitor cells to aged neurons (McKinney, 2017).

In conclusion, results presented in this chapter have firstly validated the cellular effects of the Type A and Type C alpha-synuclein oligomers first characterised by Danzer *et al.* (2007) when prepared from the N-terminally acetylated protein. To the best of the author's knowledge these are the first investigations into these oligomeric species using the modified form of the protein which is found *in vivo*. The effect of Type C oligomers on SH-SY5Y cells was then further investigated, with data suggesting that this treatment results in an OS response from the cells and subsequent secretion of phosphorylated alpha-synuclein into the culture medium. This work provides new knowledge on cellular response to exogenously applied alpha-synuclein oligomers and raises new avenues of investigation, for example by furthering the polysome profiling experiments conducted here to take an untargeted approach to determining the translational response of cells to such treatments.

Chapter 5 - General discussion

PD remains a debilitating disorder with no disease-altering treatments currently available. The lack of such treatments is due in part to incomplete knowledge of the molecular mechanisms involved in the disease. Alpha-synuclein has been irrefutably linked to PD through genetic and pathological evidence, with data pointing towards oligomeric forms as the toxic species (for a review see Bengoa-Vergniory *et al.* 2017). As such, increasing knowledge of both the normal cellular function of the protein and its potentially pathogenic forms could conceivably enhance preclinical therapeutic development for PD.

The overall aim of this thesis was to investigate the structural and functional aspects of alpha-synuclein and its oligomers. Chapter 2 presents data from investigations into the copper binding and subsequent alterations to conformation and aggregation propensity of alpha-synuclein. Specifically, the effects of a familial PD mutation and a physiologically relevant modification on these factors were characterised, with the importance of N-terminal acetylation in metal binding being determined. Chapter 3 investigated the aggregation of alpha-synuclein, both into specific oligomers of known function and into amyloid fibrils. The focus of this section of work was on the various oligomeric species present in solutions of alpha-synuclein at different stages of aggregation, and the dynamics of these species. Data demonstrated that N-terminal acetylation has little effect on oligomer assembly and final structural state. Chapter 4 set out to further characterise the effect of alpha-synuclein oligomers with the ability to seed intracellular aggregation on an SH-SY5Y cell culture model. A summary of key findings from this body of work is provided below.

5.1 H50Q mutation of N-terminally acetylated alpha-synuclein results in a loss of the proteins ability to bind to copper.

Investigations of alpha-synuclein containing familial PD causing mutations have been intensely studied, as alterations in the structure or function of these mutants may provide insights into how this protein is associated with the disease (for a review see Sahay, Ghosh and Maji, 2017). However, a large body of this work was conducted before the realisation that alpha-synuclein is constitutively acetylated *in vivo* (Anderson *et al.*, 2006). Therefore, the effects of PD associated mutations on the physiologically relevant N-terminally acetylated form of alpha-synuclein are not well characterised. In Chapter 2 the effect of the familial H50Q mutation on N-terminally acetylated alpha-synuclein's copper binding and subsequent conformation and aggregation propensity were investigated. This previously unstudied form of the protein was found to have drastically impaired copper binding (Mason *et al.*, 2016), a finding of potential significance as it has been suggested that alpha-synuclein's ability to bind copper is important for its proposed physiological function as a ferrireductase (Davies, Moualla and Brown, 2011). Results presented here imply that the H50Q mutation may leave alpha-synuclein impaired in its ability to act as a ferrireductase. Therefore, it would be of great interest to assess the ability of N-terminally acetylated H50Q alpha-synuclein to act as a ferrireductase, and if alterations were found, assess resulting metal homeostasis and ROS levels.

5.2 N-terminal acetylation of alpha-synuclein was found to not alter the formation of oligomeric species or their function.

Characterising prefibrillar oligomers is key to understanding the aberrant aggregation of misfolding proteins, with the potential to support the design of therapeutics for protein misfolding diseases. MS methods were applied to investigate the species and dynamics of alpha-synuclein that arise during the early stages of its aggregation.

Data presented in Chapter 3 demonstrated that N-terminal acetylation does not alter the oligomeric alpha-synuclein species detectable by ESI-IMS-MS. In samples of protein prior to aggregation a range of dimers, trimers and tetramers were detected. In samples of MS compatible Type C oligomers (a specific form of the protein known to inducing intracellular alpha-synuclein aggregation), pentamers and hexamers were additionally observed. These oligomeric species were detected in preparations made from both unmodified and N-terminally acetylated protein. These results indicated that this post translational modification has little effect on the final structure of type-C oligomers. However, N-terminal acetylation does alter the rate of aggregation, as demonstrated in Chapter 2. The data presented here highlights the importance of using disease relevant versions of key proteins when investigating mechanistic actions. In Chapter 4 the effect of N-terminal acetylation on oligomeric species of known cellular function was investigated. Two species were investigated: 'Type A' oligomers, known to decrease cell viability and 'Type C' oligomers, known to induce intracellular aggregation of alpha-synuclein (Danzer *et al.*, 2007). Results demonstrated that N-terminal acetylation did not affect the cellular function of Type A or Type C oligomers. This constitutes, to the best of the author's knowledge, the first study validating the

cellular effects of the Type A and Type C oligomers characterized by Danzer *et al.* (2007) when produced from the physiologically relevant, N-terminally acetylated form of alpha-synuclein.

5.3 Treatment of SH-SY5Y cells with Type C alpha-synuclein oligomers inducing a stress response.

Type C oligomers of alpha-synuclein are known to induce intracellular aggregation of endogenous protein and it has been proposed that this represents a 'seeding mechanism', providing evidence towards the hypothesis of alpha-synuclein pathology propagating from cell-to-cell in a prion-like manner (Danzer *et al.*, 2009). In Chapter 4 the response of SH-SY5Y cells to treatment with Type C oligomers was further investigated. The data provides strong evidence that this treatment results in a stress response from these cells, with an increase in ROS, a decrease in GSH:GSSG ratio and a reduction in global translation being detected. As an increase in OS has been well documented to increase intracellular aggregation of alpha-synuclein (Scudamore and Ciosek, 2018), these results imply that OS may have a role in the apparent seeding effect of Type C oligomers. It has recently been described that treatment of iPSC-derived neurons with an oligomeric species of alpha-synuclein induced OS in the cells (Deas *et al.*, 2016), setting a precedent for the results found in this chapter. However, the oligomers used by Deas *et al.*, unlike the Type C oligomers investigated here, are not known to be associated with seeding intracellular aggregation of endogenous alpha-synuclein. Results presented in this thesis provide evidence that treatment of SH-SY5Y cells with Type C oligomers evokes a stress response and this may well be the trigger for further aggregation of the protein. This furthers knowledge of the

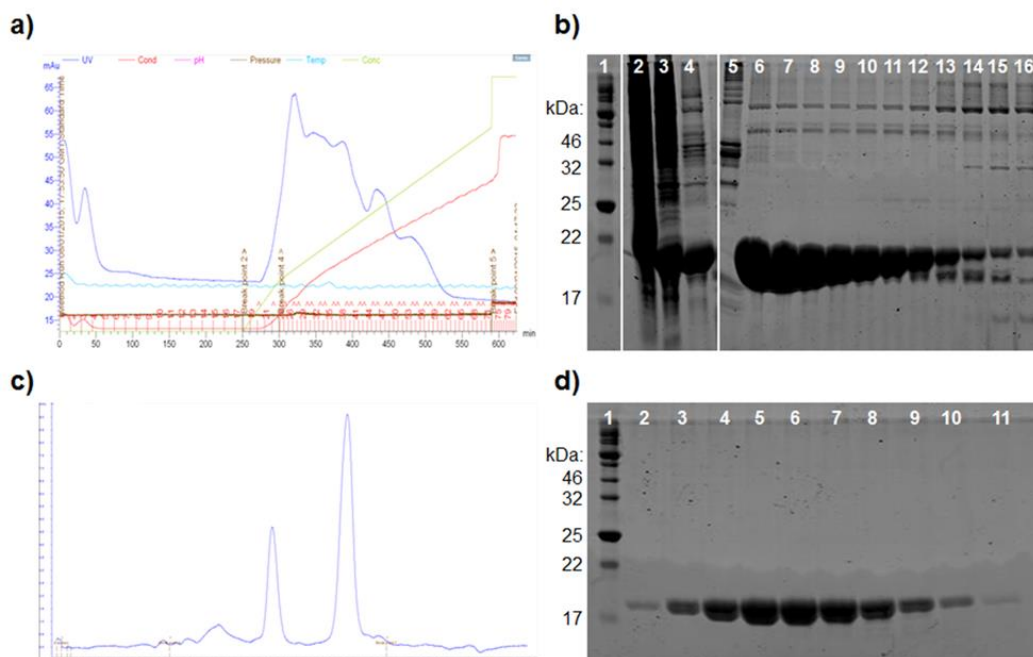
mechanism of action of these oligomers and, importantly, provides an alternate explanation of their ability to 'seed' aggregation. The data also offer a potential target for further therapy through decreasing the protein's ability to transfer pathology by damping its redox abilities. It is however important to note that the work in Chapter 4 details the response of a neuroblastoma cell line to treatment with Type C alpha-synuclein oligomers. Whether a similar response would be seen in the dopaminergic neurons of the SNpc affected in PD cannot be inferred from the experiments conducted here. To extend this work, it would be important to determine whether a stress response to Type C oligomer treatment is seen in either a more biologically relevant *in vitro* model or an *in vivo* model of PD.

5.4 Concluding remarks

It has been 200 years since Dr James Parkinson published 'An Essay on the Shaking Palsy', describing for the first time the signs and symptoms of PD. Despite the development of many treatment options to ameliorate PD symptoms, there are currently no disease-modifying treatments to slow down or reverse disease progression. Irrefutable evidence points to alpha-synuclein as a key contributor to the neurodegeneration seen in PD and, as such, much research is being carried out on this protein. Areas of interest include the use of alpha-synuclein as a biomarker of PD (Paciotti *et al.*, 2018), the use of immunotherapy to reduce levels of the protein (Weihofen *et al.*, 2018) and the use of small molecules to stabilise non-toxic forms of the protein (Price *et al.*, 2018). Whether the findings of this research will translate to clinical use remains to be seen. What is clear however is that increased understanding of the alpha-synuclein protein is of great importance to enable the development of new candidate PD therapies which target this protein.

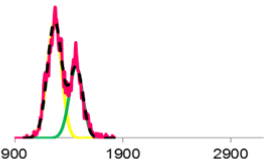
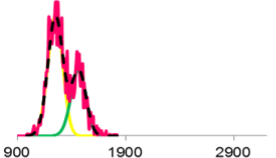
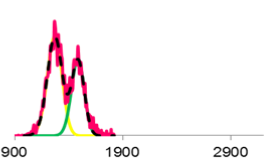
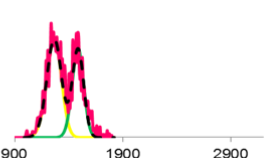
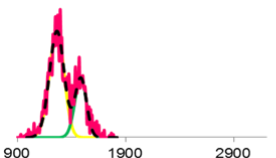
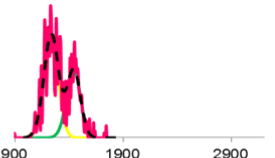
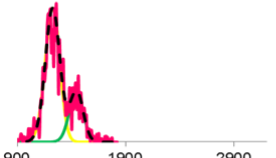
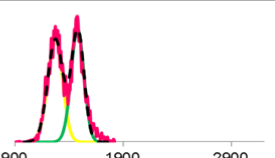
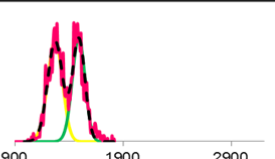
Together, data presented in this thesis have contributed novel findings and furthered knowledge in the field of alpha-synuclein research. Results have highlighted the importance of using the biologically relevant form of a protein when performing *in vitro* experiments, identified a loss of copper binding function resulting from the H50Q familial mutation, validated the cellular effects of previously characterised alpha-synuclein oligomers when produced from N-terminally acetylated protein and extended knowledge of the cellular response of the SH-SY5Y cell line to treatment with Type C oligomers. In addition, the PhD project has raised new avenues for future study, which have the potential to extend knowledge of alpha-synuclein's role in PD.

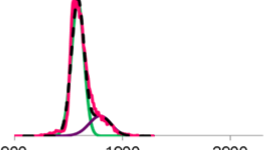
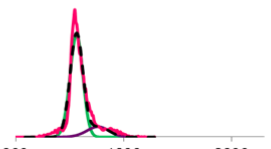
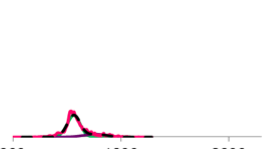
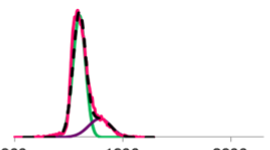
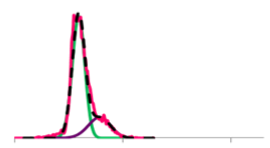
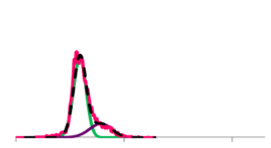
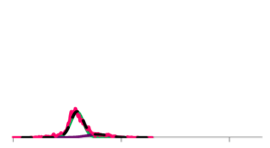
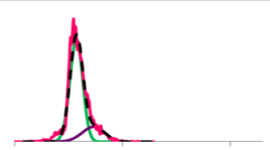
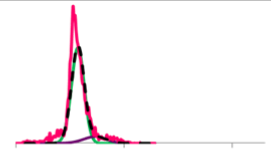
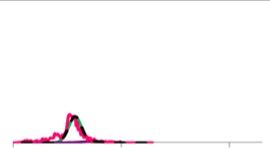
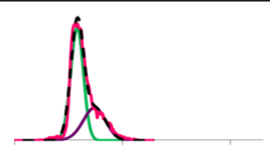
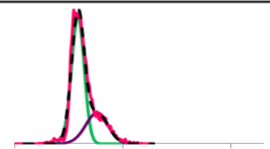
Appendix

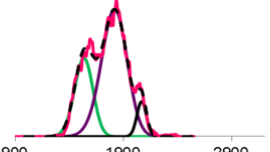
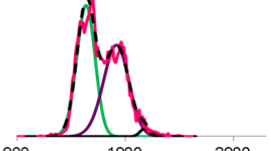
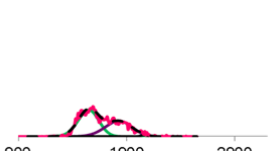
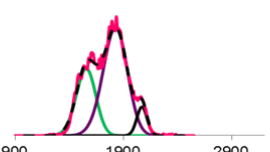
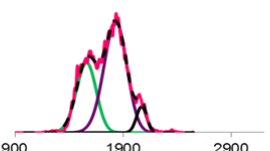
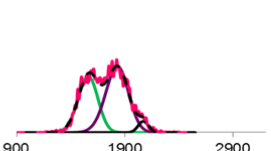
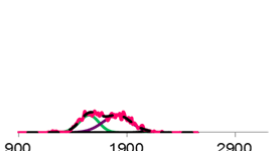
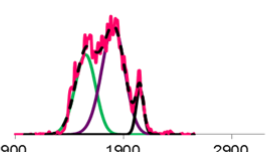
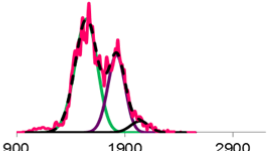
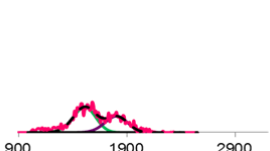
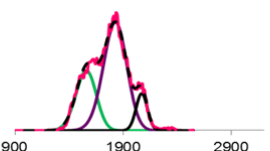
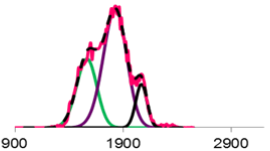


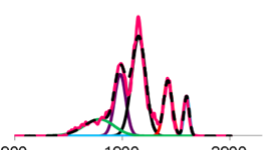
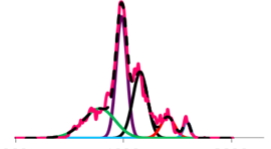
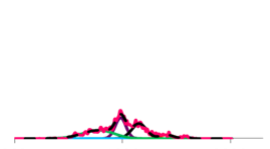
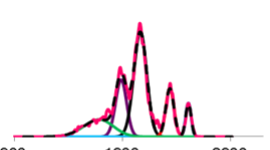
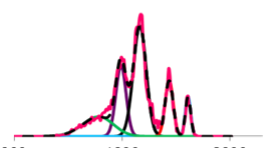
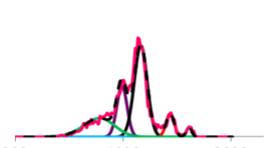
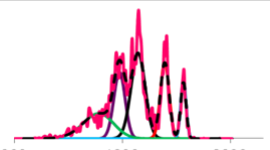
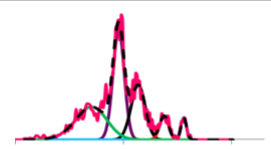
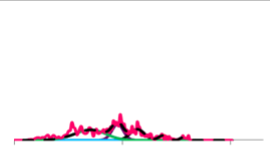
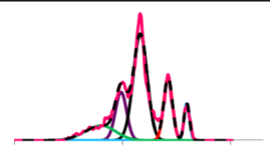
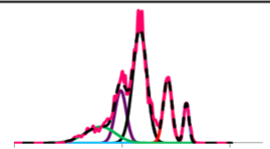
Appendix Figure 1: Typical column chromatography UV chromatograms and SDS-PAGE analysis of alpha-synuclein purification

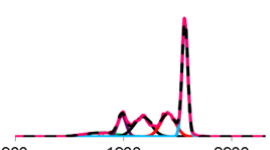
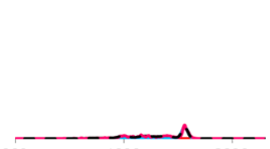
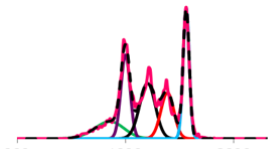
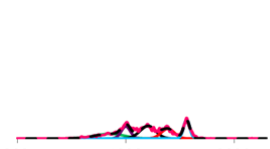
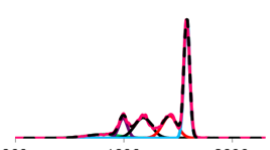
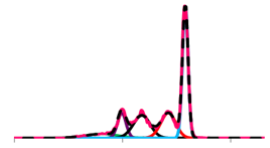
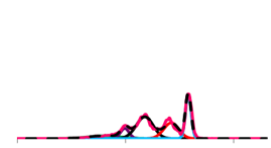
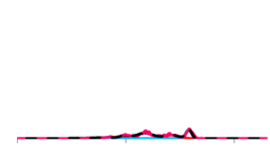
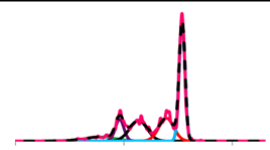
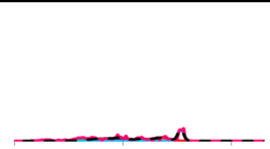
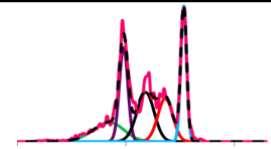
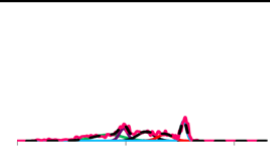
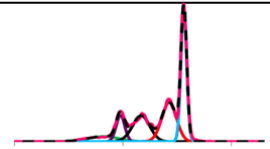
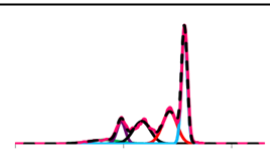
SDS-PAGE was performed at each stage of the protein purification process. (a) Shows the chromatogram obtained from running crude lysate through a 50 mL Q-Sepharose anion exchange column and (b) shows corresponding SDS-PAGE of protein containing eluted fractions. Fractions containing overexpressed alpha-synuclein are present in lanes 6 - 16. The band corresponding to alpha-synuclein has a molecular weight between the markers at 17 and 22 kDa, consistent with previous reports of this protein running on SDS-PAGE at slightly larger than its true size of 14 kDa (Moussa et al, 2004). Lanes 2 - 4 represent samples from the crude purification process prior to anion exchange, with the lysate immediately upon lysis in lane 2, the lysate after an initial centrifugation in lane 3 and the lysate following acid precipitation and centrifugation in lane 4. (c) Shows the chromatogram obtained from running pooled anion exchange fractions containing alpha-synuclein through a HiLoad® 26/600 Superdex™ 200 size exclusion column size exclusion column and (d) shows corresponding SDS-PAGE of alpha-synuclein containing eluted fractions. Here the band corresponding to overexpressed alpha-synuclein is seen in lanes 2-11 with no other visible contaminant.

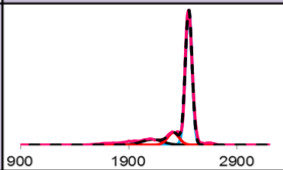
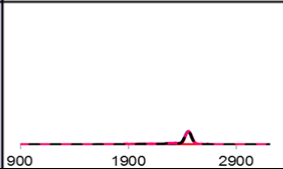
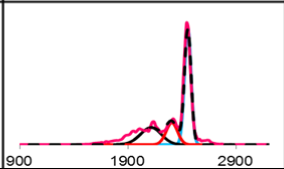
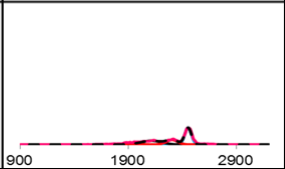
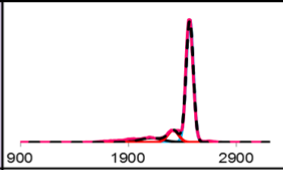
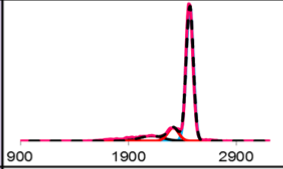
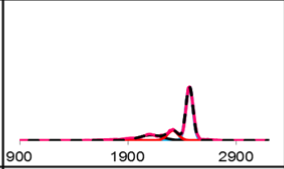
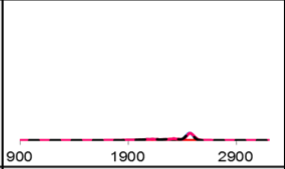
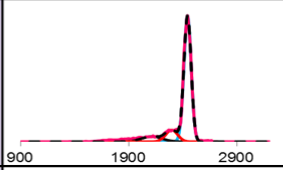
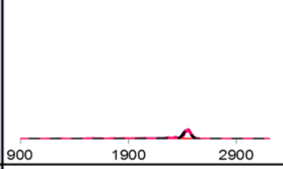
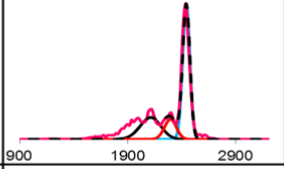
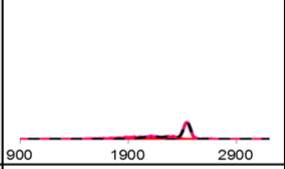
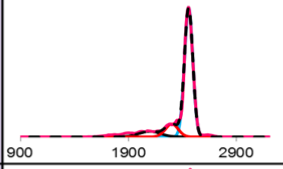
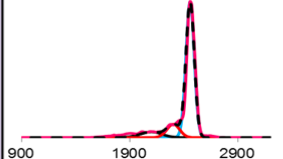
+5 ion	Unbound	1x Cu ²⁺	2x Cu ²⁺
Unmodified			
+ copper			
Acetylated			
+ copper			
H50Q			
+ copper			
Acetylated H50Q			
+ copper			

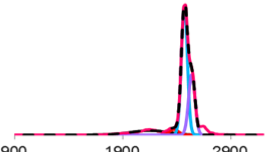
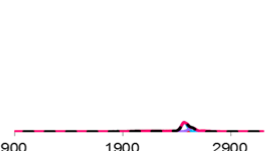
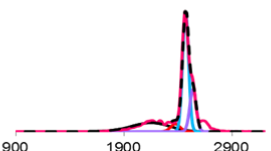
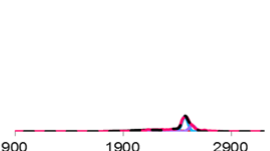
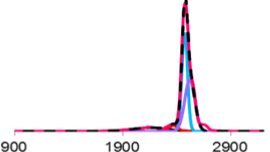
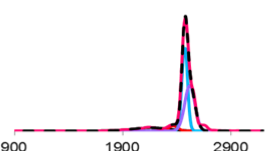
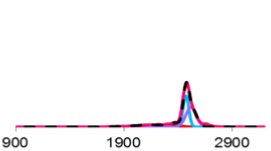
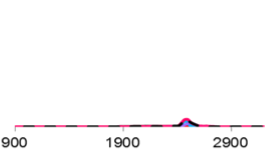
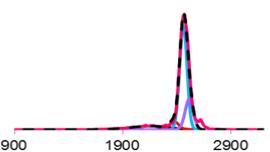
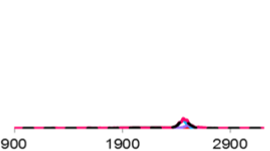
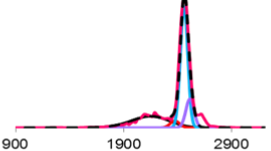
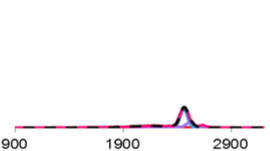
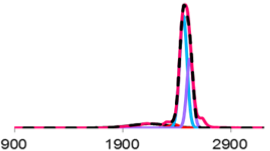
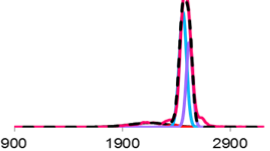
+6 ion	Unbound	1x Cu ²⁺	2x Cu ²⁺
Unmodified			
+ copper			
Acetylated			
+ copper			
H50Q			
+ copper			
Acetylated H50Q			
+ copper			

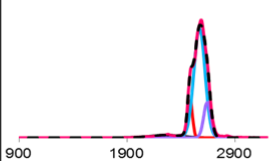
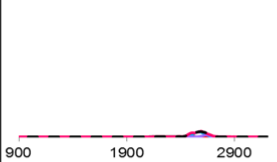
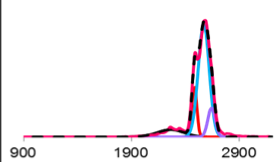
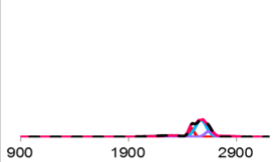
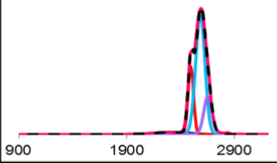
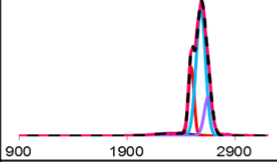
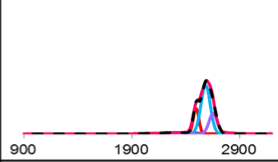
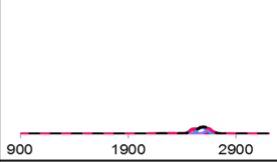
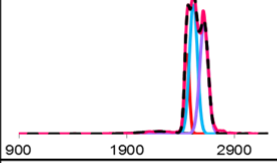
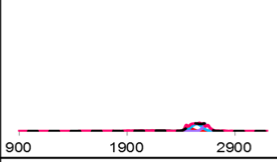
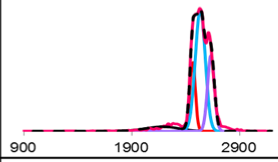
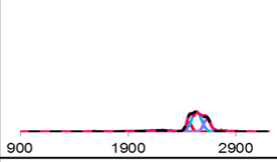
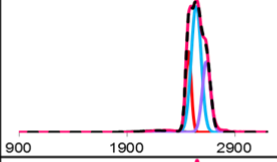
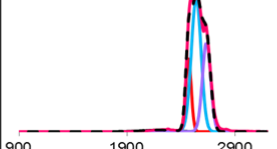
+7 ion	Unbound	1x Cu ²⁺	2x Cu ²⁺
Unmodified			
+ copper			
Acetylated			
+ copper			
H50Q			
+ copper			
Acetylated H50Q			
+ copper			

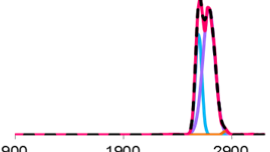
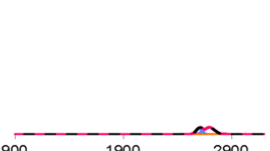
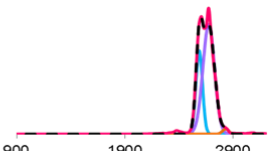
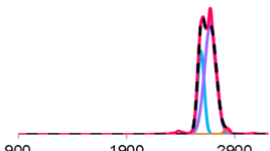
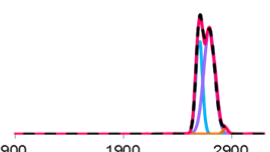
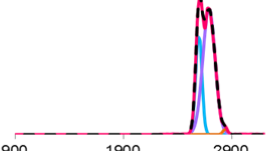
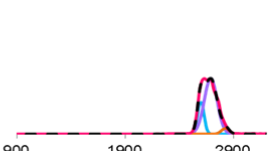
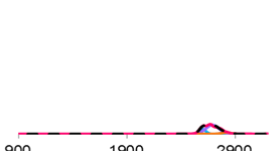
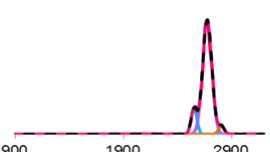
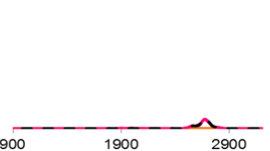
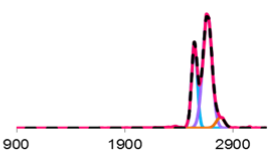
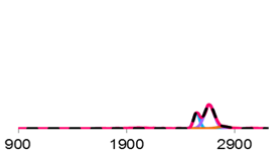
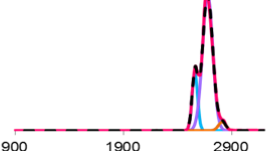
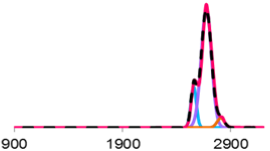
+8 ion	Unbound	1x Cu ²⁺	2x Cu ²⁺
Unmodified			
+ copper			
Acetylated			
+ copper			
H50Q			
+ copper			
Acetylated H50Q			
+ copper			

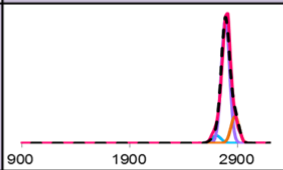
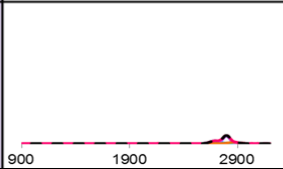
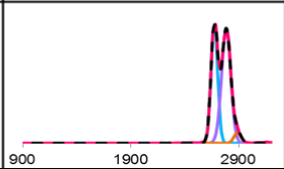
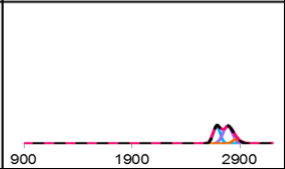
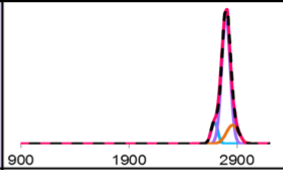
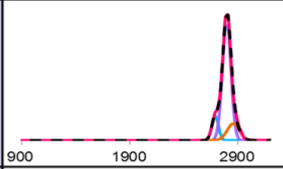
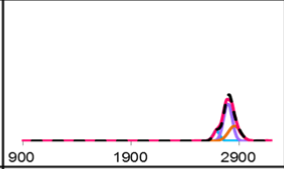
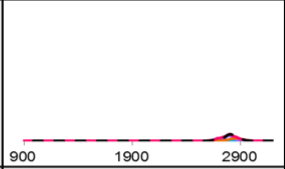
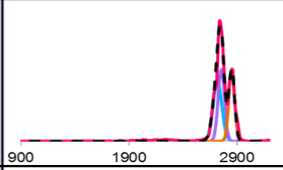
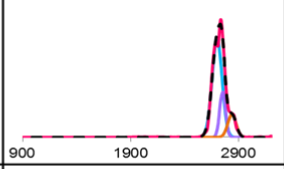
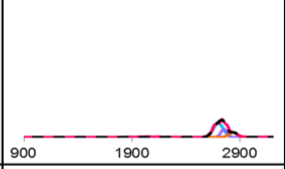
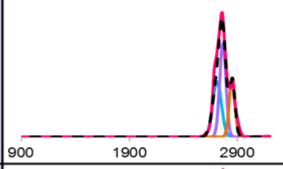
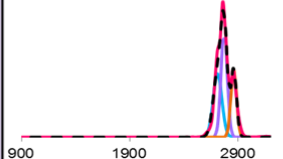
+9 ion	Unbound	1x Cu ²⁺	2x Cu ²⁺
Unmodified			
+ copper			
Acetylated			
+ copper			
H50Q			
+ copper			
Acetylated H50Q			
+ copper			

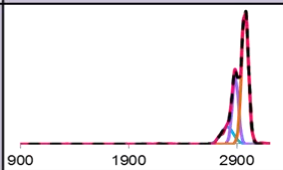
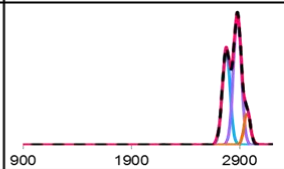
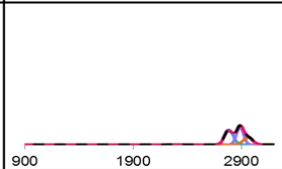
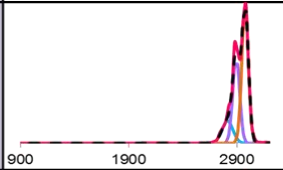
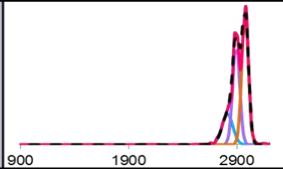
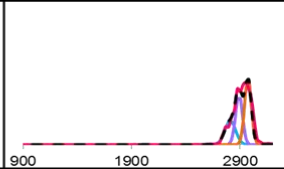
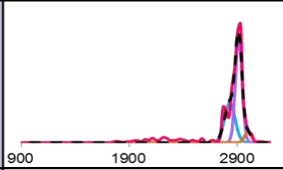
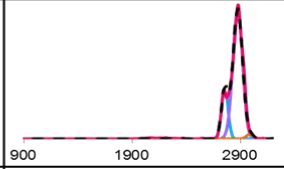
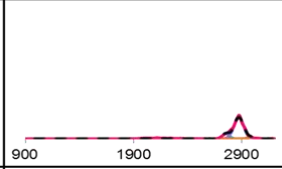
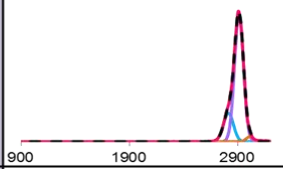
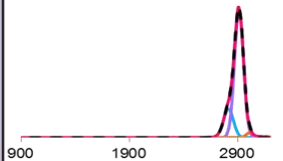
+10 ion	Unbound	1x Cu ²⁺	2x Cu ²⁺
Unmodified			
+ copper			
Acetylated			
+ copper			
H50Q			
+ copper			
Acetylated H50Q			
+ copper			

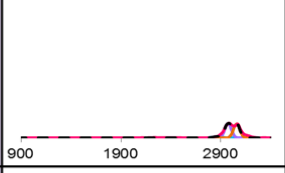
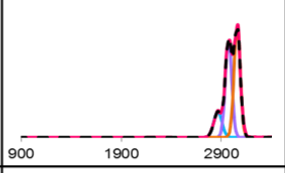
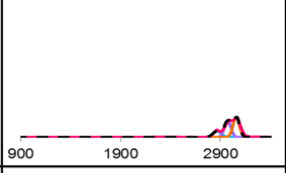
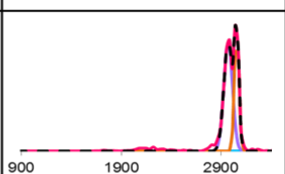
+11 ion	Unbound	1x Cu ²⁺	2x Cu ²⁺
Unmodified			
+ copper			
Acetylated			
+ copper			
H50Q			
+ copper			
Acetylated H50Q			
+ copper			

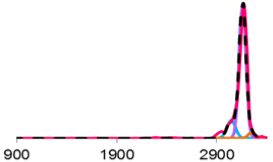
+12 ion	Unbound	1x Cu²⁺	2x Cu²⁺
Unmodified			
+ copper			
Acetylated			
+ copper			
H50Q			
+ copper			
Acetylated H50Q			
+ copper			

+13 ion	Unbound	1x Cu²⁺	2x Cu²⁺
Unmodified			
+ copper			
Acetylated			
+ copper			
H50Q			
+ copper			
Acetylated H50Q			
+ copper			

+14 ion	Unbound	1x Cu²⁺	2x Cu²⁺
Unmodified			
+ copper			
Acetylated			
+ copper			
H50Q			
+ copper			
Acetylated H50Q			
+ copper			

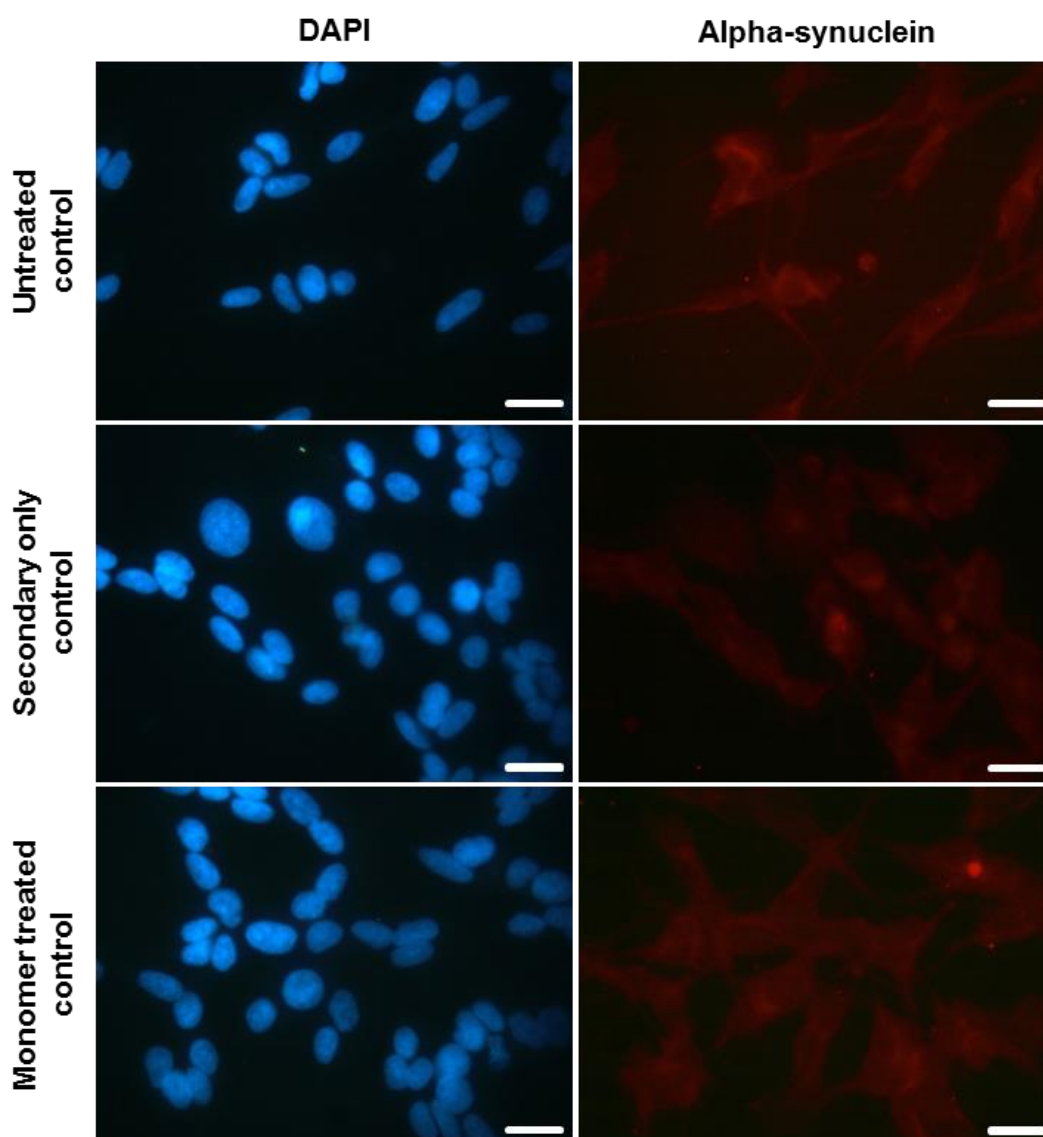
+15 ion	Unbound	1x Cu ²⁺	2x Cu ²⁺
Unmodified			
+ copper			
Acetylated			
+ copper			
H50Q			
+ copper			
Acetylated H50Q			
+ copper			

+ 16 ion	Unbound	1x Cu ²⁺	2x Cu ²⁺
Unmodified			
+ copper	 <p>Mass spectrum showing a single peak at approximately 2900 m/z. The x-axis is labeled with 900, 1900, and 2900.</p>	 <p>Mass spectrum showing a peak at approximately 2900 m/z with a blue peak and a red peak. The x-axis is labeled with 900, 1900, and 2900.</p>	 <p>Mass spectrum showing a single peak at approximately 2900 m/z. The x-axis is labeled with 900, 1900, and 2900.</p>
Acetylated			
+ copper			
H50Q			
+ copper			
Acetylated H50Q		 <p>Mass spectrum showing a peak at approximately 2900 m/z with a blue peak and a red peak. The x-axis is labeled with 900, 1900, and 2900.</p>	
+ copper			

+17 ion	Unbound	1x Cu ²⁺	2x Cu ²⁺
Unmodified			
+ copper			
Acetylated			
+ copper			
H50Q			
+ copper			
Acetylated H50Q			
+ copper			

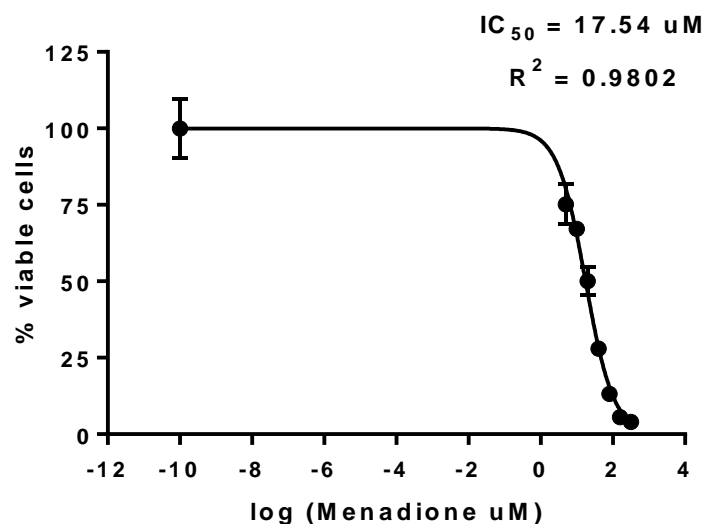
Appendix Figure 2: Arrival time distribution and Gaussian fitting of each charge state distribution of all alpha-synuclein species studied in Chapter 2.

Experimental collisional cross sections of all charge state of unmodified and acetylated WT and H50Q alpha-synuclein. Apo and Cu²⁺ bound forms resulting from mixing a 50 mM aqueous ammonium acetate solution of 10 μM alpha-synuclein with 10 μM CuCl₂. The percentages of alternate populations of differing CCS were calculated using Gaussian fitting. The raw ATD is displayed in pink and the sum of the fitted Gaussians is shown as a black broken line. The area under the curve of each Gaussian was used to calculate the percentage of protein in each conformational family under different conditions, presented in the main text in Figure 2.10, Figure 2.14 and Figure 2.17.



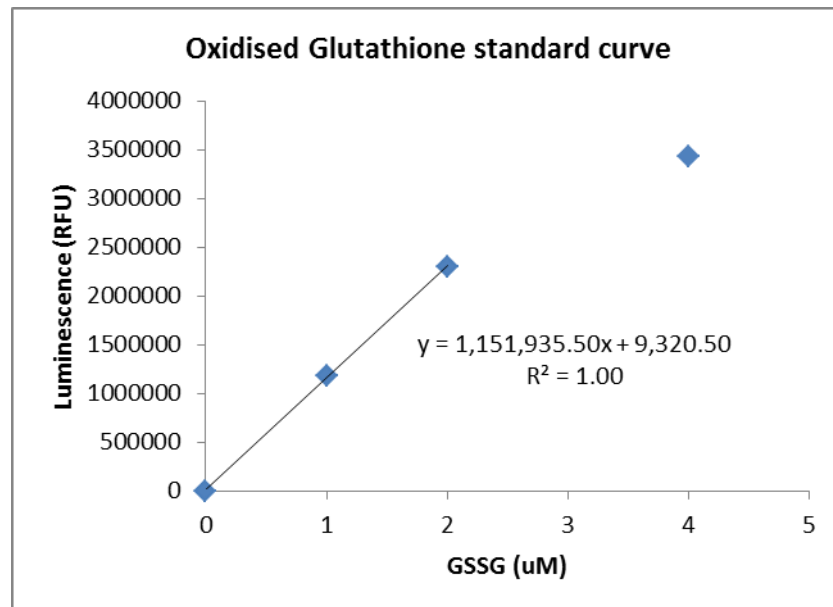
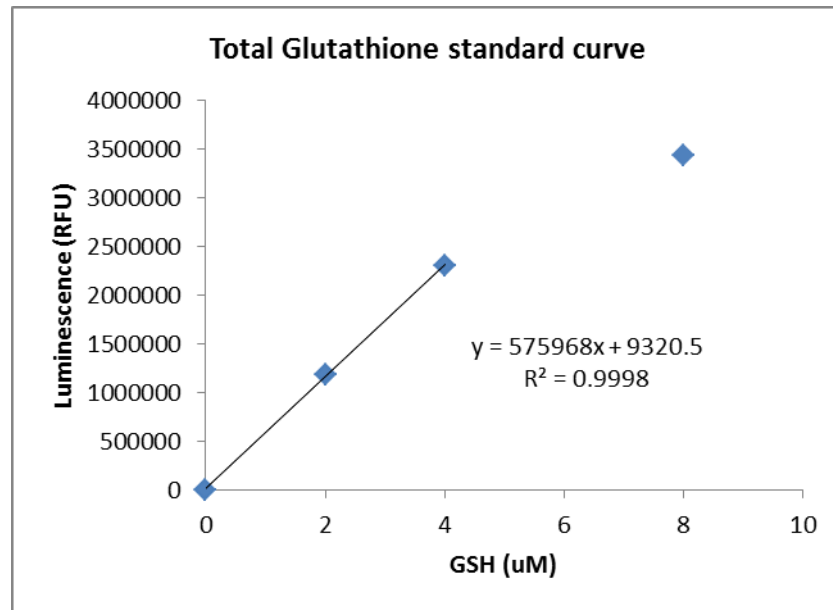
Appendix Figure 3: Immunocytochemistry images of SH-SY5Y control experiments for the data presented in Figures 4.4 and 4.5

Representative ICC images at 100x magnification of nuclear DAPI staining in blue and alpha-synuclein in red (scale bar = 20 μm). Untreated control represents cells without the addition of any treatment, stained with both primary and secondary antibodies. Secondary only control represents cells treated with 10% (v/v) Type C oligomers for 16 hours, stained with the emission of the primary antibody. The lack of fluorescence compared to the images of treated cells stained with both antibodies demonstrates the specificity of the secondary antibody for the primary antibody. Monomer treated control represents cells treated for 16 hours with 10% (v/v) 98 μM alpha-synuclein monomer, demonstrating that the alterations in alpha-synuclein staining seen following Type C oligomer treatment is not a general response to all conformations of the protein.



Appendix Figure 4: Nonlinear transform plot displaying amount of Menadione required to reduce SH-SY5Y cell activity by 50% (IC₅₀) following 2 hour treatment.

IC₅₀ was calculated to aid in the selection of a concentration of Menadione to use as a positive control in stress experiments, the results of which as shown in Figures 4.7, 4.8 and 4.9. Based on the IC₅₀ value of 17.54 μ M found here, a Menadione concentration of 10 μ M was used in these experiments.



Appendix Figure 5: Total and oxidised glutathione calibration curves.

A calibration curve of total and oxidised glutathione was produced using the GSH/GSSG-Glo™ Assay following manufacturer guidelines to enable the calculation of glutathione concentration in SH-SY5Y cells following treatment as displayed in Figure 4.8.

Bibliography

- About, S. *et al.* (2016) 'Tunneling nanotubes spread fibrillar α -synuclein by intercellular trafficking of lysosomes', *The EMBO Journal*, 35(19), pp. 2120–2138.
- de Almeida, N. E. C. *et al.* (2017) '1,2,3,4,6-penta-O-galloyl- β -D-glucopyranose binds to the N-terminal metal binding region to inhibit amyloid β -protein oligomer and fibril formation', *International Journal of Mass Spectrometry*, 420, pp. 24–34.
- Anderson, C. P. *et al.* (2012) 'Mammalian iron metabolism and its control by iron regulatory proteins', *Biochimica et biophysica acta*, 1823(9), pp. 1468–1483.
- Anderson, J. P. *et al.* (2006) 'Phosphorylation of Ser-129 is the dominant pathological modification of alpha-synuclein in familial and sporadic Lewy body disease.', *The Journal of biological chemistry*, 281(40), pp. 29739–52.
- Anderson, V. L. and Webb, W. W. (2011) 'Transmission electron microscopy characterization of fluorescently labelled amyloid β 1-40 and α -synuclein aggregates', *BMC Biotechnology*, 11(125).
- Angot, E. *et al.* (2012) 'Alpha-Synuclein Cell-to-Cell Transfer and Seeding in Grafted Dopaminergic Neurons In Vivo', *PLoS ONE*, 7(6), p. e39465.
- Appel-Cresswell, S. *et al.* (2013) 'Alpha-synuclein p.H50Q, a novel pathogenic mutation for Parkinson's disease.', *Movement disorders*, 28(6), pp. 811–3.
- Arawaka, S. *et al.* (2017) 'Mechanisms underlying extensive Ser129-phosphorylation in α -synuclein aggregates', *Acta neuropathologica communications*, 15(1), pp. 48.
- Babu, M. M. (2016) 'The contribution of intrinsically disordered regions to protein function, cellular complexity, and human disease', *Biochemical Society Transactions*, 44(5), pp. 1185-1200.
- Bartels, T., Choi, J. G. and Selkoe, D. J. (2011) ' α -Synuclein occurs physiologically as a helically folded tetramer that resists aggregation.', *Nature*, 477(7362), pp. 107–10.
- Bengoa-Vergniory, N. *et al.* (2017) 'Alpha-synuclein oligomers: a new hope', *Acta Neuropathologica*, 134(6), pp. 819–838.
- Bernstein, S. L. *et al.* (2004) 'Alpha-synuclein: stable compact and extended monomeric structures and pH dependence of dimer formation.', *Journal of the American Society for Mass Spectrometry*, 15(10), pp. 1435–43.
- Bernstein, S. L. *et al.* (2005) 'Amyloid β -protein: Monomer structure and early aggregation states of A β 42 and its Pro¹⁹ alloform', *Journal of the American Chemical Society*, 127(7), pp. 2075-2084.

- Bernstein, S. L. *et al.* (2009) 'Amyloid- β protein oligomerization and the importance of tetramers and dodecamers in the aetiology of Alzheimer's disease', *Nature Chemistry*, 1, p. 326.
- Betarbet, R. *et al.* (2000) 'Chronic systemic pesticide exposure reproduces features of Parkinson's disease', *Nature Neuroscience*, 3, p. 1301.
- Beveridge, R. *et al.* (2015) 'Relating gas phase to solution conformations: Lessons from disordered proteins', *Proteomics*, 15(16), pp. 2872–2883.
- Binolfi, A. *et al.* (2006) 'Interaction of α -Synuclein with Divalent Metal Ions Reveals Key Differences: A Link between Structure, Binding Specificity and Fibrillation Enhancement', *Journal of the American Chemical Society*, 128(30), pp. 9893–9901.
- Binolfi, A. *et al.* (2010) 'Bioinorganic chemistry of Parkinson's disease: structural determinants for the copper-mediated amyloid formation of alpha-synuclein.', *Inorganic chemistry*, 49(22), pp. 10668–79.
- Binolfi, A. *et al.* (2012) 'Bioinorganic chemistry of copper coordination to alpha-synuclein: Relevance to Parkinson's disease', *Coordination Chemistry Reviews*, 256(19–20), pp. 2188–2201.
- Blesa, J., Lanciego, J. L. and Obeso, J. A. (2015) 'Editorial: Parkinson's disease: cell vulnerability and disease progression', *Frontiers in Neuroanatomy*, 9, p. 125.
- Bliederhaeuser, C. *et al.* (2016) 'Age-dependent defects of alpha-synuclein oligomer uptake in microglia and monocytes.', *Acta neuropathologica*, 131(3), pp. 379–91.
- Bonifati, V. *et al.* (2003) 'Mutations in the DJ-1 gene associated with autosomal recessive early-onset parkinsonism', *Science*, 299(5604), p. 256.
- Borghi, R. *et al.* (2000) 'Full length α -synuclein is present in cerebrospinal fluid from Parkinson's disease and normal subjects', *Neuroscience Letters*, 287(1), pp. 65–67.
- Bosco, D. A. *et al.* (2011) 'Proteostasis and Movement Disorders: Parkinson's Disease and Amyotrophic Lateral Sclerosis', *Cold Spring Harbor Perspectives in Biology*, 3(10), p. a007500.
- Braak, H. *et al.* (2003) 'Idiopathic Parkinson's disease: possible routes by which vulnerable neuronal types may be subject to neuroinvasion by an unknown pathogen.', *Journal of neural transmission*, 110(5), pp. 517–36.
- Braak, H. *et al.* (2006) 'Pathology associated with sporadic Parkinson's disease--where does it end?', *Journal of neural transmission. Supplementum* (70), p. 89.
- Bradshaw, R. A. (1989) 'Protein translocation and turnover in eukaryotic cells.', *Trends in biochemical sciences*, 14(7), pp. 276–9.

- Breuker, K. and McLafferty, F. W. (2008) 'Stepwise evolution of protein native structure with electrospray into the gas phase, 10^{-12} to 10^2 s', *Proceedings of the National Academy of Sciences*, 105(47), pp. 18145-18152.
- Brown, D. R. (2009) 'Metal binding to alpha-synuclein peptides and its contribution to toxicity.', *Biochemical and biophysical research communications*, 380(2), pp. 377-81.
- Brundin, P. and Melki, R. (2017) 'Prying into the Prion Hypothesis for Parkinson's Disease', *The Journal of Neuroscience*, 37(41), pp. 9808-9818.
- Bu, B. *et al.* (2017) 'N-Terminal Acetylation Preserves α -Synuclein from Oligomerization by Blocking Intermolecular Hydrogen Bonds', *ACS Chemical Neuroscience*, 8(10), pp. 2145-2151.
- Buell, A. K. *et al.* (2014) 'Solution conditions determine the relative importance of nucleation and growth processes in α -synuclein aggregation', *PNAS*, 111(21), pp. 7671-7676.
- Burke, R. E., Dauer, W. T. and Vonsattel, J. P. G. (2008) 'A critical evaluation of the Braak staging scheme for Parkinson's disease', *Annals of Neurology*, 64(5), pp. 485-91.
- Burré, J. *et al.* (2010) ' α -Synuclein Promotes SNARE-Complex Assembly in vivo and in vitro', *Science*, 329(5999), pp. 1663-1667.
- Burré, J. (2015) 'The synaptic function of α -synuclein', *Journal of Parkinson's Disease*, 5(4), pp. 699-713.
- Bush, M. F. *et al.* (2010) 'Collision Cross Sections of Proteins and Their Complexes: A Calibration Framework and Database for Gas-Phase Structural Biology', *Analytical Chemistry*, 82(22), pp. 9557-9565.
- Bussell, R. and Eliezer, D. (2003) 'A Structural and Functional Role for 11-mer Repeats in α -Synuclein and Other Exchangeable Lipid Binding Proteins', *Journal of Molecular Biology*, 329(4), pp. 763-778.
- von Campenhausen, S. *et al.* (2005) 'Prevalence and incidence of Parkinson's disease in Europe', *European Neuropsychopharmacology*, 15(4), pp. 473-490.
- Carboni, E. and Lingor, P. (2015) 'Insights on the interaction of alpha-synuclein and metals in the pathophysiology of Parkinson's disease', *Metallomics*, 7(3), pp. 395-404.
- Cartelli, D. *et al.* (2016) ' α -Synuclein is a Novel Microtubule Dynamase', *Scientific Reports*, 6:33289.
- Caudle, W. M. *et al.* (2012) 'Industrial toxicants and Parkinson's disease', *Neurotoxicology*, 33(2), pp. 178-188.
- Chang, D. *et al.* (2017) 'A meta-analysis of genome-wide association studies identifies 17 new Parkinson's disease risk loci', *Nature Genetics*, 49(10), pp. 1511-1516.

- Chen, P., Miah, M. R. and Aschner, M. (2016) 'Metals and Neurodegeneration.', *F1000Research*, 5.
- Chen, S.-H. and Russell, D. H. (2015) 'How Closely Related Are Conformations of Protein Ions Sampled by IM-MS to Native Solution Structures?', *Journal of The American Society for Mass Spectrometry*, 26(9), pp. 1433–1443.
- Choi, B.-K. *et al.* (2013) 'Large α -synuclein oligomers inhibit neuronal SNARE-mediated vesicle docking.', *PNAS*, 110(10), PP. 4087-92.
- Clayton, D. F. and George, J. M. (1998) 'The synucleins: a family of proteins involved in synaptic function, plasticity, neurodegeneration and disease', *Trends in Neurosciences*, 21(6), pp. 249–254.
- La Cognata, V. *et al.* (2017) 'Copy number variability in Parkinson's disease: assembling the puzzle through a systems biology approach', *Human Genetics*, 136(1), pp. 13-37.
- Colla, E. *et al.* (2012a) 'Accumulation of toxic α -synuclein oligomer within endoplasmic reticulum occurs in α -synucleinopathy in vivo.', *The Journal of Neuroscience*, 32(10), pp. 2201-5.
- Colla, E. *et al.* (2012b) 'Endoplasmic reticulum stress is important for the manifestations of α -synucleinopathy in vivo.', *The Journal of Neuroscience*, 32(10), pp. 3306-20.
- Connolly, B. S. and Lang, A. E. (2014) 'Pharmacological treatment of Parkinson disease: A review.', *JAMA*, 311(16), pp. 1670–1683.
- Constantinescu, R. *et al.* (2007) 'Neuronal differentiation and long-term culture of the human neuroblastoma line SH-SY5Y.', *J Neural Transm, Suppl* 72, pp. 17-28.
- Conway, K. A. *et al.* (2000) 'Acceleration of oligomerization, not fibrillization, is a shared property of both alpha -synuclein mutations linked to early-onset Parkinson's disease: Implications for pathogenesis and therapy', *Proceedings of the National Academy of Sciences*, 97(2), pp. 571–576.
- Conway, K. A., Harper, J. D. and Lansbury, P. T. (2000) 'Fibrils formed in vitro from α -synuclein and two mutant forms linked to Parkinson's disease are typical amyloid', *Biochemistry*, 39(10), pp. 2552-63.
- Cookson, M. R. (2012) 'Parkinsonism due to mutations in PINK1, Parkin, and DJ-1 and oxidative stress and mitochondrial pathways', *Cold Spring Harbor Perspectives in Medicine*, 2(9).
- Cookson, M. R. (2015) 'LRRK2 Pathways Leading to Neurodegeneration', *Current Neurology and Neuroscience Reports*, 15(7), pp. 42.

- Cookson, M. R., Hardy, J. and Lewis, P. A. (2008) 'Genetic Neuropathology of Parkinson's Disease', *International Journal of Clinical and Experimental Pathology*, 1(3), pp. 217–231.
- Correia Guedes, L. *et al.* (2010) 'Worldwide frequency of G2019S LRRK2 mutation in Parkinson's disease: A systematic review', *Parkinsonism & Related Disorders*, 16(4), pp. 237–242.
- Criddle, D. N. *et al.* (2006) 'Menadione-induced reactive oxygen species generation via redox cycling promotes apoptosis of murine pancreatic acinar cells', *Journal of Biological Chemistry*, 281(52), pp. 40485-92.
- Cumeras, R. *et al.* (2015) 'Review on Ion Mobility Spectrometry. Part 1: Current Instrumentation', *The Analyst*, 140(5), pp. 1376–1390.
- Van Damme, P. *et al.* (2012) 'N-terminal acetylome analyses and functional insights of the N-terminal acetyltransferase NatB.', *Proceedings of the National Academy of Sciences of the United States of America*, 109(31), pp. 12449–54.
- Danzer, K. M. *et al.* (2007) 'Different Species of α -Synuclein Oligomers Induce Calcium Influx and Seeding', *Journal of Neuroscience*, 27(34), pp. 9220-32.
- Danzer, K. M. *et al.* (2009) 'Seeding induced by α -synuclein oligomers provides evidence for spreading of α -synuclein pathology', *Journal of Neurochemistry*, 111(1), pp. 192-203.
- Danzer, K. M. *et al.* (2012) 'Exosomal cell-to-cell transmission of alpha synuclein oligomers', *Molecular Neurodegeneration*, 7(1), pp. 42.
- Davies, P. *et al.* (2011) 'The synucleins are a family of redox-active copper binding proteins.', *Biochemistry*, 50(1), pp. 37–47.
- Davies, P., Moualla, D. and Brown, D. R. (2011) 'Alpha-synuclein is a cellular ferrireductase.', *PLoS one*, 6(1), p. e15814.
- Deas, E. *et al.* (2016) 'Alpha-Synuclein Oligomers Interact with Metal Ions to Induce Oxidative Stress and Neuronal Death in Parkinson's Disease', *Antioxidants & Redox Signaling*, 24(7), pp. 376-91.
- Desplats, P. *et al.* (2009) 'Inclusion formation and neuronal cell death through neuron-to-neuron transmission of alpha-synuclein.', *Proceedings of the National Academy of Sciences of the United States of America*, 106(31), pp. 13010–5.
- Di Maio, R. *et al.* (2016) ' α -Synuclein binds to TOM20 and inhibits mitochondrial protein import in Parkinson's disease.', *Science translational medicine*, 8(342)
- Dias, V., Junn, E. and Mouradian, M. M. (2013) 'The role of oxidative stress in parkinson's disease', *Journal of Parkinson's Disease*, 3(4), pp. 461-91.

- Dikiy, I. and Eliezer, D. (2014) 'N-terminal acetylation stabilizes N-terminal helicity in lipid- and micelle-bound α -synuclein and increases its affinity for physiological membranes.', *The Journal of biological chemistry*, 289(6), pp. 3652–65.
- Dimant, H. *et al.* (2013) 'Direct detection of alpha synuclein oligomers in vivo', *Acta Neuropathologica Communications*, 1, pp. 6.
- Diogenes, M.-J. *et al.* (2012) 'Extracellular alpha-synuclein oligomers modulate synaptic transmission and impair LTP via NMDA-receptor activation.', *The Journal of Neuroscience*, 32(34), pp. 11750–62.
- Dong, J. *et al.* (2014) 'Unique effect of Cu(II) in the metal-induced amyloid formation of β -2-microglobulin', *Biochemistry*, 53(8), pp. 1263.
- Donor, M. T. *et al.* (2017) 'Extended Protein Ions Are Formed by the Chain Ejection Model in Chemical Supercharging Electrospray Ionization', *Analytical Chemistry*, 89(9), pp. 5107–5114.
- Doty, R. L. (2012) 'Olfaction in Parkinson's disease and related disorders', *Neurobiology of disease*, 46(3), pp. 527–552.
- Drew, S. C. *et al.* (2008) 'Cu²⁺ binding modes of recombinant alpha-synuclein--insights from EPR spectroscopy.', *Journal of the American Chemical Society*, 130(24), pp. 7766–73.
- Dusa, A. *et al.* (2006) 'Characterization of oligomers during alpha-synuclein aggregation using intrinsic tryptophan fluorescence', *Biochemistry*, 45(8), pp. 2752–60.
- Dusek, P. *et al.* (2015) 'The neurotoxicity of iron, copper and manganese in Parkinson's and Wilson's diseases.', *Journal of trace elements in medicine and biology*, 31, pp. 193–203.
- Dyson, H. J. (2016) 'Making Sense of Intrinsically Disordered Proteins', *Biophysical Journal*, 110(5), pp. 1013–1016.
- Eastwood, T. A. *et al.* (2017) 'An enhanced recombinant amino-terminal acetylation system and novel in vivo high-throughput screen for molecules affecting α -synuclein oligomerisation', *FEBS Letters*, 593(6), pp. 833–841.
- Eisele, Y. S. *et al.* (2015) 'Targeting protein aggregation for the treatment of degenerative diseases', *Nature Reviews Drug Discovery*, 14, p. 759.
- El-Agnaf, O. M. A. *et al.* (2003) 'Alpha-synuclein implicated in Parkinson's disease is present in extracellular biological fluids, including human plasma.', *FASEB journal*, 17(13), pp. 1945–7.
- Elbaz, A. *et al.* (2009) 'Professional exposure to pesticides and Parkinson disease', *Annals of Neurology*, 66(4), pp. 494–504.

- Eliezer, D. *et al.* (2001) 'Conformational properties of α -synuclein in its free and lipid-associated states', *Journal of Molecular Biology*, 307(4), pp. 1061–1073.
- Fagerqvist, T. *et al.* (2013) 'Off-pathway α -synuclein oligomers seem to alter α -synuclein turnover in a cell model but lack seeding capability in vivo', *Amyloid*, 20(4), pp. 233–244.
- Fauvet, B. *et al.* (2012) ' α -Synuclein in central nervous system and from erythrocytes, mammalian cells, and Escherichia coli exists predominantly as disordered monomer.', *The Journal of biological chemistry*, 287(19), pp. 15345–64.
- Febbraro, F. *et al.* (2012) ' α -Synuclein expression is modulated at the translational level by iron.', *Neuroreport*, 23(9), pp. 576–80.
- Feng, L. R. *et al.* (2010) ' α -Synuclein mediates alterations in membrane conductance: a potential role for α -synuclein oligomers in cell vulnerability', *The European journal of neuroscience*, 32(1), pp. 10–17.
- Fernandez de la Mora, J. (2000) 'Electrospray ionization of large multiply charged species proceeds via Dole's charged residue mechanism', *Analytica Chimica Acta*, 406(1), pp. 93–104.
- Fink, A. L. (2006) 'The aggregation and fibrillation of alpha-synuclein', *Accounts of Chemical Research*, 39(9), pp. 628–34.
- Fitzpatrick, P. F. (1989) 'The metal requirement of rat tyrosine hydroxylase', *Biochemical and Biophysical Research Communications*, 161(1), pp. 211–215.
- Florance, H. V. *et al.* (2011) 'Evidence for α -helices in the gas phase: A case study using Melittin from honey bee venom', *Analyst*, 136(17), pp. 3446–52.
- Foulds, P. G. *et al.* (2013) 'A longitudinal study on α -synuclein in blood plasma as a biomarker for Parkinson's disease', *Scientific Reports*, 3(2540).
- Franco-Iborra, S., Vila, M. and Perier, C. (2015) 'The Parkinson Disease Mitochondrial Hypothesis: Where Are We at?', *The Neuroscientist*, 22(3), pp. 266–277.
- Frigerio, R. *et al.* (2011) 'Incidental Lewy Body Disease: Do some cases represent a preclinical stage of Dementia with Lewy Bodies?', *Neurobiology of Aging*, 32(5), pp. 857–863.
- Frimpong, A. K. *et al.* (2010) 'Characterization of intrinsically disordered proteins with electrospray ionization mass spectrometry: conformational heterogeneity of alpha-synuclein.', *Proteins*, 78(3), pp. 714–22.
- Funayama, M. *et al.* (2002) 'A new locus for Parkinson's Disease (PARK8) maps to chromosome 12p11.2-q13.1', *Annals of Neurology*, 51(3), pp. 296–301.

- Fussi, N. *et al.* (2018) 'Exosomal secretion of α -synuclein as protective mechanism after upstream blockage of macroautophagy', *Cell Death and Disease*, 9(757).
- Gaki, G. S. and Papavassiliou, A. G. (2014) 'Oxidative stress-induced signaling pathways implicated in the pathogenesis of Parkinson's disease', *NeuroMolecular Medicine*, 16(2), pp. 217-30.
- Gardner, B. *et al.* (2017) 'Metal concentrations and distributions in the human olfactory bulb in Parkinson's disease', *Scientific Reports*, 7, pp. 10454.
- Gaskell, B. J. M. and S. J. (2009) 'Using Electrospray Ionisation Mass Spectrometry to Study Non-Covalent Interactions', *Combinatorial Chemistry & High Throughput Screening*, pp. 203–211.
- George, J. M. *et al.* (1995) 'Characterization of a novel protein regulated during the critical period for song learning in the zebra finch', *Neuron*, 15(2), pp. 361–372.
- Gessel, M. M. *et al.* (2012) ' $A\beta$ (39–42) Modulates $A\beta$ Oligomerization but Not Fibril Formation', *Biochemistry*, 51(1), pp. 108–117.
- Ghosh, D. *et al.* (2013) 'The Parkinson's disease-associated H50Q mutation accelerates α -Synuclein aggregation in vitro.', *Biochemistry*, 52(40), pp. 6925–7.
- Giasson, B. I. *et al.* (2001) 'A Hydrophobic Stretch of 12 Amino Acid Residues in the Middle of α -Synuclein Is Essential for Filament Assembly', *Journal of Biological Chemistry*, 276(4), pp. 2380-6.
- Gidden, J. and Bowers, M. T. (2003) 'Gas-phase conformations of deprotonated trinucleotides (dGTT⁻, dTGT⁻, and dTTG⁻): the question of zwitterion formation', *Journal of the American Society for Mass Spectrometry*, 14(2), pp. 161–170.
- Giehm, L., Lorenzen, N. and Otzen, D. E. (2011) 'Assays for α -synuclein aggregation', *Methods*, 53(3), pp. 295-305.
- Giles, K. *et al.* (2004) 'Applications of a travelling wave-based radio-frequency-only stacked ring ion guide', *Rapid Communications in Mass Spectrometry*, 18(20), pp. 2401–2414.
- Goedert, M. *et al.* (2012) '100 years of Lewy pathology', *Nature Reviews Neurology*, 9, pp. 13.
- Goldberg, M. S. *et al.* (2005) 'Nigrostriatal Dopaminergic Deficits and Hypokinesia Caused by Inactivation of the Familial Parkinsonism-Linked Gene DJ-1', *Neuron*, 45(4), pp. 489–496.
- Goldman, S. M. *et al.* (2012) 'Solvent Exposures and Parkinson's Disease Risk in Twins', *Annals of Neurology*, 71(6), pp. 776–784.

- Gorell, J. M. *et al.* (1999) 'Occupational Metal Exposures and the Risk of Parkinson's Disease', *Neuroepidemiology*, 18(6), pp. 303–308.
- Gorell, J. M. *et al.* (2004) 'Multiple risk factors for Parkinson's disease.', *Journal of the neurological sciences*, 217(2), pp. 169–74.
- Grabenauer, M. *et al.* (2008) 'Spermine binding to Parkinson's protein alpha-synuclein and its disease-related A30P and A53T mutants.', *The journal of physical chemistry*, 112(35), pp. 11147–54.
- Greaves, L. C. *et al.* (2012) 'Mitochondrial DNA and disease', *Journal of Pathology*, 226(2), pp. 274-86.
- Hall, Z., Schmidt, C. and Politis, A. (2016) 'Uncovering the early assembly mechanism for amyloidogenic β 2-microglobulin using cross-linking and native mass spectrometry', *Journal of Biological Chemistry*, 291(9), pp. 4626-37.
- Han, J. Y., Choi, T. S. and Kim, H. I. (2018) 'Molecular Role of Ca²⁺ and Hard Divalent Metal Cations on Accelerated Fibrillation and Interfibrillar Aggregation of α -Synuclein', *Scientific Reports*, 8(1), pp. 1895.
- Hansen, C. *et al.* (2011) ' α -Synuclein propagates from mouse brain to grafted dopaminergic neurons and seeds aggregation in cultured human cells.', *The Journal of Clinical Investigation*, 121(2), pp. 715-25.
- Hartl, F. U., Bracher, A. and Hayer-Hartl, M. (2011) 'Molecular chaperones in protein folding and proteostasis', *Nature*, 475, pp. 324.
- Hartmann, A. (2004) 'Postmortem studies in Parkinson's disease', *Dialogues in Clinical Neuroscience*, 6(3), pp. 281-293.
- Hawkes, C. H., Del Tredici, K. and Braak, H. (2007) 'Parkinson's disease: A dual-hit hypothesis', *Neuropathology and Applied Neurobiology*, 33(6), pp. 599-614.
- Heck, A. J. R. and Van Den Heuvel, R. H. H. (2004) 'Investigation of intact protein complexes by mass spectrometry', *Mass Spectrometry Reviews*, 23(5), pp. 368-89.
- Herva, M. E. *et al.* (2014) 'Anti-amyloid Compounds Inhibit alpha-synuclein Aggregation Induced by Protein Misfolding Cyclic Amplification (PMCA)', *Journal of Biological Chemistry*, 289(17), pp. 11897-905.
- Hopper, J. T. S. and Oldham, N. J. (2009) 'Collision induced unfolding of protein ions in the gas phase studied by ion mobility-mass spectrometry: the effect of ligand binding on conformational stability.', *Journal of the American Society for Mass Spectrometry*, 20(10), pp. 1851–8.
- Hoyer, W. *et al.* (2002) 'Dependence of α -Synuclein Aggregate Morphology on Solution Conditions', *Journal of Molecular Biology*, 322(2), pp. 383–393.

- Iakoucheva, L. M. *et al.* (2002) 'Intrinsic Disorder in Cell-signaling and Cancer-associated Proteins', *Journal of Molecular Biology*, 323(3), pp. 573–584.
- Illes-Toth, E. *et al.* (2015) 'Distinct higher-order α -synuclein oligomers induce intracellular aggregation.', *The Biochemical Journal*, 468(3), pp. 485–93.
- Illes-Toth, E., Dalton, C. F. and Smith, D. P. (2013) 'Binding of Dopamine to Alpha-Synuclein is Mediated by Specific Conformational States.', *Journal of the American Society for Mass Spectrometry*, 24(9), pp. 1346–54.
- Ingelsson, M. (2016) 'Alpha-Synuclein Oligomers—Neurotoxic Molecules in Parkinson's Disease and Other Lewy Body Disorders', *Frontiers in Neuroscience*, 10, pp. 408.
- Invernizzi, G. *et al.* (2012) 'Protein aggregation: Mechanisms and functional consequences', *The International Journal of Biochemistry & Cell Biology*, 44(9), pp. 1541–1554.
- Iwai, A. *et al.* (1995) 'The precursor protein of non-A β component of Alzheimer's disease amyloid is a presynaptic protein of the central nervous system', *Neuron*, 14(2), pp. 467–475.
- Iwanaga, K. *et al.* (1999) 'Lewy body-type degeneration in cardiac plexus in Parkinson's and incidental Lewy body diseases', *Neurology*, 52(6), pp. 1269–1271.
- Jackson, R. J., Hellen, C. U. T. and Pestova, T. V. (2010) 'The mechanism of eukaryotic translation initiation and principles of its regulation', *Nature Reviews Molecular Cell Biology*, 11(2), pp. 113–27.
- Jang, A. *et al.* (2010) 'Non-classical exocytosis of α -synuclein is sensitive to folding states and promoted under stress conditions', *Journal of Neurochemistry*, 113(5), pp. 1263–74.
- Jenner, M. *et al.* (2011) 'Detection of a protein conformational equilibrium by electrospray ionisation-ion mobility-mass spectrometry.', *Angewandte Chemie*, 50(36), pp. 8291–4.
- Jiang, P. *et al.* (2017) 'Impaired endo-lysosomal membrane integrity accelerates the seeding progression of α -synuclein aggregates', *Scientific Reports*, 7(1), pp. 7690.
- Jin Lee, H. *et al.* (2018) 'Calprotectin influences the aggregation of metal-free and metal-bound amyloid-b by direct interaction', *Metallomics*, 10, pp. 1116.
- Johannes, G. *et al.* (1999) 'Identification of eukaryotic mRNAs that are translated at reduced cap binding complex eIF4F concentrations using a cDNA microarray', *Proceedings of the National Academy of Sciences*, 96(23), pp. 13118–13123.
- Johnson, M. *et al.* (2010) 'Targeted amino-terminal acetylation of recombinant proteins in *E. coli.*', *PloS one*, 5(12), p. e15801.

- Junn, E. and Mouradian, M. M. (2002) 'Human α -Synuclein over-expression increases intracellular reactive oxygen species levels and susceptibility to dopamine', *Neuroscience Letters*, 320(3), pp. 146–150.
- Kakimura, J. *et al.* (2001) 'Release and aggregation of cytochrome c and α -synuclein are inhibited by the antiparkinsonian drugs, talipexole and pramipexole', *European Journal of Pharmacology*, 417(1–2), pp. 59–67.
- Kang, L. *et al.* (2012) 'N-terminal acetylation of α -synuclein induces increased transient helical propensity and decreased aggregation rates in the intrinsically disordered monomer.', *Protein science*, 21(7), pp. 911–7.
- Kang, L. *et al.* (2013) 'Mechanistic insight into the relationship between N-terminal acetylation of α -synuclein and fibril formation rates by NMR and fluorescence.', *PloS one*, 8(9), p. e75018.
- Karas, R. M., Bahr, U and Dülcks, T (2000) 'Nano-electrospray ionization mass spectrometry: addressing analytical problems beyond routine', *Fresenius J Anal Chem*, 366, pp. 669–676.
- Kaufmann, T. *et al.* (2016) 'Intracellular soluble α -synuclein oligomers reduce pyramidal cell excitability.', *The Journal of Physiology*, 594(10), pp. 2751-72.
- Kessler, J. C., Rochet, J. C. and Lansbury, P. T. (2003) 'The N-terminal repeat domain of α -synuclein inhibits β -sheet and amyloid fibril formation', *Biochemistry*, 42(3). pp. 672-8.
- Khalaf, O. *et al.* (2014) 'The H50Q mutation enhances α -synuclein aggregation, secretion, and toxicity', *Journal of Biological Chemistry*, 289(32), pp. 21856-76.
- Kitada, T. *et al.* (1998) 'Mutations in the parkin gene cause autosomal recessive juvenile parkinsonism', *Nature*, 392, pp. 605.
- Klucken, J. *et al.* (2012) 'Alpha-synuclein aggregation involves a bafilomycin A 1-sensitive autophagy pathway.', *Autophagy*, 8(5), pp. 754-66.
- Konermann, L. *et al.* (2013) 'Unraveling the mechanism of electrospray ionization', *Analytical Chemistry*, 85(1), pp. 2-9.
- Konijnenberg, A. *et al.* (2016) 'Opposite Structural Effects of Epigallocatechin-3-gallate and Dopamine Binding to α -Synuclein', *Analytical Chemistry*, 88(17), pp. 8468–8475.
- Kordower, J. H. *et al.* (2008) 'Lewy body-like pathology in long-term embryonic nigral transplants in Parkinson's disease.', *Nature medicine*, 14(5), pp. 504–6.
- Kozlowski, H. *et al.* (2012) 'Copper, zinc and iron in neurodegenerative diseases (Alzheimer's, Parkinson's and prion diseases)', *Coordination Chemistry Reviews*, 256(19–20), pp. 2129–2141.

- Krasnoslobodtsev, A. V *et al.* (2012) 'Effect of Spermidine on Misfolding and Interactions of Alpha-Synuclein', *PLOS ONE*, 7(5), pp. e38099.
- Krishna, A. *et al.* (2014) 'Systems genomics evaluation of the SH-SY5Y neuroblastoma cell line as a model for Parkinson's disease', *BMC Genomics*, 15(1154), pp. 1–21.
- Krüger, R. *et al.* (1998) 'Ala30Pro mutation in the gene encoding alpha-synuclein in Parkinson's disease', *Nature genetics*, 18(2), pp. 106.
- Langston, J. W. *et al.* (1983) 'Chronic Parkinsonism in humans due to a product of meperidine-analog synthesis', *Science*, 219(4587), p. 979 LP-980.
- Larini, L. *et al.* (2013) 'Initiation of Assembly of Tau(273–284) and its Δ K280 Mutant: An Experimental and Computational Study', *Physical chemistry chemical physics*, 15(23), pp. 8916–8928.
- Lashuel, H. A. *et al.* (2013) 'The many faces of α -synuclein: From structure and toxicity to therapeutic target', *Nature Reviews Neuroscience*, 14(1), pp. 38-48.
- de Lau, L. M. and Breteler, M. M. (2006) 'Epidemiology of Parkinson's disease', *The Lancet Neurology*, 5(6), pp. 525–535.
- Lee, H.-J. (2005) 'Intravesicular Localization and Exocytosis of alpha-synuclein and its Aggregates', *Journal of Neuroscience*, 25(25), pp. 6016-24.
- Lee, H.-J. *et al.* (2008) 'Assembly-dependent endocytosis and clearance of extracellular α -synuclein', *The International Journal of Biochemistry & Cell Biology*, 40(9), pp. 1835–1849.
- Lee, H.-J. (2010) 'Direct transfer of alpha-synuclein from neuron to astroglia causes inflammatory responses in synucleinopathies.', *Journal of Biological Chemistry*, 285(12), pp. 9262-72.
- Lee, J.-G. *et al.* (2016) 'Unconventional secretion of misfolded proteins promotes adaptation to proteasome dysfunction in mammalian cells', *Nature Cell Biology*, 18, pp. 765.
- Leney, A. C. *et al.* (2014) 'Insights into the role of the beta-2 microglobulin D-strand in amyloid propensity revealed by mass spectrometry', *Molecular BioSystems*, 10(3), pp. 412–420.
- Lesage, S. *et al.* (2013) 'G51D α -synuclein mutation causes a novel Parkinsonian-pyramidal syndrome', *Annals of Neurology*, 73(4), pp. 459-71.
- Lesage, S. and Brice, A. (2009) 'Parkinson's disease: From monogenic forms to genetic susceptibility factors', *Human Molecular Genetics*, 18(R1), pp. R48-59.
- LeVine, H. B. T.-M. in E. (1999) 'Quantification of β -sheet amyloid fibril structures with thioflavin T', *Amyloid, Prions, and Other Protein Aggregates*, pp. 274–284.

- Li, J.-Y. *et al.* (2008) 'Lewy bodies in grafted neurons in subjects with Parkinson's disease suggest host-to-graft disease propagation.', *Nature medicine*, 14(5), pp. 501–3.
- Li, J. *et al.* (1999) 'Influence of solvent composition and capillary temperature on the conformations of electrosprayed ions: unfolding of compact ubiquitin conformers from pseudonative and denatured solutions', *International Journal of Mass Spectrometry*, 185–187, pp. 37–47.
- Liao, J. *et al.* (2014) 'Parkinson disease-associated mutation R1441H in LRRK2 prolongs the "active state" of its GTPase domain', *Proceedings of the National Academy of Sciences*, 111(11), pp. 4055-60.
- Lim, J. and Vachet, R. W. (2004) 'Using mass spectrometry to study copper-protein binding under native and non-native conditions: b-2-microglobulin', *Analytical Chemistry*, 76(13), pp. 3498-504.
- Liu, Y. *et al.* (2014) 'Gallic acid interacts with α -synuclein to prevent the structural collapse necessary for its aggregation', *Biochimica et Biophysica Acta*, 1844(9), pp. 1481–1485.
- Longhena, F. *et al.* (2017) 'The Contribution of α -Synuclein Spreading to Parkinson's Disease Synaptopathy', *Neural Plasticity*, vol. 2017, Article ID 5012129.
- Loor, G. *et al.* (2010) 'Menadione triggers cell death through ROS-dependent mechanisms involving PARP activation without requiring apoptosis', *Free Radical Biology and Medicine*, 49(12), pp. 1925–1936.
- Loureiro, C., Campêlo, C. and Silva, R. H. (2017) 'Genetic Variants in SNCA and the Risk of Sporadic Parkinson's Disease and Clinical Outcomes: A Review', *Parkinson's Disease*, 4318416.
- Ludtmann, M. H. R. *et al.* (2018) ' α -synuclein oligomers interact with ATP synthase and open the permeability transition pore in Parkinson's disease', *Nature Communications*, 9(1), pp. 2293.
- Luk, K. C. *et al.* (2012) 'Pathological α -synuclein transmission initiates Parkinson-like neurodegeneration in nontransgenic mice.', *Science*, 338(6109), pp. 949–53.
- Mackenzie, I. (2001) 'The Pathology of Parkinson's Disease', *BCMJ*, 43(3), pp. 142–147.
- Manning-Bog, A. B. *et al.* (2002) 'The herbicide paraquat causes up-regulation and aggregation of alpha-synuclein in mice: paraquat and alpha-synuclein.', *The Journal of biological chemistry*, 277(3), pp. 1641–4.
- Mao, X. *et al.* (2016) 'Pathological α -synuclein transmission initiated by binding lymphocyte-activation gene 3', *Science*, 353(6307), pp. 3374.

- Mason, E. A. and Schamp, H. W. (1958) 'Mobility of gaseous ions in weak electric fields', *Annals of Physics*, 4(3), pp. 233–270.
- Mason, R. J. *et al.* (2016) 'Copper Binding and Subsequent Aggregation of α -Synuclein Are Modulated by N-Terminal Acetylation and Ablated by the H50Q Missense Mutation', *Biochemistry*, 55(34), pp. 4737–4741.
- Masuda-Suzukake, M. *et al.* (2013) 'Prion-like spreading of pathological α -synuclein in brain', *Brain*, 136(4), pp. 1128–1138.
- May, J. C., Morris, C. B. and McLean, J. A. (2017) 'An Ion Mobility Collision Cross Section Compendium', *Anal Chem*, 89(2), pp. 1032-1044.
- McDowall, J. S., Ntai, I., Honeychurch, K. C., *et al.* (2017) 'Alpha-synuclein ferrireductase activity is detectable in vivo, is altered in Parkinson's disease and increases the neurotoxicity of DOPAL', *Molecular and Cellular Neuroscience*, 85, pp. 1–11.
- McDowall, J. S., Ntai, I., Hake, J., *et al.* (2017) 'Steady-State Kinetics of α -Synuclein Ferrireductase Activity Identifies the Catalytically Competent Species', *Biochemistry*, 56(19), pp. 2497–2505.
- McKinney, C. (2017) 'Using induced pluripotent stem cells derived neurons to model brain diseases.(Invited Review)', *Neural Regeneration Research*, 12(7), pp. 1062.
- Mendez, I. *et al.* (2008) 'Dopamine neurons implanted into people with Parkinson's disease survive without pathology for 14 years.', *Nature Medicine*, 14(5), pp. 507-9.
- Mendoza, V. L. *et al.* (2011) 'Structural Insights into the Pre-Amyloid Tetramer of β -2-Microglobulin from Covalent Labeling and Mass Spectrometry', *Biochemistry*, 50(31), pp. 6711–6722.
- Minezaki, Y. *et al.* (2006) 'Human Transcription Factors Contain a High Fraction of Intrinsically Disordered Regions Essential for Transcriptional Regulation', *Journal of Molecular Biology*, 359(4), pp. 1137–1149.
- Mizuno, N. *et al.* (2012) 'Remodeling of lipid vesicles into cylindrical micelles by α -synuclein in an extended α -helical conformation', *Journal of Biological Chemistry*, 287(35), pp. 29301-11.
- Moriarty, G. M. *et al.* (2014) 'A revised picture of the Cu(II)- α -synuclein complex: the role of N-terminal acetylation.', *Biochemistry*, 53(17), pp. 2815–7.
- Munishkina, L. A., Fink, A. L. and Uversky, V. N. (2009) 'Accelerated fibrillation of alpha-synuclein induced by the combined action of macromolecular crowding and factors inducing partial folding.', *Current Alzheimer research*, 6(3), pp. 252–60.

- Murray, I. V. J. *et al.* (2003) 'Role of α -synuclein carboxy-terminus on fibril formation in vitro', *Biochemistry*, 42(28), pp. 8530-40.
- Murray, M. M. *et al.* (2009) 'Amyloid beta protein: Abeta40 inhibits Abeta42 oligomerization', *Journal of the American Chemical Society*, 131(18), p. 6316.
- Naiki, H. *et al.* (1989) 'Fluorometric determination of amyloid fibrils in vitro using the fluorescent dye, thioflavine T', *Analytical Biochemistry*, 177(2), pp. 244–249.
- Nalls, M. A. *et al.* (2014) 'Large-scale meta-analysis of genome-wide association data identifies six new risk loci for Parkinson's disease', *Nature genetics*, 46(9), pp. 989–993.
- Natalello, A. *et al.* (2011) 'Compact conformations of α -synuclein induced by alcohols and copper', *Proteins*, 79(2), pp.611-21.
- Nettleton, E. J. *et al.* (2000) 'Characterization of the oligomeric states of insulin in self-assembly and amyloid fibril formation by mass spectrometry.', *Biophysical Journal*, 79(2), pp. 1053–1065.
- Nguyen, S. and Fenn, J. B. (2007) 'Gas-phase ions of solute species from charged droplets of solutions.', *PNAS*, 104(4), pp. 1111-7.
- Ohrfelt, A. *et al.* (2011) 'Identification of novel α -synuclein isoforms in human brain tissue by using an online nanoLC-ESI-FTICR-MS method.', *Neurochemical research*, 36(11), pp. 2029–42.
- Ostremova-Golts, N. *et al.* (2000) 'The A53T-Synuclein Mutation Increases Iron-Dependent Aggregation and Toxicity.', *The Journal of Neuroscience*, 20(16), pp.6048-54.
- Outeiro, T. F. *et al.* (2008) 'Formation of Toxic Oligomeric α -Synuclein Species in Living Cells', *PLOS ONE*, 3(4), pp. e1867.
- Ouyang, Z. *et al.* (2003) 'Preparing Protein Microarrays by Soft-Landing of Mass-Selected Ions', *Science*, 301(5638), pp. 1351.
- Pacheco, C. R. *et al.* (2015) 'Extracellular α -synuclein alters synaptic transmission in brain neurons by perforating the neuronal plasma membrane', *Journal of Neurochemistry*, 132(6), pp. 731–741.
- Paciotti, S. *et al.* ' Are We Ready for Detecting α -Synuclein Prone to Aggregation in Patients? The Case of "Protein-Misfolding Cyclic Amplification" and "Real-Time Quaking-Induced Conversion" as Diagnostic Tools.', *Frontiers in neurology*, 9:415.
- Paillusson, S. *et al.* (2017) ' α -Synuclein binds to the ER–mitochondria tethering protein VAPB to disrupt Ca(2+) homeostasis and mitochondrial ATP production', *Acta Neuropathologica*, 134(1), pp. 129–149.

- Paisán-Ruiz, C. *et al.* (2004) 'Cloning of the Gene Containing Mutations that Cause PARK8-Linked Parkinson's Disease', *Neuron*, 44(4), pp. 595–600.
- Paleologou, K. E. *et al.* (2009) 'Detection of elevated levels of soluble α -synuclein oligomers in post-mortem brain extracts from patients with dementia with Lewy bodies', *Brain*, 132(4), pp. 1093–1101.
- Parihar, M. S. *et al.* (2008) 'Mitochondrial association of alpha-synuclein causes oxidative stress', *Cellular and Molecular Life Sciences*, 65(7), pp. 1272–1284.
- Parihar, M. S. *et al.* (2009) 'Alpha-synuclein overexpression and aggregation exacerbates impairment of mitochondrial functions by augmenting oxidative stress in human neuroblastoma cells', *The International Journal of Biochemistry & Cell Biology*, 41(10), pp. 2015–2024.
- Parnetti, L. *et al.* (2014) 'Cerebrospinal Fluid Lysosomal Enzymes and Alpha-Synuclein in Parkinson's Disease', *Movement Disorders*, 29(8), pp. 1019–1027.
- Pasanen, P. *et al.* (2014) 'A novel α -synuclein mutation A53E associated with atypical multiple system atrophy and Parkinson's disease-type pathology', *Neurobiology of Aging*, 35(9), p. 2180.e1-2180.e5.
- Paxinou, E. *et al.* (2001) 'Induction of-Synuclein Aggregation by Intracellular Nitrate Insult.', *The Journal of Neuroscience*, 21(20), pp. 8053-61.
- Perez, R. G. *et al.* (2002) 'A role for alpha-synuclein in the regulation of dopamine biosynthesis', *The Journal of neuroscience*, 22(8), p. 3090.
- Perni, M. *et al.* (2017) 'A natural product inhibits the initiation of α -synuclein aggregation and suppresses its toxicity', *Proceedings of the National Academy of Sciences*, 114(6), p. E1009.
- Peschke, M., Blades, A. and Kebarle, P. (2002) 'Charged States of Proteins. Reactions of Doubly Protonated Alkyldiamines with NH₃: Solvation or Deprotonation. Extension of Two Proton Cases to Multiply Protonated Globular Proteins Observed in the Gas Phase', *Journal of the American Chemical Society*, 124(38), pp. 11519–11530.
- Pham, C., Kwan, A. and Sunde, M. (2014) 'Functional amyloid: widespread in Nature, diverse in purpose', *Amyloids In Health And Disease*, 56, pp. 207–219.
- Phillips, A. S. *et al.* (2015) 'Conformational dynamics of α -synuclein: insights from mass spectrometry.', *The Analyst*, 140(9), pp. 3070–81.
- Pickrell, A. M. and Youle, R. J. (2015) 'The Roles of PINK1, Parkin, and Mitochondrial Fidelity in Parkinson's Disease', *Neuron*, 85(2), pp. 257–273.

- Poljsak, B., Šuput, D. and Milisav, I. (2013) 'Achieving the balance between ROS and antioxidants: When to use the synthetic antioxidants', *Oxidative Medicine and Cellular Longevity*, vol. 2013, Article ID 956792.
- Polymeropoulos, M. H. *et al.* (1996) 'Mapping of a Gene for Parkinson's Disease to Chromosome 4q21-q23', *Science*, 274(5290), pp. 1197-1199.
- Polymeropoulos, M. H. *et al.* (1997) 'Mutation in the α -synuclein gene identified in families with Parkinson's disease', *Science*, 276(5321), pp. 2045-7.
- Porcari, R. *et al.* (2015) 'The H50Q mutation induces a 10-fold decrease in the solubility of α -synuclein.', *The Journal of biological chemistry*, 290(4), pp. 2395–404.
- Pozo Devoto, V. M. and Falzone, T. L. (2017) 'Mitochondrial dynamics in Parkinson's disease: a role for α -synuclein?', *Disease Models & Mechanisms*, 10(9), pp.1075-1087.
- Price, D. *et al.* 'The small molecule alpha-synuclein misfolding inhibitor, NPT200-11, produces multiple benefits in an animal model of Parkinson's disease.', *Scientific Reports*, 8(1):16165.
- Proukakis, C. *et al.* (2013) 'A novel α -synuclein missense mutation in Parkinson disease', *Neurology*, 80(11), pp. 1062–1064.
- Rahal, A. *et al.* (2014) 'Oxidative stress, prooxidants, and antioxidants: The interplay', *BioMed Research International*, vol. 2014, Article ID 761264.
- Rajasekhar, V. K. *et al.* (2003) 'Oncogenic Ras and Akt Signaling Contribute to Glioblastoma Formation by Differential Recruitment of Existing mRNAs to Polysomes', *Molecular Cell*, 12(4), pp. 889–901.
- Ranjan, P. *et al.* (2017) 'Differential copper binding to alpha-synuclein and its disease-associated mutants affect the aggregation and amyloid formation', *Biochimica et Biophysica Acta*, 1861(2), pp. 365–374.
- Rasheed, M. S. ur *et al.* (2017) 'Coherent and Contradictory Facts, Feats and Fictions Associated with Metal Accumulation in Parkinson's Disease: Epicenter or Outcome, Yet a Demigod Question', *Molecular Neurobiology*, 54(6), pp. 4738–4755.
- Raychaudhuri, S. *et al.* (2009) 'The Role of Intrinsically Unstructured Proteins in Neurodegenerative Diseases', *PLOS ONE*, 4(5), p. e5566.
- Recasens, A. and Dehay, B. (2014) 'Alpha-synuclein spreading in Parkinson's disease', *Frontiers in Neuroanatomy*, 8, pp. 159.
- Rekas, A. *et al.* (2010) 'The structure of dopamine induced alpha-synuclein oligomers', *European Biophysics Journal*, 39(10), pp.1407-19.

- De Ricco, R. *et al.* (2015) 'Remote His50 Acts as a Coordination Switch in the High-Affinity N-Terminal Centered Copper(II) Site of α -Synuclein.', *Inorganic chemistry*, 54(10), pp. 4744–51.
- de Rijk, M. C. *et al.* (2000) 'Prevalence of Parkinson's disease in Europe: A collaborative study of population-based cohorts. Neurologic Diseases in the Elderly Research Group', *Neurology*, 54(11 Suppl 5), pp. S21–3.
- Rodríguez-Leyva, I. *et al.* (2014) ' α -Synuclein inclusions in the skin of Parkinson's disease and parkinsonism', *Annals of Clinical and Translational Neurology*, 1(7), pp. 471-478.
- Roosen, D. A. and Cookson, M. R. (2016) 'LRRK2 at the interface of autophagosomes, endosomes and lysosomes', *Molecular Neurodegeneration*, 11(73).
- Roostae, A. *et al.* (2013) 'Aggregation and neurotoxicity of recombinant α -synuclein aggregates initiated by dimerization', *Molecular Neurodegeneration*, 8(5).
- Ross, O. A. *et al.* (2008) 'Genomic investigation of α -synuclein multiplication and parkinsonism', *Annals of Neurology*, 63(6), pp. 743–50.
- Ross, O. A. *et al.* (2010) 'LRRK2 variation and Parkinson's disease in African Americans', *Movement Disorders*, 25(12), pp. 1973–1976.
- Rudenko, I. N. and Cookson, M. R. (2014) 'Heterogeneity of Leucine-Rich Repeat Kinase 2 Mutations: Genetics, Mechanisms and Therapeutic Implications', *Neurotherapeutics*, 11(4), pp. 738–50.
- Ruotolo, B. T. *et al.* (2002) 'Observation of Conserved Solution-Phase Secondary Structure in Gas-Phase Tryptic Peptides', *Journal of the American Chemical Society*, 124(16), pp. 4214–4215.
- Ruotolo, B. T. *et al.* (2008) 'Ion mobility–mass spectrometry analysis of large protein complexes', *Nature Protocols*, 3, p. 1139.
- Sahay, S. *et al.* (2017) 'Alteration of Structure and Aggregation of Alpha-Synuclein by Familial Parkinson's Disease Associated Mutations', *Current Protein & Peptide Science*, 18(7), pp. 656–676.
- Sanders, L. H. *et al.* (2014) 'LRRK2 mutations cause mitochondrial DNA damage in iPSC-derived neural cells from Parkinson's disease patients: Reversal by gene correction', *Neurobiology of Disease*, 62, pp. 381–386.
- Santner, A. and Uversky, V. N. (2010) 'Metalloproteomics and metal toxicology of α -synuclein.', *Metallomics : integrated biometal science*, 2(6), pp. 378–92.
- Scarff, C. A. *et al.* (2008) 'Travelling wave ion mobility mass spectrometry studies of protein structure: biological significance and comparison with X-ray crystallography

and nuclear magnetic resonance spectroscopy measurements', *Rapid Communications in Mass Spectrometry*, 22(20), pp. 3297–3304.

Schapira, A. H. (2008) 'Mitochondria in the aetiology and pathogenesis of Parkinson's disease', *The Lancet Neurology*, 7(1), pp. 97–109.

Schapira, A. H. V., Chaudhuri, K. R. and Jenner, P. (2017) 'Non-motor features of Parkinson disease', *Nature Reviews Neuroscience*, 18(7), pp. 435–450.

Schneider, K. and Bertolotti, A. (2015) 'Surviving protein quality control catastrophes - from cells to organisms', *Journal of Cell Science*, 128, pp. 3861–3869.

Schulte, C. and Gasser, T. (2011) 'Genetic basis of Parkinson's disease: Inheritance, penetrance, and expression', *Application of Clinical Genetics*, 4, pp. 67–80.

Scudamore, O. and Ciossek, T. (2018) 'Increased Oxidative Stress Exacerbates α -Synuclein Aggregation In Vivo', *Journal of Neuropathology & Experimental Neurology*, 77(6), pp. 443–453.

Segura-Aguilar, J. *et al.* (2014) 'Protective and toxic roles of dopamine in Parkinson's disease', *Journal of Neurochemistry*, 129(6), pp. 898–915.

Shannon, K. M. *et al.* (2012) 'Alpha-synuclein in colonic submucosa in early untreated Parkinson's disease', *Movement Disorders*, 27(6), pp. 709–15.

Sharon, M. and Robinson, C. V (2007) 'The Role of Mass Spectrometry in Structure Elucidation of Dynamic Protein Complexes', *Annual review of biochemistry*, 76(1), pp. 167–193.

Shelimov, K. B. *et al.* (1997) 'Protein Structure in Vacuo: Gas-Phase Conformations of BPTI and Cytochrome *c*', *Journal of the American Chemical Society*, 119(9), pp. 2240–2248.

Shimura, H. *et al.* (2000) 'Familial Parkinson disease gene product, parkin, is a ubiquitin-protein ligase', *Nature Genetics*, 25(3), pp. 302–5.

Shoffner, S. K. and Schnell, S. (2016) 'Estimation of the lag time in a subsequent monomer addition model for fibril elongation', *Physical Chemistry Chemical Physics*, 18(31), pp. 21259–21268.

Smith, A. M. *et al.* (2006) 'Direct Observation of Oligomeric Species formed in the Early Stages of Amyloid Fibril Formation using Electrospray Ionisation Mass Spectrometry', *Journal of Molecular Biology*, 364(1), pp. 9–19.

Smith, D. P. *et al.* (2009) 'Deciphering drift time measurements from travelling wave ion mobility spectrometry-mass spectrometry studies.', *European journal of mass spectrometry*, 15(2), pp. 113–30.

- Smith, D. P. *et al.* (2011) 'Structure and Dynamics of Oligomeric Intermediates in β 2-Microglobulin Self-Assembly', *Biophysical Journal*, 101(5), pp. 1238–1247.
- Smith, D. P., Radford, S. E. and Ashcroft, A. E. (2010) 'Elongated oligomers in β 2-microglobulin amyloid assembly revealed by ion mobility spectrometry-mass spectrometry', *Proceedings of the National Academy of Sciences*, 107(15), pp. 6794–6798.
- Sode, K. *et al.* (2007) 'Effect of Repetition of Repeat Sequences in the Human α -Synuclein on Fibrillation Ability', *International Journal of Biological Sciences*, 3(1), pp. 1–7.
- Spillantini, M. G. *et al.* (1997) ' α -Synuclein in Lewy bodies', *Nature*, 388, p. 839.
- Stephens, A. D. *et al.* (2018) 'Different Structural Conformers of Monomeric α -Synuclein Identified after Lyophilizing and Freezing', *Analytical Chemistry*, 90(11), pp. 6975–6983.
- Tanner, C. M. *et al.* (2011) 'Rotenone, Paraquat, and Parkinson's Disease', *Environmental Health Perspectives*, 119(6), pp. 866–872.
- Tapiero, H., Townsend, D. M. and Tew, K. D. (2003) 'Trace elements in human physiology and pathology. Copper', *Biomedicine & Pharmacotherapy*, 57(9), pp. 386–398.
- Tavassoly, O. *et al.* (2014) 'Cu(II) and dopamine bind to α -synuclein and cause large conformational changes', *FEBS Journal*, 281(12), pp. 2738–2753.
- Tenreiro, S. *et al.* (2014) 'Phosphorylation Modulates Clearance of Alpha-Synuclein Inclusions in a Yeast Model of Parkinson's Disease', *PLOS Genetics*, 10(5), p. e1004302.
- Testa, I. *et al.* (2013) 'Extracting structural information from charge-state distributions of intrinsically disordered proteins by non-denaturing electrospray-ionization mass spectrometry', *Intrinsically Disordered Proteins*, 1(1), e25068.
- Thalassinos, K. *et al.* (2009) 'Characterization of Phosphorylated Peptides Using Traveling Wave-Based and Drift Cell Ion Mobility Mass Spectrometry', *Analytical Chemistry*, 81(1), pp. 248–254.
- Theillet, F.-X. *et al.* (2016) 'Structural disorder of monomeric α -synuclein persists in mammalian cells.', *Nature*, 530(7588), pp. 45–50.
- Thomas, J. D. and Johannes, G. J. (2007) 'Identification of mRNAs that continue to associate with polysomes during hypoxia', *RNA*, 13(7), pp. 1116–31.
- Toyama, B. H. and Weissman, J. S. (2011) 'Amyloid Structure: Conformational Diversity and Consequences', *Annual review of biochemistry*, 80, pp. 557–85.

- Uversky, V. N. (2011) 'Intrinsically disordered proteins from A to Z', *The International Journal of Biochemistry & Cell Biology*, 43(8), pp. 1090–1103.
- Uversky, V. N. (2016) 'Dancing protein clouds: The strange biology and chaotic physics of intrinsically disordered proteins', *Journal of Biological Chemistry*, 291(13), pp. 6681–8.
- Uversky, V. N., Li, J. and Fink, A. L. (2001a) 'Evidence for a partially folded intermediate in alpha-synuclein fibril formation.', *The Journal of biological chemistry*, 276(14), pp. 10737–44.
- Uversky, V. N., Li, J. and Fink, A. L. (2001b) 'Metal-triggered structural transformations, aggregation, and fibrillation of human alpha-synuclein. A possible molecular NK between Parkinson's disease and heavy metal exposure.', *The Journal of biological chemistry*, 276(47), pp. 44284–96.
- Vahidi, S., Stocks, B. B. and Konermann, L. (2013) 'Partially Disordered Proteins Studied by Ion Mobility-Mass Spectrometry: Implications for the Preservation of Solution Phase Structure in the Gas Phase', *Analytical Chemistry*, 85(21), pp. 10471–10478.
- Valente, E. M. *et al.* (2004) 'Hereditary early-onset Parkinson's disease caused by mutations in PINK1', *Science*, 304(5674), pp. 1158–60.
- Vargas, K. J. *et al.* (2014) 'Synucleins Regulate the Kinetics of Synaptic Vesicle Endocytosis', *Journal of Neuroscience*, 34(28), pp. 9364–76.
- Varland, S., Osberg, C. and Arnesen, T. (2015) 'N-terminal modifications of cellular proteins: The enzymes involved, their substrate specificities and biological effects.', *Proteomics*, 15(14), pp. 2385–401.
- Vlad, C. *et al.* (2011) 'Autoproteolytic Fragments are Intermediates in the Oligomerization- Aggregation of Parkinson's Disease Protein Alpha-Synuclein as Revealed by Ion Mobility Mass Spectrometry', *Chembiochem : a European journal of chemical biology*, 12(18), pp. 2740–2744.
- Volles, M. and Lansbury, P. (2002) ' Vesicle permeabilization by protofibrillar alpha-synuclein is sensitive to Parkinson's disease-linked mutations and occurs by a pore-like mechanism.', *Biochemistry*, 41(14), pp. 4595-602.
- Walker, D. G. *et al.* (2013) 'Changes in properties of serine 129 phosphorylated α -synuclein with progression of Lewy-type histopathology in human brains', *Experimental Neurology*, 240, pp. 190–204.
- Wang, J. and Pantopoulos, K. (2011) 'Regulation of cellular iron metabolism.', *The Biochemical journal*, 434(3), pp. 365–81.

- Wang, W. *et al.* (2011) 'A soluble α -synuclein construct forms a dynamic tetramer.', *Proceedings of the National Academy of Sciences of the United States of America*, 108(43), pp. 17797–802.
- Wei, Z. *et al.* (2018) 'Oxidative Stress in Parkinson's Disease: A Systematic Review and Meta-Analysis', *Frontiers in Molecular Neuroscience*, 11, p. 236.
- Weihofen, A. *et al.* (2018) 'Development of an aggregate-selective, human-derived α -synuclein antibody B1B054 that ameliorates disease phenotypes in Parkinson's disease models.', *Neurobiology of Disease*, S0969-9961(18)30448-0.
- Wijaya, C. H., Wijaya, W. and Mehta, B. M. (2015) 'General Properties of Major Food Components', in *Handbook of Food Chemistry*. Berlin, Heidelberg: Springer Berlin Heidelberg, pp. 15–54.
- Willis, A. W. *et al.* (2010) 'Metal Emissions and Urban Incident Parkinson Disease: A Community Health Study of Medicare Beneficiaries by Using Geographic Information Systems', *American Journal of Epidemiology*, 172(12), pp. 1357–1363.
- Wilm, M. S. and Mann, M. (1994) 'Electrospray and Taylor-Cone theory, Dole's beam of macromolecules at last?', *International Journal of Mass Spectrometry and Ion Processes*, 136(2–3), pp. 167–180.
- Wilms, H. *et al.* (2009) 'Suppression of MAP kinases inhibits microglial activation and attenuates neuronal cell death induced by alpha-synuclein protofibrils.', *International Journal of Immunopathology and Pharmacology*, 22(4), pp. 897-909.
- Winner, B. *et al.* (2011) 'In vivo demonstration that alpha-synuclein oligomers are toxic.', *Proceedings of the National Academy of Sciences of the United States of America*, 108(10), pp. 4194–9.
- Wirdefeldt, K. *et al.* (2011) 'Epidemiology and etiology of Parkinson's disease: a review of the evidence', *Eur J Epidemiol*, 26, pp. 1–58.
- Wollnik, H. and Przewlaka, M. (1990) 'Time-of-flight mass spectrometers with multiply reflected ion trajectories', *International Journal of Mass Spectrometry and Ion Processes*, 96(3), pp. 267–274.
- Woods, L. A. *et al.* (2011) 'Ligand binding to distinct states diverts aggregation of an amyloid-forming protein', *Nature Chemical Biology*, 7(10), pp. 730–739.
- Wrasidlo, W. *et al.* (2016) 'A de novo compound targeting α -synuclein improves deficits in models of Parkinson's disease', *Brain*, 139(12), pp. 3217–3236.
- Wytttenbach, T., von Helden, G. and Bowers, M. T. (1996) 'Gas-Phase Conformation of Biological Molecules: Bradykinin', *Journal of the American Chemical Society*, 118(35), pp. 8355–8364.

- Xicoy, H., Wieringa, B. and Martens, G. J. M. (2017) 'The SH-SY5Y cell line in Parkinson's disease research: a systematic review', *Molecular Neurodegeneration*, 12(1), pp. 1–11.
- Young, L. M. *et al.* (2014) 'Ion Mobility Spectrometry–Mass Spectrometry Defines the Oligomeric Intermediates in Amylin Amyloid Formation and the Mode of Action of Inhibitors', *Journal of the American Chemical Society*, 136(2), pp. 660–670.
- Zarranz, J. J. *et al.* (2004) 'The New Mutation, E46K, of α -Synuclein Causes Parkinson and Lewy Body Dementia', *Annals of Neurology*, 55(2), pp. 164–73.
- Zecca, L. *et al.* (2008) 'Neuromelanin can protect against iron-mediated oxidative damage in system modeling iron overload of brain aging and Parkinson's disease', *Journal of Neurochemistry*, 106(4), pp. 1866–1875.
- Zhang, W. *et al.* (2005) 'Aggregated alpha-synuclein activates microglia: a process leading to disease progression in Parkinson's disease.', *FASEB J*, 19(6), PP. 533-42.
- Zhu, M. and Fink, A. L. (2003) 'Lipid binding inhibits alpha-synuclein fibril formation', *Journal of Biological Chemistry*, 278(19), pp. 16873–7.
- Zucca, F. A. *et al.* (2017) 'Interactions of Iron, Dopamine and Neuromelanin pathways in Brain Aging and Parkinson's Disease', *Progress in neurobiology*, 155, pp. 96–119.